NORTH ATLANTIC TREATY ORGANIZATION

SCIENCE AND TECHNOLOGY ORGANIZATION

AC/323(AVT-239)TP/901

www.sto.nato.int

STO TECHNICAL REPORT **TR-AVT-239**

Innovative Control Effectors for Manoeuvring of Air Vehicles

(Effecteurs de contrôle innovants destinés à manœuvrer les véhicules aériens)

Summary Report of the NATO STO AVT-239 Task Group.

Published November 2020

NORTH ATLANTIC TREATY ORGANIZATION

SCIENCE AND TECHNOLOGY ORGANIZATION

AC/323(AVT-239)TP/901

www.sto.nato.int

STO TECHNICAL REPORT **TR-AVT-239**

Innovative Control Effectors for Manoeuvring of Air Vehicles

(Effecteurs de contrôle innovants destinés à manœuvrer les véhicules aériens)

Summary Report of the NATO STO AVT-239 Task Group.

The NATO Science and Technology Organization

Science & Technology (S&T) in the NATO context is defined as the selective and rigorous generation and application of state-of-the-art, validated knowledge for defence and security purposes. S&T activities embrace scientific research, technology development, transition, application and field-testing, experimentation and a range of related scientific activities that include systems engineering, operational research and analysis, synthesis, integration and validation of knowledge derived through the scientific method.

In NATO, S&T is addressed using different business models, namely a collaborative business model where NATO provides a forum where NATO Nations and partner Nations elect to use their national resources to define, conduct and promote cooperative research and information exchange, and secondly an in-house delivery business model where S&T activities are conducted in a NATO dedicated executive body, having its own personnel, capabilities and infrastructure.

The mission of the NATO Science & Technology Organization (STO) is to help position the Nations' and NATO's S&T investments as a strategic enabler of the knowledge and technology advantage for the defence and security posture of NATO Nations and partner Nations, by conducting and promoting S&T activities that augment and leverage the capabilities and programmes of the Alliance, of the NATO Nations and the partner Nations, in support of NATO's objectives, and contributing to NATO's ability to enable and influence security and defence related capability development and threat mitigation in NATO Nations and partner Nations, in accordance with NATO policies.

The total spectrum of this collaborative effort is addressed by six Technical Panels who manage a wide range of scientific research activities, a Group specialising in modelling and simulation, plus a Committee dedicated to supporting the information management needs of the organization.

- AVT Applied Vehicle Technology Panel
- HFM Human Factors and Medicine Panel
- IST Information Systems Technology Panel
- NMSG NATO Modelling and Simulation Group
- SAS System Analysis and Studies Panel
- SCI Systems Concepts and Integration Panel
- SET Sensors and Electronics Technology Panel

These Panels and Group are the power-house of the collaborative model and are made up of national representatives as well as recognised world-class scientists, engineers and information specialists. In addition to providing critical technical oversight, they also provide a communication link to military users and other NATO bodies.

The scientific and technological work is carried out by Technical Teams, created under one or more of these eight bodies, for specific research activities which have a defined duration. These research activities can take a variety of forms, including Task Groups, Workshops, Symposia, Specialists' Meetings, Lecture Series and Technical Courses.

The content of this publication has been reproduced directly from material supplied by STO or the authors.

Published November 2020

ISBN 978-92-837-2226-7

Table of Contents

List of Figures

List of Tables

List of Acronyms

AFC	Active Flow Control
ALM	Additive Layer Manufacturing
AMT	All-Moving Wingtip
Apex_L	Left Apex Leading-Edge Slot-Jet Effector
Apex_R	Right Apex Leading-Edge Slot-Jet Effector
AR	Aspect Ratio
BWB	Blended Wing-Body
CC	Circulation Control
CFD	Computational Fluid Dynamics
CG	Centre of Gravity
FCE	Fluidic Control Effector
FTV	Fluidic Thrust Vectoring
IB	Inboard
IBC	Inboard CC device
KPP	Key Performance Parameter
LAMT	Left All-Moving Wingtip
LE	Leading Edge
LEF	Leading-Edge Flap
LELE	Left Elevon
LSSD	Left Spoiler Slot Deflector
M	Pitching Moment
MAC	Mean Aerodynamic Chord
Midspan_L	Left Midspan Leading-Edge Slot-Jet Effector
Midspan_R	Right Midspan Leading-Edge Slot-Jet Effector
Mn	Mach Number
MRL	Moment Reference Line
MRP	Moment Reference Point
MTOW	Maximum Take-off Weight
NPR	Nozzle Pressure Ratio
OB	Outboard
OBC	Outboard CC device
OML	Outer Mould Line
PR	Public Relations
PSP	Pressure Sensitive Paint
PWM	Pulse Width Modulation
QFD	Quantified Function Deployment

RAMT	Right All-Moving Wingtip
RANS	Reynolds Averaged Navier-Stokes
RELE	Right Elevon
RSSD	Right Spoiler Slot Deflector
SJA	Synthetic Jet Actuator
SSD	Spoiler Slot Deflector
TE	Trailing Edge
TEL_dn	Trailing Edge Left Down Slot-Jet Effector
TEL_up	Trailing Edge Left Up Slot-Jet Effector
TER_dn	Trailing Edge Right Down Slot-Jet Effector
TER_up	Trailing Edge Right Up Slot-Jet Effector
UAV	Unmanned Air Vehicle
UCAV	Unmanned Combat Air Vehicle
YTV	Yaw Fluidic Thrust Vectoring
YTV_L	Left Yaw Fluidic Thrust Vectoring
YTV_R	Right Yaw Fluidic Thrust Vectoring

AVT-239 Membership List

CO-CHAIRS

Prof. Clyde WARSOP
BAE Systems AIR
UNITED KINGDOM
Email: clyde.warsop@baesystems.com

Dr. Douglas R. SMITH
AFOSR/EOARD
UNITED KINGDOM
Email: douglas.smith.82@us.af.mil

Dr. Jonathan IRVING
BAE Systems Submarines
UNITED KINGDOM
Email: jonathan.irving@baesystems.com

MEMBERS

Mr Oluwatobi AFILAKA
The University of Manchester
UNITED KINGDOM
Email: oluwatobi.afilaka@manchester.ac.uk

Prof. Kenneth J. BADCOCK
University of Liverpool
UNITED KINGDOM
Email: K.J.Badcock@liverpool.ac.uk

Mr. Steven S. BRANDT
United States Air Force Academy
UNITED STATES
Email: steven.brandt@usafa.edu

Prof. Dr.-Ing. Christian BREITSAMTER
Aerodynamics and Fluid mechanics
GERMANY
Email: christian.breitsamter@aer.mw.tum.de

Assist Prof. Kemal Bulent YUCEIL
Istanbul Technical University (ITU)
TURKEY
Email: yuceil@itu.edu.tr

Prof. Dr. Oksan CETINER-YILDIRIM
Istanbul Technical University (ITU)
TURKEY
Email: cetiner@itu.edu.tr

Dr. James CHARD
The University of Manchester
UNITED KINGDOM
Email: james.chard@manchester.ac.uk

Prof. Jonathan E. COOPER
University of Bristol
UNITED KINGDOM
Email: j.e.cooper@bristol.ac.uk

Dr. Joe COPPIN
Defence Science & Technology Laboratory
UNITED KINGDOM
Email: jcoppin@dstl.gov.uk

Mr. Pierre DUBOIS
Rockwell Collins
FRANCE
Email: pierre.dubois@rockwellcollins.com

Dr. Matthew FORSTER
BAE SYSTEMS Air
UNITED KINGDOM
Email: matthew.forster@baesystems.com

Prof. Ari GLEZER
George W. Woodruff School
of Mechanical Engineering
UNITED STATES
Email: ari.glezer@me.gatech.edu

Mr. Senem Ayse HASER
Turkish Aerospace Industries (TAI)
TURKEY
Email: shaser@tai.com.tr

Dr. Stephan HITZEL
Airbus Defence and Space
GERMANY
Email: stephan.hitzel@airbus.com

Dr. -Ing. Andreas N. HOEVELMANN
Airbus Defence and Space
GERMANY
Email: andreas.hoevelmann@airbus.com

Dr. George A. HOHOLIS
University of Liverpool
UNITED KINGDOM
Email: g.hoholis@liverpool.ac.uk

Ms. Kerstin HUBER
German-Dutch Wind Tunnels (DNW)
GERMANY
Email: kerstin.huber@dnw.aero

Prof. Dr. -Ing Dietrich HUMMEL
Technische Universität Braunschweig
GERMANY
Email: dietrich.hummel@t-online.de

Mr. Christopher R. HUTCHIN
Defence Science and Technology Laboratory
UNITED KINGDOM
Email: crhutchin@dstl.gov.uk

Mr. Thomas IMMISCH
DLR - Institute of Flight Systems
Flight Dynamics and Simulation
GERMANY
Email: thomas.immisch@dlr.de

Dr. Olaseinde O. JEGEDE
The University of Manchester
UNITED KINGDOM
Email: olaseinde.jegede@manchester.ac.uk

Prof. Konstantinos KONTIS
University of Glasgow
UNITED KINGDOM
Email: kostas.kontis@glasgow.ac.uk

Mr. Burak KURKCU
Aselsan Inc
TURKEY
Email: bkurkcu@aselsan.com.tr

Dr. Alberto LLOPIS-PASCUAL
The University of Manchester
SPAIN
Email: alberto.llopis-pascual@postgrad.manchester.ac.uk

Mr. Patrick LOECHERT
Dstl Air and Weapons System Department
UNITED KINGDOM
Email: patrick.loechert@dlr.de

Mr. Daniel N. MILLER
Lockheed Martin ADP
UNITED STATES
Email: daniel.n.miller@lmco.com

Mr. Mauro MOLINO
Airbus Defence and Space
GERMANY
Email: mauro.molino@airbus.com

Dr. Raj NANGIA
Nangia Associates
UNITED KINGDOM
Email: nangia@blueyonder.co.uk

Dr. Michael A. NIESTROY
Lockheed Martin ADP
UNITED STATES
Email: michael.a.niestroy@lmco.com

Mr. Robert OSTERHUBER
Airbus Defence and Space
GERMANY
Email: robert.osterhuber@airbus.com

Mr. Bradley ROBERTSON-WELSH
The University of Manchester
UNITED KINGDOM
Email: bradley.robertsonwelsh@manchester.ac.uk

Dr. Jurgen SEIDEL
US Air Force Academy
GERMANY
Email: jurgen.seidel@usafa.edu

Mr. Omur SERAN
Turkish Aerospace Industries (TAI)
TURKEY
Email: oseran@tai.com.tr

Dr. Rene STEIJL
University of Glasgow
NETHERLANDS
Email: rene.steijl@glasgow.ac.uk

Dr. Jana STUECKE
University of the West of England, Bristol
GERMANY
Email: jana.stucke@uwe.ac.uk

Mr. Umut SUSUZ
Turkish Aerospace Industries (TAI)
TURKEY
Email: ususuz@tai.com.tr

Mr. Erhan E. TARHAN
Turkish Aerospace Industries (TAI)
TURKEY
Email: ertarhan@tai.com.tr

Dr. Christine A. TOOMER
University of the West of England
UNITED KINGDOM
Email: chris.toomer@uwe.ac.uk

Mr. Anthony E. WASHBURN
NASA Langley Research Centre
UNITED STATES
Email: anthony.e.washburn@nasa.gov

Prof. David R. WILLIAMS
Illinois Institute of Technology
UNITED STATES
Email: david.williams@iit.edu

Dr. Rene WOSZIDLO
The Boeing Company
GERMANY
Email: rene.woszidlo@boeing.com

Prof. Israel J. WYGNANSKI
The University of Arizona
UNITED STATES
Email: wygy@email.arizona.edu

ADDITIONAL CONTRIBUTORS

Brock H. CRAWFORD
United States Air Force Academy
UNITED STATES
Email: unavailable

William J. CROWTHER
The University of Manchester
UNITED KINGDOM
Email: w.j.crowther@manchester.ac.uk

Jason A. HOLMES
United States Air Force Academy
UNITED STATES
Email: unavailable

Brandt H. MAINES
Lockheed Martin ADP
UNITED STATES
Email: brandt.h.maines@lmco.com

Thomas E. MCLAUGHLIN
United States Air Force Academy
UNITED STATES
Email: tom.mclaughlin@usafa.edu

Ryan OSTEROOS
United States Air Force Academy
UNITED STATES
Email: ryan.osteroos@usafa.edu

Thomas SHEARWOOD
The University of Manchester
UNITED KINGDOM
Email: Thomas.shearwood@manchester.ac.uk

PANEL MENTOR

Mr. Peter G. MARTIN
Defence Science and Technology Laboratory
UNITED KINGDOM
Email: pgmartin@dstl.gov.uk

Innovative Control Effectors for Manoeuvring of Air Vehicles

(STO-TR-AVT-239)

Executive Summary

Next generation military aircraft will confront increasingly contested and increasingly sophisticated threat environments. To enhance the survivability of future aircraft in these environments will require new approaches to flying aircraft. Legacy approaches, using deflecting surfaces that open gaps and seams in the aircraft surface, are at odds with the demand for enhanced survivability. Novel approaches focussed around the application of Active Flow Technology (AFC), involving seamless technologies without the requirement to deflect conventional flight control surfaces, offer the promise of full aircraft flight control without compromising low detectability.

The NATO STO AVT-239 Research Task Group came together to investigate the application of novel flight control technologies to aircraft manoeuvring. Candidate AFC technologies were identified, developed, and assessed against key vehicle performance and vehicle integration criteria (e.g., complexity, maintainability, reliability). The goal was to identify the technologies that minimized the reliance on conventional control surfaces during different portions of the vehicle mission profiles. The aerodynamic performance of these technologies was tested on two platforms representative of next generation tailless aircraft (ICS and SACCON/MULDICON) for a representative ingress mission phase. These evaluations combined experimental measurements in wind tunnels and high-fidelity numerical simulations. The aerodynamic data were then incorporated into flight dynamics simulations where flow control technologies were used to provide flight control in lieu of conventional control surface deflections. These flight simulations were run for a representative one-hour ingress mission scenario with the aircraft subject to light/moderate turbulence and moderate gusts. In tandem with these performance evaluations, conceptual design studies provided interior aircraft layouts in which the control technologies were integrated. These studies allowed team members to evaluate the 'ilities' metrics of the aircraft design and to perform a technology readiness assessment. The culmination of these three activities was a Quality Function Deployment (QFD) evaluation where each flow control technology was graded in an objective and consistent manner against a set of defined measures. The objective of the research activity was to identify system integration impact, the barriers to implementation and the next steps required to implement these technologies on a full-scale aircraft.

This study concludes that AFC technology is both feasible and reasonable for application to next generation air vehicle platforms represented by the ICE and SACCON/MULDICON platforms with respect to the impact such systems would have on mission performance, integration, and propulsion integration. For the ingress mission phases, both trailing edge tangential blowing/circulation control and yaw fluidic thrust vectoring appear to be the most promising technologies.

Areas highlighted for future R&D investment include: AFC valve reliability/maintainability and the maturation of technology, integration, and manufacturing readiness to level 5 or greater. Further assessments are proposed to explore the application of AFC to the take-off/landing and manoeuvring mission phases. A comprehensive framework for integrating flow control into the preliminary aerodynamic design process of a next generation UAV and assessing its system impact on that aircraft has been established.

Effecteurs de contrôle innovants destinés à manœuvrer les véhicules aériens

(STO-TR-AVT-239)

Synthèse

Les aéronefs militaires de prochaine génération seront confrontés à des environnements de plus en plus contestés et à des menaces de plus en plus sophistiquées. L'amélioration de la survivabilité des futurs aéronefs dans ces conditions nécessitera de nouvelles approches des aéronefs volants. Les approches héritées, consistant à utiliser des surfaces déflectrices qui donnent lieu à des ouvertures et des joints à la surface de l'aéronef, entrent en conflit avec la demande d'amélioration de la survivabilité. Les approches inédites concentrées sur l'application de l'Active Flow Technology (AFC, technologie de l'écoulement actif), qui font appel à des technologies sans joint et n'exigent pas de braquer les surfaces des commandes de vol classiques, promettent une maîtrise complète du vol de l'aéronef sans compromettre la faible détectabilité.

Le groupe de recherche AVT-239 de la STO de l'OTAN s'est réuni pour étudier l'application des nouvelles technologies de commande de vol aux manœuvres des aéronefs. Les technologies AFC envisageables ont été identifiées, développées et évaluées au regard des performances clés du véhicule et des critères d'intégration du véhicule (par exemple, la complexité, la maintenabilité, la fiabilité). Le but était d'identifier les technologies qui minimisaient l'utilisation des surfaces de commande conventionnelles pendant différentes parties des profils de mission du véhicule. Les performances aérodynamiques de ces technologies ont été testées sur deux plateformes représentatives des aéronefs sans queue de prochaine génération (ICS et SACCON/MULDICON) pour une phase de mission d'entrée représentative. Ces évaluations ont associé des mesures expérimentales en soufflerie et des simulations numériques à haute fidélité. Les données aérodynamiques ont ensuite été incorporées dans des simulations de dynamique du vol, dans lesquelles le vol est commandé par des technologies de contrôle de l'écoulement et non par le braquage des surfaces de commande classiques. Ces simulations de vol ont été exécutées selon un scénario représentatif d'une mission d'entrée d'une heure soumettant l'aéronef à des turbulences légères/modérées et à des rafales modérées. En association avec ces évaluations des performances, des études de définition ont fourni l'agencement intérieur de l'aéronef dans lequel les technologies de commande étaient intégrées. Ces études ont permis aux membres de l'équipe d'évaluer les indicateurs d'attribut de qualité de la conception des aéronefs et de réaliser une évaluation de la maturité technologique. Ces trois activités ont débouché sur l'évaluation d'un déploiement de la fonction qualité (QFD), où chaque technologie de contrôle de l'écoulement a été notée de manière objective et cohérente par rapport à un ensemble de mesures définies. L'objectif de l'activité de recherche était d'identifier l'effet de l'intégration du système, les obstacles à la mise en œuvre et les étapes suivantes nécessaires pour appliquer ces technologies dans un aéronef en grandeur réelle.

La présente étude conclut que l'utilisation de la technologie AFC est à la fois faisable et raisonnable sur les plateformes de véhicule aérien de prochaine génération représentées par les plateformes ICE ET SACCON/MULFICON, du point de vue de l'impact qu'auraient ces systèmes sur l'exécution de la mission, l'intégration et l'intégration de la propulsion. Pour les phases de mission d'entrée, le soufflage tangentiel/contrôle de circulation du bord de fuite et l'orientation de la poussée fluidique en lacet semblent les technologies les plus prometteuses.

Les domaines mis en avant pour les futurs investissements de R&D sont les suivants : fiabilité/maintenabilité des vannes AFC et maturation de la technologie, intégration et aptitude à la fabrication de niveau 5 ou plus. D'autres évaluations sont proposées pour étudier l'application de l'AFC aux phases de décollage/atterrissage et manœuvres des missions. Un cadre complet a été établi, qui régit l'intégration du contrôle de l'écoulement dans le processus d'étude aérodynamique préliminaire des UAV de prochaine génération et l'évaluation de l'impact de son système sur l'aéronef.

Chapter 1 – INTRODUCTION AND OVERVIEW

Douglas R. Smith
USAF European Office of Aerospace
Research and Development,
UNITED KINGDOM

Clyde Warsop
BAE Systems Air, Filton
UNITED KINGDOM

1.1 OVERVIEW

Active Flow Control (AFC) holds the potential to transform the flight control of current and next generation aircraft by eliminating conventional, mechanically-deflected control surfaces. Such a system could reduce the weight and complexity of the vehicle while maintaining the same or superior system performance. A recent NATO research task group has investigated a suite of AFC-based flight control systems for use in next generation tailless military aircraft. The group has evaluated and generated performance data for individual AFC technologies on representative aircraft and developed flight control models from these data. Simulated mission scenarios were then 'flown' with the models to inform a systems/trades assessment of the AFC flight controlled vehicle. This paper describes the motivation for the study, the formation and organization of teams within the task group, and an introduction to the specific tasks undertaken by each team. Companion papers describe in greater detail each part of the task group's effort.

1.2 INTRODUCTION

Next generation military aircraft will confront increasingly contested and increasingly sophisticated threat environments. To enhance the survivability of future aircraft in these environments will require new approaches to flying aircraft. Legacy approaches, using deflecting surfaces that open gaps and seams in the aircraft surface, are at odds with the demand for enhanced survivability. Novel approaches, involving seamless technologies without deflecting surfaces, offer the promise of full aircraft flight control without compromising low detectability.

The NATO STO AVT-239 Research Task Group came together to investigate the application of novel flight control technologies to aircraft manoeuvring. Candidate technologies were identified, developed, and assessed against key vehicle performance and vehicle integration criteria (e.g., complexity, maintainability, reliability). The goal was to identify candidate technologies that minimized the reliance on conventional control surfaces during different portions of the vehicle mission profiles. The aerodynamic performance of these technologies was tested on two platforms representative of next generation tailless aircraft (UCAV). These evaluations combined experimental measurements in wind tunnels and high-fidelity numerical simulations. The aerodynamic data were then incorporated into flight dynamics simulations where flow control technologies were used to provide flight control in lieu of conventional control surface deflections. These flight simulations were run for a representative one-hour ingress mission scenario with the aircraft subject to light/moderate turbulence and moderate gusts. In tandem with these performance evaluations, conceptual design studies provided interior aircraft layouts in which the control technologies were integrated. These studies allowed team members to evaluate the '-ilities' metrics of the aircraft design and to perform a technology readiness assessment. The culmination of these three activities was a Quality Function Deployment (QFD) evaluation where each flow control technology was graded in an objective and consistent manner against a set of defined measures.

This paper will provide a broad overview of the structure of the task group, the participation of NATO members within that structure, the basic test platforms and mission scenarios, and a brief introduction to each of the three assessment tasks. Subsequent papers will provided a detailed exploration of the efforts in each of the tasks. The broader goal of the NATO research activity is to identify the next steps and the barriers to implementation of these technologies on a full-scale aircraft.

1.3 BACKGROUND

The motivation for the AVT-239 group arose from the recommendations of a NATO workshop held in May 2013 (NATO STO AVT-215), but the impetus has its origins slightly earlier. An AVT Symposium on Morphing Vehicles (Evora, Portugal, April 2009, RTO-MP-AVT-168) examined many approaches that involve seamless geometry movement including morphing leading and trailing edges, morphable wings and wing tips, and continuous mould-line technology, to name just a few. The workshop in 2013 explored a wider range of concepts including many pneumatic/fluidic control approaches to creating 'virtual geometry changes'. Such approaches involve blowing or suction to increase the effectiveness of (or even replace) conventional aerodynamic control surfaces. They have a wide range of potential uses from separation control for improving high alpha performance, to lift augmentation and full 3-axis flight control. However, to date, exploitation on production platforms has been limited, often due to the perceived complexity, unknown power requirements, and concern over the impact on cruise performance. Successfully implemented flow control technologies, however, have the potential to revolutionise the performance and manoeuvring characteristics of modern air and maritime platforms. It was this potential that motivated the AVT-215 workshop, and a key objective from the workshop was to explore, assess and baseline the current state of the art in innovative control effector technologies. The conclusion of the workshop was that, if the Technology Readiness Level (TRL) of these technologies were raised, they could offer a promising route to providing a new range of control effectors suitable for application to aircraft that are constrained by low-observability considerations.

The AVT-215 workshop clearly established that the flow control landscape contains many potential flow control technologies and when coupled to the many prospective next generation NATO vehicle platforms spans a large parameter space. A comprehensive exploration of this space was well-beyond both the staffing of the group and the timeline for its work. In addition, the unfunded, volunteer nature of NATO task groups constrains the space that the group can examine, depending importantly on the interests and experience of the contributing researchers and on leveraging available prior work. This leveraging of prior work was an important consideration in the selection of aircraft test platforms. Moreover, the group wanted to establish a comprehensive framework for integrating flow control into the aerodynamic design of a next generation UAV and assessing its system impact on that aircraft. It is the hope of the group that this framework will become the enduring standard by which future novel control technologies are assessed.

An important challenge to be addressed by this group was identifying technologies that reduce or minimize 'seams', 'gaps', or moving surfaces to effect flight control. Recognizing that no single technology may provide control throughout the full flight envelope, combinations of control effectors were an essential part of the evaluation.

The following sections of this paper will, first, briefly introduce the baseline vehicles and missions used by the AVT-239 group to do the AFC assessments, and then describe how the group was organized to undertake the assessments.

1.4 AVT-239 VEHICLE PLATFORMS AND MISSION SETS

In the first year of the AVT-239 task, the group identified two baseline aircraft configurations for the flow control effector evaluations and a set of mission scenarios under which the performance of the technologies could be evaluated against conventional flight control effectors.

1.4.1 Vehicle Platforms

The criteria for candidate vehicle platforms were that:

1) The vehicle should be characteristic of a next generation combat vehicle, preferably tailless;

2) An existing vehicle performance and control database for the platform was readily available in the open literature; and

3) The platforms should be sufficiently distinct to provide an assessment of the control effector performance against different aerodynamic characteristics, e.g., wing sweep.

Two vehicles matched well against these criteria, the stability and control (SACCON) design (Figure 1-1) from AVT-161, and the Lockheed Martin Innovative Control Effectors (ICE) design (Figure 1-2). The SACCON is a generic UCAV designed to challenge the ability of RANS-based CFD methods at predicting the stability and control characteristics of highly-swept wings [1]. The ICE aircraft is an all-wing, tailless configuration that can be manned or unmanned. The aircraft with the baseline conventional control effectors indicated in Figure 1-2, evolved from 1991 Internal Research and Development (IRAD) studies at Lockheed Martin Aeronautics and was subsequently studied in depth under AFRL sponsorship [2], [3].

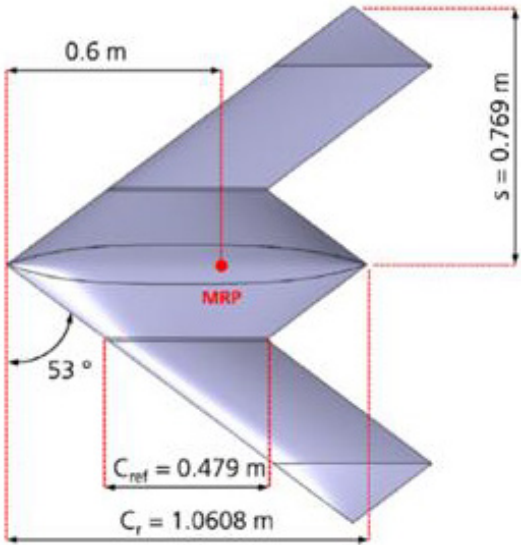

Figure 1-1: SACCON Platform.

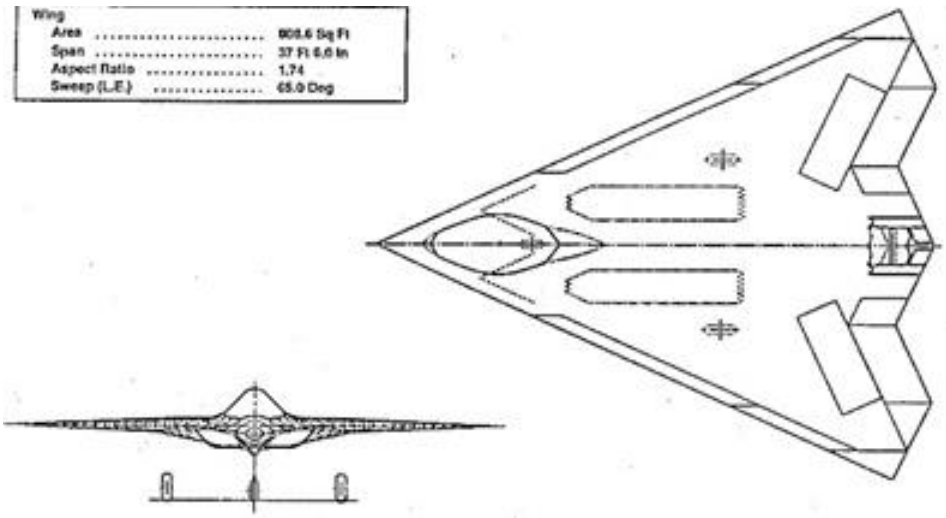

Figure 1-2: Innovative Control Effectors Platform (ICE).

1.4.2 Mission Profiles

A set of three mission profiles were initially chosen for the assessment of control effector and vehicle performance. The mission profiles were (1) ingress/cruise, (2) egress with high manoeuvrability, and (3) high-lift take-off and landing. These profiles were structured such that the control authority from the novel effectors would be increasingly demanding in moving from the first mission to the third. Although performance data relevant to all three missions were collected in the course of this task group, a full system assessment was only performed for the ingress mission profile.

The flight conditions for the ingress profile were Mach 0.9 and 30,000 ft. (Figure 1-3). For this profile, the required performance was full flight control in the presence of light-to-moderate turbulence over 99% of the flight time and moderate gusts for the remaining 1% of the flight time (ref. MIL-HDBK-1797). This performance was assessed against the required engine bleed mass flow rate as a percentage of the total engine mass flow.

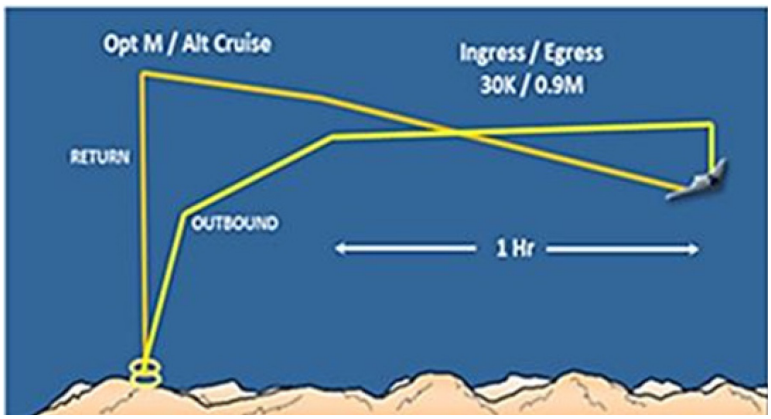

Figure 1-3: Ingress/Egress Mission Profile.

1.5 AVT-239 RESEARCH TASK GROUP STRUCTURE

The structure of the task group participation was established around the three key components of the assessment framework: the flow control effector technologies, the vehicle performance evaluation, and the trade study and system requirements evaluation. Although each of these groups had distinct responsibilities, the expectation from the beginning of the effort was that there would be important and ongoing interactions between these efforts (Figure 1-4).

1.5.1 Flow Control Technology

The Flow Control Technology sub-group was composed primarily of academic participants bringing expertise with specific flow control technologies. The composition of this group determined which technologies were likely candidates for vehicle manoeuvring. They were responsible for defining a consistent means for comparing the relative merits of different flow control technologies. For the technologies used in this effort, all candidates were pneumatic-based, and all performance evaluations were measured against the momentum coefficient (C_μ) required to achieve a specific effect e.g., ΔC_L. Participants in this sub-group undertook the task of doing all of the component level evaluations of the candidate technologies. These evaluations were done with both experimental testing in wind tunnel facilities and numerical simulations. When possible, experiments and simulations were performed for the same configurations at the same test conditions (Re, Ma).

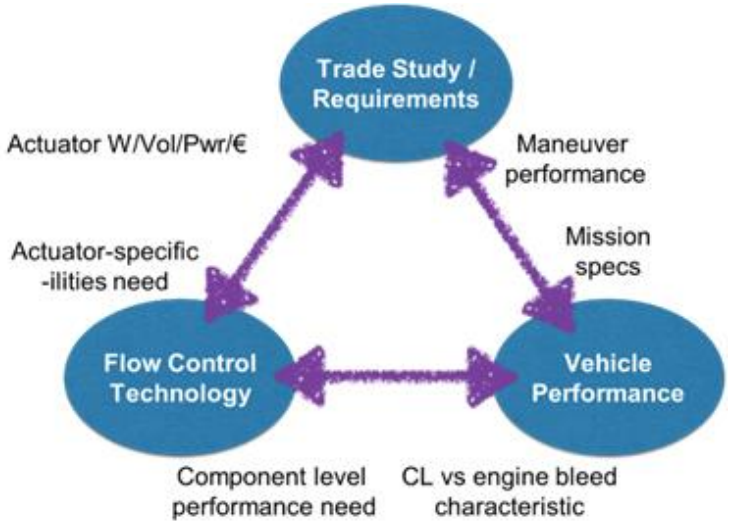

Figure 1-4: NATO AVT-239 Sub-Groups and Example Interactions.

The output of this group was aerodynamic performance changes as a function of actuator momentum coefficient. As the source of high pressure air for the actuator technologies is likely to be engine bleed air in practice, an estimate of percentage mass flow relative to core mass flow was also reported.

1.5.1.1 Subsonic Wind Tunnel Tests at USAFA

A wind tunnel test campaign at the US Air Force Academy (USAFA) evaluated an active flow control system designed to provide roll, pitch, and yaw control on a tailless aircraft. The vehicle geometry was derived from the ICE configuration with a 65 degree sweep leading edge and a thickness distribution borrowed from SACCON [4]. The control effectors consist of three pairs of variable-strength air jets exiting from slots parallel to the wing leading and trailing edges (Figure 1-5). The pair of actuators located near the apex primarily provided yaw control. A second pair positioned at the mid-span along the wing leading edge primarily provided side force control, and the third pair of actuators located at the trailing edge primarily provided roll and pitch control. Due to cross-axis coupling, the actuators are required to be operated in combination to produce pure yaw, pitch and roll control outputs. The wind tunnel tests were complemented with high-fidelity numerical simulations. The primary and cross control derivatives were measured as functions of vehicle angle of attack and actuator momentum coefficient.

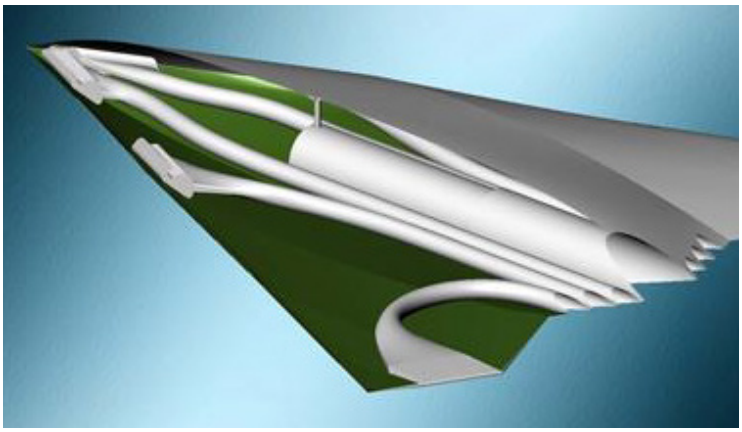

Figure 1-5: USAFA ICE Configuration Showing Internal Plumbing Channels to Flow Control Effectors.

1.5.1.2 Circulation Control and Thrust Vectoring Studies at Manchester University

Research efforts at the University of Manchester, in collaboration with BAE Systems, led to an improved understanding of supersonic wall jets and their attachment and separation behaviours [5]. These concepts were then applied to the development of practical Circulation Control (CC) and Fluidic Thrust Vectoring (FTV) technologies. The research was both experimental and numerical. The experimental efforts informed RANS simulations of CC approaches applied to the SACCON vehicle configuration (Figure 1-1). The supersonic wall jet concept was also used to develop an FTV nozzle (Figure 1-6).

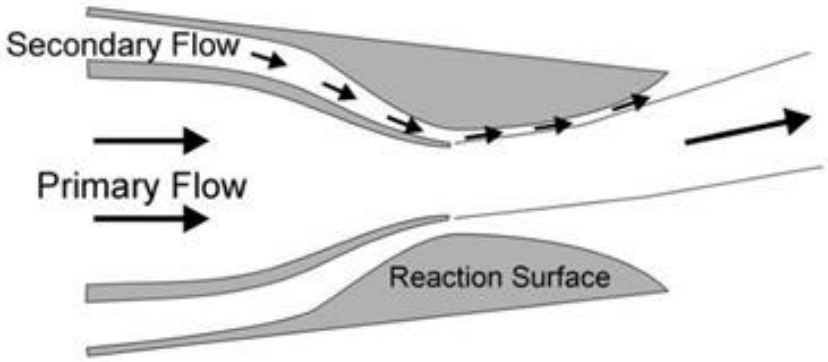

Figure 1-6: Schematic of the Co-Flow Fluidic Thrust Vectoring Scheme.

1.5.1.3 Wind Tunnel Testing at the University of Arizona

A campaign of experimental tests was undertaken to control the non-linear aerodynamic stability behaviours of thin, highly-swept wings at high incidence [6]. The test article was a sub-scale model of the SACCON configuration which has a 53 degree swept leading and trailing edges. At angles of attack above 10 degrees, the configuration exhibits a highly non-linear pitch break behaviour arising from separated flow on the outboard section of the wing. Sweeping jets, with differing distribution densities, were placed at two chordwise locations along the span of the wing: leading edge, and flap/aileron hinge point (Figure 1-7). Flow streamline topologies and extensive parametric studies of the aerodynamic performance were collected and studied.

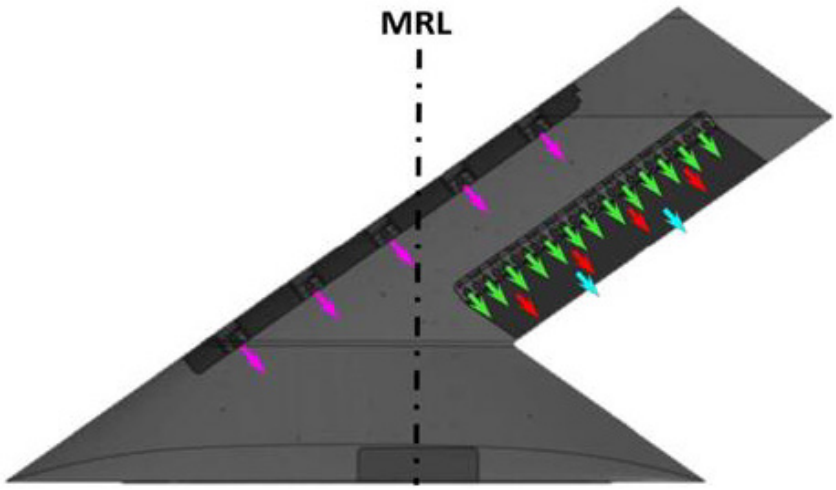

Figure 1-7: Sweeping Jet Actuator Locations on SACCON for the University of Arizona Wind Tunnel Tests.

1.5.2 Vehicle Performance

The Vehicle Performance sub-group assessed the impacts of component level flow control technologies on vehicle mission performance. In coordination with the Trade Study and Requirements sub-group, this team defined figures of merit for evaluating a flow control technology at the vehicle level. As the AFC technologies of interest all required engine bleed air, the figures of merit were based on the average and peak engine bleed demand during the prescribed mission. The average mass flow rate demand giving an estimate of the impact of AFC flight control on engine TSFC and hence range. Component level performance measures (data obtained from the Flow Control Technology sub-group) were integrated into the flight control laws of a 6-DOF MATLAB-based flight simulator.

1.5.2.1 Lockheed Martin ICE Flight Simulations

Using the component level control effector results from the USAFA wind tunnel tests, a flight control model was built for the ICE platform [7]. The control effector data was included as a look-up table, and the control derivatives were computed from these data. A series of 100 ingress mission simulations were then run with this model to provide a statistical estimate of the engine bleed mass flow demand for flight control. In addition to the basic ingress mission profile, these simulations also considered, among other parameters, light and heavy aircraft configurations, and permutations of the gust direction, e.g., streamwise axis only, streamwise + pitch axes.

1.5.2.2 DSTL SACCON Flight Simulation

Using the control effector results provided by the University of Arizona wind tunnel tests and the University of Manchester, a flight control model was built for the SACCON platform [8]. These simulations were run only for the heavy aircraft configuration and assumed trimmed flight without AFC control. An estimate for the mass flow rate demand for re-trimming the aircraft to a light configuration was later added to the control results. Here too, a parametric study of gust direction and length was undertaken.

1.5.3 Trade Study and Requirements

The Trade Study and Requirements sub-group defined the overall requirements for the study, identified the mission profiles for the vehicle performance trials, and conducted the trade studies in which the control technologies were evaluated against the system performance requirements. This evaluation used a Design of Experiments (DOE) Quality Function Deployment (QFD) matrix to give qualitative, relative comparisons with objective metric scoring. The approach is based on the statistical analysis methods of Box et al. [9]. The QFD approach assessed each technology in four areas: performance, integration, ‘-ilities’, and maturity. These four assessment areas including metrics and grading criteria are shown in Table 1-1.

The performance assessment was described briefly above in Section 1.5.2. The outcomes of these assessments have a direct impact on the airframe integration of the AFC technologies by defining, for example, the mass flow rate demand and hence the size of the piping to the control effectors. An AFC system layout for the ICE platform is shown in Figure 1-8. For ease of interpretation and to provide a relative measure of the integration impact on the system design, the integration metrics are expressed in percentages derived by normalizing with conventional control systems weight and volume.

The ‘-ilities’ are metrics that cover a range of non-functional operational and support requirements that are assessed as a part of a cost-benefit analysis of a system. These metrics assess important life cycle requirements that are of interest to the operational community who provide important full life cycle support for a system. Although there is a wide range of ‘-ilities’ metrics, only four were chosen to capture the key non-functional requirements that would be of most interest to a potential system developer.

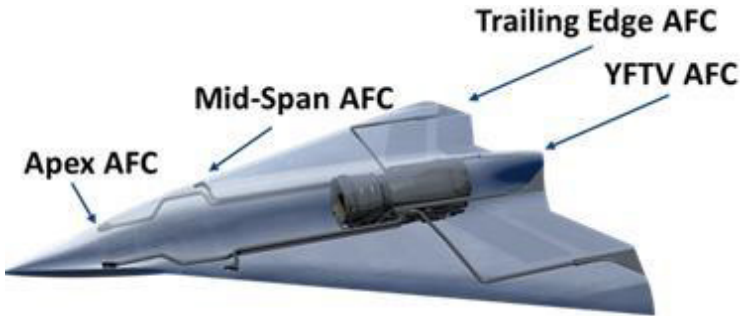

Figure 1-8: AFC System Layout in the ICE Platform for Ingress/Egress.

Table 1-1: Example QFD Assessment Table Showing Metrics, Objectives, and Grading Criteria.

	Metric	Quantity	Objective	Grading Criteria			Wt Factor
				3	2	1	
Maturity	Technology Readiness Level	TRL	Maximize	>5	3,4	<3	3
	Integration Readiness Level	IRL	Maximize	>4	2,3	<2	2
	Manufacturing Readiness Level	MRL	Maximize	>5	2,3,4	<2	1
	Transferability	# Applicable Cross-Deck Platforms	Maximize	>2	2	1	1
Integration	Volumetric Impact	% AFC Volume Impact	Minimize	<70%	70%<x<100%	>100%	3
	Weight Impact	% AFC Weight Impact	Minimize	<90%	90%<x<110%	>110%	3
	Engine Bleed Impact	% AFC Bleed Impact	Minimize	<1%	1%<x<3%	>3%	2
	OML Complexity	% AFC seam length (relaive to conventional)	Minimize	<80%	80%<x<120%	>120%	1
Ilities	Reliability	MTBF per Mil Spec	Maximize	>500	300<x<500	<300	3
	Maintainability & Supportability	Maintainability factor based on Parts Counts, weights Sourcing, Maintenance Access (relative to conventional)	Maximize	<50%	50%<x<100%	>100%	2
	Scalability	Re, M Manufacturability Compared to Spec (proven, not proven but expected, disproved)	Maximize	all proven	2 proven, 1 expected	2 proven, 1 disproved	1
	Affordabilty (Cost Impact)	% Cost (relative to conventional) based on a factor derived from parts count, weight, material, design and manufacturing complexity	Minimize	<50%	50%<x<100%	>110%	1
Performance	Reject light turbulence	Peak flow (10s simulation)	Minimise	<3lb/s	3 < x < 6	>6lb/s	1
	Reject light gust	Peak flow (10s simulation)	Minimise	<3lb/s	4 < x < 6	>6lb/s	2
	Reject moderate gust	Peak flow (10s simulation)	Minimise	<3lb/s	5 < x < 6	>6lb/s	3
	Accommodate trim	Flow to retrim from 90-60% fuel weight	Minimise	<3lb/s	6 < x < 6	>6lb/s	3

The maturity evaluation, or readiness assessment, is a process that assesses the maturity of, and the risk associated with, critical technologies that are under consideration for use in system acquisition programs. The purpose of these assessments is to understand the maturity of the technologies so that the associated risks of using them can be either managed or eliminated. Typically, the readiness assessment focuses on the technology readiness level; that is, the degree to which the technology has been demonstrated in a relevant environment. Here, we will broaden our readiness assessment to include system integration and component manufacturing readiness levels in addition to the technology readiness. A fourth metric assesses the applicability of a particular control effector evaluated on one platform to provide the same control effect on a similar, but different, platform.

1.5.4 Participation by Organization

The sub-group composition and participation is shown in Table 1-2.

1.6 AVT-295 COOPERATIVE DEMONSTRATION OF TECHNOLOGY

Mid-way through the work of the AVT-239 activity, two opportunities arose to demonstrate the innovative control effector technologies on sub-scale air vehicles through a NATO-sponsored Cooperative Demonstration of Technology (CDT). These demonstrations would prove the feasibility of

implementing the novel control technologies and to validate the model-based analysis undertaken within AVT-239. The hope was that the CDT would increase confidence that the technologies could be implemented on a full-scale vehicle, thereby reducing the design compromises imposed by expected future design demands such as low observability, and realizing the potential performance and manoeuvring benefits for future NATO air vehicles.

Table 1-2: AVT-239 Task Group Participants and Contributions.

Organization	Contribution					
	Vehicle		Flow Control Technology		Vehicle	Trade
	SACCON	Hybrid ICE	Experiments	Computations	Performance	Study/Requirements
AFOSR	x	x				x
U. Arizona	x		x			
BAE Systems	x		x	x		x
DLR	x					x
DSTL	x				x	
IIT		x	x			
U. Liverpool	x					
Lockheed	x	x			x	x
U. Manchester	x					
USAFA		x		x		

The aim of the CDT was to integrate pneumatic-based control effectors onto a sub-scale air vehicle with a representative tailless planform and ultimately demonstrate effective flight control, whole or in part, with minimal, or no, conventional control surface input. The CDT used reduced-scale versions of the configurations similar to those studied in the research efforts of AVT-239. The aircraft and the control approaches were developed by two teams, one based in the UK and one in the US. Their testing programmes were separate but complementary in scope.

1.7 CONCLUDING REMARKS

A recent NATO task group has investigated AFC technologies for feasibility and use as the flight control effectors in a next generation tailless aircraft. To make a systematic study of the technologies, the group was organized around three highly-coupled teams, the flow control technology team, the vehicle performance team, and the trade study/requirements team. The flow control team performed component level testing of AFC technologies in wind tunnel and numerical experiments. The aerodynamic performance data from this testing was used by the vehicle performance team to construct a 6-DOF flight control model for a representative tailless aircraft. This representative aircraft, with the new control model, was then ‘flown’ through a one-hour ingress mission that included freestream turbulence and intermittent gusts. The performance demands derived from these simulated mission flights were subsequently used to size a full-scale AFC flight control system for a representative tailless aircraft. In the last task of the group assessment, the trade study team evaluated the full aircraft against integration, ‘-ilities’, and maturity metrics. Although described here as a sequential process, in practice there was close interaction and frequent iteration between the teams.

The assessment process outlined here and discussed in greater detail in the following chapters forms a rigorous framework in which to assess the application of active flow control technologies to aircraft systems. The authors encourage future efforts to embrace the same or a similar process when assessing new AFC technologies.

1.8 ACKNOWLEDGEMENTS

The authors would like to thank BAE Systems, DSTL, and Lockheed Martin Aero for their generous contributions of time and resources without which this effort would not have been possible. The authors would also like to thank the members of the group for their continuous dedication to the effort and unfailing participation in the bi-annual meetings. Finally, the authors gratefully acknowledge the leadership and guidance of Dr. Jonathan Irving who served as a co-chair during the early years of the task group.

1.9 REFERENCES

[1] Cummings, R.M., and Schutte, A. An Integrated Computational/Experimental Approach to UCAV Stability and Control Estimation: Overview of NATO RTO AVT-161. *AIAA Paper 2010-4392, 20*10.

[2] Dorsett, K.M., and Mehl, D.R. WL-TR-96-3043 Innovative Control Effectors (ICE). WPAFB: Wright Laboratory, 1996.

[3] Dorsett, K., Fears, S., and Houlden, H. Innovative Control Effectors (ICE) Phase II. Phase II Final Report, WL-TR-97-3059, 1997.

[4] Williams, D.R., Seidel, J., Osteroos, R., and McLaughlin, T.E. Flight Control Derivatives Using Active Flow Control Effectors on the ICE/SACCON UAS Model. AIAA Paper 2019-0043, AIAA SciTech Forum. San Diego, CA, 2019.

[5] Warsop, C., Forster, M., and Crowther, W.J. Supercritical Coanda Based Circulation Control and Fluidic Thrust Vectoring. AIAA Paper 2019-0044, AIAA SciTech Forum. San Diego, CA, 2019.

[6] Phillips, E., Jentzsch, M., Menge, M., Forster, M., Taubert, L., and Wygnanski, I. On the Use of Active Flow Control to Change the Spanwise Flow on Tailless Aircraft Models, Thus Affecting their Trim and Control. AIAA Paper 2019-0045, AIAA SciTech Forum. San Diego, CA, 2019.

[7] Niestroy, M.A., Williams, D.R., and Seidel, J. Flow Control Simulation of the ICE Aircraft. AIAA Paper 2019-0279, AIAA SciTech Forum. San Diego, CA, 2019.

[8] Hutchin, C. Control Effectiveness and System Sizing Requirements for Integration of Fluidic Flight Controls on the SACCON Aircraft Configuration. AIAA Paper 2019-0280, AIAA SciTech Forum. San Diego, CA, 2019.

[9] Box, G., Hunter, S., and Hunter, W.G. *Statistics for Experimenters: Design, Innovation, and Discovery.* Wiley-Interscience, 2005.

Chapter 2 – APPROACH TO ASSESS PROSPECTS OF ACTIVE FLOW CONTROL ON A NEXT GENERATION AIRCRAFT

Daniel N. Miller
Lockheed Martin Aero
UNITED STATES

David R. Williams
Illinois Institute of Technology
UNITED STATES

Clyde Warsop
BAE Systems Air
UNITED KINGDOM

Douglas R. Smith
USAF European Office of Aerospace
Research and Development
UNITED KINGDOM

2.1 OVERVIEW

A trade study approach is described to evaluate modern flow control technology integrated on a representative future military tailless aircraft configuration. A North Atlantic Treaty Organization technical task group was commissioned to investigate the feasibility of active flow control for providing disturbance rejection during ingress/egress flight conditions. A design of experiments trade study approach is defined to assess the feasibility of employing a suite of active flow control technologies for this application relative to a conventional mechanical flap-based control suite. The trade study approach employs four categorical metric groups (each with four metric parameters) including:

1) Flight control performance;
2) Aircraft integration;
3) Technology 'ilities' including reliability, maintainability, scalability, and affordability; and
4) Technology maturity.

The overall process of the trade study approach is discussed including supporting engineering modeling and simulation, conceptual design, and analyses. Prospects for this approach to support AVT-239 objectives are outlined with initial results described in a companion report.

2.2 INTRODUCTION AND BACKGROUND

Next generation military unmanned aerial system (UAS) aircraft will confront an increasingly contested and more sophisticated threat environment. UAS aircraft will require an unprecedented level of flight performance while simultaneously becoming more affordable. To meet these future challenges, the North Atlantic Treaty Organization (NATO) launched an Applied Vehicle Technology (AVT) technical task group AVT-239 to evaluate and flight test scaled versions of conceptual next generation UAS platforms. These platforms will be equipped with modern Active Flow Control (AFC) technologies that might eliminate the need for complex, moving flight control surfaces which constrain current UAS performance. The goals for the AFC technologies under investigation are to enable reduced weight, size, complexity and cost, with increased availability and agility during enhanced, evasive tactics.

The task group identified two candidate conceptual aircraft platforms to conduct this study: (1) The innovative control effector (a.k.a. ICE) [1], [2]; and (2) The stability and control (a.k.a. SACCON) [3] configurations, both shown in Figure 2-1. The scope of this initial report is confined to the trade study conducted on the ICE platform. The ICE aircraft is an all-wing, tailless configuration that can be manned or unmanned. The aircraft with the baseline conventional control effectors indicated, evolved from 1991 Internal Research And Development (IRAD) studies at Lockheed Martin Aeronautics and was subsequently studied in depth under AFRL sponsorship [1], [2].

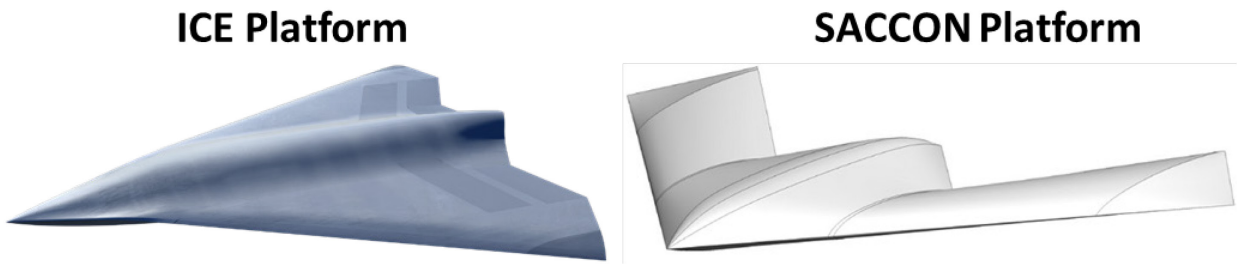

Figure 2-1: ICE and SACCON Tailless Platforms Selected for Investigation.

2.3 NATO AVT-239 TASK GROUP OVERVIEW

New control effector strategies are desired for future UAS configurations. Approaches that minimize 'seams', 'gaps' or moving surfaces have been studied in the past and continue to evolve toward ever improving efficiency and ease of integration. The need to be seamless invokes a very critical characteristic – in general because control power for any one control effector is limited, a suite of control effectors are required to provide all-envelope control of a vehicle. This is true even for a vehicle that only requires mild maneuvering. Control effectors for take-off and landing requirements have particularly difficult integration issues. There are many approaches that involve seamless geometry movement including morphing leading and trailing edges, morphable wings and wing tips, and continuous mould line technology [4].

Likewise there are many AFC approaches to create 'virtual geometry changes' that involve blowing or suction to increase the effectiveness of (or even replace) conventional aerodynamic control surfaces. Successfully implemented AFC technologies have the potential to revolutionize the performance and maneuver characteristics of modern air and maritime platforms. Flow control technologies have a wide range of uses from separation control for improving high alpha performance, to lift augmentation and full 3-axis flight control. However, to date, implementation on production platforms has been limited, often due to the complexity, power requirements and impact on cruise performance [5]. A STO workshop (May 2013, AVT-215, Novel Control Effectors for Military Vehicles) explored innovative control effector technologies including AFC techniques for providing control power. The conclusion of the workshop was that the application of novel AFC technologies to the maneuvering of a future UAS offers the most promising route to raising the Technology Readiness Level (TRL) sufficiently to allow exploitation onto future NATO UAS platforms. The AVT-215 workshop set the stage for the AVT-239 working group study.

NATO AVT-239 was launched to investigate AFC technologies to provide flight control power for next-gen tailless UAS platforms. The AFC technology feasibility would be assessed by assessing their feasibility against platform integration criteria. The goal is to minimize reliance on conventional control surfaces during select portions of the UAS mission profile. Three flight regimes of interest include mission ingress/egress, maneuver, and take-off/landing. For the Phase I of the NATO study, the scope was confined to an ingress/egress mission profile, with tentative plans to address the other two regimes in a subsequent phase. To accomplish this objective, the AVT-239 task group was organized into three sub-groups that to focus on principal topic areas and collaborate together including:

1) Flow Control Technology;
2) Vehicle Performance; and
3) Trade Study/Requirements (see Figure 2-2).

Initial UAS platform requirements were defined by sub-group #3. These requirements were used to direct computational and experimental research being conducted by group #1. The requirements and data resulting from these tasks were used in a flight control simulation under sub-group #2 to conduct vehicle performance

assessments. Details on the AVT-239 organization are provided in a companion paper [6]. This report addresses the trade study approach conducted under sub-group #3.

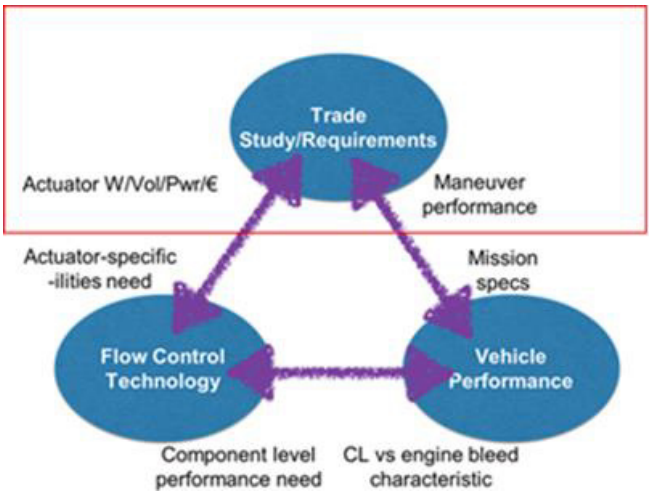

Figure 2-2: NATO AVT-239 Task Group Organization.

2.4 TRADE STUDY APPROACH

2.4.1 Objective

The objective of the trade study is to assess the feasibility of AFC technology for future tailless UAS platform. Consistent with the Phase I trade study, the scope is confined to implementation of an AFC suite on the ICE platform to manage turbulence and gust disturbance rejection and trim for a representative ingress/egress mission. As such, the goal is to provide sufficient control power for this regime at an acceptable 'opportunity cost'. Flight conditions are defined as 30Kft altitude and Mach 0.9 speed across a 1 hour ingress/egress flight duration.

As a basis to evaluate an integrated AFC system, a basic layout and internal arrangement of the ICE platform was updated for this effort. While integration of an AFC system onto a vehicle during the conceptual design phase allows the most flexibility in the arrangement, it is important to understand how the AFC system must integrate with the other interfaces and subsystems on the aircraft at a high level. Figure 2-3 highlights the basic arrangement of the conventional and AFC effector flight control suite for the baseline ICE configuration. The conventional hinged control effector suite includes pitch flaps, elevons leading edge flaps and a spoiler slot deflector.

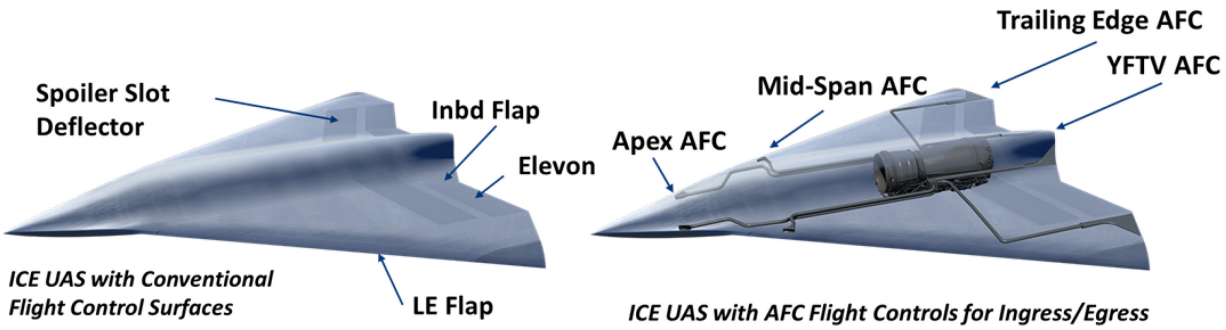

Figure 2-3: ICE with Conventional Control Suite (Left) and AFC Flow Control Suite (Right).

The AFC effector suite includes a bilaterally symmetric installation of control effectors distributed at four principal locations on the aircraft. The control effectors are located along the:

1) Exhaust Nozzle wall to achieve Yaw-plane Fluidic Thrust Vectoring (YFTV);
2) Outboard wing Trailing Edge (TE);
3) Wing Leading Edge (LE) apex; and
4) Wing Leading Edge (LE) mid-span.

The AFC effector suite is distributed to provide multiple options for control power in aircraft pitch, roll, and yaw axes. Each AFC effector is supplied with bleed air extracted from the inter-stage port of a representative modern military turbofan engine. The bleed air is transported to each AFC location via a valve and duct assembly.

The AFC effector suite uses an array of surface-integrated slot-jets at each of the four locations, as shown in Figure 2-4. The AFC suite injects high pressure air that interacts with the boundary or shear layer to modify the local pressure distribution on the aircraft and therefore provide control power. The YFTV AFC creates a virtual aero-surface on the internal nozzle wall that emulates the function of a moving mechanical flap, but with no hinges or variable geometry [7]. The TE AFC modifies the local airfoil circulation and pressure distribution using a tangential wall jet [8]. The LE Apex and Mid-Span AFC similarly modify the local lift distribution along the airfoil [9].

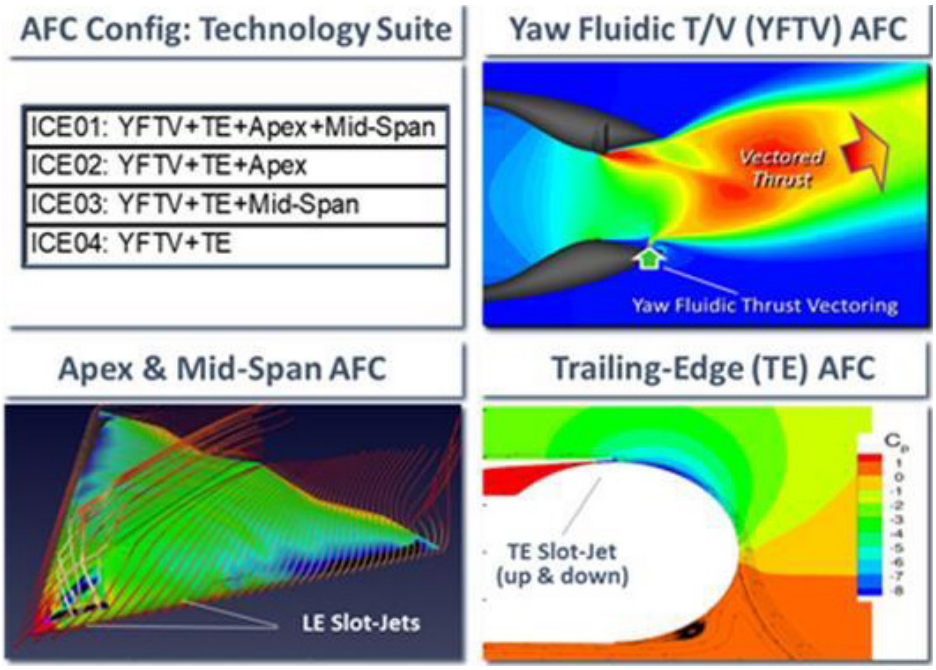

Figure 2-4: ICE AFC Technology Suite and Configurations ICE01-04.

2.4.2 Trade Study Matrix

A relatively simple 'house of quality' or Quality Function Deployment (QFD) experimental design [10] matrix is developed to conduct the trade study, as shown in Figure 2-5. Architecturally, the trade matrix features 4 configuration combinations (dubbed ICE01-04) of the AFC effector suite evaluated on the ICE platform, shown Figure 2-4. The AFC configurations employ the entire suite in ICE01 (forward and rear) and sequentially remove AFC effectors/locations until ICE04 (rear only).

Four groups of trade study metrics each with four Key Performance Parameters (KPPs) are employed to represent the AFC performance and platform integration 'opportunity cost'. Group I (or G-I) measures AFC flight control performance on the ICE platform, G-II measures the integration impacts, G-III measures the so-called 'ilities' impacts, and G-IV measures the technology maturity. The aim of the matrix is to provide a structured tool to compile and compare relative qualitative and quantitative measures of the metric groups/KPPs. Details on the metric groups, their respective KPPs, and the scoring criteria are described below in the subsequent sections.

		G-I: Performance						G-II: Integration						G-III: Ilities				G-IV: Maturity					
		Reject light turbulence Minimize Wbleed% (peak)	Reject light gust Minimize Wbleed% (peak)	Reject moderate gust Minimize Wbleed% (peak)	Accommodate trim Minimize Wbleed% (mean)	Volumetric Impact Minimize VNconventional	Weight Impact Minimize MMconventional	Engine Bleed Impact Minimize Wbleed% (mean)	OML Complexity Minimize LEconventional	Reliability Maximize RRconventional	Maintainability Minimize MMconventional	Scalability Maximize	Affordability Minimize Cost Factor	TRL Maximize	IRL Maximize	MRL Maximize	Transitability Maximize	Totals		
Weighting Factors		3X	1X	3X	2X	3X	3X	2X	1X	3X	2X	1X	1X	3X	1X	2X	1X	Wt Factors		
QFD Matrix																				
Actuator/Location																		Scores	Score %	
ICE01: YFTV+TE+Apex+Mid-Span		1	3	9	1	3	9	1	3	9	1	3	9	1	3	9	1	142	49%	
ICE02: YFTV+TE+Apex		3	9	1	3	9	1	3	9	1	3	9	1	3	9	1	3	114	40%	
ICE03: YFTV+TE+Mid-Span		9	1	3	9	1	3	9	1	3	9	1	3	9	1	3	9	160	56%	
ICE04: YFTV+TE		1	3	9	1	3	9	1	3	9	1	3	9	1	3	9	1	142	49%	

Figure 2-5: QFD Matrix for 4 ICE01-04 Configurations Across 4 Metric Groups (Scores Hypothetical).

2.4.3 Trade Study Process

The QFD process is a powerful technique to make more objective (or at least less subjective) assessments and design decisions. An overview of the QFD trade study process is illustrated in Figure 2-6. Generally, engineering analysis and design is conducted across the four metric groups to define values for the KPPs and their consequent scores that feed into the QFD matrix. Weight factors are defined across the metric groups and KPPs to reflect relative importance in the overall assessment. The trade study results are used to generate KPP response plots (or bar graphs) across the four AFC configurations to permit side-by-side relative comparisons. The resultant KPP scores for each configuration also permit assessment of AFC feasibility against defined criteria.

More specifically, the overall process work flow (Figure 2-6) for the AVT-239 trade study moves from tasks to define data for metric groups G-I to G-IV. A flight control model is developed under the vehicle performance sub-group to define performance characteristics of each AFC effector and combination of effectors on the ICE platform. The flight control model is calibrated with experimental and computational flow control data provided by researchers in the AVT-239 flow control sub-group and the literature (cited prior). Mission simulations are run using this flight control model to define required AFC flow rate profiles that provide the basis data for G-I performance KPPs. The required AFC flow rate profiles are then provided to the trade study sub-group to define the subsequent AFC architecture, component sizing, and design integration into the ICE platform. With the integration concepts completed, the basis data is available for the G-II integration, G-III 'ilities', and G-IV maturity KPPs. A QFD score of 9, 3, or 1 is applied based on predefined grading criteria that are associated respectively with the preferred target value, an acceptable value, or an unacceptable value.

2.4.4 G-I Performance Group

Details of the G-I performance KPPs are provided in Table 2-1. A series of 100 flight control simulations are run on the four AFC configurations and a random turbulent intensity. Prior results have shown that this

approach achieves a near-Gaussian probabilistic distribution of results. The simulation results are processed to compute an ensemble average of the peak bleed air mass flow across a 10 second period of the mission to obtain a representative peak bleed air requirement. Time-averaged mean values of bleed flow are also computed to obtain a representative average. Details of the flight control simulation are provided in a companion paper [11].

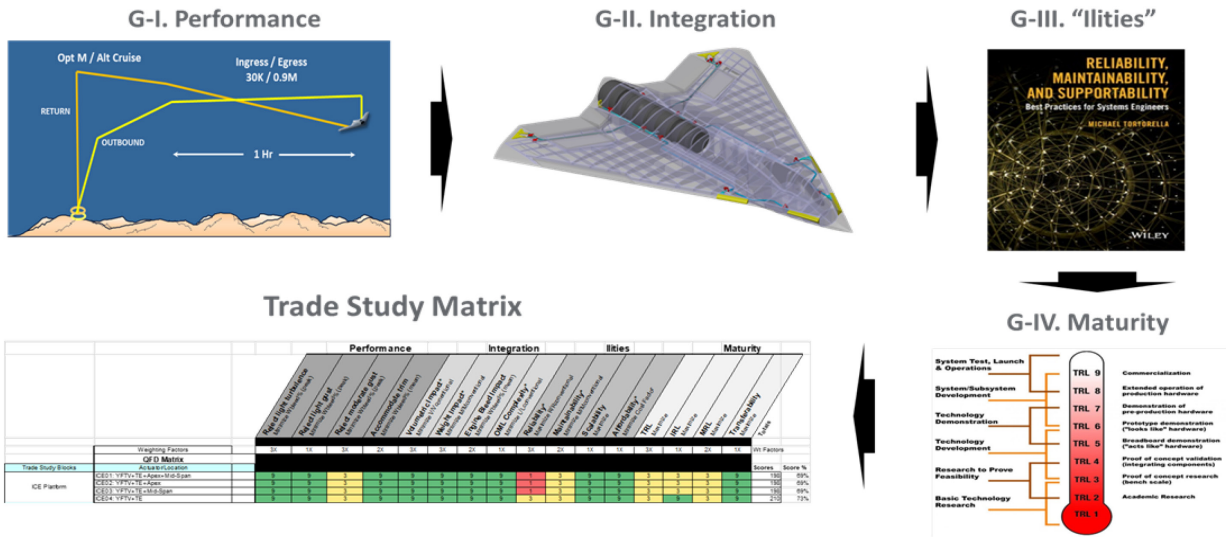

Figure 2-6: Trade Study Process Incorporates Analysis and Design Task Across 4 Groups of Metrics.

Table 2-1: G-I Performance 4 Metric Values Defined by Flight Controls Modeling and Simulation Results.

	Metric	Quantity	Units	Objective	Grading Criteria			Metric Value	QFD Score	Wt Factor
					9	3	1			
PERFORMANCE METRICS (G-I)	Reject light turbulence	Peak flow (10s simulation)	%	Minimize	<2%	2 < x < 4	>4%	TBD	TBD	3
	Reject light gust	Peak flow (10s simulation)	%	Minimize	<2%	2 < x < 4	>4%	TBD	TBD	2
	Reject moderate gust	Peak flow (10s simulation)	%	Minimize	<2%	2 < x < 4	>4%	TBD	TBD	1
	Accommodate trim	Flow to re-trim 90-60% fuel	%	Minimize	<2%	2 < x < 4	>4%	TBD	TBD	1

The four G-I KPPs are measures of a 'cost function' (bleed air flow rate %) required to:

1) Reject light turbulence;
2) Reject light gust;
3) Reject a moderate gust; and
4) Accommodate trim.

The bleed air mass flow rates are normalized by the total engine air mass flow rate to obtain a percent bleed flow ($\%W_{bleed}$). The goal is to minimize the engine bleed percentage since it reduces engine performance and aircraft range. With the KPPs metric values defined, the QFD score is applied using the grading criteria in Table 2-1. For the ICE engine, range is reduced by 2% for each 1% bleed flow extracted. Thus, a bleed air mass flow percentage less than 2% corresponds to a preferred impact of less than 4% range and receives a score of 9. If the bleed air mass flow percentage is greater than 4%, then it has a greater than 8% range reduction, which is unacceptable, and the score is 1.

2.4.5 G-II Integration Group

Details of the G-II integration KPPs are provided in Table 2-2. The required AFC flow rate profiles are obtained from the flight simulations for each AFC configuration. The AFC flow rate requirement is obtained by simulating a 1 hr mission profile with light turbulence and moderate gust superimposed for 1% of the time. The subsequent AFC architecture, component sizing, and design integration is completed for the ICE platform.

The four G-II KPPs are:

1) Volumetric impact (defined as the AFC system volume normalized by the conventional control suite volume);
2) Weight impact (defined as the AFC system weight and normalized by the conventional control suite weight);
3) Engine bleed impact (defined as the mission time-averaged % bleed rate); and
4) Outer Mould Line (OML) complexity (defined as the aggregate width of the AFC slot-jets normalized by the conventional control suite aggregate seam/hinge lengths).

The objective is to minimize all integration KPPs. With the KPPs metric values defined, the QFD score is applied using the grading criteria in Table 2-2. The preferred impact of AFC KPP is defined to be less than 50% and an unacceptable impact greater than 150%.

Table 2-2: G-II Integration 4 Metric Values Defined by Conceptual Design Results.

	Metric	Quantity	Units	Objective	Grading Criteria			Metric Value	QFD Score	Wt Factor
					9	3	1			
INTEGRATIION METRICS (G-II)	Volumetric Impact	%Volume AFC/Conventional	%	Minimize	<50%	50%<x<150%	>150%	TBD	TBD	3
	Weight Impact	%Weight AFC/Conventional	%	Minimize	<50%	50%<x<150%	>150%	TBD	TBD	3
	Engine Bleed Impact	%Flow Bleed/Engine	%	Minimize	<1%	1%<x<2%	>2%	TBD	TBD	2
	OML Complexity	%Seam Length AFC/Conventional	%	Minimize	<50%	50%<x<150%	>150%	TBD	TBD	1

2.4.6 G-III 'Ilities' Group

Details of the G-III 'ilities' KPPs are shown in Figure 2-7 and Table 2-3. The four KPPs are:

1) Reliability (normalized by the conventional control suite value);
2) Maintainability (normalized by the conventional control suite value);
3) Scalability; and
4) Affordability cost impact (normalized by the conventional control suite value).

The KPPs are computed using inputs from the AFC designs in the G-II integration task using the methodologies detailed in Appendix 2-1. The objective is to maximize reliability, minimize the maintainability metric (relates to maintenance hours), maximize scalability, and minimize the affordability metric (relates to cost impact). With the KPPs metric values defined, the QFD score is applied using the grading criteria in Table 2-2. The preferred impact of AFC KPP is less than 50% and unacceptable greater than 150%.

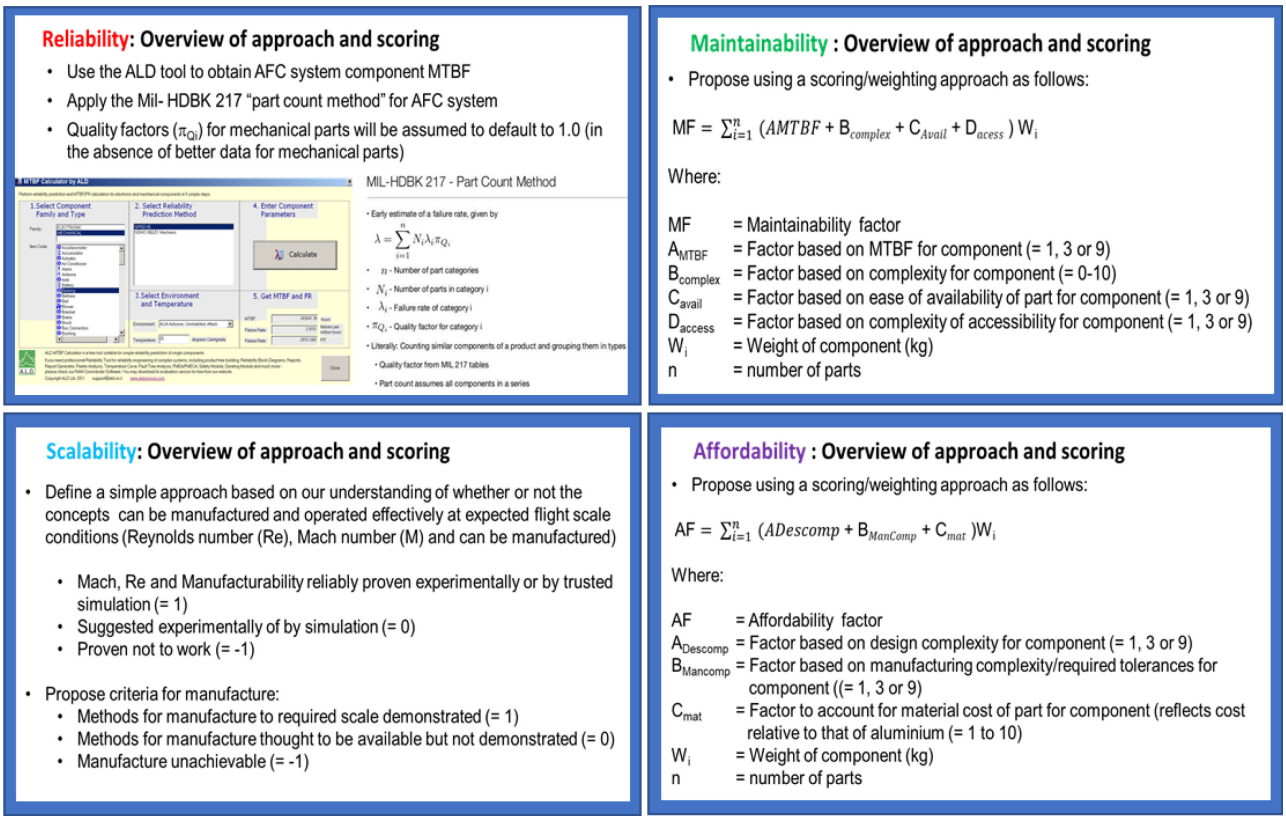

Figure 2-7: G-III 'Ilities' Metric Definitions.

Table 2-3: G-III 'Ilities' 4 Metrics Values Defined by Analysis Using G-II Integration Design.

	Metric	Quantity	Units	Objective	Grading Criteria 9	Grading Criteria 3	Grading Criteria 1	Metric Value	QFD Score	Wt Factor
ILITIES METRICS (G-III)	Reliability	MTBF per Mil Spec (rel. to conventional)	%	Maximize	>150%	150%>x>50%	<50	TBD	TBD	3
	Maintainability	MF per parts, sourcing, parts access (rel. to conventional)	%	Minimize	<50%	50%<x<100%	>150%	TBD	TBD	2
	Scalability	Per Re, Mach, manufacturability (proven, expected, disproved)		Maximize	all proven	2 proven, 1 expected	1+ disproved	TBD	TBD	1
	Affordabilty (Cost)	Per parts, weight, material, complexity (rel. to conventional)	%	Minimize	<50%	50%<x<150%	>150%	TBD	TBD	1

2.4.7 G-IV Maturity Group

Details of the G-IV maturity KPPs are shown in Figure 2-8 and Table 2-4. The four G-IV KPPs are:

1) Technology Readiness Level (TRL);
2) Integration Readiness Level (IRL);
3) Manufacturing Readiness Level (MRL); and
4) Transferability (related to the AFC applicability to platforms based on LE sweep).

The KPPs are assessed using inputs from the AFC designs from the G-II integration task.

The objective is to the maximize maturity in TRL, MRL, and IRL, and utility across different platforms. With the KPPs values defined, the QFD score is applied using the grading criteria in Table 2-4.

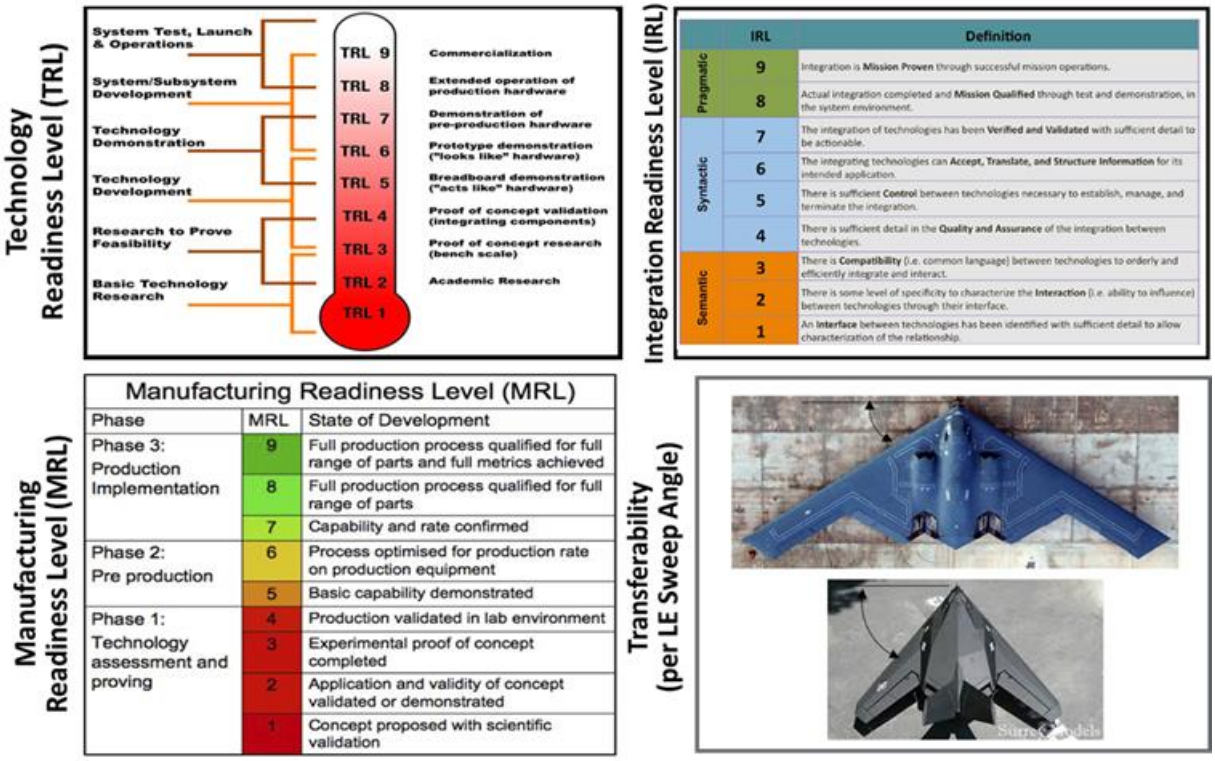

Figure 2-8: G-IV Maturity Metric Definitions.

Table 2-4: G-IV Maturity 4 Metrics Values Defined by Analysis Using G-II Integration Design Results.

	Metric	Quantity	Units	Objective	Grading Criteria			Metric Value	QFD Score	Wt Factor
					9	3	1			
MATURITY METRICS (G-IV)	TRL	DoD TRL	-	Maximize	>5	3,4	<3	TBD	TBD	3
	IRL	DoD IRL	-	Maximize	>4	2,3	<2	TBD	TBD	3
	MRL	DoD MRL	-	Maximize	>5	3,4	<3	TBD	TBD	2
	Transferability	# Applicable Cross-Deck Platforms	-	Maximize	>2	2	1	TBD	TBD	1

2.5 CONCLUSIONS

The trade study approach outlined in this report will be used to assess the feasibility of AFC technology for application to the ICE platform [12]. The approach is based on 16 KPPs that address AFC technology performance, integration, 'ilities', and maturity. Once completed on ICE, the approach can be used on future phases of the NATO AVT-239 task group that will investigate other critical flight regimes and platforms.

2.6 ACKNOWLEDGEMENTS

The authors are indebted to the following supporting contributors from LM Skunk Works to this report including: Dan Baruzzini, Derek Bye, Ken Dorsett, Bryan Guzzardo, Brant Maines, Mike Niestroy, and Andrew Ross, as well as Gary Dale (AFRL), Jurgen Seidel (USAFA), and Chris Hutchins (UK NATO AVT-239 representative).

2.7 REFERENCES

[1] Dorsett, K.M., Mehl, D.R., Innovative Control Effectors (ICE), Phase 1 Final Report, WL-TR-96-3043, January 1996.

[2] Dorsett, K.M., Fears, S.P., Houlden, H.P., Innovative Control Effectors (ICE) Phase II, Phase II Final Report, WL-TR-97-3059, August 1997.

[3] Cummings, R.M., Introduction: SACCON Uninhabited Combat Aerial Vehicle Experimental and Numerical Simulations, *Journal of Aircraft*, Vol. 49, No. 6, November-December 2012.

[4] Wu, C.R., Soutis, C., Zhong, S. and Filippone, A., A Morphing Aerofoil with Highly Controllable Aerodynamic Performance, *The Aeronautical Journal*, Volume 121, Issue 1235, pp. 54-72, January 2017.

[5] Joslin, R.D. and Miller, D.N., *Fundamentals and Applications of Modern Flow Control, Progress in Astronautics and Aeronautics*, 1st edition, AIAA, 2009.

[6] Smith, D.R., and Warsop, C., NATO AVT-239: Innovative Control Effectors for Manoeuvring of Air Vehicles – Introduction and Overview, AIAA Paper 2019-0041, *AIAA SciTech Conference*, January 2019.

[7] Miller, D.N. and McCallum, B.N., Prospects for Fluidic Thrust Vectoring Technology on a Next-Generation Air Vehicle, *NATO STO Workshop*, Session 4, Paper #10, May 2013.

[8] Hoholis, M.G., Steijl, R., and Badcock, K., Circulation Control as a Roll Effector for Unmanned Combat Aerial Vehicles, *Journal of Aircraft*, Vol. 53, No. 6, November-December 2016.

[9] Williams, D.R. and Seidel, J., Crossed-Actuation AFC for Lateral-Directional Control of an ICE-101/Saccon UCAV, *AIAA 2016-3167, 8th Annual Flow Control Conference*, 2016.

[10] Box, G.E.P., Hunter, W.G., Hunter, J.S., *Statistics for Experimenters*, Wiley, 1978.

[11] Niestroy, M.A., Williams, D, and Seidel, J., NATO AVT-239 Task Group: Flow Control Simulation of the Tailless ICE Aircraft, AIAA Paper 2019- 0279, *AIAA SciTech Conference*, January 2019.

[12] Miller, D.N., Maines, B.H., Niestroy, M.A., Williams, D., Warsop, C., Smith, D.R., NATO AVT-239 Task Group: Results to Assess Prospects of Active Flow Control on a Next-Gen Tailless Aircraft, AIAA Paper 2019-0281, *AIAA SciTech Conference*, January 2019.

Appendix 2-1: 'ILITIES'APPROACH TO ASSESSMENT AND SCORING

2A1.1 INTRODUCTION

The 'ilities' are a group of metrics that cover a range of non-functional operational and support requirements that need to be assessed as part of a cost-benefit analysis of a system. The 'ilities' are a way for customer needs to be captured by the systems engineer early in the development lifecycle. They are properties of the system that are important to customers and other stakeholders and are not necessarily specific requirements of the system. Each 'ility' is likely to have a different level of importance to each stakeholder and a system developer often needs to produce a solution that balances all stakeholder interests. In practice there are a wide range of 'ilities' that a development programme must assess (e.g., vulnerability, affordability, availability, affordability, reliability, supportability, maintainability, scalability, adaptability, usability, security, safety, etc.). Within the scope of the present study a small subset of the possible 'ilities' was chosen to represent the key non-functional requirements a potential developer or customer of a fluidic controlled air platform might consider important. Namely:

- Reliability;
- Maintainability;
- Scalability; and
- Affordability.

'Safety' was an additional 'ility' that was originally considered at the outset of the study. However, it was assessed as being too difficult to evaluate in any tractable and meaningful way. Instead it was considered better to design in failsafe/redundancy within the fluidic system in order to achieve similar levels for both a conventionally controlled aircraft and one with fluidic systems and have this impact weight, cost, reliability, etc. The current focus of this study was to explore the use of fluidic flight control systems as supplementary to conventional control surfaces to achieve lower signature levels during an ingress mission. Therefore, failure of the fluidic controls could be tolerated through the ability to revert to the conventional control effectors in case of emergency, albeit with potential implications for mission success.

Each of the four 'ilities' considered in this study was assessed for the two baseline aircraft configurations using approaches that were developed to capture the preliminary nature of design maturity at this stage. The methodologies used are therefore based on the simplistic preliminary design level information available but provide a consistent approach to their application that is suitable for a QFD analysis of this type.

The measures and grading criteria applied for each of the 'ilities' are presented in Table 2A1-1.

The control surface sizing for both the ICE and MULDICON configurations together with the 'ilities' grading criteria and the assessment methodology are described in the sections below.

2A1.2 SYSTEM COMPONENT AND MASS BREAKDOWN

The quantification of the 'ilities' in this study (see subsequent sections) was based on breakdowns of the AFC systems into a number of subcomponents to which quantifiable attributes could be assigned. A similar level of component breakdown was also undertaken for the 'equivalent' conventional control system in the aircraft.

Table 2A1-1: The 'Ilities' Grading Criteria.

				Grading Criteria		
Metric	**Quantity**	**Units**		**9**	**3**	**1**
Reliability	**MTBF** per Mil Spec	hrs	Maximize	>500	300< x <500	<300
Maintainability and Supportability	**Maintainability factor** based on Parts Counts, weights, Sourcing, Maintenance Access (relative to conventional)	%	Minimize	<70%	70%≤x≤130%	>130%
Scalability	**Re, Mach, Manufacturability.** Compared to Spec (proven, not proven but expected, disproved)			all proven	2 proven, 1 expected	2 proven 1 unproved
Affordability (Cost Impact)	**% Cost** (relative to conventional) based on a factor derived from parts count, weight, material, design and manufacturing complexity	%	Minimize	<70%	70%≤x≤130%	>130%

The component breakdown for the AFC system was to the level of individual ducts, joints, supports, bellows, gimbals, control valves and nozzles. Each AFC valve was further broken down into subcomponents (control signals, electrical power supply, electrical controller/inverter, motor windings, motor bearings, motor gearbox, sleeve valve) assuming dual lane redundancy up to and including the motor windings (single motor/gearbox/sleeve valve with fault tolerant architecture (see subsequent section for details).

The component breakdown for the conventional flight control system was to the level of individual control surfaces, hinges and actuators. The conventional flight control surface actuators were assumed to be Electro Hydraulic Actuators (EHAs) having quad channel, dual redundant architecture with Analogue voting (see subsequent section for details).

System subcomponent masses for the AFC systems were derived from the outputs of the system integration and sizing study (See Chapter 6).

System subcomponent masses for the 'equivalent' conventional control surface systems were estimated using the following process.

2A1.2.1 ICE Configuration

A mass estimate of 1500 lb for the complete conventional control surface system for the ICE configuration was available (structure, power supplies, bearings, supports, actuators for the pitch flaps, elevons, tip flaps and slot-spoiler deflectors). This mass compared to an estimate of 1136 lb obtained using the conceptual design methodology of Raymer (equation 15.17) [2A1-1] based on design Mach number (0.8), total planform surface area of the control surfaces (146 ft^2) and total number of control surfaces (8). The total control system mass was then distributed among individual control surfaces in proportion to their individual

projected planform area. In the absence of better data the mass of the actuators for each control surface was then estimated as a proportion of the total mass allocated to each control surface derived based on a factor derived from public domain data available for the F35 JSF rudder (actuator mass = 42 kg surface area estimated as $16m^2$). The residual mass allocated to each flight control was then distributed between the flight control surfaces themselves, their bearings and support structures. The estimated subcomponent mass breakdown for the ICE conventional control systems is presented in Table 2A1-2.

Table 2A1-2: Estimated Mass Breakdown for Conventional Control System on ICE Configuration (Values are for Both Port and Starboard Controls).

Component	Pitch flap	Elevon	Tip flap	Spoiler Slot Deflector
Projected Planform Area (Ft2) (Port + Starboard)	7.7	22.77	19.89	22.7
Total Control System Mass (lb)	79.0	233.7	204.2	233
Mass of EHA Actuators (lb)	44.6	131.8	115.1	131.4
Mass of Control Surface Structure (lb)	31.0	91.8	80.2	91.5
Mass of Hinge Bearings (lb)	3.5	10.2	8.9	10.2

2A1.2.2 MULDICON Configuration

Due to a lack of better design data and for consistency of the 'ilities'; evaluation a mass estimate of the conventional control surface system for MULDICON was obtained based on scaling parameters derived from the mass breakdown for the ICE configuration. This was considered acceptable since both aircraft are of a similar size and operate at similar flight conditions. Firstly the conceptual design method of Raymer (Equation 15.17) (2A1-1) was used to estimate the control system mass based on control surface projected areas, flight Mach no., etc. The value obtained was then factored by 1.32 which is the ratio of the calculated control system mass for ICE to the estimate derived from the Raymer method. The overall mass of the conventional control surface system on MULDICON was 1021 lb. This was distributed and proportioned to individual control surface components based on projected control surface planform area using an identical approach to that used for ICE. The estimated subcomponent mass breakdown for the MULDICON conventional control systems is presented in Table 2A1-3.

2A1.3 RELIABILITY

Reliability has been graded according to the expected Mean Time Between Failure (MTBF) estimated for the system. Conventional flight control systems on combat aircraft are designed to be fault tolerant and highly redundant in order to ensure high levels of safety and mission success. These control systems typically have to meet the requirements of MIL-F-9490 Probability of Loss of Control (PLOC), MIL-F-9490 Probability of Mission Abort (PMA), and MIL-STD 882B Fail-Operational/Fail-Operational redundancy requirements. In achieving these requirements military combat aircraft with conventional controls typically exhibit a MTBF of components within their flight control systems of approximately 750-1000 hrs. System redundancy and architecture design means that these failures rarely result in mission abort ($<10^{-5}$ per mission) or loss of control ($<10^{-7}$) [2A1-2]. Based on these figures for conventional control systems and on the acceptance that the fluidic control systems simply augmented the conventional control systems in the aircraft it was considered possible for an MTBF between 300 and 500 hrs to be acceptable (QFD score = 3). An MTBF below 300 hrs would be considered poor (QFD score = 1) and a value above 500 hrs good (QFD score = 9).

Table 2A1-3: Estimated Mass Breakdown for Conventional Control System on MULDICON Configuration (Values are for Both Port and Starboard Controls).

Component	Inboard Elevons	Outboard Elevons	Yaw Spoiler
Projected Planform Area (Ft2) (Port + Starboard)	32.2	32.2	24
Total control system mass (lb)	186	186	138.5
Mass of EHA Actuators (lb)	93.3	93.3	69.4
Mass of Control surface structure (lb)	83.5	83.5	62.1
Mass of Hinge Bearings (lb)	9.3	9.3	6.9

In this study MTBF has been calculated using an approach based on the MIL-HDBK 217 "part count method" for a complete system where the failure rate (λ) is defined by the expression:

$$\lambda = \sum_{i=1}^{n} N_i \lambda_i \pi Q_i \qquad (2A1\text{-}1)$$

where:

n = Number of part categories in the system

N = Number of parts in category i

λ_i = Failure rate of category i

πQ_i = Quality factor of category i

In this study the Quality factors (π_{Qi}) for mechanical parts were assumed to default to a value of 1.0 (in the absence of better data). To apply the above approach both the conventional and fluidic flight control systems in both the ICE and MULDICON configurations were broken down into their separate individual components to the level of fidelity defined in Table 2A1-4.

MTBF values for each system component were derived from a number of sources [2A1-3], [2A1-4], [2A1-5] and [2A1-6] (as defined in Table 2A1-4. Where possible representative values for military aerospace application were chosen. The impact of operation of fluidic systems components at elevated temperature (nominally 440 °F) was also accounted for where possible.

Since it was expected that the performance of the active flow control valves would be dominant in determining the overall system failure rate, each valve was broken down into its key subcomponents in order to calculate its overall MTBF. For consistency, similar architectures were adopted for the actuators used to control the AFC valves and those used for the conventional controls. The baseline architecture for the actuators was based on the assumption that the conventional control system would employ Electro Hydraulic Actuators (EHAs) (as typified by the actuators used on the F35 Joint Strike Fighter) rather than a more traditional piped hydraulic system (Figure 2A1-1). The assumed architecture for the conventional control surface actuators was 'Quad channel, dual redundant electrohydraulic actuators with Analogue voting'. This concept was determined by Sadeghi and Lyons [2A1-2] as being one of the most optimal to meet MIL Standard probability of mission abort and loss of control requirements whilst minimizing a cost parameter based on failure rate and system mass (Figure 2A1-2).

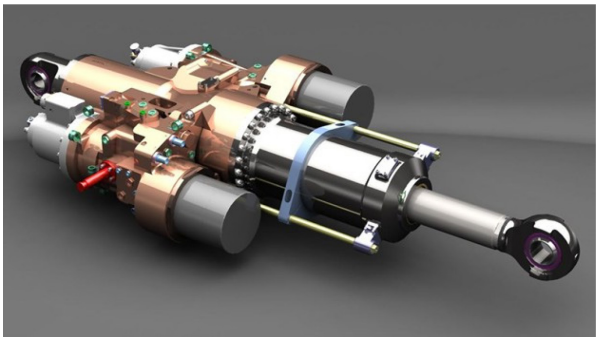

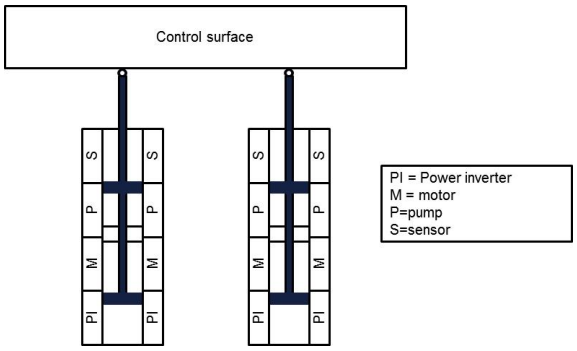

(a) Typical Dual Architecture EHA (MOOG). (b) Schematic Dual Tandem EHA Architecture.

Figure 2A1-1: Dual-Tandem EHA.

Table 2A1-4: Assumed MTBF for Control System Components.

Component	MTBF (hrs)	Source
Duct	750638	NSWC-11 Mechanic (tubing) [2A1-3]
Duct joint	375319	NSWC-11 Mechanic (tubing) [2A1-3]
Duct insulation	16339869	NPRD-95 [2A1-4]
Duct bellows	375319	NPRD-95 [2A1-4]
Duct support	555555566	NPRD-95 [2A1-4]
Duct gimbal	375319	NPRD-95 [2A1-4]
Engine bleed off-take port/valve	22350	Derived from [2A1-5]
AFC sleeve valve	161168	NPRD-95 [2A1-4]
Actuator nozzle	750638	NSWC-98/LE1 Mechanic (tubing) [2A1-3]
Electrical control signals to motor	76923	Derived from [2A1-5]
Electrical power supply	18519	Derived from [2A1-5]
Electric controller/inverter	11696	Derived from [2A1-5]
Motor windings	72463768	Derived from [2A1-5]
Motor bearings	1515152	Derived from [2A1-5]
Motor gearbox	151515	Derived from [2A1-5]
Actuator mechanism (EMA actuator drive)	666667	Derived from [2A1-5]
Conventional Control surface hinge bearing	108771	NSWC-11 Mechanic [2A1-3]
Conventional Control surface structure	76300000	NPRD-95 based on generic value for a structural shaft [2A1-4]

Similar actuator system architecture was assumed for the electromechanical AFC valves. However, unlike for a single hydraulic end effector which will still operate in the case that one of the hydraulic supply

systems jams the direct mechanical link between the AFC valve sleeve and a drive motor means that independent motors cannot be used to operate the valve in redundant mode (if one motor jams the entire system will be jammed). Thus the architecture of the best achievable electromechanical valve system that can be achieved is depicted in the fault tree architecture of Figure 2A1-2. In this case the electromechanical valve can be described as dual lane fault tolerant with redundancy up to the point of the motor windings. Effectively the valve sleeve is driven through a single gearbox by a single motor that incorporates dual redundant windings, power supplies and signalling. The AFC valve architecture therefore achieves a loss of valve output probability of $8x10^{-6}$ which meets the MIL-F-9490 Probability of Mission Abort (PMA) requirement ($<10^{-5}$) but not the MIL-F-9490 Probability of Loss of Control (PLOC) requirement ($<10^{-7}$). This would probably be satisfactory for an AFC system that augments a conventional control system although a fully AFC aircraft would require revision of the AFC valve architecture with additional redundancy to meet PLOC requirements.

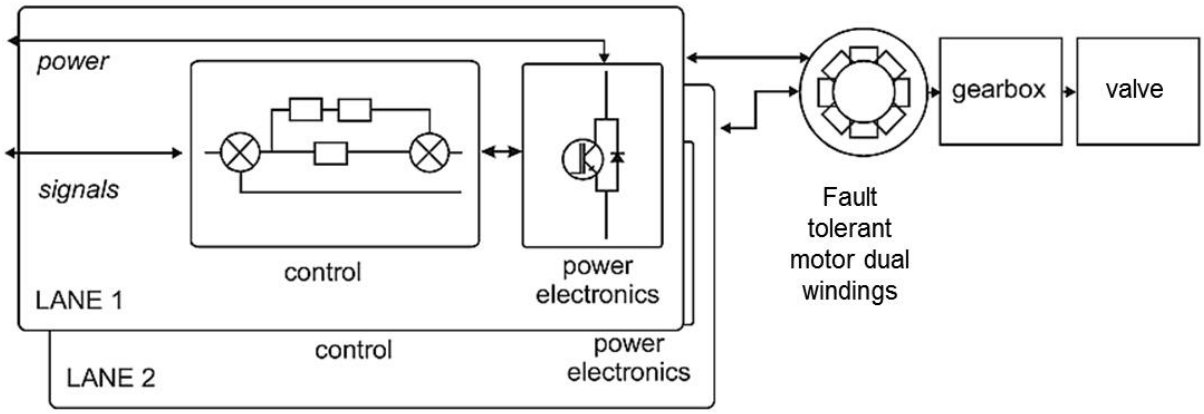

(a) Dual Lane Fault Tolerant AFC Valve Architecture.

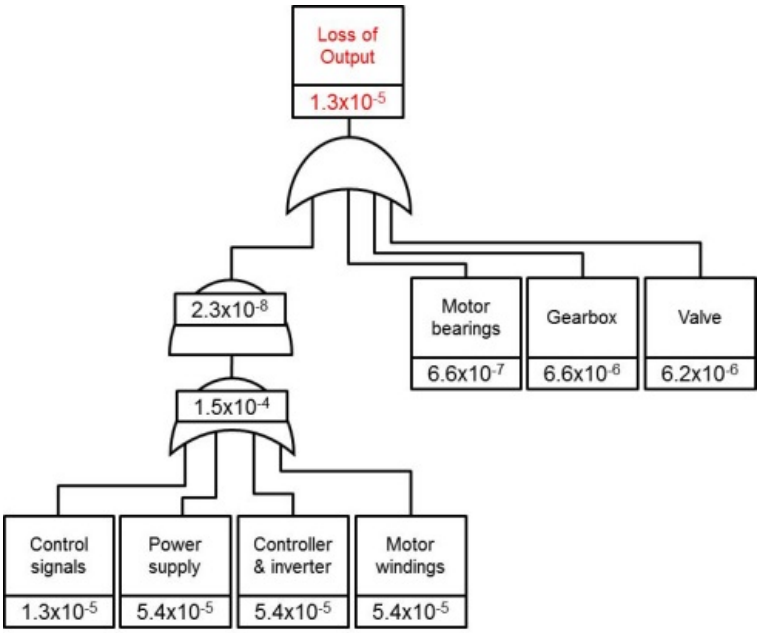

(b) Fault Tree with Failure Probabilities per Flight Hour.

Figure 2A1-2: Architecture for a Dual Lane Fault Tolerant EMA AFC Valve.

MTBF was calculated using Equation (2A1-1) and the data in Table 2A1-4 for each of the AFC and conventional control surface architectures on both the SACCON and MULDICON configurations.

2A1.4 MAINTAINABILITY

Maintainability has been graded according to a Maintainability Ratio defined as:

$$\text{Maintainability Ratio } M_r = \frac{MF_{Fluidic}}{MF_{Conventional)}} \tag{2A1-2}$$

where:

M_r = Maintainability Ratio.

$MF_{Fluidic}$ = Maintainability Factor for the complete AFC system on the aircraft.

$MF_{Conventional}$ = Maintainability Factor for the complete conventional control system on the aircraft.

For each of the fluidic and conventional control systems the Maintainability Factor is defined as:

$$\text{Maintainability Factor } MF = \sum_{i=1}^{n} \left(A_{MTBF} + B_{complex} + C_{avail} + D_{access}\right) w_i \tag{2A1-3}$$

where:

A_{MTBF} = Factor based on MTBF for the component (see Table 2A1-5).

$B_{complex}$ = Factor based on design and manufacturing complexity of the component based on judgement (an integer between 1 and 10).

C_{avail} = Factor based on likely availability of the component (see Table 2A1-6).

D_{access} = Factor based on accessibility of the component for maintenance (see Table 2A1-7).

The Maintainability Factor for each control system is therefore a number that is proportional to the weight (cost) of its constituent parts and factored according to how often they need to be replaced, how complex they are and how easy they are to procure and install which is then normalized by the total system weight. The choice of values for the factors; A_{MTBF}, $B_{complex}$, C_{avail} and D_{access} were determined using engineering judgement by a trial and error approach. The key here was the adoption of a realistic and consistent approach to the definition and application of the values for both the AFC and conventional control systems. The final values used for these factors are based on the QFD approach of penalising 'poor' and accentuating 'good' (Table 2A1-5, Table 2A1-6 and Table 2A1-7). Maintainability Ratio is a measure of the maintainability 'cost' for the system.

Table 2A1-5: MTBF Factor Used for Estimating Maintainability.

MTBF of Component (hrs)	A_{MTBF}
MTBF>5000	1
1000≤MTBF≤5000	3
MTBF<1000	9

Table 2A1-6: Availability Factor Used for Estimating Maintainability.

Availability of Component	C_{avail}
COTS or line spare	1
Short lead time item (≤ 3 months)	3
Long lead time item (> 3 months)	9

Table 2A1-7: Accessibility Factor Used for Estimating Maintainability.

Availability of Component	D_{access}
COTS or line spare	1
Short lead time item (≤ 3 months)	3
Long lead time item (> 3 months)	9

2A1.5 SCALABILITY

A simple approach to grading was adopted based on an understanding of whether or not the concepts can be manufactured and operated effectively at expected flight scale conditions (Reynolds number (Re) and Mach number (M)) and can be manufactured.

Firstly, a numeric value was applied for each of the scalability parameters for AFC concept as follows:

Criteria for Re and M:

- Reliably proven experimentally or by well validated simulation (= 1).
- Suggested experimentally of by simulation (= 0).
- Proven not to work (= -1).

Criteria for manufacture:

- Methods for manufacture to required scale demonstrated (= 1).
- Methods for manufacture thought to be available but not demonstrated (= 0).
- Manufacture unachievable (= -1).

The following approach was then used to determine the final QFD scoring:

- QFD score of 9 if Re, M and manufacturing all score 1.
- QFD score of 3 if 2 out of 3 scalability parameters score 1 and the other scores 0.
- QFD score of 1 if more than two out of 3 scalability parameters score less than 1 or if any score -1.

2A1.6 AFFORDABILITY

Affordability has been graded according to an Affordability Ratio defined as:

$$\text{Affordability Ratio } A_r = \frac{AF_{Fluidic}}{AF_{Conventional)}} \qquad \text{(2A1-4)}$$

where:

A_r = Affordability ratio.

$AF_{fluidic}$ = Affordability Factor for the complete AFC system on the aircraft.

$AF_{Conventional}$ = Affordability Factor for the complete conventional control system on the aircraft.

For each of the fluidic and conventional control systems the Affordability Factor is defined as:

$$\text{Affordability factor } AF = \sum_{i=1}^{n} \left(A_{Descomp} + B_{mancomp} + C_{mat}\right)w_i \quad \text{(2A1-5)}$$

where:

$B_{complex}$ = Factor based on design and manufacturing complexity of the component based on judgement (an integer between 1 and 10).

$A_{descomp}$ = Factor based on based on design complexity for component Integer between 1 (simple component) and 10 (complex component with multiple parts) assigned using engineering judgement).

$B_{mancomp}$ = Factor based on manufacturing complexity/required tolerances for component Integer between 1 (simple processes) and 10 (complex processes) assigned using engineering judgement).

C_{mat} = Factor to account for material cost of part (reflects cost per unit mass relative to that of aluminium) (see Table 2A1-8).

The Affordability Factor for each control system is therefore a number that is proportional to the weight (cost) of parts factored according to what they are made of, how complex they are in design and manufacture. The choice of values for the factors; $A_{descomp}$, $B_{mancomp}$ and C_{mat} were determined using engineering judgement. The key here was the adoption of a realistic and consistent approach to the definition and application of the values for both the AFC and conventional control systems. The final values used for these factors are based on the QFD approach of penalising 'poor' and accentuating 'good'.

Table 2A1-8: Material Factor Used for Estimating Affordability.

Primary Material of Component	C_{mat}
Aluminium alloy	1
Electronics	1
Steel alloy	2
Titanium/Inconel	8
Carbon composite	10
Complex electromechanical/electrohydraulic	10

2A1.7 REFERENCES

[2A1-1] Raymer, D., *Aircraft Design: A Conceptual Approach*, AIAA, Washington DC.

[2A1-2] Sadeghi, T., and Lyons, A., Fault Tolerant EHA Architectures, IEEE AES Systems Magazine, March 1992, pp. 32-42.

[2A1-3] *Handbook of Reliability Prediction Procedures for Mechanical Equipment*, Naval Surface Warfare Centre, Bethesda, May 2011.

[2A1-4] *Nonelectronic Parts Reliability Data*, Quanterion Solutions Incorporated, 1995.

[2A1-5] Bennett, J.W., Fault Tolerant Electromechanical Actuators for Aircraft, PhD Thesis, Newcastle University School of Electrical, Electronic and Computer Engineering, 2010.

[2A1-6] Fitzpatrick, M., and Paasch, R., Analytical Method for the Prediction of Reliability and Maintainability Based Life-Cycle Labor Costs, *J. Mech. Des*, Vol. 121 No. 4, Dec 01, 1999, pp. 606-613. doi:10.1115/1.2829506.

Appendix 2-2: READINESS ASSESSMENT DESCRIPTION

2A2.1 INTRODUCTION

A Readiness Assessment (RA) is a process that assesses the maturity of, and the risk associated with, critical technologies that are under consideration for use in a major defence acquisition program. The purpose of these assessments is to understand the maturity of the technologies so that the associated risks of using them can be either managed or eliminated. In an actual acquisition program, these assessments would be completed in the Technology Development (TD) Phase of the program – this is the second phase of the system life cycle and comes after the Materiel Solution Analysis (MSA) phase where candidate technologies would have been identified. For critical technologies, a minimum readiness level would need to be demonstrated prior to the inclusion of the technology in the next phase, the Engineering and Manufacturing Development phase.

Typically, the readiness assessment focuses on the technology readiness level; that is, the degree to which the technology has been demonstrated in a relevant environment. Here, we broaden our readiness assessment to also include system integration and component manufacturing readiness levels.

In doing this assessment, we are looking for a technology that is effective and mature with a stable implementation design and readily manufactured.

From the perspective of the system acquisition lifecycle, we assume that the MSA phase has identified fluidic-based control effectors as a candidate technology to provide the desired flight control capability in the aircraft. As a next step, the tasks of the AVT-239 group have been to consider this set of novel aerodynamic effectors, measure their performance in modifying the aerodynamic forces and moments on the two baseline aircraft configurations, determine if the aerodynamic performance changes are sufficient to control the aircraft during an ingress/cruise mission with prescribed gust rejection requirements, and pass an assessment on the system performance readiness for consideration in system acquisition.

In using the defence acquisition life cycle system as a basis for our analysis, we are also defining a baseline framework for assessing all ‘flow control’ technologies, past and future, as candidate technologies for insertion into system development programs.

2A2.2 ACTIVE FLOW CONTROL TECHNOLOGY DESCRIPTION

This readiness assessment considers the development of a new flight control system that can be used to minimize, or eliminate, the use of conventional, deflecting control surfaces during certain mission segments where conventional control compromises overall aircraft system performance.

The new control systems were evaluated on two baseline aircraft configurations, ICE and SACCON. For each of these baseline configurations, different control systems were evaluated and a readiness assessment was made for each aircraft configuration. The full control system was comprised of distinct control effector technologies that were tested in isolation before assembly in to the complete system. Non-linear interactions between two or more effectors were not considered.

The ICE platform combines the planform of the original ICE vehicle which has a 65 deg swept LE with the thickness distribution along the span that follows the SACCON distribution (Figure 2-1). Steady air jets issued from slot actuators located at three positions on the vehicle: near the apex, near the wing LE and midway along span, and along the TE of the wing. At the first two locations, the jets issued from slots that directed the flow along the surface rather than vertically in to the cross-flow. The TE actuators were used for circulation control of the local wing section. A fluidic thrust vectoring nozzle was assumed to be integrated in to the engine nozzle exit, providing yaw and pitch control.

The SACCON platform is a representative UCAV configuration with a 53 deg swept LE and similarly swept TEs as shown in Figure 2-1. Here, steady blowing at the wing TE and along a segment of the span provided circulation control. Sweeping jet actuators were deployed along the LE and at the flap hinge line along the outboard span of the wing. Steady blowing, in the form of a wall jet, was used in the engine nozzle exit to perform fluidic thrust vectoring for pitch and yaw control.

The high pressure air supply needed to drive the pneumatic flight control technologies was provided by engine compressor bleed; alternative air sources, independent of engine bleed, were not considered, nor was on-board storage either as an accumulator or as an on-demand compressed air supply.

Based on preliminary layout designs, these pneumatic systems were assembled from COTS components including Inconel tubing with insulation, bleed air control valves, and bellows with high-temperature couplings. The effector nozzles are custom fabrications requiring ‘precise’ manufacturing to ensure the expected performance characteristics.

2A2.3 TECHNOLOGY RISKS SUMMARY AND READINESS ASSESSMENT

This section describes how the readiness assessment was made including the metrics used in the assessment, how these metrics were evaluated, and how the evaluated technologies were identified.

The readiness assessments for the new flight control systems will include three metrics: TRL, IRL, MRL. Readiness assessment used industry established standards for determining readiness level.

2A2.3.1 Technology Readiness Level (TRL)

The technology readiness assessment is made using the TRL metric. TRL has a long history going back to the 1980s at NASA, and the DoD acquisition process has largely adopted this technology readiness metric. This metric assesses how mature a technology is in terms of its capability to achieve a desired effect on a full-scale system under operational conditions. Figure 2-8 shows the TRL level, definition and description of the requirement to attain the readiness level. The assessment was made using a combination of test results from teams participating in the NATO group activity, and SME knowledge of prior work with the same or similar technology elements.

2A2.3.2 Integration Readiness Level (IRL)

The integration readiness assessment looked at the interoperability of discrete technologies within the entire flight control systems. This assessment used the IRL metric (Figure 2-8). Here we are evaluating the interaction and integration of AFC technologies for effecting flight control with some general awareness that there is an interface with the aircraft engine. In light of the resource-constrained control effector testing, very limited information was available about the interactions between different effector systems, between the pneumatic control system and a conventional control system, and between the pneumatic control system and the engine providing the bleed air. There has been no study of the individual technologies operating on the same vehicle at the same time. We have assumed that control effectiveness is simply a super-position of the individual effects. Transient effects have not been considered, and whilst these will have a very limited effect on the aerodynamic performance, there may be a more significant effect on the engine arising from fluctuating bleed demands.

2A2.3.3 Manufacturing Readiness Level (MRL)

The manufacturing readiness assessment is intended to manage risks prior to the phases of manufacturing development and low-rate initial production. The assessment helps to enable a design for producibility; to

develop affordable and executable manufacturing processes; and to ensure affordability and operational supportability. An assessment of manufacturing readiness also supports system integration, interoperability, safety, and utility goals. This assessment used the MRL metric (Figure 2-8).

Broadly speaking, manufacturing readiness is the ability to harness the manufacturing, production, quality assurance, and industrial functions to achieve an operational capability from the original technology concept. Manufacturing Readiness Levels (MRLs) are designed to be measures used to assess the maturity of a given technology from a manufacturing prospective and provide perspective on the level of manufacturing risk associated with the other maturity metrics and system level uncertainties. Relevant considerations for assessing MRL include the technology base maturity (TRL), challenges associated with scaling up production, design maturity and % of design that is new, design stability, use of COTS, dual-use of technology components, and the industrial capacity to produce components that may require specialized fabrication.

The installed pneumatic flight control systems are composed primarily of COTS components with only a few custom fabricated parts. These systems should be straightforward to assemble and require few parts with limited capacity constraints. For example, the circulation control system on ICE requires only four custom fabricated nozzles. With such a low part count per vehicle and requiring custom, but not demanding, fabrication, it is reasonable to expect that MRL might be comparable to large part count items with a wider manufacturing base.

2A2.3.4 Identification of Technologies Assessed

For each baseline aircraft configuration, the readiness assessment evaluated the circulation control and fluid thrust vectoring technologies first in isolation, then in combination with each other and the other effector technologies. The combinations of technologies for the assessment were selected based on the flight control performance during the ingress mission.

The maturity of individual technologies was assessed based on the highest maturity level the technology had achieved under any testing condition. That is, the technology was not evaluated against its ability to achieve a particular level, or degree, of flight control. Note that the technologies were selected based on their ability to provide some level of aerodynamic control useful for flight control. When assessed in combinations, the maturity of the combined system was assumed to be no better than the most immature sub-system.

2A2.3.5 Technology Transfer-Ability, or Cross-Decking

A fourth readiness metric attempts to capture the ability of an AFC technology assessed on one specific platform to provide comparable performance on a similar, but different, platform. We called this metric the ‘transfer-ability’, or more colloquially, ‘cross-decking’. This metric was assessed by considering how the technology effected the control from a (fluid) mechanics perspective. For example, engine exhaust thrust vectoring effects control by re-directing the engine exhaust thrust to create a moment about the aircraft center-of-gravity. This technology could be expected to work on any aircraft where the engine is mounted in the main fuselage and aligned with the symmetry axis of the aircraft. As such, the technology would score well on the transfer-ability metric.

Chapter 3 – FLIGHT CONTROL DERIVATIVES USING ACTIVE FLOW CONTROL EFFECTORS ON THE ICE/SACCON UAS MODEL

David R. Williams
Illinois Institute of Technology
UNITED STATES

Jurgen Seidel, Ryan Osteroos, and Thomas E. McLaughlin
United States Air Force Academy
UNITED STATES

3.0 NOMENCLATURE

C_μ	Momentum coefficient, $\frac{\dot{m}_{jet}V_{jet}}{qS}$
$C_{L,D,Y}$	Lift, drag, side force coefficients, $\frac{L\ (or\ D,Y)}{qS}$
C_{L0}	Lift coefficient at α = 0
$C_{l,n}$	Roll and yaw moment coefficients, $\frac{L,N}{qSb}$
C_m	Pitch moment coefficients, $\frac{M}{qS\bar{c}}$
L	Lift force or roll moment
M	Mach number or pitching moment
N	Yaw moment
$Re_{\bar{c}}$	Reynolds number based on mean aerodynamic chord
S	Planform area
U	Freestream speed
b	Span
$\bar{c}$	Mean aerodynamic chord
$\dot{m}_{jet}$	Mass flow rate through actuator
q	Dynamic pressure, $\frac{1}{2}\rho U^2$
Λ	Leading edge sweep angle
α	Angle of attack
β	Side slip angle
MRP	Moment Reference Point

3.1 OVERVIEW

An active flow control system was designed to provide roll, pitch, and yaw control on a tailless ICE/SACCON UAS vehicle that has a 65 degree sweep leading edge. The active flow control effectors consist of three pairs of variable strength slot jets that exit tangentially to the surface. The slot jet pairs are located at the apex and midspan leading edge as well as the outboard trailing edges of the wing. The pair of actuators located near the apex provides primary yaw control. A second pair positioned at the midspan along the wing provides side force control, and the third pair of actuators located at the trailing edge provides roll and pitch control. The effectiveness of the actuators was evaluated with scale-model wind tunnel tests and by high-fidelity numerical simulations. The primary and cross control derivatives were measured as functions of vehicle angle of attack and actuator momentum coefficient. The yaw and roll control authority appear to be sufficiently strong to provide lateral-directional control of the tailless aircraft at M = 0.2. The data set obtained from the measurements was used in an ICE-101 flight simulator for mission performance predictions, and the data provide the benchmarks for a scale-model flight test program underway at the US Air Force Academy.

3.2 INTRODUCTION

The NATO task group AVT-239 was organized in the Spring of 2014 to study the application of innovative control effectors to tailless aircraft for the purpose of reducing (or eliminating) the need for conventional flight control effectors. Active Flow Control (AFC) technology was applied to three different platforms investigated by the task group; namely, MAGMA, SACCON, and an ICE/SACCON hybrid. This chapter reports on the effort by Illinois Institute of Technology (IIT) and the US Air Force Academy (USAFA) to develop a flight control system that uses AFC on the ICE aircraft.

Active flow control technology in the form of 'boundary layer control' has been used for decades as a means for improving the flight performance of aircraft. Usually AFC is applied as a 'fix' to a specific performance issue. For example, increasing the low-speed lift on final approach by blowing air over the trailing-edge flaps was a method used to enhance pilot visibility by reducing the approach angle of attack, and for decreasing landing distances by reducing final approach speeds. Dowgwillo [1] provides a detailed account of the development and use of blown flaps on a Phantom F-4C. The F-104 Starfighter also used blown flaps to provide additional lift for wings during landing, which reduced final approach speed and landing distance.

'Pneumatic' vortex control effectors for flight control were studied by Valasek and Walchli [2] using a high-fidelity flight simulator model of the F-16XL aircraft. The term 'pneumatic' control effector refers to air jets that were located on the forebody, wing, and tail of the aircraft. The control effector performance was obtained from wind tunnel data by Langan and Samuels [3] on a SHARC model, and Maines and Peters [4] for the F-16XL. Valasek and Walchli [2] used the high-fidelity flight simulator to execute various maneuvers with conventional control effectors and the AFC actuators on the forebody, wing, and tail. With a momentum coefficient of $C_\mu = 0.0026$ they determined that the rudder and ailerons could be completely replaced by the pneumatic control system. They also determined that much lower mass flow requirements were necessary to execute a simulated penetration and strike mission.

The tailless ICE-101 aircraft of interest in this chapter was first studied by a joint US Air Force-US Navy program conducted by LMTAS and Bihrle Applied Research [5], [6]. The objective was to investigate innovative control concepts for tailless aircraft. The novel approaches to control effectors that were studied included mechanical all-moving wing tips and spoiler-slot-deflectors. The mechanical control effectors were shown to be effective in maintaining the required yaw control. At that time, active flow control techniques were not investigated with this aircraft.

The NATO/STO AVT-239 task group revisited the topic of using active flow control effectors to improve the flight performance of tailless UAS aircraft. The initial focus was on enhanced lateral-directional control of tailless aircraft, and reducing or eliminating the reliance on conventional control effectors. Sub-groups within AVT-239 explored different AFC approaches and different platforms. Each vehicle has different flight characteristics, so different AFC actuation schemes are needed. In 2014 the British Aerospace / University of Manchester group had an effort underway with the MAGMA demonstrator project. The MAGMA has a $\Lambda = 47$ deg. leading edge sweep angle, and uses thrust vectoring and trailing-edge circulation control actuators for roll, pitch, and yaw control. The University of Arizona investigated the effectiveness of using sweeping jet actuators on the SACCON/MULDICON aircraft. The SACCON has a $\Lambda = 53$ deg. leading edge sweep angle. Results of these investigations will be presented in separate papers. After an AFC effector concept was chosen for a particular platform, its performance on the flight vehicle was evaluated at high- subsonic cruise conditions by using flight simulators. A QFD system level analysis was performed to assess engine bleed air requirements, volume, weight, and AFC system complexity.

In this chapter we describe the IIT/USAFA effort to use slot jet actuators at different locations along the leading and trailing edges of the wing on a modified Lockheed Martin ICE-101 profile. The ability of the proposed active flow control effector system to produce forces and moments large enough for control of the tailless ICE aircraft was assessed in wind tunnel and high-fidelity numerical simulations. The data resulting from this investigation is used in ICE flight vehicle simulations by Niestroy [7] to determine the controllability of the aircraft with AFC during cruise conditions in light and moderate turbulence. The data were also used as the benchmark for actual flight tests on a sub-scale vehicle with AFC.

Section 3.4 describes the details of the experimental methods. The measurements obtained in experiment are presented in Section 3.5, and some selected results from the computational fluid dynamic studies are described in Section 3.6. The conclusions are reviewed in Section 3.7.

3.3 METHODS OF INVESTIGATION

Wind tunnel experiments and numerical simulations are used in a complimentary approach to explore a wide parameter space of AFC conditions and obtain flow specific information that cannot be achieved by experiment. The wind tunnel was used to measure the forces, moments, and control derivatives acting on the ICE model with and without AFC. Numerical simulations provide detailed information about the flow field in a smaller set of the parameter space.

Because the emphasis of the NATO group was on lateral-directional control of tailless aircraft, the decision was made to use a full three-dimensional model in experiments and simulations to obtain 6 degree of freedom measurements. Although half-models enable larger Reynolds numbers to be achieved, they force the midspan streamline to be straight, so that the flow field is symmetric between the model in the wind tunnel and its image pair. The numerical simulations presented later in this report show that flow field streamlines are not symmetric across the span when actuation is applied or when the aircraft is in sideslip.

3.3.1 Experimental Methods

Experiments were performed in the USAFA Subsonic Wind Tunnel in Colorado to evaluate the effectiveness of the active flow control effector system. The test section cross-sectional dimensions are 0.91 m x 0.91 m. Test conditions were at free stream Mach numbers over the range from M = 0.15 to 0.4; however, the most extensive results were obtained at M = 0.2 which are presented here. Angles of attack, α, were varied from $-4° \leq \alpha \leq 28°$ in 2° increments. Measurements at side slip angles between $-10° \leq \beta \leq 10°$ were also acquired.

The 1:37 scale model is a hybrid of the Lockheed Martin ICE-101 planform [6] and NATO SACCON profiles [8]. We will refer to the ICE/SACCON hybrid as simply ICE in the remainder of this report. SACCON profiles were matched at the midspan, at the 1/3 halfspan and 2/3 halfspan locations. The leading edge has a 65 degree sweep angle as shown in Figure 3-1(a). The leading edge blended from sharp at the apex, to round in the midspan, and then returned to sharp at the outer third of the wing. The model was mounted to a 6-component 667 N force and moment transducer inside a sting as shown in Figure 3-1(b).

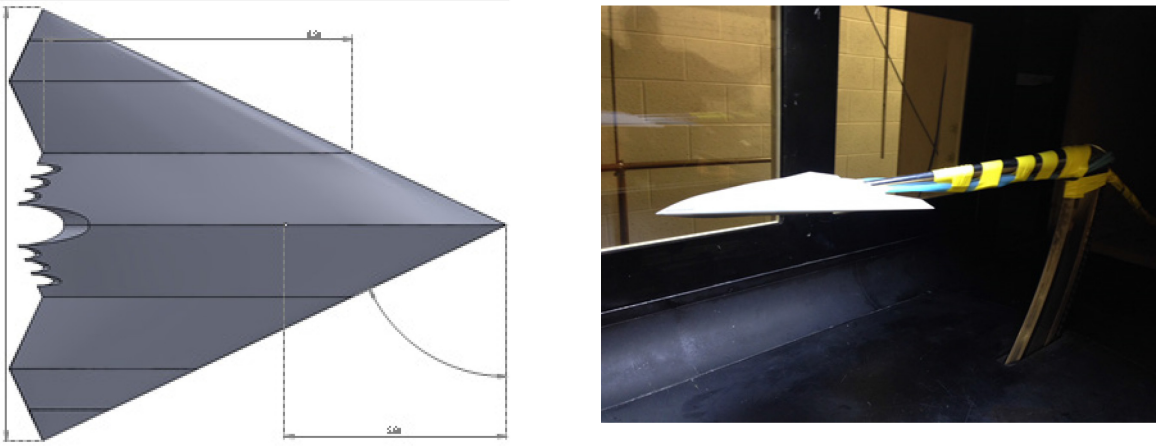

(a) 1:37 Scale Model (Dimensions in Inches). **(b) ICE Model in Subsonic Wind Tunnel.**

Figure 3-1: Model Definition and Wind Tunnel Installation.

The Reynolds number based on the mean aerodynamic chord, $\bar{c}$, was $Re_{\bar{c}}$ = 730,000 at M = 0.2. The planform area S = 0.0472 sq. m (73.2 sq.in.) with a span b = 287 mm (11.3 in.). The Moment Reference Point (MRP) is located at $0.46\bar{c}$.

Variable strength steady blowing actuators are used as the control effectors. Three pairs of actuators are installed along the leading edges of the model as shown in Figure 3-2(a). A pair of slots was positioned at the apex of the model for yaw and pitch control, and a second pair of slots was located at the midspan position of the leading edge for side force control, and a third pair of slots at the trailing edge was used for roll and pitch control. Internal passageways in the model connected the slots to air supply lines at the trailing edge of the model. The air flow rate was controlled by an external Pneumatic Control Box (PCB). High pressure air in the laboratory is reduced by regulators to 276 kPa gage (40 psig). Electro/pneumatic valves direct the flow to tubing that connects with the model in the wind tunnel. Flow rates are set manually by needle valves in the PCB. The maximum pressure to the actuators was 103.4 kPa gage (15 psig) pressure, which corresponds to a flow rate of 2.9 grams/s through the apex and midspan actuators, and 1.9 grams/s through the trailing-edge actuators.

3.3.2 Numerical Simulations

The DoD HPCMP CREATE–AV/Kestrel software suite was employed for the numerical simulations. Kestrel is second order in space and time and features a number of turbulence models. The SARC turbulence model was employed in this effort. The computational model was set up such that the model was described using a no-slip wall boundary condition and the wind tunnel walls were not included in the model. Instead, far-field boundary conditions were placed 20 mean aerodynamic chord lengths from the model. For active flow control, the boundary condition at the base of the corresponding forcing duct (Figure 3-2(b)) was changed from a no-slip wall to a constant total-pressure, total-temperature source boundary condition, with the conditions approximately matching the experiments. Using the partial duct allowed for a more realistic velocity distribution at the slot jet exit.

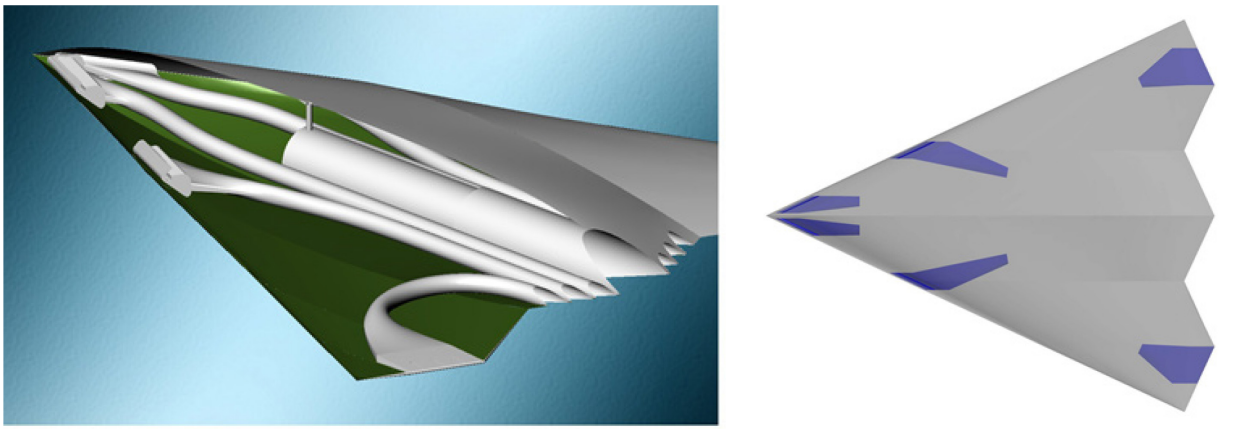

(a) CAD Drawing with Internal Plumbing. **(b) CFD Model with Actuator Ducts (Blue).**

Figure 3-2: Flow Control Ducting in Wind Tunnel Model and CFD Model.

3.4 RESULTS

Comparisons between the wind tunnel measurements, numerical simulations, and published data for the ICE-101 model are presented in this section. The ICE-101 has the same planform as the ICE model, but the profiles are different. Furthermore, the ICE-101 has a cockpit that was removed in the ICE design.

Therefore, close agreement cannot be expected between the ICE and the ICE-101. Nevertheless, this is the only data available for a similar platform acquired in an independent facility, and we believe the comparisons build confidence in the measurements of ICE.

3.4.1 Baseline – Without Forcing

Baseline measurements of the lift and drag forces and the pitching moment acting on ICE without AFC are shown in Figure 3-3, which have been reproduced from Williams and Seidel [9]. Only data at M = 0.2 are presented. The angle of attack is varied between $-4° \leq \alpha \leq 26°$. Side slip angles $\beta = \pm 5°$, and $\pm 10°$ are shown. The results from the USAFA numerical simulations are labeled as 'sim', and the original ICE-101 data from Gillard et al., [6] are labeled as 'ICE'.

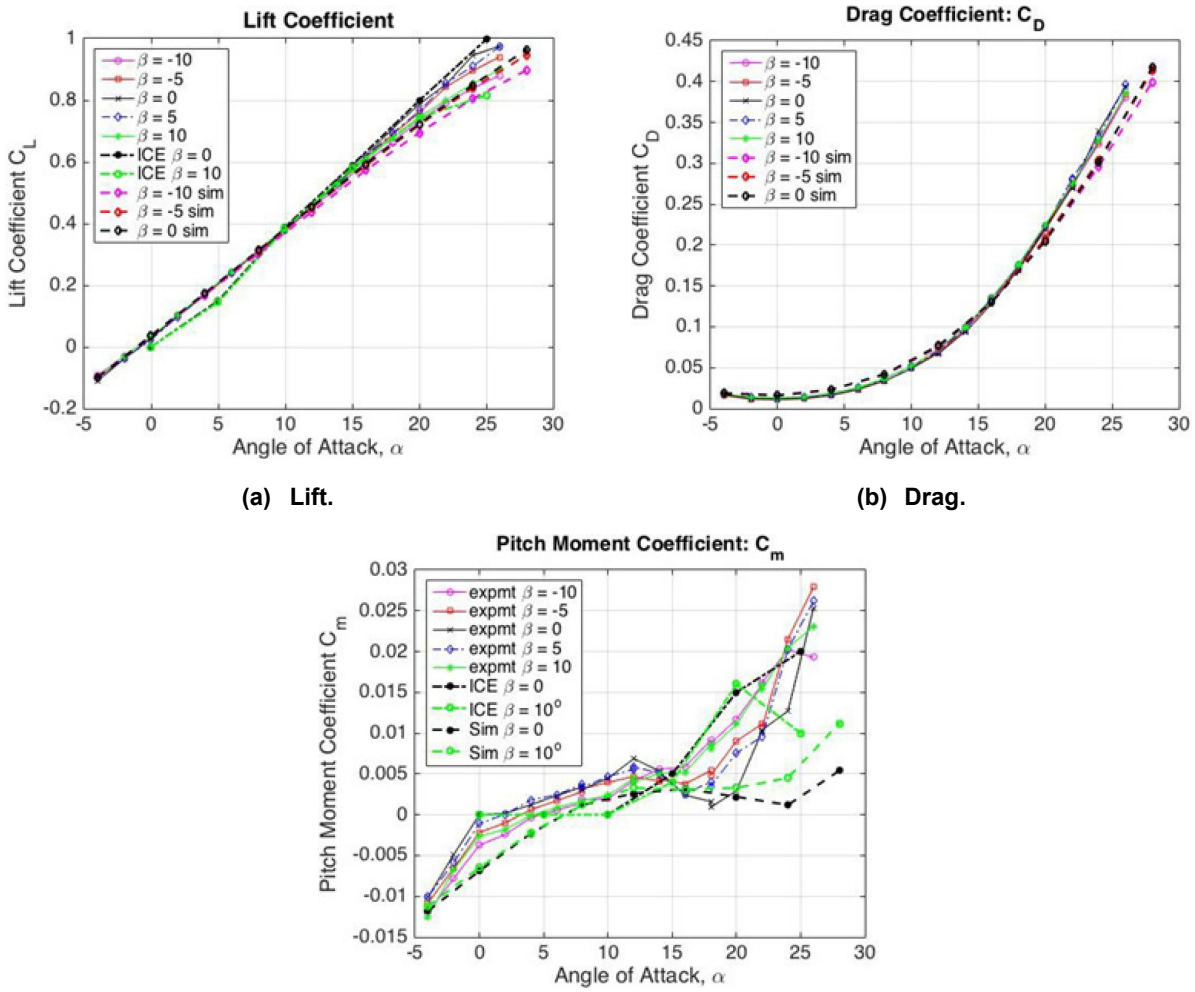

(a) Lift. **(b) Drag.**

(c) Pitching Moment.

Figure 3-3: Baseline Measurements. Reproduced from Ref.[9].

The data are in reasonable agreement when the flow is attached between $-4° \leq \alpha \leq 15°$. By $\alpha = 20°$ the flow separation is substantial and differences in lift and pitching moment appear. The AVT-239 study considered flight at cruise conditions at low angles of attack, so the agreement between simulations, past and current configurations of the aircraft was considered to be reasonable.

3.4.2 Active Flow Control

Each flow control actuator was individually calibrated to determine the mass flow rate and momentum coefficient dependence on the supply line pressure. Needle valves were used to control the flow rate between the PCB and the actuators. The supply line pressure was monitored to determine the momentum coefficient.

The momentum coefficient was defined as $C_\mu = \frac{\dot{m}_{jet} V_{jet}}{0.5 \rho U_\infty^2 S}$. At the maximum supply line pressure (103.4 kPa gage, 15 psig) the flow rate from the apex and midspan jets was $\dot{m}_{jet}$ = 2.9 grams/s. The corresponding maximum flow rates through the trailing-edge actuators were smaller (1.9 grams/s), because the trailing-edge actuators have a smaller exit area.

The reaction forces and moments produced by the slot jet actuators (due to the momentum flux associated with their jets of air) were measured by operating the actuators at their maximum C_μ value when there was no flow in the wind tunnel. To make comparisons with wind tunnel results obtained at M = 0.2, the forces and moments from the quiescent tunnel measurements were converted to coefficient form by normalizing with the dynamic pressure of the flow at M = 0.2. The values are listed in Table 3-1. These offset values were subtracted from the wind tunnel measurements to obtain the corrected AFC results.

Table 3-1: Control Effector Forces and Moments in a Quiescent Wind Tunnel (Normalized by Dynamic Pressure at M = 0.2).

C_L	C_D	C_Y	C_l	C_m	C_n
-0.0053	-0.007	-0.0146	-0.0014	-0.0055	-0.0058

3.4.2.1 Pitching Moment Control and Trim

Trailing-edge slot jet control effectors with upward blowing capability were used to trim the model. The left and right trailing-edge slot jets must operate symmetrically to prevent introducing an undesired roll moment. A shift of the moment reference point by -0.04$\bar{c}$ produced a more stable moment distribution, although the aircraft will not reach a trim condition without the application of AFC. The effect of increasing C_μ on the pitching moment can be seen in Figure 3-4. The aircraft will be statically stable and trimmed at $\alpha = 4°$ when there is a net C_μ = 0.0028 as indicated by the circle in the figure at C_μ = 0.

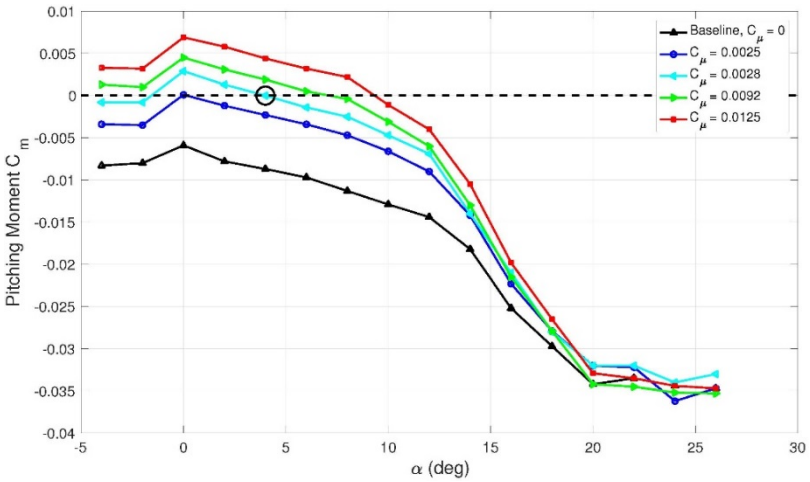

Figure 3-4: Pitching Moment Coefficients with Both Left and Right Upward Blowing Trailing-Edge AFC Control Effectors.

3.4.2.2 Roll and Yaw Moment

The effects of AFC on the roll moment increment and the yaw moment increment are shown as surface plots in Figure 3-5. The independent variables are actuator control voltage and angle of attack. Positive actuator

voltage corresponds to right side actuator forcing, and negative voltage is left-side forcing. The maximum voltage (2.5 V) for the apex actuator corresponds to C_μ = 0.006, and C_μ = 0.004 for the trailing-edge actuators. At a fixed angle of attack, the slope of the surface $\frac{dC_l}{dC_\mu}|_{apex}$ shown in Figure 3-5(a) gives the roll control derivative. The open circles are the measured values and the colored surface is a multi-dimensional least squares curve fit to the data. At low angles of attack the roll increment shows a monotonic increase with forcing. The control authority increases as the angle of attack increases, at least up to α = 15°.

We are particularly interested in the control derivatives near α = 4°, because this angle of attack is close to the maximum L/D condition where the aircraft will fly during cruise conditions.

In Figure 3-5(b) the roll moment increments used in the ICE-101 flight simulator with left elevon deflection angles δ_{elev} = ±10° and ±30° are compared to the roll moment that is produced by the individual trailing-edge AFC effectors. By comparing the roll moment produced we see that the AFC control with C_μ = 0.004 is equivalent to a 10 degree elevon deflection on one side of the aircraft. Niestroy's flight simulations showed that this is sufficient roll control for cruise flight in light and moderate turbulence.

The yaw moment increment to left/right apex actuation is shown in Figure 3-6(a) and Figure 3-6(b). The right side actuator produces a positive (nose to the right) yaw moment. Apex actuation on the left side of the model produces a negative (nose to the left) yaw moment. The yaw results presented in 6a also show that proportional control of the yaw moment can be achieved, and the control authority increases with increasing angle of attack. When the model is at a β = 5° side slip angle, the results in Figure 3-6(b) show that there is more than sufficient control authority to compensate for the directional instability.

The yaw control derivative at β = 0° was determined to be $\frac{dC_n}{dC_\mu}|_{apex}$ = 0.433 at α = 0°, and it nearly doubles to $\frac{dC_n}{dC_\mu}|_{apex}$ = 0.792 at α = 10°.

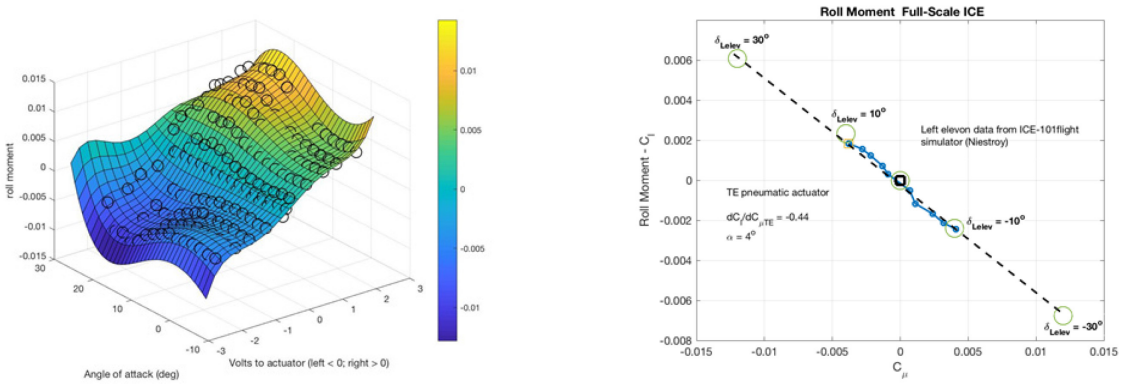

(a) (b)

Figure 3-5: (a) Roll Moment Increment with Left/Right Trailing-Edge Actuation; (b) Roll Moment Increment Comparison Between AFC and Conventional Elevon Deflection.

The measured stability and control derivatives at α = 4° are shown in Table 3-2. From the magnitude of the coefficients it is clear that the apex actuators are dominant over other actuators for yaw control, while the midspan actuator is the strongest for roll control. However, there are cross control effects that must be compensated. For example, producing a roll moment with the midspan actuator produces an adverse yaw moment that must be compensated with apex actuation. This is analogous to the classic 'adverse yaw' produced by conventional ailerons, which is corrected by rudder input. The solution with pneumatic control effectors is to use crossed-actuation, i.e., right-side apex actuation is combined with left-side midspan actuation.

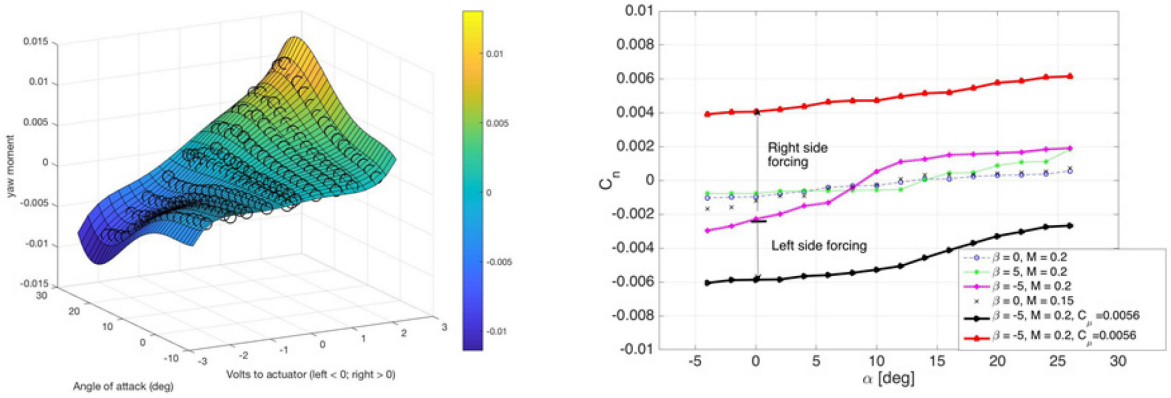

(a) (b)

Figure 3-6: (a) Yaw Moment Increment with Apex Actuation; (b) Yaw Moment Control Envelope at β = 5° Side Slip.

Table 3-2: Stability and Control Derivatives at α = 4°.

	$C_{x,\beta}$	$C_{x,C\mu apex}$	$C_{x,C_{\mu_{mid}}}$	$C_{x,TEup}$
Roll Cl	-0.049	-0.205	-0.429	-0.44
Yaw Cn	-0.0115	0.624	0.214	-0.463
Side CY	-0.019	1.57	2.14	-0.735
Pitch Cm		-0.220	-0.026	1.56

3.5 CFD FLOW FIELDS

Figure 3-7 shows streamlines and surface pressure coefficients over the ICE model when the aircraft is at α = 4°. The left side apex actuator is activated with C_μ = 0.006. The asymmetry of the flow pattern produced by the AFC effector and the low pressure in the vicinity of the actuator exit combine to produce a negative yaw moment. The air exiting the apex slot crosses over the centerline of the vehicle and produces a streamwise oriented vortex over the right wing.

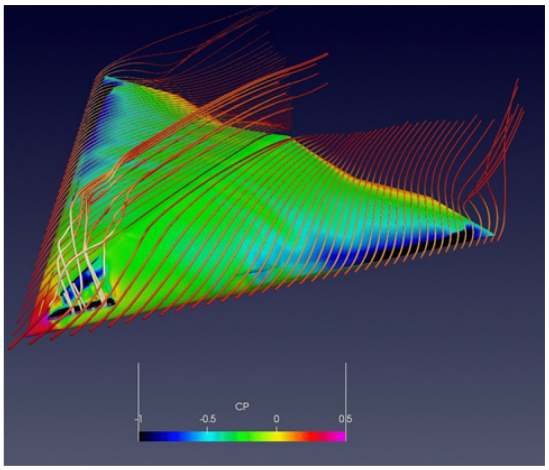

Figure 3-7: Streamlines and Surface Pressures.

3.6 CONCLUSIONS

Slot jet active flow control actuators located at the apex, midspan, and trailing-edge locations of a tailless ICE aircraft were shown to be effective in controlling the roll and yaw moments necessary for flight control. Force and moment data obtained from experimental measurements and CFD simulations were used to obtain the control derivatives that are used in an ICE-101 flight simulation. The apex actuators were shown to be most effective in controlling yaw moments, while the trailing-edge actuators had the largest effect in controlling the pitch and roll moments.

3.7 ACKNOWLEDGEMENTS

Support by the US Air Force Office of Scientific Research under grant FA9550-16-1-0098 with past program managers Douglas Smith and Ivett Leyva and current program manager Gregg Abate is gratefully acknowledged. This research was supported in part by a grant of computer time from the DoD High Performance Computing Modernization Program at the US Air Force Research Laboratory DoD Supercomputing Resource Center (AFRL DSRC). This material is based in part on research sponsored by the US Air Force Academy under agreement number FA7000-13-2-0009 and FA7000-18-2-0012. The US Government is authorized to reproduce and distribute reprints for Governmental purposes notwithstanding any copyright notation thereon.

3.8 REFERENCES

[1] Dowgwillo, R., A Stake in the Ground: How Boundary Layer Control Was Implemented on a Production Tactical Aircraft, AIAA Paper 2018-0561, 2018.

[2] Valasek, J., and Walchli, L.A., High Speed, Low Angle-of-Attack Pneumatic Vortex Control, AIAA Paper 98-4449, 1998.

[3] Langan, K. and Samuels, J., Effects of Wing Jet Blowing on the SHARC 55 Percent-Scale Fighter Configuration, Tech. Rep., AIAA Paper 97-0039, 1997.

[4] Maines, B. and Peters, S., Pneumatic Aerodynamic Device Development (PADD), Tech. Rep., WL-TR-96-3141, 1996.

[5] Dorsett, K., Fears, S., and Houlden, H., Innovative Control Effectors (ICE) Phase II, Tech. Rep. WL-TR-97-3059, Wright Laboratory, 1997.

[6] Gillard, W.J., Innovative Control Effectors (Configuration 101), Tech. Rep. AFRL-VA-WP-TR-1998-3043, Air Force Research Laboratory Wright Patterson, 1998.

[7] Niestroy, M., Williams, D., and Seidel, J., NATO AVT-239 Task Group: Active Flow Control Simulation of the Tailless ICE Aircraft, AIAA Paper 2019-0279, 2019.

[8] Huber, K.C., Vicroy, D., Schutte, A., and Hubner, A., UCAV Model Design and Static Experimental Investigations to Estimate Control Device Effectiveness and Stability and Control Capabilities, AIAA Paper 2014-2002, 2014.

[9] Williams, D., and Seidel, J., Crossed-Actuation AFC for Lateral-Directional Control of an ICE-101/SACCON UCAV, AIAA Paper 2016-3167, 2016.

Chapter 4 – SUPERCRITICAL COANDA BASED CIRCULATION CONTROL AND FLUIDIC THRUST VECTORING

Clyde Warsop, and Matthew Forster
BAE Systems AIR
UNITED KINGDOM

William J. Crowther
The University of Manchester
UNITED KINGDOM

4.0 NOMENCLATURE

$C\mu$	Momentum coefficient = $\dot{m}V_j/q_\infty S$
C_D	Drag coefficient for complete aircraft
C_L	Lift coefficient for complete aircraft
C_l	Section lift coefficient / Aircraft Rolling moment coefficient
C_n	Yawing moment coefficient for complete aircraft
C_m	Pitching moment coefficient
C_{ref}	Reference chord
C_y	Side force coefficient for complete aircraft
C_Z	Normal force coefficient
c	Chord (m)
h	Height of blowing slot (m)
h*	Throat height of convergent-divergent nozzle (m)
r	Radius (m)
Δ	Increment
α	Angle of attack
δ	Deflection angle of control surface or vector angle of a jet (deg.) or boundary layer thickness (m)

4.1 OVERVIEW

This chapter overviews research undertaken to develop and demonstrate active flow control technologies with the objective of developing systems having adequate control authority to trim and manoeuvre an aircraft flying at transonic speed without the use of conventional control surfaces. The research has led to an improved understanding of supersonic wall jets and their attachment and separation which has then been applied to the development of practical Circulation Control and Fluidic Thrust Vectoring concepts. The research has been both experimental and numerical in nature and has led to the determination of control powers and efficiencies for a generic UCAV configuration used as the basis for performance assessments by the NATO AVT-239 task group.

4.2 INTRODUCTION

This chapter outlines and draws conclusions from a series of studies [1] to [30] conducted by the authors and their co-researchers to develop Circulation Control (CC) and Fluidic Thrust Vectoring (FTV) concepts based on the application of supersonic Coanda wall jets.

A principal driver for Fluidic Control Effectors (FCEs) for military aircraft is signature reduction. Conventional moving control surfaces create changes in aircraft external geometry during flight and are the sources of additional edges and gaps that must be carefully treated to minimise radar reflection. FCE's also provide opportunities for lower maintenance requirements since they have fewer, highly-loaded, moving parts compared to conventional control surfaces and are therefore less prone to wear and mechanical failure. FCE's may also be more volumetrically efficient compared with conventional trailing edge control surfaces – allowing for additional fuel or improved structural layout.

On the other side of the balance is the 'systems cost' of implementing fluidic controls. Historically, despite a number of high profile attempts (e.g., blown flaps on the Blackburn Buccaneer / F104 Starfighter / some

MiG 21 variants and circulation control on the Grumman A-6A and NASA X-Wing prototypes) the uptake of flow control has, in general, been frustrated by a lack of cost-effectiveness. This is not to say that the solutions are not aerodynamically effective; it is that the life cycle cost of implementing them outweighs the benefits. Such 'costs' relate to:

- Systems: Dedicated blowing air supply, control and distribution systems for flow control introduce additional systems size, weight and power costs.
- Maintainability: Flow control devices typically require precise control of flow path geometry at the interface between the device and the external flow. Small, high precision slots and orifices are subject to blockage from ingress of water and dirt from the environment. Also, engine bleed used as the air source is hot, leading to thermal stressing of components.
- Flight safety and mission availability: FCEs generally have a high level of dependency on the primary propulsion system for their effectiveness as they are generally reliant on engine compressor bleed as their primary power source. Flight safety considerations therefore require the use of twin engines, an auxiliary power unit or reliance on conventional control surfaces in the event of an engine failure.

The impact of all the above considerations can be reduced by improving the efficiency of the flow control system relative to historical values and has been the primary objective of the research described in this chapter.

This chapter sets out a comprehensive definition of terms and performance metrics suitable for characterizing fluidic control effectors. It then overviews the research undertaken by the authors that has led to the development of effective and efficient flow control effectors suitable for application to the three axis control of a full-scale, transonic UCAV configuration. After summarising the basic fluid mechanics studies the chapter concludes by applying these to a generic UCAV (the NATO SACCON configuration) and presenting control effectiveness and efficiency data for these fluidic controls. This information formed the input that was used for subsequent performance and system integration studies [31].

4.3 OVERVIEW OF CIRCULATION CONTROL AND FLUIDIC THRUST VECTORING TECHNOLOGIES

4.3.1 Circulation Control

4.3.1.1 Description of the CC Concept

In its simplest form the Trailing Edge CC concept is one characterized by the blowing of a tangential jet sheet through spanwise slots placed just upstream of a cylindrical trailing edge (Figure 4-1). The jet sheet remains attached to the cylindrical surface and entrains the air passing over the upper surface of the wing through the Coanda effect [32]. As a consequence, 'circulation' develops around the aerofoil and a lift increment is generated in a similar way to that produced from a conventional trailing edge flap (Figure 4-2).

By independently controlling blowing from the upper and lower slots on a trailing edge (Figure 4-1d) it is possible to control wing circulation (lift) in both a positive and negative sense thereby creating the same effect as a conventional control surface that may be deflected both upwards and downwards. The dual-slot CC concept can also be employed as a thrust/yaw generating device by operating both upper and lower blowing jets simultaneously. A further embodiment of the dual-slot concept also allows for operation at continuous blowing whereby a control valve is used to modulate the percentage of the total flowrate applied to the upper and lower slots at any point in time. The advantage of such a system is the ability to generate full control authority while operating the engine at a continuous bleed condition which, under some circumstances, may be better for engine performance.

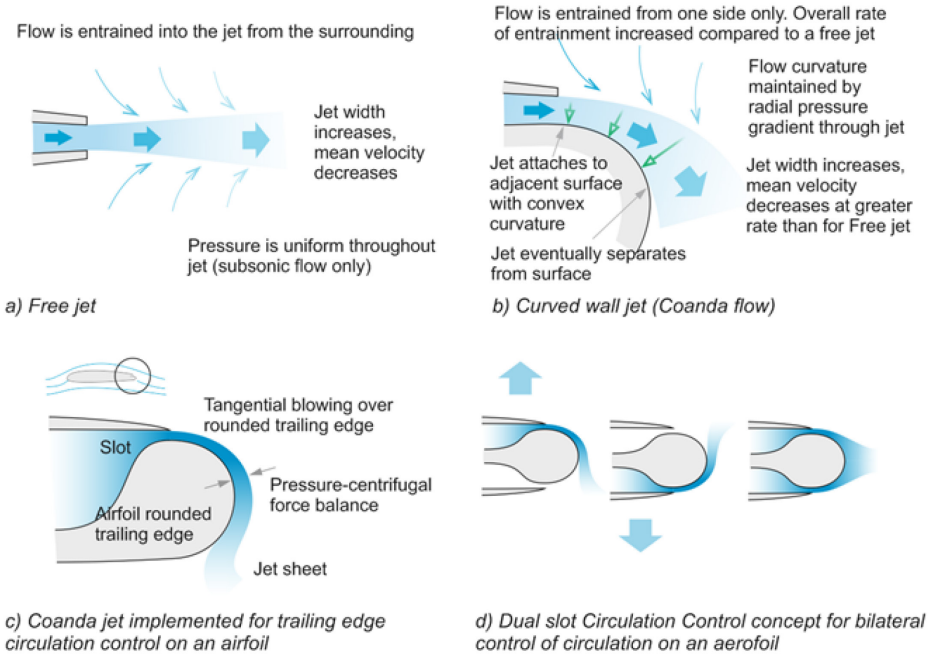

Figure 4-1: Trailing Edge Circulation Control. Fundamental concepts and evolution of implementation as a bilateral control on the trailing edge of a wing.

4.3.1.2 Historical Development of CC

A full outline of the history and subsequent development of CC technology by the present authors was published in Ref. [31]. However, for completeness of the present chapter this description is presented again below.

Wing trailing edge Circulation Control (CC) was first patented by Davidson in 1962 [33] and further developed by various researchers during the 1970s, 80s and 90s [34], [35], [36], [37], [38], [39]. More recently, researchers have continued to study and develop our understanding of CC through the application of more advanced experimental and modelling techniques [40], [41]. Concise reviews of this early development of CC have been documented among others by Wood and Nielsen [42], [43], Frith [1], Llopis-Pascual [2], Robertson-Welsh [3] and Kweder et al. [44]. Much of the early research into effectiveness was carried out by Englar [34], [35], [36] focusing on the performance of CC for high-lift applications. More recent studies have extended the application of the CC concept to a variety of other applications [45] including the control of slender bodies and projectiles by modifying after-body flows [46]. The pioneering work of Englar suggested that there was a non-linear relationship between lift coefficient increment and blowing coefficient are characterized by a low blowing 'boundary layer control' regime that transitions to a 'CC' regime at a blowing momentum coefficient of 0.03 [47]. However, this distinction has not been found that useful in practice, see, for example, Refs. [4], [36]. Jones and Englar [48] also proposed that there is an optimum range for slot height to Coanda surface radius ratio, h/r, and radius to chord ratio, r/c. Englar [34], [35] and later Abramson and Rogers [37] carried out research into the effects of geometry on CC effectiveness. These studies agreed that h/r and r/c have a significant impact on lift and drag increments. This is shown graphically in Figure 4-3 where the shaded area highlights the optimum geometry region proposed by Englar and Williams [49].

The proposed optimum design space is based on the trade-off between increased efficiency due to a large Coanda radius and reduced drag through the use of a smaller radius. Jones et al. [48] also proposed a lower limit to the value of r/c (2%) below which the decrease in lift augmentation was perceived as too great. Whilst development of these rules of thumb has been useful, there has been tendency for newer researchers

to consider these outcomes as universal facts rather than guidelines. As such, work to further explore the available design space has been slower than it might have been has these rules not been in place.

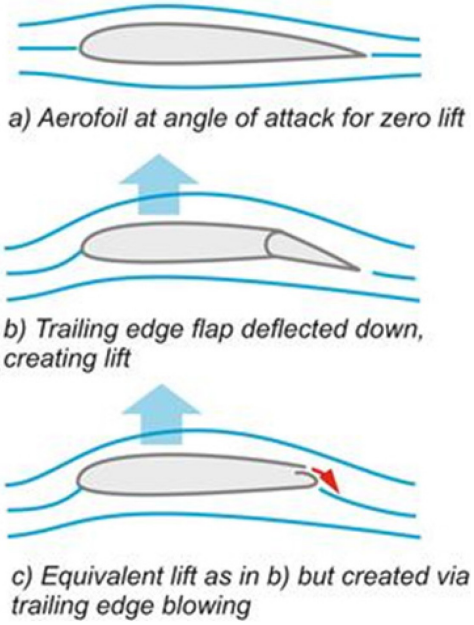

Figure 4-2: Equivalence of Circulation Control via a Trailing Edge Flap and Trailing Edge Blowing.

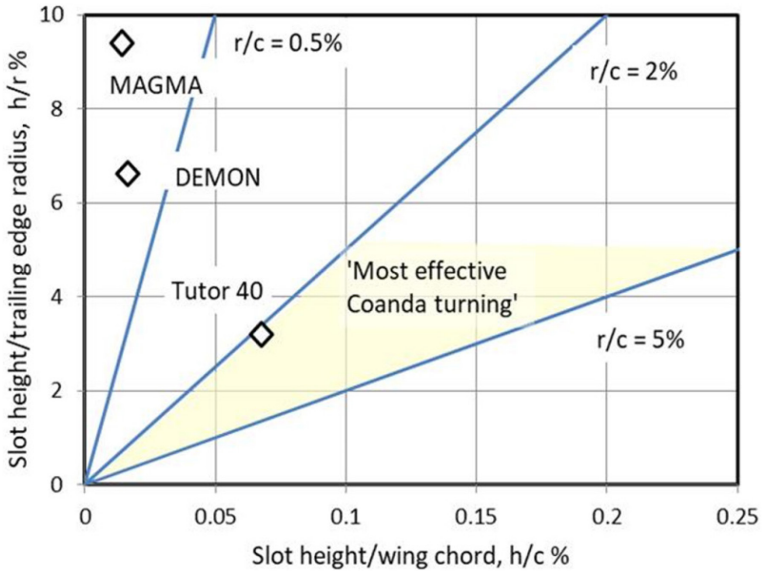

Figure 4-3: CC System Geometry Sizing Diagram, with Area for Optimal Operation as Identified by Englar [49] in Yellow Shading.

4.3.1.3 The Perceived Problem with CC

By the end of the 1990s it was generally considered that CC for enhanced high-lift capability was too difficult to implement into practical aircraft concepts. For the Grumman A6 aircraft the high engine bleed mass-flows and the additional drag of the bluff wing trailing edge severely compromised

aircraft performance. The high bleed mass-flow requirements also gave rise to system integration issues caused by the large duct and valve sizes required. Similar practical implementation issues also curtailed the X-wing programme.

During the late 1990s and early 2000s the present authors and their colleagues began to consider CC not as a means of generating high-lift but also as a means of providing control forces. A key driver for this change in emphasis is that the bleed air requirement for generation of useful control forces is significantly reduced compared to that needed for useful high-lift and can be met using existing engine bleed budgets of 1 – 2 %. However, there remain a number of hurdles to overcome:

- To meet various performance requirements (including low drag) it needed to be shown that CC could be integrated into a wing having a trailing edge thickness not much greater than that of a conventional control surface and provide equivalent control power. A target of 5 to 15 mm was set for the trailing edge height, based on the size of military platforms that these devices might be deployed on. For a full-scale wing having a chord of several metres this means operating at values of r/c well below those explored by previous researchers (below 1%, refer to Figure 4-3 for context).
- It needed to be shown that CC for flight control purposes could be made to operate on configurations flying at practical (at least transonic) flight speeds. This demands that the CC blowing velocities be supersonic in order to achieve required velocity ratios of greater than unity.
- It needed to be shown that CC could be operated efficiently from the perspectives of the required power offtake from the engine and integration of the necessary bleed air control and distribution system. Simple considerations of mass flow, exit velocity, and momentum show that, for a given mass flow, the momentum is maximised by operating at as high a jet exit velocity as possible. This suggests that operating a CC system at as high a pressure ratio as possible should lead to the most compact and efficient systems provided that:
    - The required pressure ratio is available; and
    - The high pressure ratio wall jet will both attach to the trailing edge and achieve entrainment of the outer flow at a similar rate to that achieved using subsonic jets.

The hurdles identified above focussed the authors' subsequent CC research activity on understanding the design and performance of CC systems where the r/c is exceedingly small by previous standards, e.g., below 1%, and understanding the design and performance of CC systems where the wall jet exit velocity is supersonic (pressure ratios greater than ~2).

4.3.1.4 Recent Research

The authors' research into CC commenced in 2000 following research conducted by colleagues Frith and Wood [1], [8] who explored the application of CC to low aspect ratio swept wings. Frith [1] and Frith and Wood [8] showed the viability of using CC for flight control low subsonic speed aircraft and suggested that the trailing edge radius to chord ratio (r/c) could be reduced to 0.05 compared to existing practice, provided that a suitable value of slot height to radius (h/r) was maintained. Subsequently, work by Michie [9] showed that the use of a further reduced Coanda radius (r/c = 0.003) had no detrimental impact on CC system performance. A design methodology for CC systems for flight control application was developed as an outcome of this [50], [51]. In addition, many obstacles with respect to implementing flight hardware to achieve these goals were overcome including:

- Operating a small gas turbine engine with compressor bleed;
- Design and manufacture of the bleed air distribution and control hardware;
- Design and manufacture of the CC trailing edge with small radii (3 mm) and slot heights (0.2 mm) capable of operating with hot (200° C) bleed air; and

- Integration of the CC system into the aircraft flight control system (FCS) in a way in which allowed the FCS to treat the control as a conventional control surface [50], [51].

Overlapping with Michie's research Wilde [4], [7] demonstrated the viability of employing a pair of wing mounted dual-slot CC actuators to provide three axis control of a flying wing configuration. Wilde showed how both exclusive and non-exclusive blowing concepts (see Section II of Ref. [30]) could be used to generate not only independent control about the pitch and roll axes but also about the yaw axis using an asymmetric dual blowing approach [7].

Building on the success of the research done in the 2000s, interest turned to full-scale application on vehicles flying at transonic speed which implicitly required much higher blowing velocities. It was also understood that CC blowing at as high a pressure ratio as possible minimises the required mass flow to achieve a given C_μ and results in a positive impact on engine performance and system integration. Englar [35] appreciated the need to understand supersonic wall jet detachment and demonstrated a supersonic curved wall jet remaining attached for a CC aerofoil having a large radius to chord ratio of 0.09 [34]. He also noted that the attachment of the supersonic curved wall jet under varying operating conditions was 'unpredictable'. Subsequent investigations found that there was a significant loss in CC performance due to the separation of the supersonic curved wall jet once the nozzle had become choked [37], [52], [53]. Steered by the outcome of the author's research into the Coanda based FTV of supersonic jets in the 2000s (see following section) research was conducted to exploit the application of this knowledge to super-critically blown CC trailing edges. Between 2012 and 2017 Llopis-Pascual [2], Forster [14], and Forster and Steijl [15], [16] successfully showed that, with appropriate shaping of the CC slot and trailing edge geometry, a CC effector with very low radius to chord ratio can give sufficient control authority to manoeuvre an aircraft flying at Mach 0.8. Much of the success achieved by Llopis-Pascual and Forster was based on applying the findings of:

- Bevilaqua and Lee [54], who developed a convergent-divergent slot design approach which skews the velocity and pressure profile along the jet exit to create a correctly-expanded supersonic turning flow.
- Gregory-Smith and Senior [55] and Carpenter and Smith [56] who showed how a small, aft-facing step placed just downstream of the exit of a convergent slot greatly improved the attachment of an under-expanded jet to an adjacent Coanda surface.

Llopis-Pascual [2] and Forster and Steijl [18] showed how a high pressure ratio slot flow (PR of any value but demonstrated to PR = 7), combined with the appropriate selection of h/c can enable a Coanda jet to remain attached to the trailing edge and entrain a transonic outer flow. They also demonstrated the efficacy of combining a rearward facing step just downstream of the exit of a convergent nozzle to avoid the complication of manufacturing a convergent-divergent nozzle to achieve flow attachment at high pressure ratios (Figure 4-4).

In parallel with this work, Robertson-Welsh [3] provided further insight into the mechanisms associated with the attachment and separation of high pressure ratio Coanda wall jets which is expressed in Figure 4-5.

Figure 4-5 summarises the different design points of Coanda jets in terms of h*/r and the nozzle pressure ratio at which the jet separates, where h* is the throat height of a con-di nozzle. The use of h* as opposed to the exit height h allows more meaningful comparison of different nozzles as the product of h* and NPR provides a measure of the design mass flow of the nozzle. The important outcome from this figure is that most of the nozzle designs, be they 'convergent only', 'con-di', or 'skewed con-di', fall approximately along the same curve. It is apparent that the advanced skewed nozzles of Llopis-Pascual [18] (black crosses) do slightly better in terms of attachment compared to 'convergent only'. However, this is of the same order as for a 'convergent only nozzle with a step'. The important implication of this understanding is the realisation that practical high speed Coanda devices can make use of a simple convergent nozzle followed by a step. This type of geometry costs much less to implement compared to that required for a con-di nozzle.

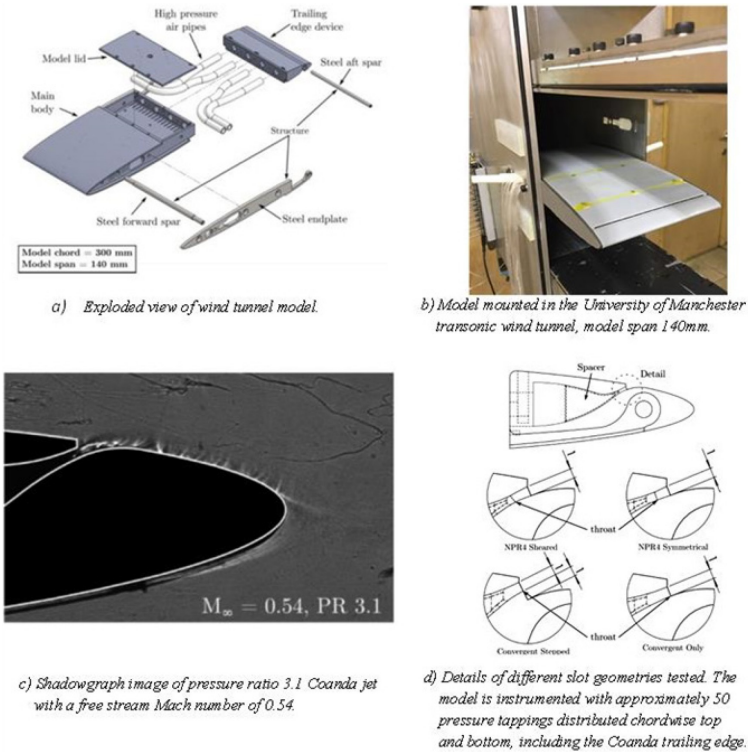

Figure 4-4: Demonstration of a Supersonic CC Effector in a Transonic Wind Tunnel by Llopis-Pascual [2].

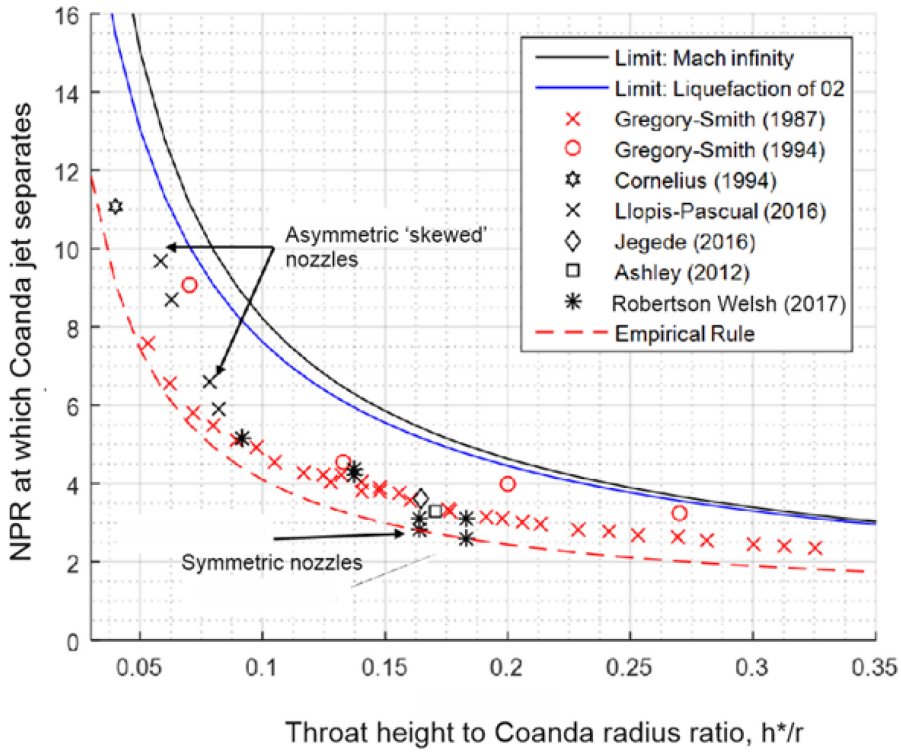

Figure 4-5: The Nozzle Pressure Ratio (NPR) at Which Coanda Jet Separation Occurs is Driven Predominantly by h*/r, Where h* is the Height of the Throat and r is the Coanda Surface Radius, Adapted from [3].

In supporting the experimental work of Llopis-Pascual and Robertson-Welsh; Forster [14], Forster and Steijl [16], Hoholis [13] and Hoholis et al. [18], [19] exploited the capabilities of modern CFD methods to guide fundamental experimental studies and to explore applications to large-scale configurations at full-scale flight conditions including the results presented later in the chapter for the SACCON configuration.

4.3.2 Fluidic Thrust Vectoring

4.3.2.1 Description of FTV Concepts

Vectoring the thrust of a jet engine can be a powerful method of providing control power to effect both trim and manoeuvre. Historically, thrust vectoring has been implemented on aircraft such as the X31 and F22 through provision of complex mechanical systems in which the exhaust nozzle geometry is physically deformed or where movable vanes are provided (Figure 4-6a) and Figure 4-6b)). While most researchers have exploited flow turning through shock waves, the research undertaken by the present authors has focussed on the exploitation of the Coanda effect (Figure 4-6c) and Figure 4-6d)). The primary reasons for this were pre-existing experience with wall bounded flows combined with the expectation that significantly greater vector angles for a given mass flow budget were achievable than could be achieved using shock turning techniques. A major challenge has been the development of approaches to make such systems work when the primary exhaust jet and the flow control jets are supersonic. The understanding of how to condition such high pressure ratio flows to achieve controllable attachment to, and detachment from, the reaction surfaces that has been a significant achievement of this work.

Figure 4-6 depicts FTV concepts exemplified by systems that employ separate upper and lower exhaust nozzle reaction surfaces to achieve both positive and negative vectoring of the jet. Some engine installations, particularly for signature driven reasons require the engine exhaust to be placed on the upper surface of the wing ahead of the trailing edge (e.g., B2 bomber). Such aft-deck installations are less amenable to implementation of a two-reaction surface system. However, with appropriate geometric consideration such installations can be given a pitch vectoring capability as depicted in the schematic of Figure 4-7.

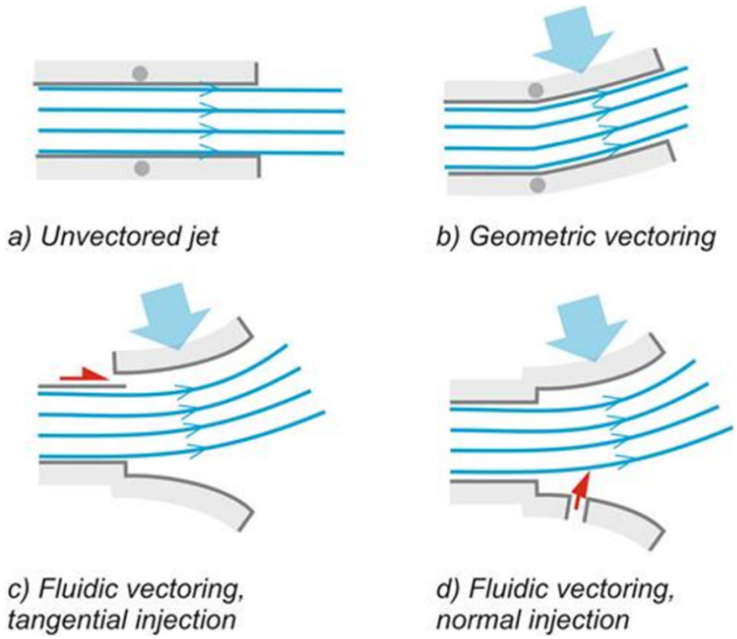

Figure 4-6: Schematic Comparison of Mechanical Thrust Vectoring and the Fluidic Thrust Vectoring Schemes Explored by the Authors.

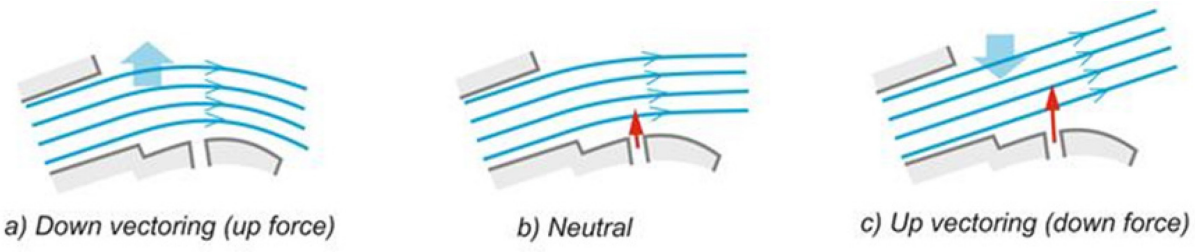

With no fluidic actuation applied, the jet attaches to the adjacent surface and is vectored downwards, case a). As actuation is applied, the jet detachment point moves progressively upstream until the jet separates at the nozzle exit, case c), corresponding to maximum up vectoring. In between there exists a point at which the jet exits horizontally which is the neutral position. Blue arrow is the control output force; red arrow is the fluidic input.

Figure 4-7: Example Implementation of Single Surface (Aft Deck) Fluidic Thrust Vectoring.

4.3.2.2 Historical Development of FTV

A number of Fluidic Thrust Vectoring (FTV) concepts have been developed over the past three decades all of which achieve deflection of a primary jet through flow control as opposed to changes in geometry. Examples of FTV concepts include shock vector control [57]; throat shifting [58]; dual throat [59], [60]; counter-flow [61], [62], [63], [64] and co-flow [5]. Most of these studies have explored jet vectoring about a single axis but others, such as Washington and Alvi [65] have extended this to multiple axis vectoring. Good overviews of the shock control, throat shifting, dual throat and counter-flow methods, their benefits and drawbacks were given by Deere et al. [59], [66], [67], [68], Chambers [69] and Miller et al. [70].

In the early 1990s, work at NASA under the Fluidic Injection Nozzle Technology (FLINT) programme predicted that the potential benefits of fluidic thrust vectoring nozzles would be a 28 – 40 % percent weight reduction by implementing fluidic throat area control, a 43 – 80 % weight reduction by implementing fluidic throat area and exit area control, a 7 – 12 % improvement in engine thrust-to-weight ratio, and a 37 – 53 % reduction in nozzle procurement and life cycle costs [69]. In addition to these considerations, fixed aperture nozzles were said to enhance low-observable characteristics by eliminating moving flaps, discontinuities, and gaps. The improved performance predictions were perhaps in hindsight rather optimistic; or at least it has not been possible to realise the proposed technologies at acceptable cost/risk.

Prior to the year 2000, the majority of research was concentrated on the counter-flow, shock vector control and throat shifting techniques, demonstrating vectoring angles up to approximately 15 degrees for secondary injection mass-flows of around 5 – 10 % of the primary nozzle mass flow [67]. Typically, the best vectoring efficiencies approached 4° of vector angle per percent injected mass flow and system thrust efficiencies were in the range 0.86 to 0.94. Prior to the current authors' research, the co-flow concept does not appear to have been investigated in great depth by others. Inspired and guided by their ongoing research into CC concepts the authors undertook preliminary research into Coanda based co-flow FTV concepts in the late 1990s [5]. This work produced promising results for subsonic primary jets and led to the substantial body of research on applying the technique to supersonic jets being undertaken over the following 17 years (described more fully later in this report).

The research addressed the following challenges:

- To meet various performance requirements the thrust vectoring concept should work efficiently with supersonic primary jets. Ideally deflection efficiencies of better than 5° per percent injection mass flow were desirable in order to meet bleed offtake limitations of the engine.

- It needed to be shown that thrust vector angle response should be substantially linear in order to simplify control implementation, i.e., the force output should vary monotonically with increasing control input and suffer minimal hysteresis.
- It was desirable to show that in addition to vectoring about the pitch axis that concepts could also achieve vectoring about the yaw axis.
- Operation needed to be shown to be insensitive to operation of a fixed geometry exhaust nozzle at 'off-design' conditions.
- Operation needed to be compatible with low-observable design typified by high aspect ratio, rectangular nozzle cross sections and scarfed (swept) nozzle trailing edges It was also desired that nozzle concepts be sympathetic to integration into a an aft-deck configuration.

Subsequent fluidic thrust vectoring research activity then focussed on:

- Understanding the performance of Coanda wall jets operating at supersonic speeds (pressure ratios between 2 and 10) and their ability to entrain a supersonic primary jet (the outer flow in this case). Primary jets from both convergent only (under-expanded) and convergent-divergent (correctly-expanded) nozzles were of interest.
- Developing and validating concepts capable of operating effectively at 'off-design' primary nozzle flow conditions.
- Developing and validating concepts compatible with the requirements of practical implementation (operation, manufacture, and maintainability).

4.3.2.3 Recent Research

Inspired and guided by their ongoing research into CC, the authors initiated a study into the co-flow FTV concept in the late 1990s (undertaken by Mason [20], [21]). This work applied the co-flow approach to subsonic jets from rectangular nozzles and demonstrated vector angles of approximately 20° using secondary/primary mass flow ratios of approximately 5 – 6 %. Subsequently Pilmoor [22] demonstrated the application of high subsonic FTV for the pitch control of a low-observable planform UAV in the wind tunnel and Gill [12] extended this to application on a jet powered flying demonstrator aircraft.

Work on applying the co-flow technique to the vectoring of supersonic primary jets was conducted by Lytton [23] between 2002 and 2005. Lytton demonstrated the ability to deflect an under-expanded, pressure ratio 2.5, supersonic jet through angles in excess of 25° using tangential secondary blowing jets having a secondary to primary mass flow ratio of approximately 15% (Figure 4-8).

Lytton found that, for an under-expanded primary jet with a pressure ratio in excess of approximately 2.7, the interaction of shock waves resulted in premature detachment of the secondary wall jet and rapid loss of thrust vectoring capability. Subsequently, Chippendall [24] explored the co-flow thrust vectoring technique applied to fully-expanded primary jets with a view to overcoming the limitations imposed by shock boundary layer interactions. He concluded that fully expanding the primary jet improved the performance of the co-flow vectoring technique at pressure ratios above 2.7, particularly for the on-design operating condition of the convergent-divergent nozzle. Chippendall [24] also identified key pieces of literature [55], [56] relating to the design and operation of gas burning Coanda flares employed in the gas and oil industry. This literature details many of the shock structure and detachment mechanisms exhibited by supersonic curved wall jets and was subsequently used in the research activities of Forster [14], Llopis-Pascual [2] and Afilaka [25].

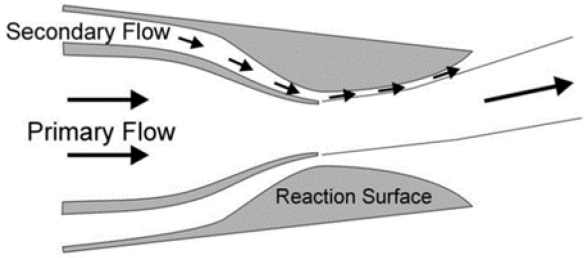

(a) Schematic of the Co-Flow Fluidic Thrust Vectoring Concept.

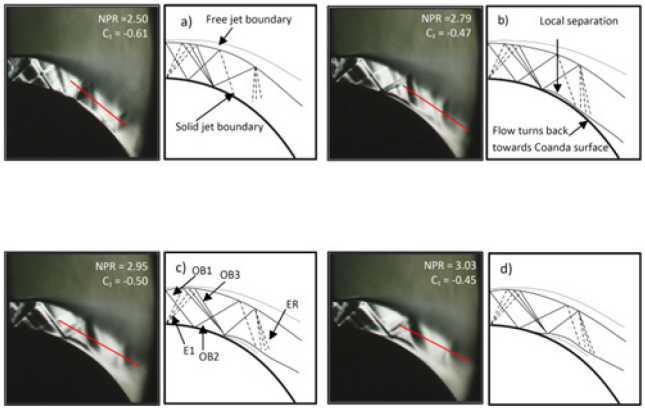

(b) Schlieren Images of Co-Flow Fluidic Thrust Vectoring at a Range of Supercritical Primary Jet Pressure Ratios.

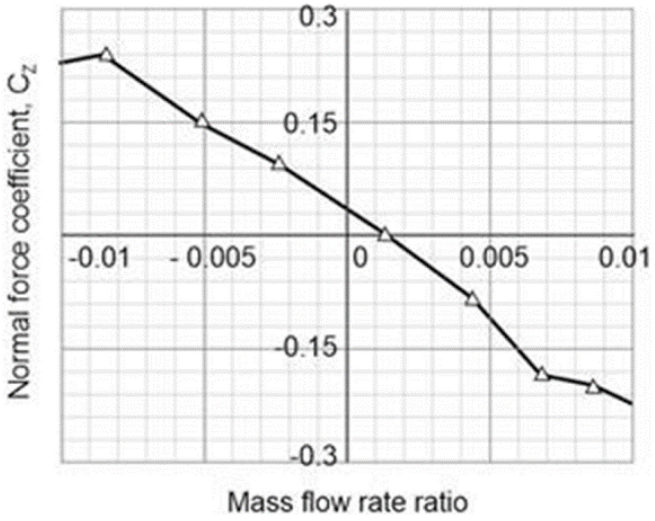

(c) Effectiveness of Co-Flow Fluidic Thrust Vectoring for an NPR 3.0 Primary Jet. C_z is the normal force relative to the undeflected thrust of the primary jet. Mass flow ratio is the ratio of the secondary jet blowing mass flow to that of the primary jet.

Figure 4-8: Co-Flow Fluidic Thrust Vectoring Concept.

Chippendall also identified a publication by Bevilaqua and Lee [54] who proposed a method of improving the attachment of supersonic curved wall jets through skewing a convergent-divergent nozzle to produce a radial pressure profile at the nozzle exit. The method of Bevilaqua and Lee was also explored by Ashley [26] who incorporated the approach to an FTV exhaust nozzle having a single reaction surface (aft deck). Ashley demonstrated the ability of this technique to maintain a pressure ratio 3 primary jet fully attached around a 90° reaction surface (Figure 4-9). Jegede [27] extended this concept to design a nozzle capable of achieving yaw as well as pitch vectoring. Afilaka [25] demonstrated the concept of applying normal blowing through holes, as opposed to tangential blowing through a slot, on the reaction surface to achieve monotonic vectoring of the primary jet using significantly lower secondary mass-flows (Figure 4-10). This was done to overcome the potential structural and manufacturing issues associated with provision of a tangential blowing slot.

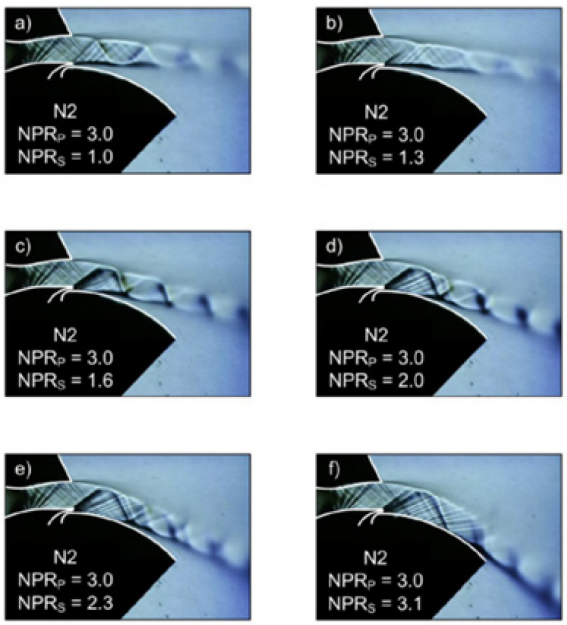

(a) Schlieren Images of Single Reaction Surface Thrust Vectoring System Where Actuation is by Tangential Slot Blowing at the Primary Nozzle Exit.

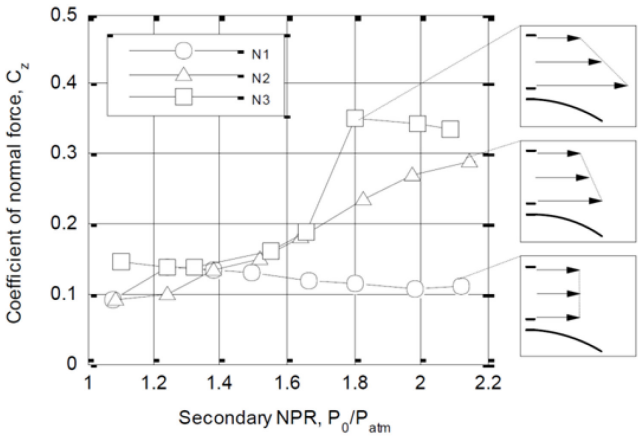

(b) Variation of Normal Force Coefficient with Secondary Blowing for Concept (N2) Depicted in (a)

Figure 4-9: Single Reaction Surface (Aft Deck) Fluidic Thrust Vectoring Concepts Using Tangential Blowing (From Ref. [26]).

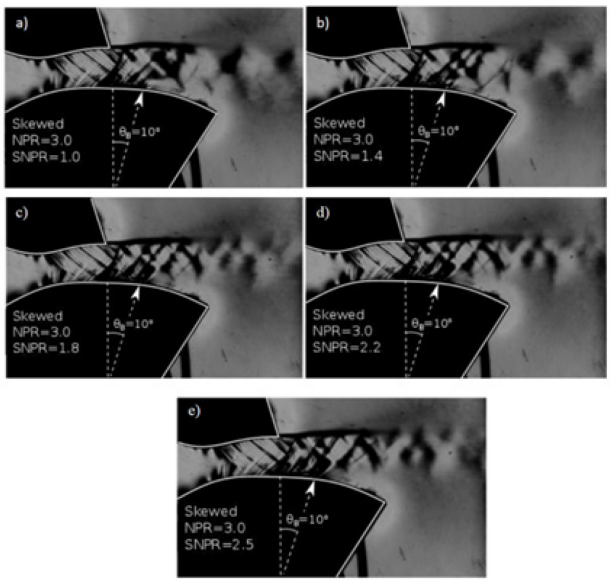

(a) Schlieren Images of Single Reaction Surface Thrust Vectoring System Where Actuation is by Injection Through Spanwise Array of Holes Located on the Reaction Surface Itself.

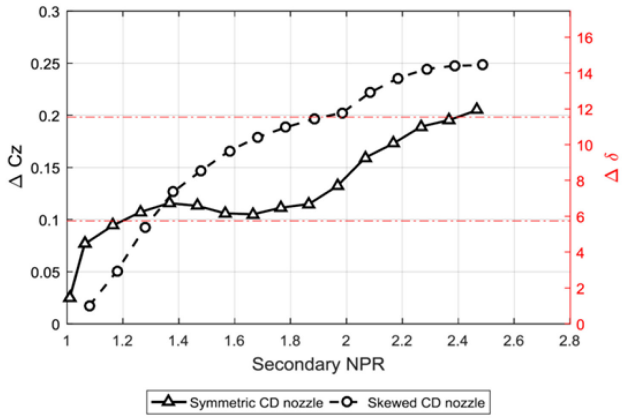

(b) Variation of Thrust Vector Angle with Secondary Blowing for Concept Depicted in (a).

Figure 4-10: Single Reaction Surface (Aft Deck) Fluidic Thrust Vectoring Concept Using Normal Blowing Through Holes in Reaction Surface (From Ref. [27]).

4.4 CIRCULATION CONTROL APPLIED TO THE SACCON CONFIGURATION

4.4.1 Introduction

In order to undertake the mission assessments for the SACCON configurations [31] it was necessary to generate control derivative data for the aircraft operating at the transonic ingress flight condition (Mach 0.7 at 30,000 ft) with CC effectors. Since resources were unavailable to derive this data experimentally it was necessary to resort to the use of CFD analysis that was validated as best as possible against experimental data for both transonic, high pressure ratio CC effectors and for the baseline SACCON configuration.

Experimental results were available for the baseline SACCON configuration from investigations conducted within AVT-201 [71]; here measurements in the BAE Systems High Speed Wind Tunnel (HSWT) at transonic conditions were made for the SACCON model which included the effects of control surface deflections. Complimentary CFD studies were also conducted as part of AVT-201. These experimental and numerical data [72] of SACCON with conventional controls formed a point of reference against which the numerical predictions of CC performance were compared.

4.4.2 Configuration and CC Nozzle Geometry

Preliminary CFD design studies into the effectiveness of supersonic CC effector nozzle geometries in a transonic freestream (Figure 4-11) were undertaken in Ref. [15]. These simulations were instrumental in determining the efficacy of simple convergent nozzles with a stepped exit prior to subsequent experimental testing [2]. Following this validation of the CC device performance, the geometry was assessed on the SACCON configuration using the validated CFD tools.

The SACCON wind tunnel geometry as tested in Ref. [71] and simulated in Ref. [72] is shown in Figure 4-11. The model had two control surfaces on the port side wing which each covered approximately 50% of the wingspan and were labelled as IB Flap and OB Flap for inboard and outboard control surfaces, respectively. Measurements were taken with the control surfaces at -10, 0, and +10 degrees, and in addition a split flap at ±10 degrees deflection was tested at the outboard location.

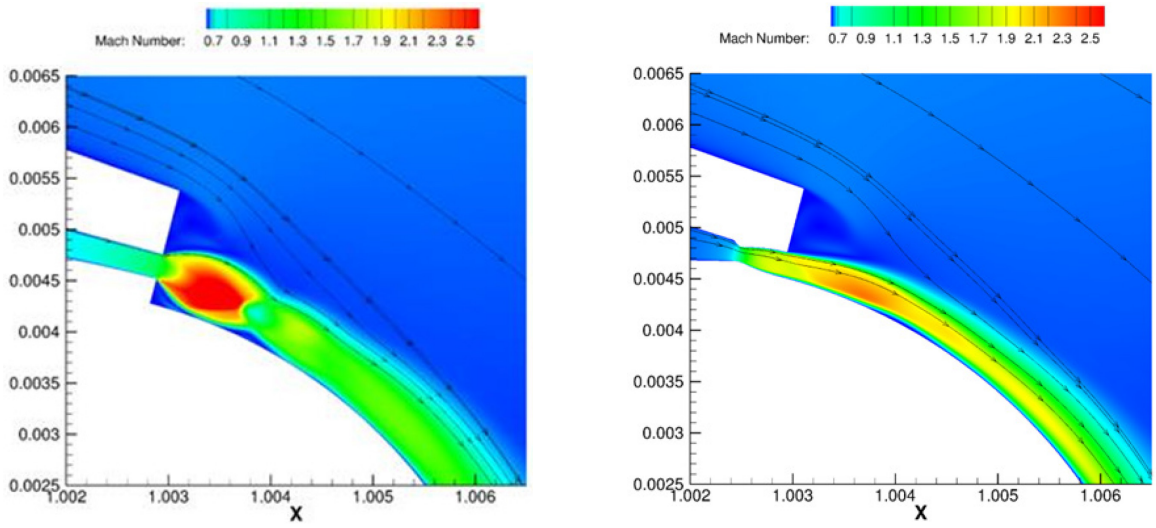

(a) Stepped.

(b) Convergent-Divergent with Skewed Velocity Profile.

Figure 4-11: Simulation of a Supersonic CC Effector for a Range of Nozzle Geometries.

To enable a like-for-like comparison between conventional controls and CC, the flaps were replaced with a CC effector which was split into an inboard and outboard (IBC and OBC) CC effector at the same place as the conventional controls, shown in Figure 4-12. The Coanda geometry shown in Figure 4-12 had a radius of 0.4% Cref at the root and 0.3% C_{ref} at the tip, with a 20:1:1 radius-to-step-to-slot ratio. All CFD results presented here use only the inboard (IBC) and are compared against IB Flap results from experiments [71] and simulations [72].

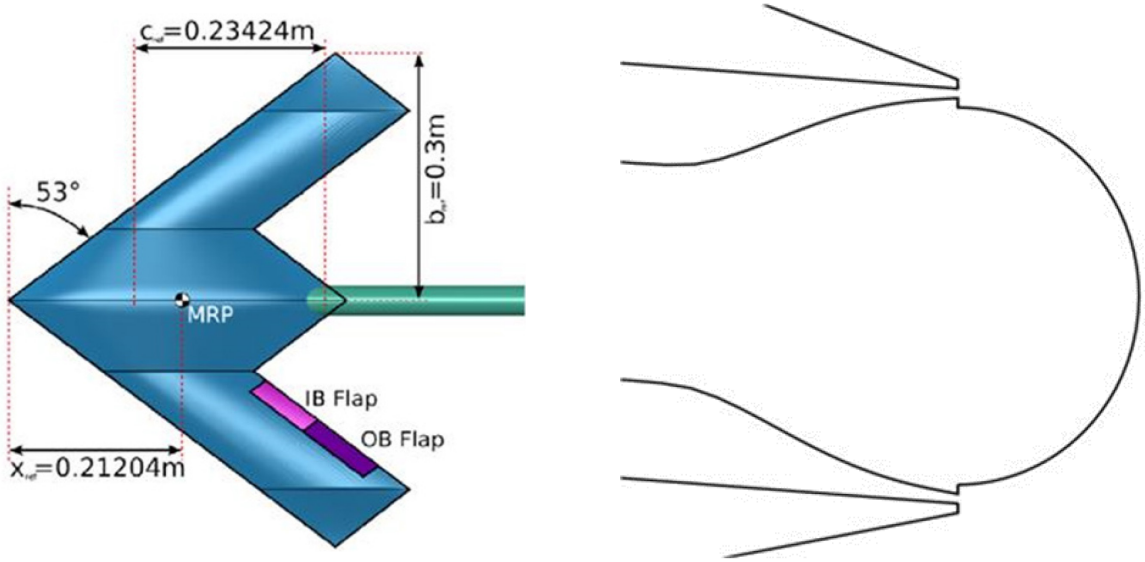

(a) SACCON Geometry and Reference Lengths [73].

(b) Cross Section of Trailing Edge Modified with CC Effector.

Figure 4-12: SACCON Configuration Showing Location of Flaps and the CC Effector Geometry.

4.4.3 Computational Methodology

The Helicopter Multi-block (HMB2) [74], [75] CFD solver of The University of Liverpool was used for this work. HMB2 is a compressible, cell-centred finite volume CFD code which solves the Reynolds-averaged Navier-Stokes equations on block-structured grids. The solver has been validated for a number of applications, including helicopters; wind turbines; turboprops; and high speed unmanned combat aerial vehicles [76]. In addition, validation of the solver and boundary conditions for CC in subsonic [18] and transonic [16] freestreams has been performed, for which comparisons with measured experimental results of circulation control were conducted. While a variety of turbulence models are available in HMB2, the simulations presented here use the Menter k-ω SST model.

CFD grids used in this study were modified using grid topologies built by Hoholis [19], which had been used to investigate CC on the SACCON at low freestream speeds. Grid spacing and block-edge dimensions used followed the recommendations of Kennett [72]. However, it was necessary to include additional cells to account for the refinement required near the Coanda surface. A grid refinement study using a half span model for the SACCON configuration with CC blowing in transonic freestream [14] concluded that a grid with 12.5 million cell volumes was appropriate to achieve mesh-independent results. Therefore, the full span model had 25 million cells. Figure 4-13 shows the grid that was used to generate CFD predictions of CC applied to the SACCON as presented in this report.

The trailing edge of the SACCON geometry was modified to accommodate CC effectors [18] by truncating and applying a rounded profile to the trailing edge. A comparison of the aerodynamic behaviour of the modified SACCON against the baseline model as studied in AVT-201 was made. Figure 4-14 shows a

comparison between CFD results from Kennett [72], the baseline transonic experimental measurements [71] and the modified SACCON configuration. The modifications to the geometry to accommodate the CC device appear to have had little effect on the response in the pitching moment for $\alpha < 10^{o}$. The peak in pitching moment at $\alpha = 17.5^{o}$ for the original unmodified geometry occurred at $\alpha = 15^{o}$ for the unblown CC. This is thought to be largely due to the differences in turbulence model chosen, since Kennett used a k-ω model with a vortex limiter and the CC simulations here are with the k-ω SST without a vortex limiter. However, these results provide confidence that meaningful comparisons between the SACCON with CC and conventional control surfaces can be made for $\alpha < 10^{o}$.

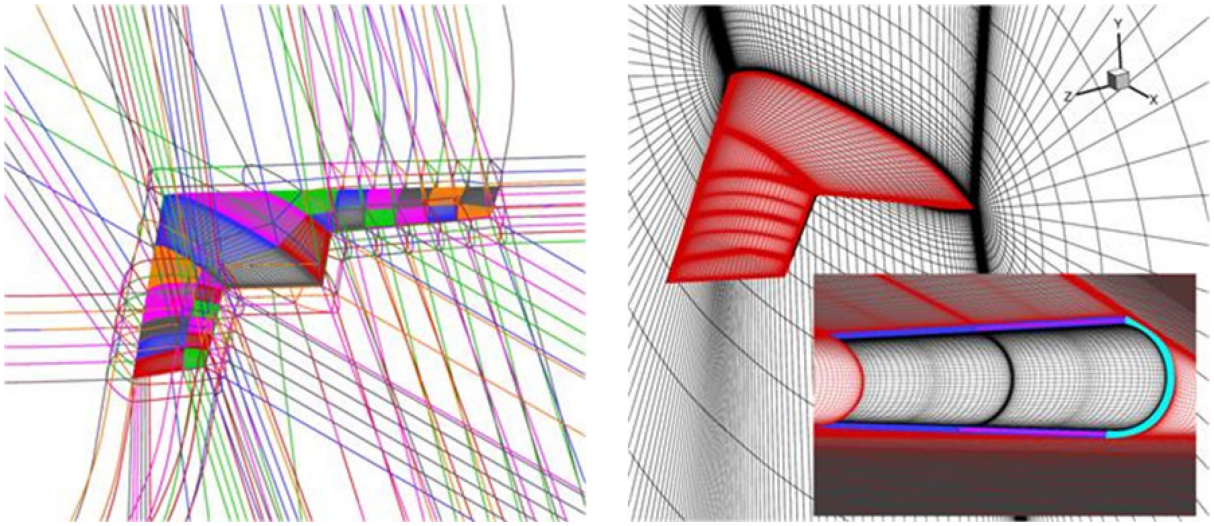

(a) Block-Structured Grid Topology.

(b) View of Surface Mesh and Slice Through Volume. Inset Shows the Surface Grid Over the CC Effector.

Figure 4-13: CFD Grid Used for Simulations of SACCON with CC (From [14]).

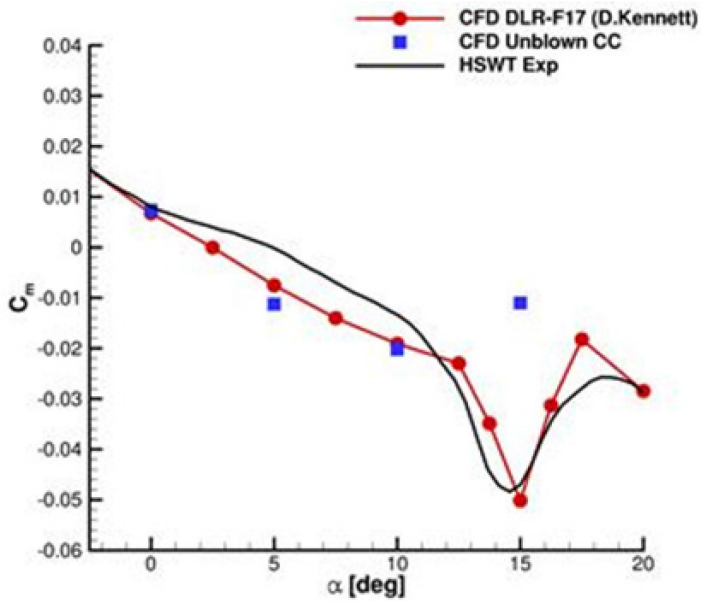

Figure 4-14: Pitching Moment Coefficient vs. Angle of Attack for Baseline SACCON CFD [72] and Experiment [71], and Modified SACCON with Unblown CC Effector.

4.4.4 Results

4.4.4.1 Control Authority of CC Effector

Results were obtained using half span simulations that were converted to full span using a first-order force reduction method which combined loads and moments from two half span results. A description of the force reduction process is given by Coppin [77] who applied this approach on CFD simulations of the baseline SACCON.

Blowing over the upper slot of the left hand side inboard Coanda (IBC+) resulted in attachment of the jet until NPR = 4.0 (Cμ = 3.0 × 10-4). At blowing rates above NPR = 4.5 (Cμ = 3.4 × 10-4) the jet detached from the upper surface. As shown in Figure 4-15 and Figure 4-16, the effect of the detachment caused a significant drop in the loads and moments generated by the circulation control device. Blowing over the lower slot (IBC-) gave an approximately symmetric shift in the loads and moments. In Figure 4-15 and Figure 4-16, "negative Cμ" corresponds to blowing over the lower surface of the Coanda. At Cμ = (-)3.0 × 10-4 (lower slot blowing) the jet starts to detach from the Coanda surface towards the root of the slot. The effect on the loads and moments are most evident at 5 degrees angle of attack. Figure 4-17 shows that the jet remained attached only to the middle section of the inboard Coanda control surface with blowing at Cμ = (-)3.0 × 10-4 and α = 5°.

A table of these results using half span simulations is given in Table 4-1, Table 4-2 and Table 4-3, which include the effect of blowing through both slots to produce yaw control in Table 4-3. These data were used in performance and system integration studies in Ref. [31].

Table 4-1: Incremental Force and Moment Coefficients Due to Port Side Inboard Blowing at 0 Degrees Angle of Attack.

NPR	C_μ	Lift ΔC_L	Drag ΔC_D	Side ΔC_Y	Roll ΔC_l	Pitch ΔC_m	Yaw ΔC_n
-4.00E+00	-2.99E-04	-2.70E-02	9.57E-04	3.65E-05	-1.34E-02	1.15E-02	-6.27E-04
-3.00E+00	-2.21E-04	-2.36E-02	6.69E-04	-1.70E-04	-1.15E-02	9.70E-03	-3.59E-04
-2.00E+00	-1.35E-04	-1.58E-02	3.44E-04	-2.20E-04	-7.66E-03	6.48E-03	-1.48E-04
0.00E+00	0.00E+00	0.00E+00	0.00E+00	0.00E+00	0.00E+00	0.00E+00	0.00E+00
2.00E+00	1.35E-04	1.52E-02	3.46E-05	6.43E-04	7.42E-03	-6.29E-03	-2.06E-04
3.00E+00	2.20E-04	2.23E-02	1.96E-04	1.09E-03	1.09E-02	-9.17E-03	-4.25E-04
4.00E+00	2.98E-04	2.72E-02	3.16E-04	1.39E-03	1.33E-02	-1.13E-02	-5.85E-04
4.50E+00	3.36E-04	6.29E-03	-2.13E-04	5.99E-05	3.05E-03	-2.61E-03	9.82E-05
5.00E+00	3.75E-04	5.58E-03	-2.40E-04	1.24E-05	2.72E-03	-2.34E-03	1.25E-04

Table 4-2: Incremental Force and Moment Coefficients Due to Port Side Inboard Blowing at 5 Degrees Angle of Attack.

NPR	C_μ	Lift ΔC_L	Drag ΔC_D	Side ΔC_Y	Roll ΔC_l	Pitch ΔC_m	Yaw ΔC_n
-4.00E+00	-2.99E-04	-1.93E-02	-6.36E-04	7.45E-04	-9.38E-03	7.88E-03	-8.36E-04
-3.00E+00	-2.21E-04	-2.57E-02	-6.70E-04	1.16E-03	-1.26E-02	1.08E-02	-1.29E-03

NPR	C_μ	Lift ΔC_L	Drag ΔC_D	Side ΔC_Y	Roll ΔC_l	Pitch ΔC_m	Yaw ΔC_n
-2.00E+00	-1.37E-04	-1.78E-02	-6.27E-04	6.14E-04	-8.65E-03	7.37E-03	-7.29E-04
0.00E+00	0.00E+00	0.00E+00	0.00E+00	0.00E+00	0.00E+00	0.00E+00	0.00E+00
2.00E+00	1.32E-04	1.29E-02	7.54E-04	-9.89E-05	6.24E-03	-5.33E-03	2.45E-04
3.00E+00	2.20E-04	2.03E-02	1.32E-03	-2.95E-05	9.85E-03	-8.40E-03	2.75E-04
4.00E+00	2.98E-04	2.54E-02	1.76E-03	9.28E-05	1.24E-02	-1.05E-02	2.35E-04
4.50E+00	3.36E-04	7.05E-03	2.11E-04	-2.34E-04	3.44E-03	-2.98E-03	2.96E-04
5.00E+00	3.74E-04	6.34E-03	1.40E-04	-2.48E-04	3.13E-03	-2.73E-03	3.03E-04

Table 4-3: Incremental Force and Moment Coefficients Due to Port Side Inboard Blowing at 0 Degrees Angle of Attack Using Both Upper and Lower Slots Together.

NPR	C_μ	Lift ΔC_L	Drag ΔC_D	Side ΔC_Y	Roll ΔC_l	Pitch ΔC_m	Yaw ΔC_n
3.00E+00	4.40E-04	-6.32E-04	-2.02E-04	-1.89E-04	-3.28E-04	2.81E-04	1.64E-04
5.00E+00	7.50E-04	-2.59E-03	-3.79E-04	2.65E-03	-4.79E-03	-2.90E-04	3.87E-04

4.4.4.2 Comparison of CC Effector with Conventional Control

Numerical simulations of CC here use the full span grid with blowing only over the port side wing, in line with the experiments. Experimental results of flaps are taken from the BAE Systems' HSWT data set [71], while the CFD flapped results are from Kennett [72].

Comparisons were made between the SACCON configuration with an inboard flap at 10 degrees positive and negative deflection angles (IB+10, IB-10 respectively) and the stepped inboard Coanda (IBC) device blowing from the upper, lower and both slots at NPR+3, NPR-3 and NPR±3, respectively. This corresponds to $C_\mu = 2.2 \times 10^{-4}$, and $C_\mu = 4.4 \times 10^{-4}$ when using both slots. Figure 4-18 shows the moment results of this comparison; up to 15 degrees angle of attack the CC effector produced a higher control authority than the equivalent conventional controls with 10 degrees flap incidence.

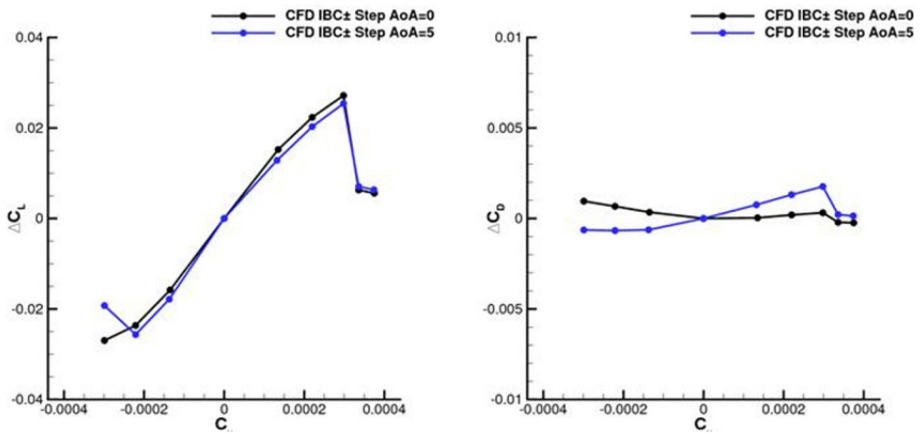

Figure 4-15: ΔC_L and ΔC_D with Respect to Blowing from the Circulation Control Device at the Inboard of the Left Wing (IBC) at 0 and 5 Degrees Angle of Attack. "Negative" C_μ Corresponds to Blowing over the Lower Slot (IBC-).

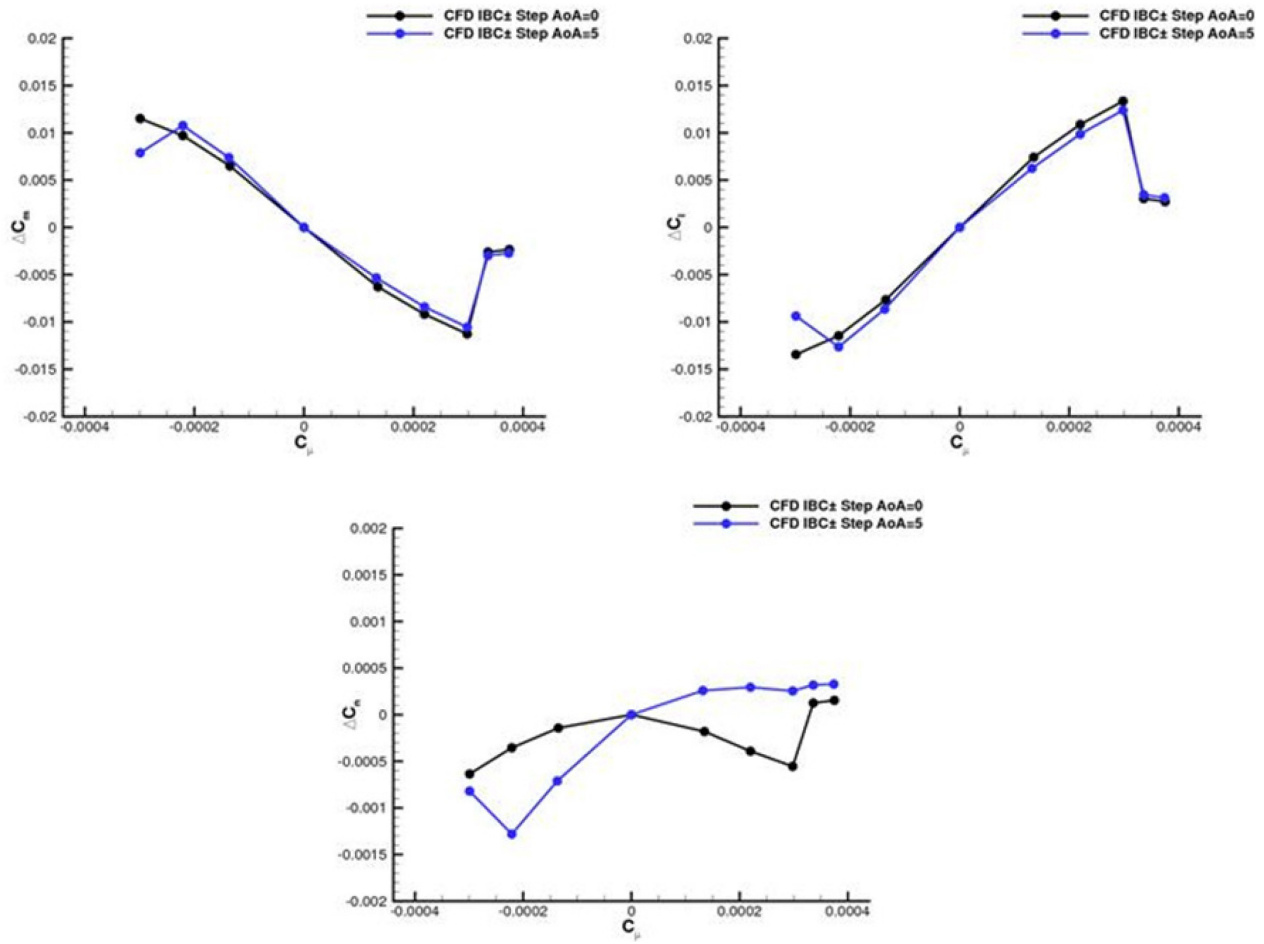

Figure 4-16: Pitch (C_m), Roll (C_l) and Yaw (C_n) Moment Coefficients with Respect to Blowing at the Inboard of the Left Wing (Lower Slot Negative C_μ).

In addition, the blue symbols in Figure 4-18 show the effect of blowing through both upper and lower slots together on the inboard port side wing. This actuation results in a thrust over the port side wing and thus produces a yawing moment of approximately $C_n = 3 \times 10^{-4}$, without a significant change in the roll and pitching moments. With split flaps deflected to 10 degrees in the outboard side of the wing a yaw moment coefficient of $C_n = -5 \times 10^{-4}$ was achieved in the experiments. Taking into account the ratio of the moment arm between the centre of the outboard and inboard flaps (~1.5), and that the split flaps produce a drag rather than a thrust; it is estimated that the CC effectors have approximately the same control authority as split flaps for yaw control.

4.5 CONCLUSIONS

This chapter has surveyed fluidic flight control effectors in the form of wing trailing edge Circulation Control and Fluidic Thrust Vectoring suitable for application to a low-observable combat aircraft configuration. The objective of employing such novel control effectors would be to negate the requirement to deflect conventional moving trailing edge control surfaces during the ingress phase of a mission. The survey has shown that both technologies have relevance to the application and are capable of providing levels of control effectiveness of a similar magnitude to that achievable with conventional trailing edge controls. Recent developments in Trailing Edge CC technology allow installation into trailing edges having a thickness similar to that of wings with conventional control surfaces. The effectiveness and efficiency of a

CC system for application to an aircraft travelling at high subsonic speeds is achieved by maximising the exit velocity of the Coanda jet which gives rise to the highest blowing momentum coefficient for a given blowing mass flow. Supersonic wall jet velocities are achievable and, with careful consideration of the CC nozzle exit height and geometry, attachment of the Coanda wall jet can be achieved for high pressure ratios and small trailing edge Coanda surface radii. Effective CC devices operating at nozzle pressure ratios of up to 7 and beyond combined with trailing edge radii of a few mm have been demonstrated experimentally.

The available experimental data for high pressure ratio CC devices applied on wing sections operating at transonic freestream speeds has been used to successfully validate CFD tools. These CFD tools have been used to generate control effectiveness data for the NATO AVT SACCON configuration operating at a transonic ingress flight condition. This data is suitable for use in a mission assessment of the aircraft to determine the ability of these control effectors to generate sufficient control power to achieve trim, manoeuvre and the rejection of gusts and turbulence.

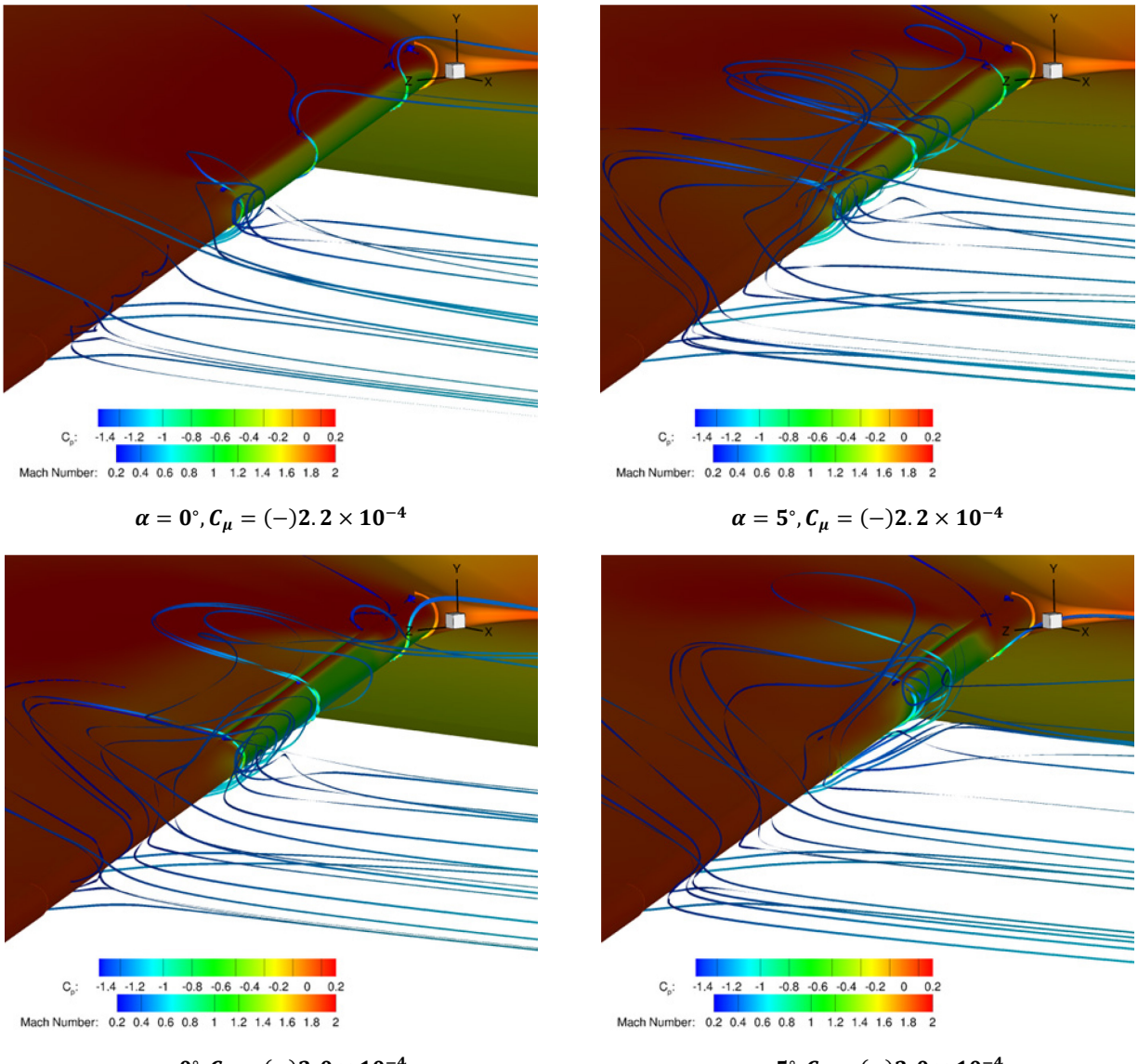

$\alpha = 0°, C_\mu = (-)2.2 \times 10^{-4}$ $\alpha = 5°, C_\mu = (-)2.2 \times 10^{-4}$

$\alpha = 0°, C_\mu = (-)3.0 \times 10^{-4}$ $\alpha = 5°, C_\mu = (-)3.0 \times 10^{-4}$

Figure 4-17: Stream-Trace Ribbons and Surface C_p with Blowing Over Lower CC Effector Slot.

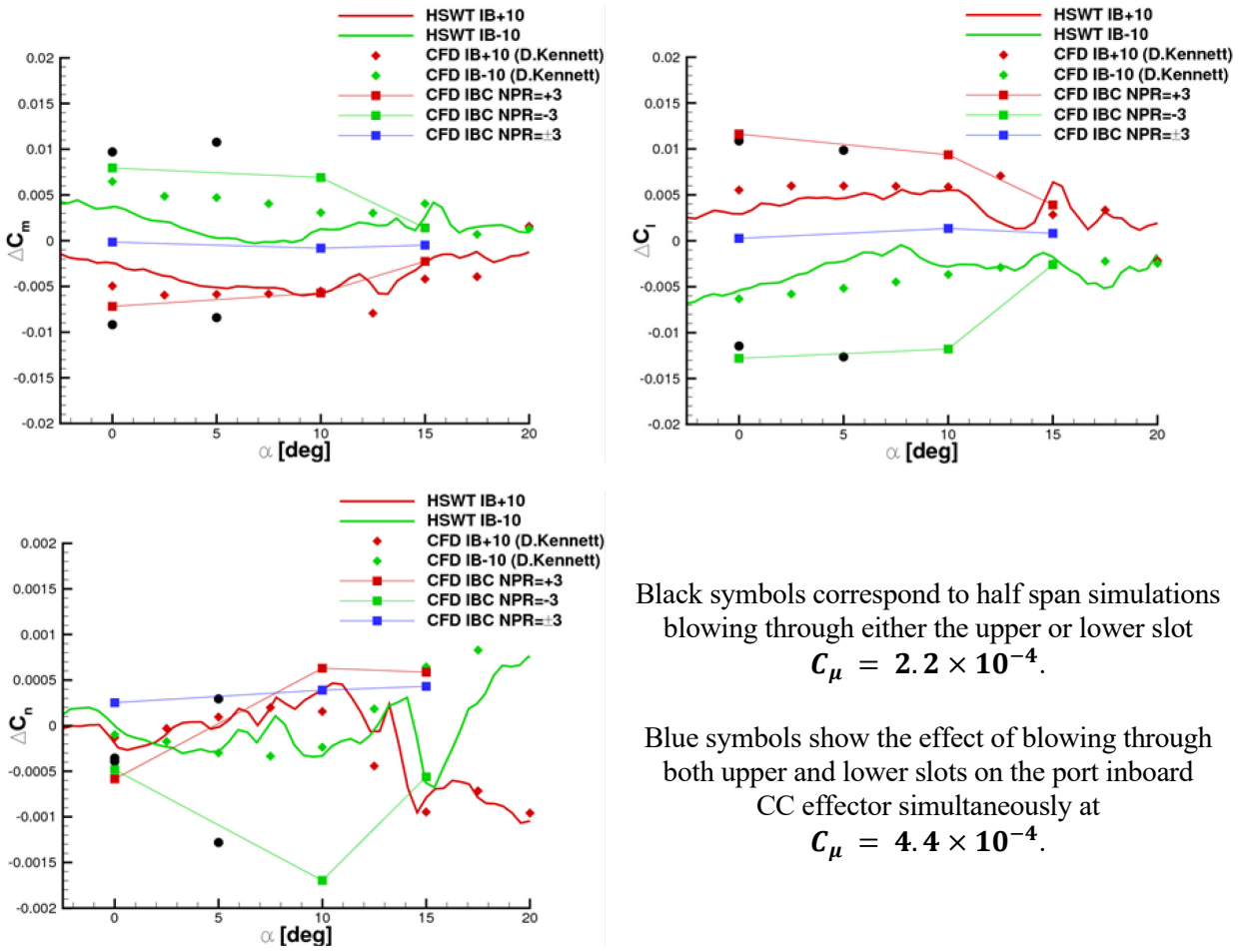

Figure 4-18: Difference in Pitch (C_m), Roll (C_l) and Yaw (C_n) Moment Coefficients Due to Control Effectors. Experimental Results from the HSWT and CFD from Kennett Correspond to the Port Side IB Flap at 10 Degrees Deflection. CC Effectors here were Applied Only to the Port Side Inboard and Were Operated at NPR = 3. (From Ref. [14]).

4.6 ACKNOWLEDGEMENTS

The authors would like to acknowledge the contributions of their co-workers and of the numerous PhD students at Manchester and Liverpool Universities who contributions over the years made the work described in this chapter possible. They would also like to acknowledge the significant financial contribution made to the various research projects discussed herein made by BAE Systems, the UK Engineering and Physical Sciences Research Council, the UK Defence Science and Technology Laboratory (Dstl) and the universities of Manchester and Liverpool.

4.7 REFERENCES

[1] Frith S., Flapless Control for Low Aspect Ratio Wings, Manchester, 2007.

[2] Llopis-Pascual, A., Supercritical Coanda Jets for Flight Control Effectors, PhD Thesis, Manchester University, Manchester, 2016.

[3] Robertson-Welsh, B., Adaptive Nozzles for High Speed Circulation Control, PhD Thesis, Manchester University, Manchester, 2017.

[4] Wilde, P.I.A., The Application of Circulation Control for Three Axis Control of a Tailless Aircraft, PhD Thesis, Manchester University, Manchester, 2009.

[5] Crowther, W.J. and Mason, M.S., Fluidic Thrust Vectoring of Low Observable Aircraft, CEAS Aerospace Aerodynamic Research Conference, Cambridge, 2002.

[6] Liddle, S., Flow Control to Enhance Aileron Effectiveness, PhD Thesis, Manchester University, Manchester, 2006.

[7] Wilde, P.I.A., Crowther, W.J. and Harley C.D., Application of Circulation Control for Three-Axis Control of a Tailless Flight Vehicle, Proceedings of the Institution of Mechanical Engineers, Part G: *Journal of Aerospace Engineering*, Vol. 224, No. 4, pp. 373-386, 2010. doi: 10.1243/09544100 JAERO568.

[8] Frith, S.P. and Wood, N.J., The Use of Circulation Control for Flight Control, NASA/ONR Circulation Control Workshop, NASA/CP-2005-213509, 2004, pp. 657-688.

[9] Michie, S., Development of Flight-Ready Circulation Control Manoeuvre Effectors, PhD Thesis, Manchester University, Manchester, 2009.

[10] Gill, K.S., Wilde, P.I.A., Geroult, R. and Crowther, W.J., Development of an Integrated Propulsion and Pneumatic Power Supply System for Flapless UAVs, 7th AIAA Aviation Technology, integration and Operations Conference (ATIO), Paper AIAA 2007-7726, Belfast, 2007. doi: 10.2514/6.2007-7726.

[11] Wilde, P.I.A., Gill, K.J., Michie, S., Sparkes, R. and Crowther, W.J., Integrated Design of a Model-Scale Gas Turbine Powered Flapless Demonstrator Aircraft: A Case Study, 7th AIAA Aviation Technology, Integration and Operations Conference (ATIO), Paper AIAA 2007-7727, Belfast, 2007. doi: 10.2514/6.2007-7727.

[12] Gill, K.J., The Development of Coflow Fluidic Thrust Vectoring Systems, PhD Thesis, Manchester University, Manchester, 2009.

[13] Hoholis, G., Assessment of Fluidic Control Effectors Using Computational Fluid Dynamics, PhD Thesis, Liverpool University, Liverpool, 2016.

[14] Forster, M.J., Computational Modelling of Transonic Circulation Control, PhD Thesis, Liverpool University, Liverpool, 2017.

[15] Forster, M.J. and Steijl, R., Design Study of Coanda Devices for Transonic Circulation Control, *The Aeronautical Journal*, Vol. 121, No. 1243, 2017, pp. 1368-1391. doi: 10.1017/aer.2017.65.

[16] Forster, M.J. and Steijl, R., Numerical Simulation of Transonic Circulation Control, 53rd AIAA Aerospace Sciences Meeting, Kissimmee, 2015. doi: 10.2514/6.2015-1709.

[17] Forster, M.J. and Steijl, R., Circulation Control for High-Speed Unmanned Combat Air Vehicles, UK Royal Aeronautical Society 2016 Applied Aerodynamics Conference, Bristol, 2016. doi: 10.13140/ RG.2.2.31209.08805.

[18] Hoholis, G., Steijl, R. and Badcock, K., Circulation Control as a Roll Effector for Unmanned Combat Aerial Vehicles, *Journal of Aircraft*, Vol. 53, No. 6, 2016, pp. 1875-1889. doi: 10.2514/1.C033642.

[19] Hoholis, G., Steijl, R. and Badcock, K., The Application of Trailing Edge Circulation Control as a Roll Effector for Unmanned Combat Aerial Vehicles, Royal Aeronautical Society Applied Aerodynamics Conference, Bristol, 2014.

[20] Mason, M. Fluidic Thrust Vectoring for Low-Observable Aircraft, PhD Thesis, Manchester University, Manchester, 2003.

[21] Mason, M. and Crowther, W.J., Fluidic Thrust Vectoring of Low Observable Aircraft, CEAS Aerospace Research Conference, Cambridge, 2002.

[22] Pilmoor, M., Pitch Control of a Low Observable UAV Using Fluidic Thrust Vectoring, PhD Thesis, Manchester University, Manchester, 2009.

[23] Lytton, A., Large-Scale Application of Fluidic Thrust Vectoring, PhD Thesis, Manchester University, Manchester, 2005.

[24] Chippindall, J., Geometric Optimisation of Nozzles for Supersonic Fluidic Thrust Vectoring, PhD Thesis, Manchester University, Manchester, 2010.

[25] Afilaka, O., Normal Blowing Fluidic Thrust Vectoring for Supercritical Aft-deck Convergent-Divergent Nozzles, PhD Thesis, Manchester University, Manchester, 2017.

[26] Ashley, J., Aft Deck Supersonic Thrust Vectoring, PhD Thesis, Manchester University, Manchester, 2011.

[27] Jegede, O., Dual-Axis Fluidic Thrust Vectoring of High Aspect-Ratio Supersonic Jets, PhD Thesis, Manchester University, Manchester, 2016.

[28] Warsop, C., and Crowther, W.J., Fluidic Thrust Vectoring and the FLAVIIR DEMON Flight Demonstration Airvehicle, NATO STO Symposium, Innovative Control Effectors for Military Vehicles, STO-MP-AVT-215, Paper No. 11, Stockholm, 2013.

[29] Chard, J., Jegede, O., Llopis-Pascual, A. and Crowther, W.J., Towards High Speed Fluidic Flight Controls, NATO STO Symposium, Innovative Control Effectors for Military Vehicles, STO-MP-AVT-215, Paper No. 14, Stockholm, 2013.

[30] Warsop, C., and Crowther, W.J., Fluidic Flow Control Effectors for Flight Control, *AIAA Journal*, Vol. 56, No. 10 (2018), pp. 3808-3824. doi: 10.2514/1.J056787.

[31] Hutchin, C., NATO AVT-239: Control Effectiveness and System Sizing Requirements for Integration of Fluidic Flight Controls on the SACCON Aircraft Configuration, AIAA Paper 2019-0280, 2019 AIAA Aerospace Sciences Meeting (AIAA 2019), San Diego, CA.

[32] Coanda, H., Device for Deflecting a Stream of Elastic Fluid Projected into an Elastic Fluid, US patent No. US2052869 A, 1936.

[33] Davidson, I.M., Aerofoil Boundary Layer Control Systems, US patent office patent number US3062483 A, 1962.

[34] Englar, R.J., Experimental Investigation of the High Velocity Coanda Wall Jet Applied to Bluff Trailing Edge Circulation Control Airfoils, David W Taylor Naval Ship Research and Development Center, Bethesda, 1975.

[35] Englar, R.J., Two-Dimensional Transonic Wind Tunnel Tests of Three 15-Percent Thick Circulation Control Airfoils, David W Taylor Naval Ship Research and Development Center, Washington, D.C., 1970.

[36] Englar, R.J., Hemmerly, R.A., Taylor, D.W., Moore, W.H., Seredinsky, V., Valckenaere, W. and Jackson, J.A., Design of the Circulation Control Wing Stol Demonstrator Aircraft, *J. Aircraft*, Vol. 18, No. 1, 1981, pp. 51-88. doi: 10.2514/3.57463.

[37] Abramson, J. and Rogers, R.E., High-Speed Characteristics of Circulation Control Airfoils, AIAA 21st Aerospace Sciences Meeting, AIAA 83-0265, Reno, 1983. doi: 10.2514/6.1983-265.

[38] Holz, R.G., Hassan, A.A. and Reed, H.L., Numerical Model for Circulation-Control Flows, AIAA Journal, Vol. 32, No. 4, 1994, pp. 701-707. doi: 10.2514/3.12042.

[39] Englar, R.J., Lynn, T. and Rodney, H.A., STOL Potential of the Circulation Control Wing for High-Performance Aircraft, *J. Aircraft,* Vol. 15, No. 3, 1978, pp. 175-181. doi: 10.2514/3.58337.

[40] Liu, Y., Sankar, L.N., Englar, R.J., Ahuja, V. and Gaeta, R., Computational Evaluation of the Steady and Pulsed Jet Effects on the Performance of a Circulation Control Wing Section, 42nd AIAA Aerospace Sciences Meeting and Exhibit, Paper AIAA 2004-56, Reno, 2004. doi: 10.2514/6.2004-56.

[41] Nishino, T. and Shariff, K. Effect of Jet Nozzle Lip Momentum Loss on Circulation Control Airfoil Performance, *AIAA Journal*, Vol. 50, No. 3, 2011, pp. 551-558. doi: 10.2514/1.J051196.

[42] Wood, N.J. and Nielsen, J.N., Circulation Control Airfoils – Past, Present, Future, 23rd AIAA Aerospace Sciences Meeting, Reno, 1985.doi: 10.2514/6.1985-204.

[43] Wood, N.J. and Nielsen J.N., Circulation Control Airfoils as Applied to Rotary-Wing Aircraft, *J. Aircraft*, Vol. 23, No. 12, 1986, pp. 865-875. doi: 10.2514/3.45394.

[44] Kweder, J., Panther, C.C. and Smith, J.E. Applications of Circulation Control, Yesterday and Today, *International Journal of Engineering*, Vol. 4, No. 5, 2010, pp. 411-429.

[45] Jones, G.D. and Joslin, R.D., Progress in Astronautics and Aeronautics: Applications of Circulation Control Technology, American Institute of Aeronautics and Astronautics, 2006. doi: 10.2514/ 4.866838.

[46] Zeidler, M., Garnier, E., Cayzak, R. and Merlen, A., Fluidic Control of a 155 Millimeter Spin-Stabilized Projectile Using Coanda Effect, *AIAA Journal,* Vol. 53, No. 5, 2015, pp. 1146-1158. doi: 10.2514/1.J053085.

[47] Englar, R.J., Circulation Control Pneumatic Aerodynamics: Blown Force and Moment Augmentation and Modification; Past, Present and Future, AIAA Fluids 2000 Conference and Exhibit, AIAA 2000-2541, Denver, 2000. doi: 10.2514/6.2000-2541.

[48] Jones, G.S. and Englar, R.J., Advances in Pneumatic – Controlled High – Lift Systems Through Pulsed Blowing, 21st AIAA Applied Aerodynamics Conference, AIAA 2003, 3411, Orlando, 2003. doi: 10.2514/6.2003-3411.

[49] Englar, R.J. and Williams, R.M., Design of a Circulation Control Stern Plane for Submarine Applications, Naval Ship Research and Development Centre Technical Note AL-200, Bethesda, 1971.

[50] Buananno, A, Aerodynamic Circulation Control for Flapless Flight Control of an Unmanned Air Vehicle, PhD Thesis, Cranfield University, Cranfield, 2009.

[51] Jamil, R., Multi-Objective Control Allocation, PhD Thesis, Cranfield University, Cranfield, 2011.

[52] Englar, R.J., Development of the A-6/Circulation Control Wing Flight Demonstrator Configuration, David W Taylor Naval Ship Research and Development Centre, DTNSR DC/ASED-79/01, Bethesda, 1979.

[53] Wood, N.J. and Conlon J.A., The Performance of a Circulation Control Airfoil at Transonic Speed, *AIAA 21st Aerospace Sciences Meeting*, Paper AIAA 83-0083, Reno, 1983. doi: 10.2514/6.1983-83.

[54] Bevilaqua, P.M. and Lee, J.D., Development of a Nozzle to Improve the Turning of Supersonic Coanda Jets, Rockwell International Corp, Final Technical Report, Columbus, 1980.

[55] Gregory-Smith, D.G. and Senior, P., The Effects of Base Steps and Axisymmetry on Supersonic Jets Over Coanda Surfaces, *International Journal of Heat and Fluid Flow*, Vol. 15, No. 4, 1994, pp. 291-298. doi: 10.1016/0142-727X(94)90014-0.

[56] Carpenter, P.W. and Smith, C., The Aeroacoustics and Aerodynamics of High-Speed Coanda Devices, Part 2: Effects of Modifications for Flow Control and Noise Reduction, *Journal of Sound and Vibration*, Vol. 208, No. 5, 1997, pp. 803-822. doi: 10.1006/jsvi.1997.1203.

[57] Abeyounis, W.K. and Bennett, B.D., Static Internal Performance of an Overexpanded, Fixed-Geometry, Nonaxisymmetric Nozzle with Fluidic Pitch-Thrust-Vectoring Capability, NASA TP-3645, 1997.

[58] Miller, D.N., Yagle, P.J. and Hamstra, J.W., Fluidic Throat Skewing for Thrust Vectoring in Fixed Geometry Nozzles, 37th AIAA Aerospace Sciences Meeting and Exhibit, paper AIAA 99-0365, Reno, 1999. doi: 10.2514/6.1999-365.

[59] Deere, K.A., Berrier, B.L., Flamm, J.D. and Johnston, S.K., A Computational Study of a New Dual Throat Fluidic Thrust Vectoring Nozzle Concept, 41st AIAA/ASME/SAE/ASEE Joint Propulsion Conference and Exhibit, Paper AIAA 2005 3502, Tucson, 2005. doi: 10.2514/6.2005-3502.

[60] Ferlauto, M. and Marsilio, R., Numerical Investigation of the Dynamic Characteristics of a Dual-Throat-Nozzle for Fluidic Thrust-Vectoring, AIAA Journal, Vol. 55, No. 1, 2017, pp. 86-98. doi: 10.2514/1.J055044.

[61] Strykowski, P.J. and Krothapalli, A., The Countercurrent Mixing Layer – Strategies for Shear-Layer Control, AIAA Shear Flow Conference, paper AIAA 93-3260, Orlando, 1993. doi: 10.2514/6.1993-3260.

[62] Flamm, J.D., Experimental Study of a Nozzle using Counterflow Thrust Vectoring, 34th AIAA/ASME/ SAE/ASEE Joint Propulsion Conference and Exhibit, Paper AIAA 99-2669, Cleveland, 1999. doi: 10.2514/6.1998-3255.

[63] Alvi, F.S. and Strykowski, P.J., Forward Flight Effects on Counterflow Thrust Vector Control of a Supersonic Jet, *AIAA Journal*, Vol. 37, No. 2, 1999, pp. 279-281. doi: 10.2514/2.705.

[64] Strykowski, P.J., Krothapalli, A. and Forliti, D.J., Counterflow Thrust Vectoring of Supersonic Jets, *J. Aircraft*, Vol. 34, No. 11, 1996, pp. 2306-2314. doi: 10.2514/3.13395.

[65] Washington, D.M., Alvi, F.S., Krothapalli, A. and Strykowski, P.J., Multiaxis Fluidic Thrust Vector Control of a Supersonic Jet Using Counterflow, *AIAA Journal*, Vol. 34, No. 8, 1996, pp. 1734-1736. doi: 10.2514/3.13296.

[66] Deere, K.A., Summary of Fluidic Thrust Vectoring Research Conducted at NASA Langley Research Centre, 21st AIAA Applied Aerodynamics Conference, Paper AIAA 2003-3800, 2003. doi: 10.2514/6.2003-3800.

[67] Deere, K.A., Berrier, B.L., Flamm, J.D. and Johnston S.K., Computational Study of Fluidic Thrust Vectoring Using Separation Control in a Nozzle, AIAA 21st AIAA Applied Aerodynamics Conference, Paper AIAA 2003-3803, Orlando, 2003. doi: 10.2514/6.2003-3803.

[68] Flamm, J.D., Deere K.A., Mason, M.L., Berrier, B.L. and Johnston, S.K., Experimental Study of an Axisymmetric Dual Throat Fluidic Thrust Vectoring Nozzle for Supersonic Aircraft Application, 43rd AIAA/ASME/SAE/ASEE Joint Propulsion Conference and Exhibit, Cincinatti, 2007. doi: 10.2514/6.2007-5084.

[69] Chambers, J.R., Innovation in Flight: Research of the NASA Langley Research Centre on Revolutionary Advanced Concepts for Aeronautics, NASA SP-2005-4539, 2005.

[70] Miller, D.N. and McCallum, B.N., Prospects for Fluidic Thrust Vectoring, NATO STO Symposium, Innovative Control Effectors for Military Vehicles, STO-MP-AVT-215, Paper No 10, Stockholm, 2013.

[71] Fairhurst, D.J., A Summary of SACCON DLR-F17E Tests Carried out on Model RA234 in the Warton 1.2 m High Speed Wind Tunnel, BAE Systems, Rept. BAE-WEIS-RP-ASF-WTD-119741 WP070-O-005, Warton UK, 2012.

[72] Kennett, D.J., Hoholis, G. and Badcock, K.J., Numerical Simulation of Control Surface Deflections over a Generic UCAV Configuration at Off-Design Flow Conditions, 32nd AIAA Applied Aerodynamics Conference, Paper AIAA 2014-2134, Atlanta, 2014. doi: 10.2514/6.2014-2134.

[73] Rein, M., Irving, J., Rigby, G. and Birch, T.J., High Speed Static Experimental Investigations to Estimate Control Device Effectiveness and S&C Capabilities, 32nd AIAA Applied Aerodynamics Conference, Paper AIAA 2014-2004, Atlanta, 2014 doi: 10.2514/6.2014-2004.

[74] Steijl, R., Barakos, G. and Badcock, K., A Framework for CFD Analysis of Helicopter Rotors in Hover and Forward Flight, *International Journal for Numerical Methods in Fluids*, Vol. 51, No. 8, 2006, pp. 819-847. doi: 10.1002/fld.1086.

[75] Badcock, K.J., Richards, B.E. and Woodgate, M.A., Elements of Computational Fluid Dynamics on Block Structured Grids Using Implicit Solvers, *Progress in Aerospace Science*s, Vol. 36, No. 5-6, 2000, pp. 351-392. doi: 10.1016/S0376-0421(00)00005-1.

[76] Lawson, S.J. and Barakos, G.N., Evaluation of DES for Weapons Bays in UCAVs, *Aerospace Science and Technology,* Vol. 14, No. 6, 2010, pp.397-414. doi: 10.1016/j.ast.2010.04.006.

[77] Coppin, J. and Birch, T.J., CFD Predictions of Control Effectiveness for a Generic Highly Swept UCAV Configuration, 32nd AIAA Applied Aerodynamics Conference, Paper AIAA, 2014-2135, Atlanta, 2014. doi: 10.2514/6.2014-2135.

Chapter 5 – ON THE USE OF ACTIVE FLOW CONTROL (AFC) ON TAILLESS AIRCRAFT MODELS TO AFFECT THEIR TRIM AND CONTROL

E. Phillips, M. Jentzsch, M. Menge, C. Heinritz, L. Taubert, I. Wygnanski
The University of Arizona
UNITED STATES

Matthew Forster
BAE Systems – Air
UNITED KINGDOM

John Ladd
Boeing Research and Technology
UNITED STATES

5.0 NOMENCLATURE

C_L	Lift coefficient
C_{LM}	Pitching moment coefficient, $\frac{M}{q_\infty Sc}$
C_{LL}	Rolling moment coefficient, $\frac{L}{q_\infty Sc}$
C_{LN}	Yawing moment coefficient, $\frac{N}{q_\infty Sc}$
C_P	Pressure coefficient
b	Wing span
c	Chord
C_μ	Dimensionless momentum coefficient
L	Rolling moment
N	Yawing moment
M	Pitching moment
Mn	Mach number
p	Pressure
q_∞	Dynamic pressure
S	Wing reference area
U_∞	Free stream velocity
α	Angle of incidence
δ	Flap deflection angle
$\Lambda_{c/4}$	Quarter chord sweep angle
Λ	Leading-edge sweep angle

5.1 OVERVIEW

Tests were carried out on a selected number of tailless aircraft planforms and swept-wings in order to understand their non-linear pitch characteristics. Although our task was to overcome the pitch-break on the SACCON (Stability and Control Configuration) model, we turned our attention to the universality of this problem and the means to control it. A small number of sweeping jet actuators were used for this purpose and they were most effective when located downstream of the local mid-chord of the wing prior to stall. It was realized that the location of the actuator, its orientation and the level of its momentum output are important parameters affecting the flow and the integral wing characteristics. Therefore, one may change these features by deploying either control surfaces, AFC or a combination of both, noting that there is a strong coupling among all the variables involved. CFD provided guidance to the location and orientation of the actuation and affirmed some of the observations made during the tests.

5.2 PROLOGUE

The 32nd AIAA Applied Aerodynamics Conference devoted a special session to the stability and control of future military aircraft reported by the NATO Science and Technology Organization (STO) AVT-201 Task Group. It focused its research on the SACCON model designed by AEDS (Airbus) that represented a generic UCAV aircraft [1], [2], [3], [4], [5], [6]. AVT-239 was to search for "Innovative Control Effectors to stabilize

and control the SACCON and other generic UCAV configurations". AEDS's SACCON model, Lockheed's ICE model and BAE's MAGMA were considered initially for this task but in 2016 the Head of the US AVT-239 Task Group selected Lockheed's ICE for model flight tests. The Active Flow Control (AFC) research group at the University of Arizona continued to work on the SACCON and joined the University of Manchester and BAE in applying sweeping jet actuators to the MAGMA. This effort represents the core of the present chapter. Although the use of sweeping jet actuators to trim the SACCON and control its yaw was reported elsewhere [7] some of the results are also shown presently for the sake of completion and are augmented by studies on other configurations that were sponsored by the Boeing Company, ONR and AFRL.

5.3 INTRODUCTION

A Blended Wing-Body (BWB) tailless aircraft, where a lifting surface is carrying the payload rather than a separate cylindrical fuselage, provides a larger volume for a given surface area and thus has lower cruise drag. Consequently, a BWB may potentially replace the traditional tube and wing design as a subsonic optimal transport planform. A typical BWB configuration has a λ wing planform with a Leading Edge (LE) that is swept-back at 45°-55° and an Aspect Ratio (AR) of 3 to 5. The outboard part of the wing is thin while the inboard, "body" part is of necessity thick, providing the needed volume for a prescribed mission. Low observability is another constraint imposed on combat air vehicles that are either manned or unmanned. According to Hitzel [8], deltas, double deltas and their derivatives that have a LE sweep of approximately 50°-60° and a Trailing Edge (TE) sweep of 25°-30° are most desirable. Vertical tails should be canted and preferably eliminated in order to lower observability. Various UCAV platforms tested in Europe and the USA that use these criteria are shown on the right side of Figure 5-1.

The higher AR planforms perform reasonably well at cruise, but they are problematic at high incidence angles needed during takeoff and landing. Furlong and McHugh [9] report that nose-up pitch departure depends mostly on Λ and AR (or weighted average sweep measured at the ¼ chord, $\Lambda_{c/4}$, for tapered and cranked wing planforms [10]). If the maximum lift coefficient, C_{Lmax}, is of order unity, the maximum usable C_L may be as low as ⅓ before reaching pitch-break, beyond which control surface deflection is required for trimming. The product $AR*\tan(\Lambda_{c/4})$ = const. approximately follows a demarcation line separating stable from unstable wing configurations (Figure 5-1, Left). Slats, flaps and fences increase the constant slightly [9] but they add complexity, weight and increase observability, all of which are undesirable. Typical method of alleviating or delaying pitch-break is to reduce AR, therefore increasing induced drag (e.g., ICE model). Introduction of a LE crank reduces $\Lambda_{c/4}$ while increasing AR and is thus a method of choice on BWB configurations (Northrop-Grumman X-47 and Boeing X-48). Since most tailless aircraft planforms are located on or near the neutral stability curve (Figure 5-1), pitch-break is a major impediment to design. Cruise performance is sacrificed in favor of stability and in most cases UCAVs do not fare well when compared with a classical long range design such as the B-52. AFC may provide a solution to this conundrum by raising the stability boundary for higher AR-configurations.

Thin airfoils used on UCAV wings tend to stall from the leading edge, enclosing a bubble in two- dimensional flow, which turns into a vortex whenever there is a substantial spanwise velocity component. At moderate incidence angle (α), the LE vortex stays at the LE and feeds into the tip vortex. At larger α, and/or larger sweep (Λ) or larger AR, the LE vortex turns in the direction of streaming inboard of the tip and lifts off the flow outboard of its trajectory leading to tip stall. The circulation associated with the LE vortex increases with incidence and the location at which it turns downstream moves inboard, thus increasing the stalled area between it and the tip.

The creation of the LE vortex, its departure from the LE and flow separation near the tip, result in non-linear pitch and roll behavior leading to stability and control problems, since it occurs within a very small range of Δα. If the outboard (further aft) portion of the wing stalls, while the inboard (further forward) portion maintains strong suction, the two effects add causing a strong nose-up pitching moment. If either the port or starboard side of the wing stalls asymmetrically, a spin can result.

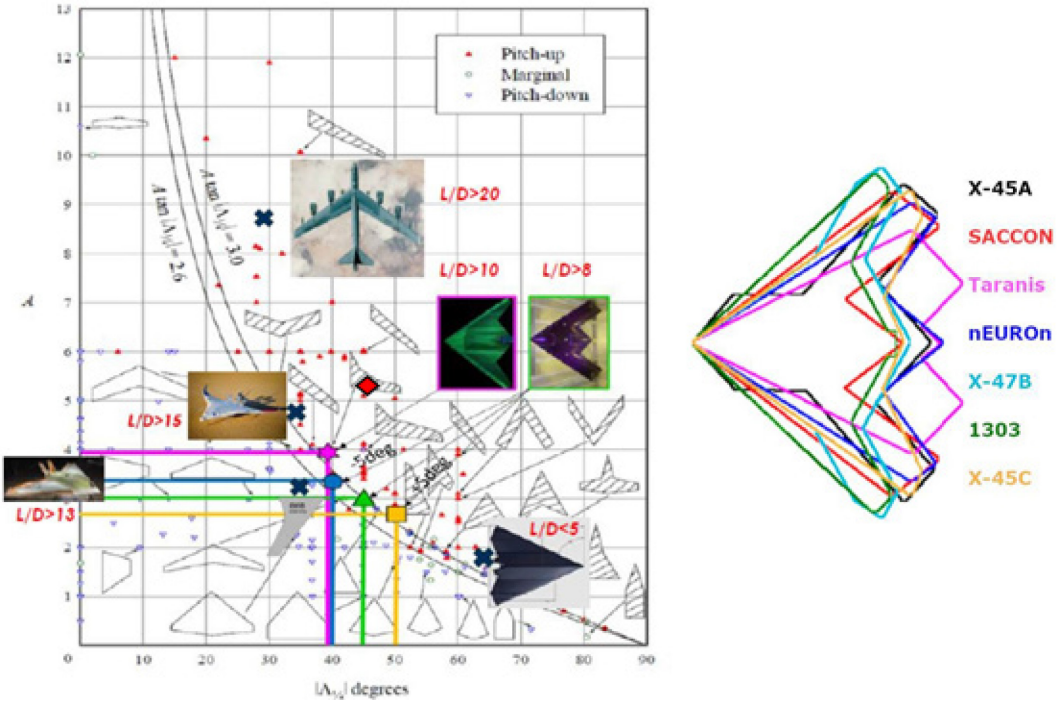

Figure 5-1: Left: AR and Λ Relations vs. Longitudinal Stability Boundary [10]. Right: Various Flying Planform Models Compared at Approximately Equal Area.

AFC may advance the design of a typical UCAV by increasing its trimmed C_L. This would affect the size of the vehicle and its ability to loiter at low speed. It could also affect its takeoff and landing capabilities. AFC can also enable yaw control with a relatively small coupling to roll, thus not requiring a large vertical tail and avoiding the use of conventional control surfaces that spoil the UCAV's stealthy configuration. The utility of AFC depends on the amount of air or other sources of energy that it requires to fulfil the "A" in the acronym.

The efficacy of a small number of sweeping jet actuators was tested on two semi-span models (the SACCON and the MAGMA (shown in Figure 5-2)) under the auspices of the AVT-239 Task Group. These tests were carried out at incompressible speeds corresponding to Mn < 0.2 and at Re based on the root chord of approximately 10^6. Since the purpose of this presentation is to provide results that are universally applicable to most tailless BWB configurations, we shall not limit our discussion to these two models but describe the features associated with sweep in general by examining the flow over relatively simple swept-back wings (Figure 5-2, right). AFC therefore has two challenges:

1) To provide as high a lift as possible while keeping the aircraft trimmed thus allowing the aircraft to takeoff and land at lower speeds; and
2) To control the yaw of the aircraft in cruise and loiter without the use of deflectable control surfaces.

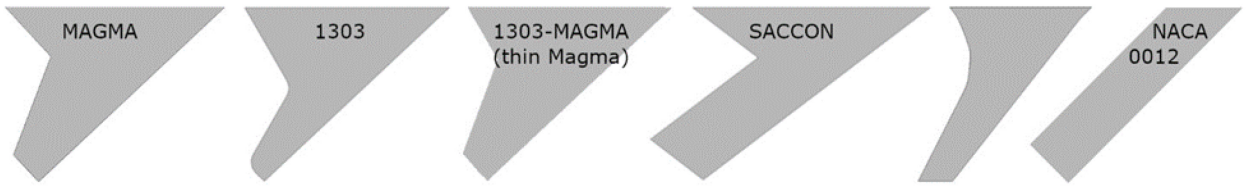

Figure 5-2: Four BWB Models (Left) and Two Swept-Back Wings (Right) Tested Using a Small Number of Sweeping Jet Actuators for the Purpose of Suppressing Spanwise Flow.

5.4 EXPERIMENTAL APPARATUS

Tests were carried out at the University of Arizona at the closed-loop subsonic research wind tunnel (see Figure 5-3). The test section is 3 ft high, 4 ft wide and 12 ft long. The tunnel can reach a maximum velocity of 80 m/s providing typical root chord maximum Re = $5*10^6$ at Mach Number Mn = 0.23. The mean flow uniformity across the test section outside the wall boundary layers was better than ± 0.5%, while the turbulence intensity measured by a linearized hot wire anemometer that was filtered between 1 Hz to 10 kHz was 0.05%. The test section temperature was maintained at 72° ± 1° F throughout the entire test campaign. An artificial wall was inserted next to the wind tunnel side wall in order to minimize the effects of the side wall boundary layer. All forces and moments were measured by a five component external pedestal balance and all semi-span wings tested were attached to the balance by means of a special mount that also passed the compressed air supply to the actuators.

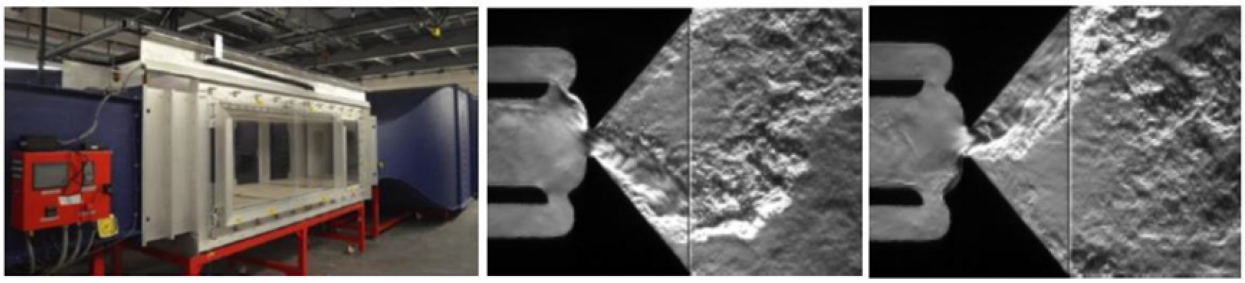

Figure 5-3: The University of Arizona Research Tunnel and the Sweeping Jet Actuators [11].

Sweeping jet actuators were used on all configurations although they are more complicated to build than ordinary jet nozzles and the pressure drop across them is larger. Consequently, they put a larger load on a compressor whose size or power consumption are defined by the mass flow and the pressure rise that it supplies. Nevertheless, by sweeping from side to side at an included angle of 100° (Figure 5-3, bottom right) they cover a large surface area, entrain more surrounding fluid than steady jets and as a result their effect on the pressure field in the vicinity is larger for comparable momentum input levels. Furthermore, since the surface flow direction on complex UCAV configurations at large incidence angles is not easily (or correctly) predicted, and the efficacy of AFC is sensitive to the surface flow direction, the sweeping jets are more forgiving than steady jets to errors in flow direction. Since these rigid devices possess no moving parts, their use is no less reliable than steady jets.

5.5 THE TEST ARTICLES

The MAGMA model was derived from the 1303 by widening its aft outboard part and hence moving its Trailing Edge (TE) crank location inboard. The sweepback of its LE is 47° and its AR = 3.4 (when based on the full span). The model has a projected reference area S = 458.2 in2 and has no washout or twist along its span. The leading-edge radius and the maximum wing thickness decrease along the span. A “zig-zag” tape that is used to trip the boundary layer on gliders is used presently for the same purpose. The trip strip is located around 10% of the chord and it spans the wing upper surface. The model has two flaps hinged around 80% of the local chord and extending from the TE crank all the way to the wing tip. They are deflected separately at 5° intervals between $-15° < \delta < +35°$. The Moment Reference Line (MRL) was located at 49.3% of the root chord (Figure 5-4(a)). The semi-span model has only two control surfaces and it does not have a vertical tail.

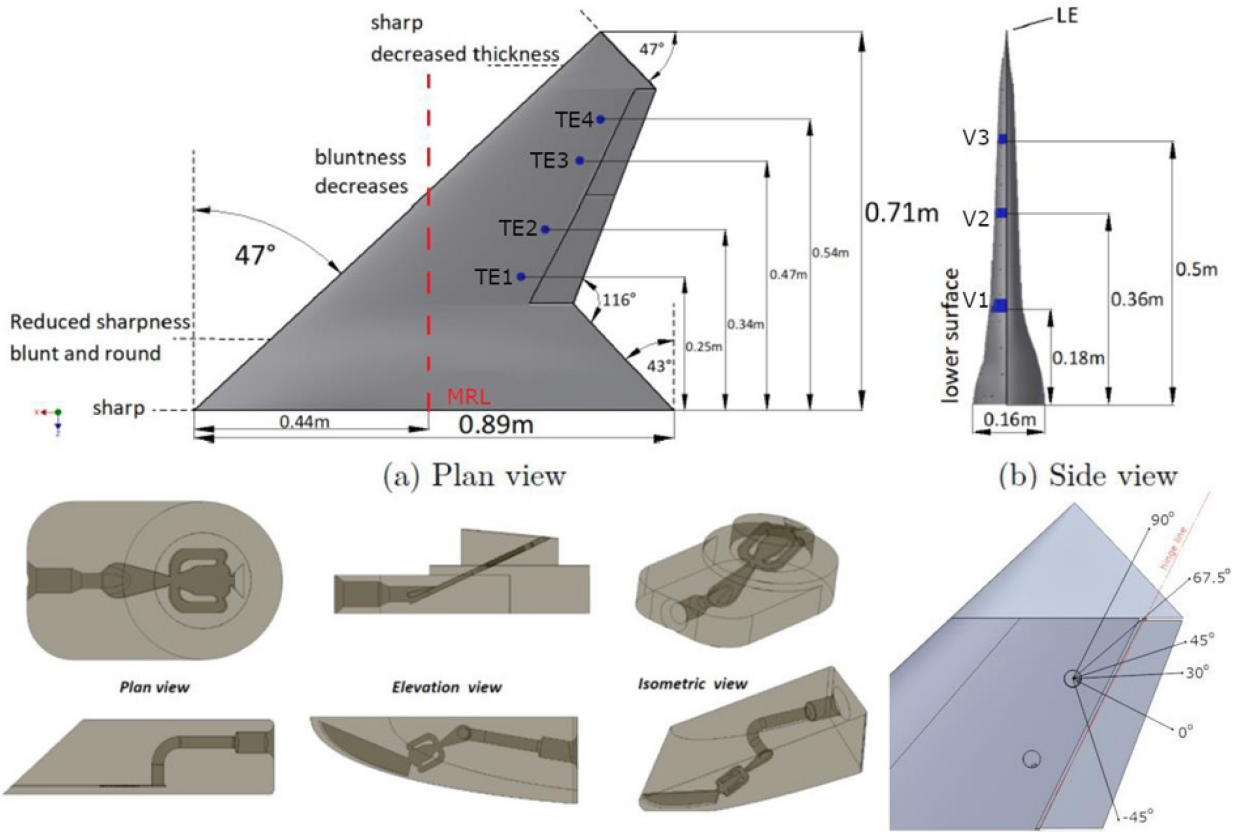

Figure 5-4: The MAGMA Model and its Actuators (Bottom Left: TE Actuators (Top Row) and LE Fluid Vortilons (Bottom Row), Bottom Right: TE Actuator Orientation).

The model has only four sweeping jet actuators located on the suction side above the flap hinge line which are sweeping in a plane that is slightly inclined to the flap's upper mould. These actuators are embedded into replaceable circular plugs that enabled one to check the sensitivity of the flow to jet orientation (Figure 5-4). In addition, there are three inserts in the lower surface of the LE containing one sweeping jet each at spanwise locations shown in Figure 5-4(b). These actuators sweep in a plane that is parallel to the free stream and their axis of blowing is oriented downward and forward. Consequently, they should emulate vortilons by blocking the spanwise flow near the attachment line. The jets' forward orientation generates drag, hence they generate a yawing moment when activated asymmetrically on one wing of a full model.

The SACCON model also represents a generic UCAV planform specifically designed to assess stability and control prediction methods for NATO unmanned air vehicles. It is a blended wing-body configuration having a swept back LE at $\Lambda = 53°$. The leading and trailing edges of the outboard part of the wing are parallel. The LE is divided into three sections distinguished by their sharpness (Figure 5-5, right) and the outer panel has an outwash of 5°. The LE at the root is very sharp and turns blunt opposite the TE crank that forms the juncture of the tapered and parallel portions of the λ wing planform. The abrupt change in the LE radius sheds the LE vortex generated inboard of this discontinuity that aligns itself with the free stream before turning outboard near the TE. The bluntness of the LE gradually decreases towards the tip. The model has two flaps of approximately 30% outer wing chord that can be deflected between $-10° < \delta < +50°$. The MRL was established by the designer (AEDS) at x/croot = 0.5656.

An array of 13 sweeping jet actuators is located above the flap hinge of this model. They could be blocked individually, thus, at times only 4 or even 2 actuators were used (Figure 5-5). Five inserts at the LE contained

actuators which injected momentum to the upper surface. The sweeping jet motion in all these actuators was almost parallel to the upper mould line, in contrast to the fluid vortilons in the MAGMA model.

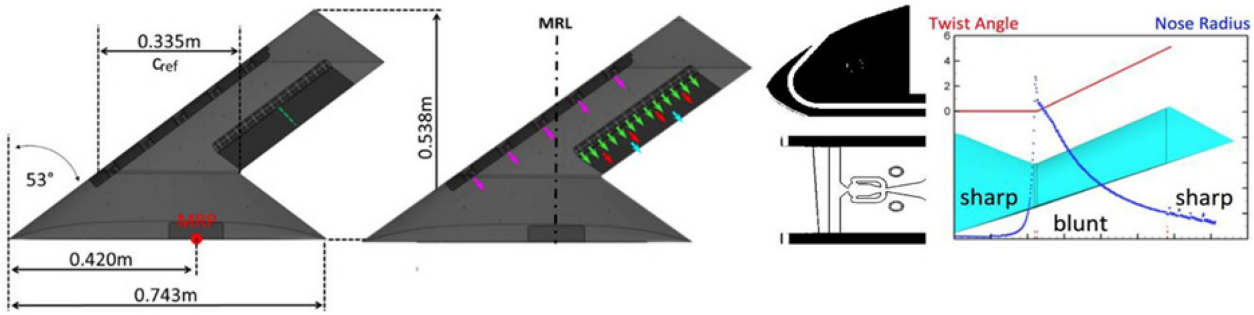

Figure 5-5: The SACCON Model Showing the Location and Number of its Actuators and their Installation at the LE. The relative dimension of the LE radius and the washout of the outboard wing are shown at the right.

The simplest test article that revealed most about the flow on swept-back wings and the way to control it is based on a NACA 0012 airfoil section [12] made out of extruded aluminum. The wing has a chord of 8" measured normal to the leading edge. It has neither taper, twist nor flaps. It has an AR of 5.18 and it is swept back at 45° to the free stream with its wing tip being perpendicular to the LE. It is thus highly unstable according to the criteria of Figure 5-1. In order to assess the behavior of the LE vortex on this wing, modular 3D printed leading-edge inserts were added as shown in Figure 5-6. They increased the chord somewhat thus reducing the AR to 4.88 and 4.82. All inserts had identical LE radii, two of them are symmetrical while the third is flat at the bottom (Figure 5-6, center), thus adding camber to the LE. In order to avoid the formation of laminar bubbles and the associated strong Reynolds number dependence, a "zig-zag" tape was used for tripping the boundary layer. Two small inserts at the LE of the wing divided its span into three equal segments and were equipped with sweeping jet actuators emulating a LE fence. Each insert contained two fluidic oscillators that were very close to each other, one blowing over the top surface and one over the bottom (Figure 5-6, right). The sweeping motion described a plane that was normal to the surface.

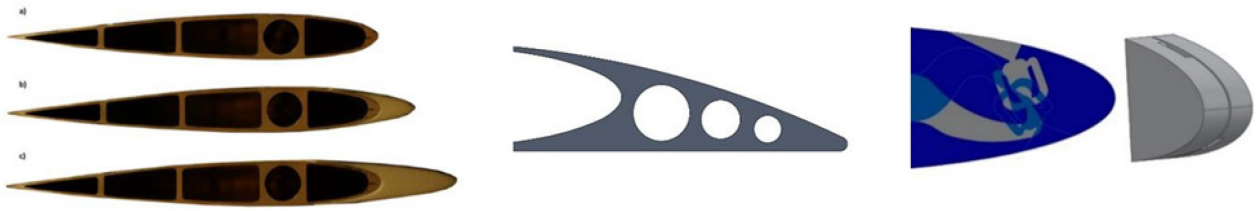

Figure 5-6: The Swept-Back Simple Wing and its Various Extensions.

5.6 SOME OBSERVATIONS OF FLOW OVER SWEPT-BACK WINGS AND ITS CONTROL

Only the chordwise velocity component stagnates at the LE of a swept-back wing. Therefore, the flow is dominated by the spanwise component along the LE attachment line and its immediate vicinity. Decomposition the flow into chordwise and spanwise components enables one to apply the "cross-flow" principle to predict the drag [13]. This principle is rooted in the boundary layer independence principle that applies to yawed cylinders (airfoils) of infinite aspect ratio. It indicates that two-dimensional boundary layer equations apply to the chordwise component of the velocity field that is completely independent of the spanwise flow. However, the spanwise boundary layer flow that is devoid of pressure gradient ($\partial p/\partial z = 0$)

depends on the other two components of velocity that have been predetermined by the two-dimensional solution. This principle applies to laminar and turbulent flows alike [14]. The chordwise velocity component decelerates toward the trailing edge where ideally it should stagnate (Kutta condition), but viscous losses lead to earlier deceleration and potential stagnation somewhere on the aft part of a high aspect ratio wing. Pressure contours obtained by Pressure Sensitive Paint (PSP) suggest that the flow near the surface should turn outboard as it selects the path of least resistance while remaining attached to the surface (Figure 5-7, left). This leads to the accumulation of a lowest momentum fluid along the trailing edge of the tip region of the wing. It is therefore there where the flow separates and its reversal has been first observed (Figure 5-7, center). The separated flow region moves inboard and upstream with increasing incidence (Figure 5-7, right).

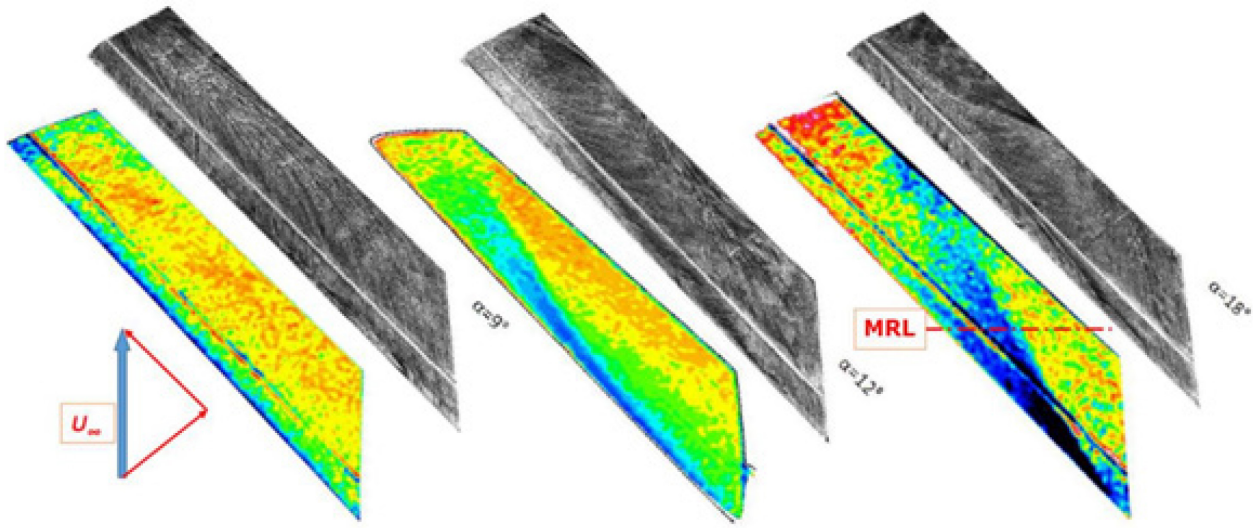

Figure 5-7: Oil Flow and Pressure Sensitive Paint Contours on a Swept-Back Finite Wing. AR = 5.2 and Λ = 45°.

The flow at the LE of a thin airfoil separates when α exceeds the designed incidence angle by a prescribed safety margin. The separated flow may reattach farther downstream enclosing a bubble whose size depends on the LE radius and on Re. The same happens on a swept-back wing except that the separation and reattachment occur in the presence of spanwise flow resulting in a LE vortex whose circulation increases along the span. LE separation and the ensuing vortex originate inboard of the wing tip, but seldom close to it because the tip vortex pulls the surface flow toward its core increasing spanwise velocity. The LE vortex merges initially into the tip vortex and strengthens it. It spreads inboard with increasing α and reaches the wing root at moderate incidence (see Figure 5-7, center corresponding to α = 12°). It also turns in the direction of streaming when its size and strength (circulation) are sufficiently large. When the LE vortex departs from the LE and bends in the direction of the free stream, it accelerates the spanwise flow inboard of its axis and lifts off the flow on its outboard side stalling the tip of the wing (Figure 5-7, center and right). An increase in α strengthens the vortex inboard of the turning location thus advancing the turning point toward the wing root. This inboard movement is not related to the initial movement of the origin of the LE vortex inboard with increasing incidence, because that movement depends on the initial location of separation, the AR and Λ.

The use of tufts helped in the interpretation of the oil flow patterns, as the latter only show the footprint of the complex three dimensional vortex flow above the upper wing surface. A good example of the correlation between the two methods of flow visualization is shown in Figure 5-8 where the two pictures were taken at α = 11° and a free stream velocity of U_∞ = 40 m/s. The LE row of tufts indicates that the flow at the LE is attached between the wing root and its mid span, where the origin of the LE vortex is located (the tufts are unsteady and point upstream, Figure 5-8, bottom). This vortex turns downstream at approximately 70% of the

span and a new LE vortex that joins the tip vortex appears outboard of this turning point. The premature downstream turn of the main LE vortex might have been triggered by the thin slot from which the sweeping jet emulating the vortilon emerges (Figure 5-6). It became later apparent that a small excrescence located near the LE attachment line turns the LE vortex in the direction of the free stream. The departure of the vortex from the LE is associated with its rapid divergence (lateral spreading angle) due to the adverse pressure gradient to which its core flow is subjected to. The diagonal path of the vortex from the LE to the TE of the wing induces an upstream flow on the inboard side of the vortex core and lifts off the flow on the outboard side of the vortex. When the LE vortex straddles the Mean Reference Line (MRL) its low pressure near the wing root and the high pressure that is associated with separation near the tip result in nose-up pitch- break (Figure 5-7, right).

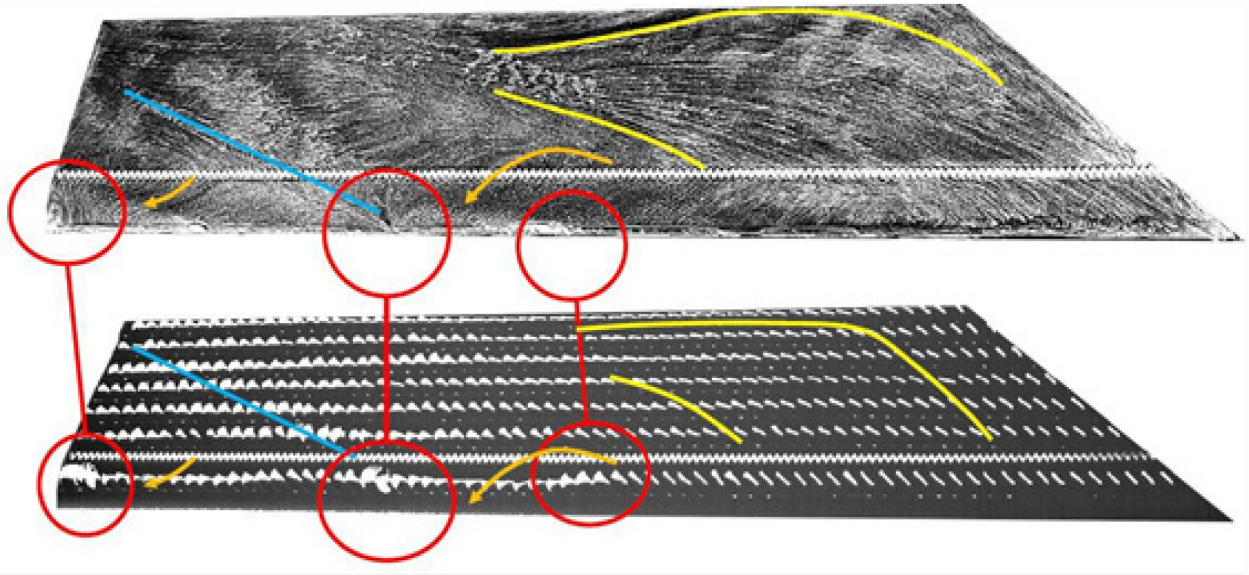

Figure 5-8: The Correlation Between Oil Flow and Tufts at α = 11° and a Free Stream Velocity of U_∞ = 40m/s.

Consider the case of the extended drooped LE (Figure 5-9). Up to α = 5.5° the flow was completely attached, but at α = 6° a LE vortex is formed at around 70% of the span which starts a nose down pitch departure since the LE vortex increased the area of low pressure located downstream of the MRL. The LE vortex expanded in outboard and inboard directions with increasing incidence. Up to α≈9°, the LE vortex was aligned with the LE and the surface flow at the aft part of the wing (x/c > 50%) was almost parallel to the leading edge. Since the low pressure associated with the vortex is mostly downstream of the MRL the expansion of the LE vortex results in a net nose down pitching moment (Figure 5-9). C_{LM} attained its minimum value when the vortex reached the wingtip; thereafter the circulation of the vortex near the apex increased with incidence lowering the pressure upstream of the axis of rotation (marked by the red dashed line) while gentle separation occurred near the wingtip's TE. Both phenomena result in pitch-up. At α>12°, the vortex turned downstream and the spanwise location of its axis moved inboard with increasing α thus stalling the wing tip and accelerating the pitch-up departure.

The appearance and growth of the LE vortex downstream of the MRL increases $\partial C_L/\partial\alpha$ and generates a nose down pitch (Figure 5-10). A sharp LE causes early LE separation and the generation of the LE vortex that also increases the lift of the wing. The angle at which these effects are noticeable increases with bluntness and with LE droop. The depth (or the maximum) of the nose down departure is insensitive to the shape of the LE, but the LE camber has the smallest $\partial C_L/\partial\alpha$ and thus its pitch-down departure is more gentle.

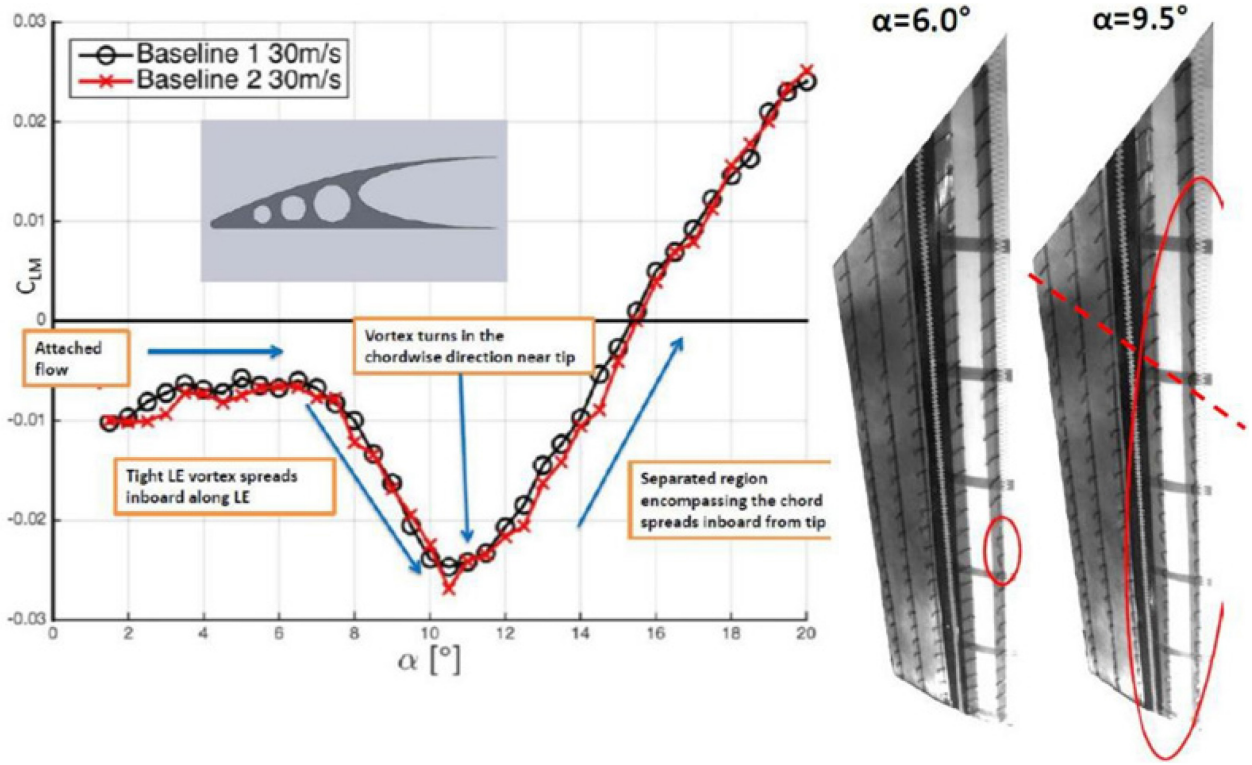

Figure 5-9: The Relationship Between the LE Vortex and Nose Down Pitch for Slightly Drooped, Sharp LE.

Actuation was introduced from the leading edge of the model as shown in Figure 5-6 at an aggregate $C_\mu = 0.25\%$. The sweeping motion of the actuator was supposed to simulate a solid fence that was wrapped around the LE, consequently the actuators injected some momentum upstream against the oncoming flow. This strengthened the analogy between the fluidic fence and the physical fence.

The magnitude of the effect that these jets have on the flow was first assessed by flow visualization using tufts (Figure 5-11, right). Green tufts correspond to baseline flow while magenta ones represent the flow generated by AFC and black color appears wherever AFC did not change the flow direction at $C_\mu = 0.25\%$. Since long exposure was used in these photographs, a sharp image of a tuft represents steady flow while a blurred one suggests unsteadiness. At $\alpha = 10°$ and in the absence of actuation the flow separated over the triangular area that extends from the midspan location at the LE to the very tip of the wing at its trailing edge, i.e., the outboard region to the right of the dashed red line. The two jets are located where there are gaps in the "zig-zag" trip strip. They attached the flow over the frontal 25% of the chord almost to the tip of the wing. A trapezoidal area (marked by yellow lines) marks the locations where the baseline flow has a larger chordwise component of velocity at the surface than the actuated flow. In this zone, the baseline flow is also steadier. This "adverse" effect of actuation inboard of the jet trajectory is caused by jet entrainment. Inboard of the left yellow line, actuation had no effect on the flow direction. Increasing the incidence results in a movement of the dashed red line to the left (i.e., towards the root of the wing) and a reduction in the effectiveness of the actuation provided C_μ is not increased. Quantitative effects of the actuation are also shown in Figure 5-11. An increase in $\partial C_L/\partial\alpha$, that marks the expansion of the LE vortex, was almost eliminated by the sweeping jets, as $\partial C_L/\partial\alpha$ remained approximately constant up to $\alpha \approx 14°$ and it decreased at higher of incidence. The stable (nose down) C_{LM} excursion was almost eliminated by AFC but the unstable pitch-up break was only slightly delayed (from $C_L = 0.7$ for the baseline flow to 0.8 for $C_\mu = 0.25\%$).

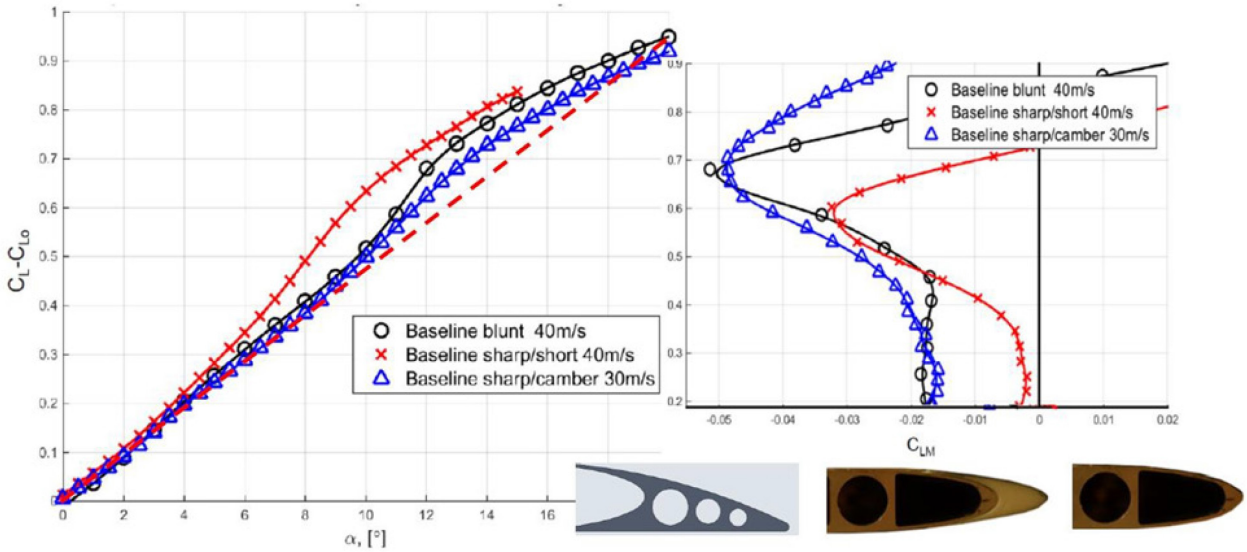

Figure 5-10: The Effect of LE Shape On lift and Pitching Moment.

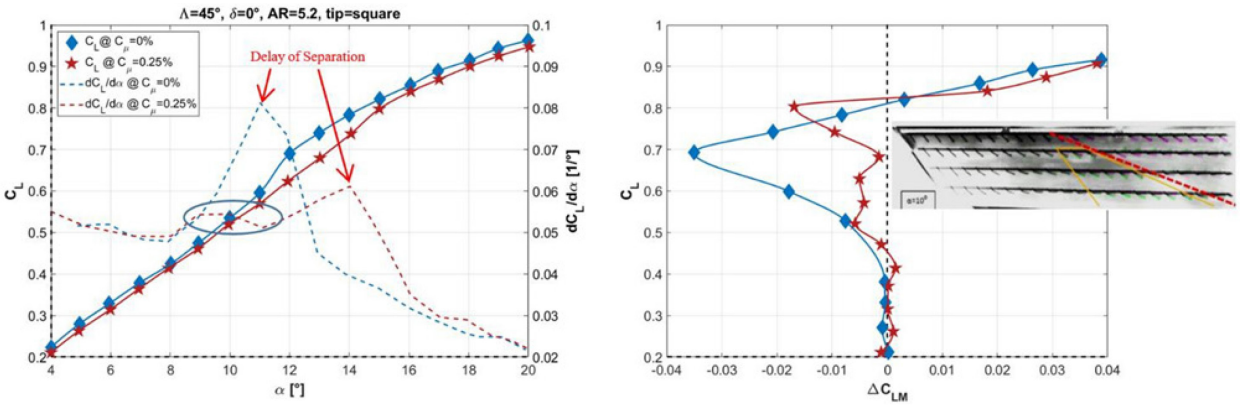

Figure 5-11: The Effects of LE Actuation Emulating a Vortilon on Lift and Pitching Moment.

The removal of the tape covering the actuator exits prior to actuation revealed the sensitivity of the flow to excrescences located near the LE attachment line, as a slot that was only 0.025" wide changed the pressure distribution over the upper surface of the wing. With the slots being taped there was a single LE vortex that turned gently downstream near the mid span of the wing (Figure 5-12, left). Removal of the tape in the absence of actuation generated three weaker vortices that separated from the LE near each of the actuator slots and near the wing tip (Figure 5-12, center). This effect was only noticeable over a narrow range of incidence angles when the attachment line straddled the actuator slots located on the bottom surface.

The effectiveness of passive devices such as a LE snag or a vortilon was thus examined. Both passive devices are used extensively in practice, snags on combat airplanes (e.g., F-4) and vortilons on commercial ones (e.g., Embraer ERJ-145). At $\alpha = 12°$ and in the absence of any device, a single vortex is originating at the LE near the root of the wing and passing diagonally over its surface, departing at the TE near the tip. Both passive devices resulted in two such vortices. The vortex originating at the root was forced downstream by the device and a new vortex originating at the device parted the wing tip somewhere close to the mid chord location. The premature shedding of the LE vortex by the device delayed the tip stall and the associated pitch-break. The snag was more effective than a single vortilon over a wider range of incidence angles.

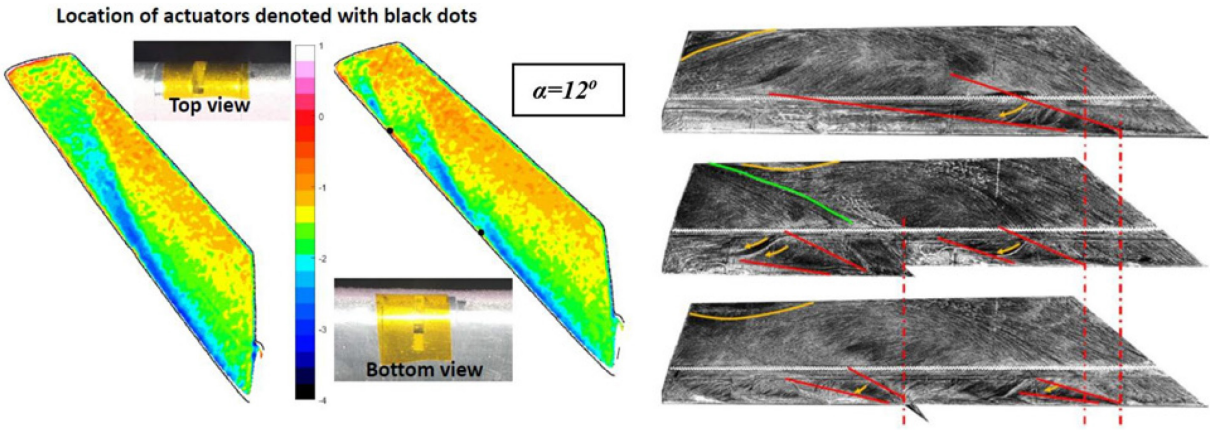

Figure 5-12: The Sensitivity of the LE Vortex to Excrescences and the Effect of a Snag and a Vortilon on the Flow.

The effect of snag location on the flow was briefly tested as it may affect the design and location of AFC near the LE. The snag location was changed from 24% of the span to 65% at 4 approximately equal intervals and the pitching moment dependence on α was compared to the baseline data obtained in the absence of the snag. Since the area of the wing changed so did the aspect ratio (increased from AR = 4.74 to AR = 4.92). The minimum (nose down) C_{LM} due to the presence of the LE vortex decreased by moving the snag outboard (Figure 5-13, right). The maximum trimmed incidence (where C_{LM} = 0) increased by moving the snag outboard up to 50% of the span. Locating the snag at 65% of the span proved to be deleterious (Figure 5-13). Tufts indicate that the snag forces the LE vortex to turn in the direction of the oncoming flow. It also initiates a new LE vortex a short distance outboard of its location. Both phenomena are indicated by the first row of tufts whose direction is reversed at some distance outboard of the snag (Figure 5-13).

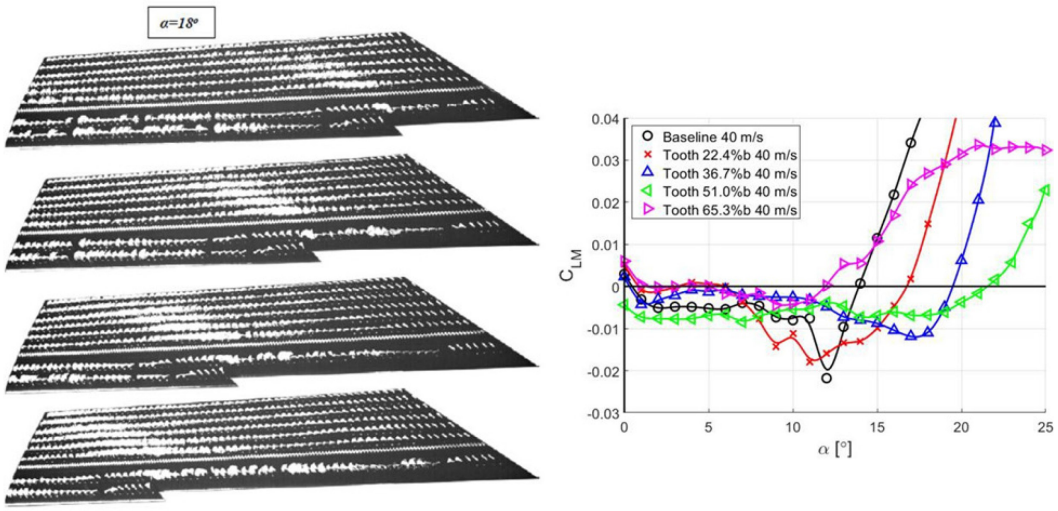

Figure 5-13: The Significance of Snag Location on the Flow and on C_{LM}.

The global effect of actuation on swept wings is demonstrated by examining the tuft pictures shown in Figure 5-14. Actuation is provided by two pairs of actuators located at x/c = 70% and dividing the span into three approximately equal segments (as marked by magenta color dots). At α = 9.6° the spanwise component of velocity dominates the area downstream of the actuators at both of their spanwise locations. The flow

upstream of the inboard actuator is fully attached (the tufts are stationary and they are white implying that actuation had no effect on their direction) and hence the actuation affects only the small region covered by the jet trajectory. In contrast, the outboard pair of actuators changed the flow over half of the wing area. In the absence of actuation (green tufts), a LE vortex originates at 35% of the span and it remains near the LE for more than half of the span turning in the direction of streaming near the tip and leaving the wing at mid chord. Four rows of tufts indicate that there is a flow reversal upstream of the outboard pair of actuators. AFC at an aggregate C_μ = 0.5% eliminated the LE vortex and attached the flow (magenta color tufts) between the LE and the outboard pair of actuators. The jets emanating from the outboard actuators entrain the flow inboard and downstream of their trajectory shifting the tuft direction outboard and upstream relative to their baseline direction. It is presumably a deleterious effect. Increasing the incidence by a single degree to $\alpha = 10.7°$ shifts the origin of the LE vortex to 20% of the span, allowing the AFC from both actuators to pull the LE flow diagonally across the wing and push the origin of the LE vortex back to its 35% spanwise location. This suggests that the effectiveness of the inboard pair of actuators is very sensitive to incidence.

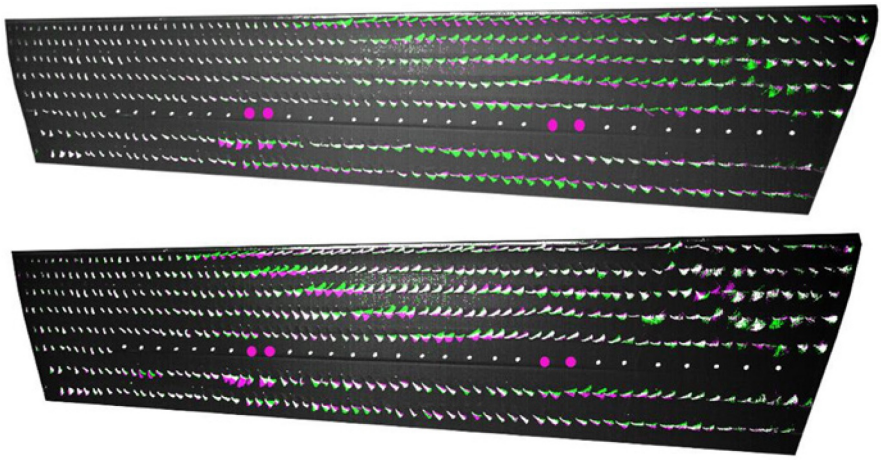

Figure 5-14: The Effect of Actuation from the Magenta Colored Locations, x/c = 70%; C_μ = 0.5% and α = 9.6° (top) and 10.7° (bottom).

Quantitative results describing the relationships among AR, sweep, incidence and actuation on a simple flapped wing based on a NACA 0012 airfoil were presented by Tewes et al. [15], [16], [17]. These results will not be discussed in this chapter and the reader is referred to the older publications. It was observed that a small number of fluidic actuators located near the natural flow separation line (or highly deflected flap hinge line) can delay separation and increase the lift on a swept-back wing. In the absence of sweep a large number of actuators and a relatively high momentum input are required to generate a similar result. This result indicates that controlling the spanwise flow is easier than the traditional two-dimensional control of the chordwise flow component. This result was confirmed on the slightly tapered and flapped, symmetrical wing representing a full-scale vertical stabilizer and rudder of a 757 airliner that was tested at NFAC [18].

5.7 STABILIZING THE SACCON MODEL IN PITCH

The SACCON model is a generic UCAV whose aerodynamic loads were determined by various NATO/STO Task Groups. Its name is an acronym standing for Stability and Control Configuration, as it focuses on the two most serious aerodynamic challenges for this design, stability and control. The 2014 AIAA Aviation Conference devoted an entire session, comprising of six papers [1], [2], [3], [4], [5], [6], to the various experimental and computational observations made on this model. The results of earlier tests were already reported at the 2010 Applied Aerodynamics conference [19], [20]. An extensive investigation of the flow over the SACCON was carried out by Vallespin et al. [21] who used two versions of the model

that differed only by the curvature of their leading edges. The Sharp Leading Edge (SLE) model, after being equipped with sweeping jet actuators, was tested at the University of Arizona.

The abrupt change in the leading-edge radius upstream of the crank in the wing planform forces a LE vortex originating at the wing apex to move downstream at moderate incidence. However the thick fuselage inboard of the crank and the mild pressure gradient along the span forces this vortical flow outboard as seen in Figure 5-15. The vortex core that schematically makes an "S" shape turn as it is displaced from the wing LE to its TE on the outboard wing portion, induces an upward flow from the surface as marked by the curved red arrows in Figure 5-15. This results in the surface chordwise flow stagnating along the dashed red line where the introduction of active flow control could create a large effect. Tuft visualization indicates that the trailing-edge region is dominated by spanwise flow (outlined in blue in Figure 5-15, right) that does not change much over a relatively wide range of incidence angles. Substantial spanwise flow was already observed at $\alpha = 3°$ and up to $\alpha = 10°$ the flow in that region remains fairly steady (i.e., attached). The abrupt change in the LE radius stabilizes the vortex path over the wing and it resembles the effect of the snag on the simple swept-back wing. It does prevent the abrupt change in the flow observed in Figure 5-14. The first indication of the existence of an LE (tip) vortex appeared at the very tip of the wing at $\alpha = 7°$. Even at $\alpha = 10°$ (Figure 5-15) the LE vortex, whose origin moves inboard with increasing α, occupied only 20% of the span (outlined in red in Figure 5-15, right). It is the outwash (twist) that moderates the strength of the tip vortex and slows its spread inboard and its turn in the direction of streaming. The joint tip/LE vortex reduces the pressure over the tip region resulting in the non-linearity in the pitching moment that extends between $10° < \alpha < 15°$ (Figure 5-15, right).

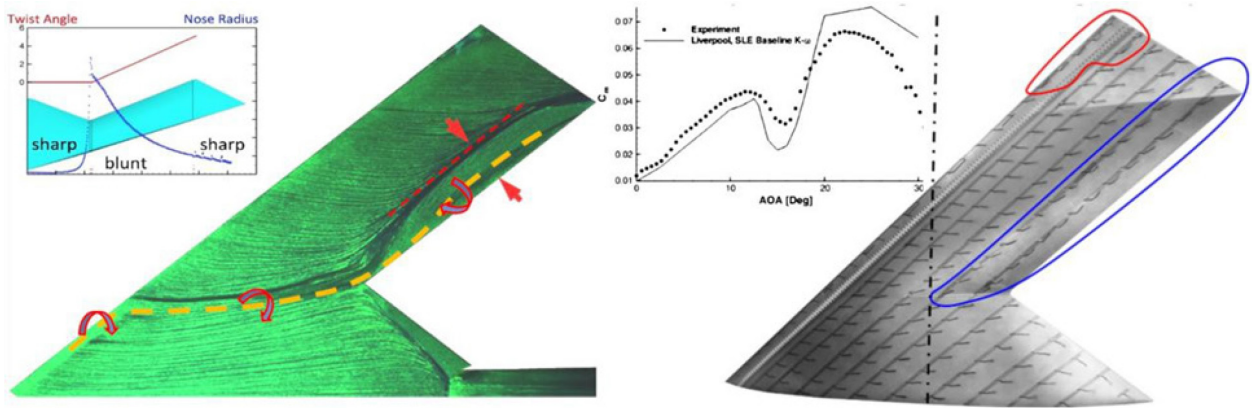

Figure 5-15: The SACCON (SLE) Model at α = 10°. Oil flow visualization [21] and the spanwise variation of nose radius and twist angle (top left inset) [22] (left). Tuft orientation in the absence of AFC (right) and the non-linear pitch departure (top right inset) [22].

Pressure contours obtained by using PSP compliment the flow visualization pictures shown in Figure 5-15 and help to assess the effects of AFC on the flow. At $\alpha = 11°$ in absence of actuation, the LE vortex that originated at the apex turned downstream toward the TE crank. It resulted in a triangular low pressure region extending from the apex to the MRL just upstream of the TE crank and back to the LE at approximately 75% of the span where a new LE tip vortex originates (Figure 5-16(a)). There is a spanwise adverse pressure gradient ($\partial C_p/\partial z$) outboard of the MRL (marked by red arrow in Figure 5-16(a)) that is almost eliminated by the actuation emanating from the flap hinge that approximately coincides with the separation line marked on the oil flow picture of Figure 5-15. The location of the actuators corresponds to the yellow dots seen in Figure 5-16(b) marking the slightly lower pressure associated with the indentations in the surface forming the sweeping jet nozzles. Pressure difference contours, ΔC_P, between the baseline and actuation (Figure 5-16(c)) indicate that the most significant change in surface pressure results from the upstream entrainment created by the sweeping jets array. The reduction in pressure downstream of the MRL contributes to nose down (stabilizing) pitching

moment. **Hence, energizing the boundary layer and changing the flow direction downstream of the actuators increases the pressure near the TE, thus provoking pitch-up** (see the orange color near the TE of Figure 5-16(c)), but this effect is small relative to the pressure reduction upstream of the actuator array. This low pressure region pulls the LE tip vortex toward the wing TE realigning it with the freestream. As long as this vortex is small and confined to the tip region (i.e., far downstream of the MRL or the neutral point), pulling it toward the actuator array is beneficial. However, by increasing α to 15°, the vortex moves upstream along the leading edge and grows in size and strength of its circulation (Figure 5-16(d)). Severe pitch-up follows, as soon as the LE vortex and the low pressure associated with it propagates upstream and inboard of the MRL (shown as dashed, vertical line in Figure 5-16). The actuation over the flap surface becomes ineffective because the actuators are located too far outboard to affect the origin of the LE vortex that moved to the apex (see arrow on Figure 5-16(e)). However, they manage to pull this vortex toward the TE thus resulting in earlier tip stall and a concomitant increase in pressure near the wing tip (Figure 5-16(f)) and this is a deleterious effect. The downstream pull of the LE vortex was already seen at α = 11° (Figure 5-16(c)). The lift and pitching moment associated with the pressure patterns discussed in conjunction with Figure 5-16 are shown on the right hand side of that figure. Clearly, the actuation had a large effect on C_{LM} proving that AFC is capable to trim the model in pitch-up to α = 11°. **This suggests that the effectiveness of AFC can improve by changing the actuators' location and adapting it to local flow conditions and this is achievable in practice provided the number of actuators is small.**

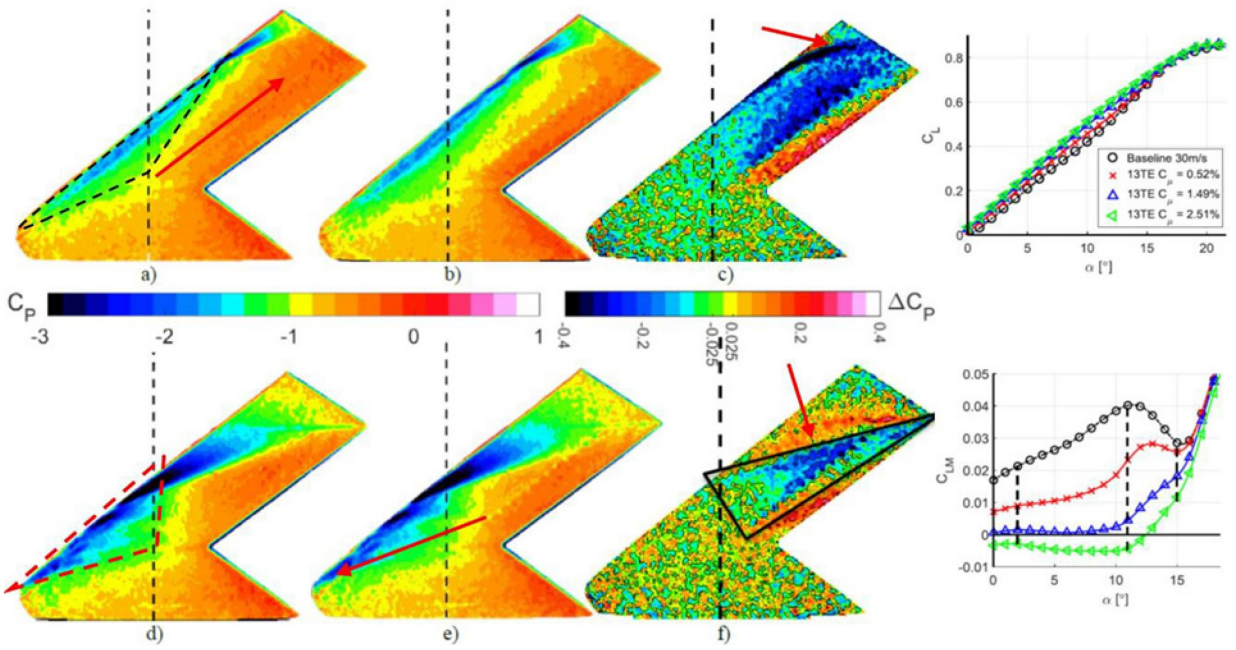

Figure 5-16: PSP Contour Lines at u_∞ = 60m/s; Top α = 11°; Bottom 15° : (a) and (d) Baseline; (b) and (e) 13 Actuators Evenly Distributed Along Flap Hinge; (c) and (f) ΔC_P = (AFC-Baseline) Right: The Effect of the 13 Actuators on C_L and C_{LM}. MRL = 0.5656.

The effect of a small fence, which was attached to the LE and aligned with the freestream, on the LE flow was monitored (Figure 5-17). The fence had no effect on the pitching moment when it was placed not far from the apex, but when placed near the MRL it eliminated the nose down pitch departure by forcing the apex vortex downstream and preventing the inboard expansion of the weaker LE tip vortex between 12° < α < 16° (Figure 5-17, bottom right). It also reduced the lift slope, $\partial C_L/\partial\alpha$, at α >12°. The tip LE vortex (whose boundaries are outlined in red in Figure 5-17, top left) almost merges with the apex LE vortex (outlined in yellow) at α = 13° in absence of the fence. Insertion of the fence changed the direction of the

flow toward the free stream outboard and downstream of the fence (Figure 5-17, top right). This stopped the growth of the LE tip vortex and eliminated the low pressure associated with it.

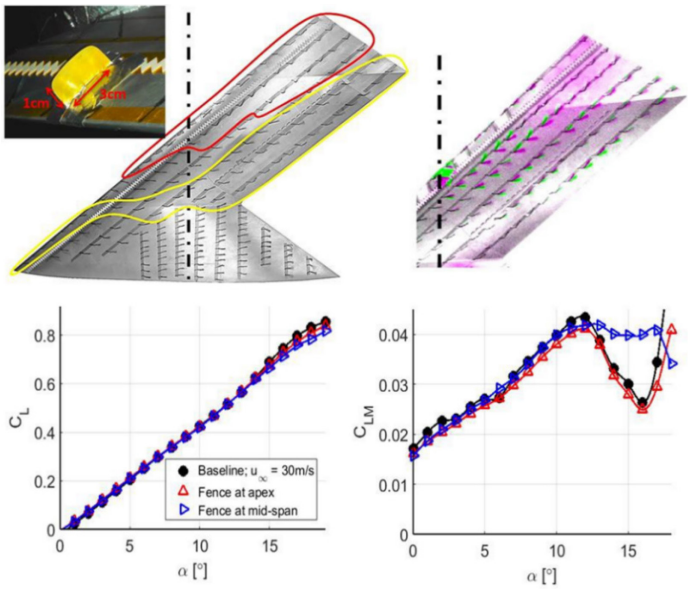

Figure 5-17: Tuft Visualization at α = 13° (Left) and at α = 14° (Right) with and Without the Fence Shown in the Inset and the Effect of the Fence on C_L and C_{LM} at Two Spanwise Locations.

PSP indicates that the flow emanating from the sweeping jet located at the LE at moderately high incidence angles raises the pressure along its path (Figure 5-18). At α = 11°, while the flow is still attached over most of the LE (see Figure 5-15) and only the flow over the flap surface is dominated by the spanwise velocity component, the path of the jet does not deviate much from the free stream direction. However, the jet path arches outboard near the TE (Figure 5-18, left). At α = 15°, the jet path is a straight line connecting the actuator location to the TE tip of the wing. Hence, the jet that was emitted normally to the LE turned almost instantly toward the tip. It did so because at α = 15° the LE vortex took the identical path (Figure 5-16(d)) and the sweeping jet merged with it. There may be a decrease of pressure outside the jet boundary resulting from jet entrainment but this effect pales in comparison to the pressure increase observed. **Thus blowing from the LE inboard (upstream) of the MRL will result in pitch-down, while blowing outboard of the MRL will result in pitch-up**.

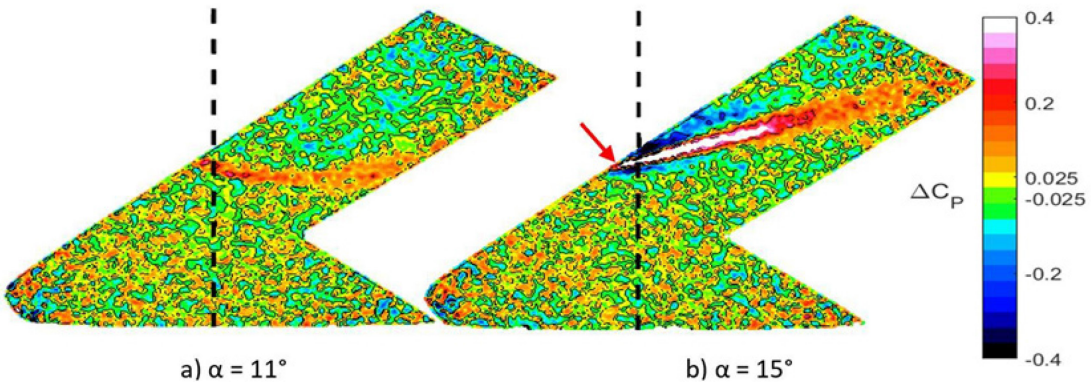

Figure 5-18: ΔC_P Contours Over the Wing When a Single Sweeping Jet Located Near the MRL is Active; C_μ = 0.10%, u_∞ = 60m/s.

In the absence of flap deflection, the pitching moment around the MRL located at $x/c_{root} = 0.5656$ is positive as is its slope $\partial C_{LM}/\partial\alpha$, making the model unstable at all incidence angles considered. The MRL location that was arbitrarily selected by previous investigators did not correspond to a neutral point (aerodynamic center) of the basic model at the Reynolds number range tested. When the MRL was switched to $x/c_{root} = 0.5505$, the baseline yields $\partial C_{LM}/\partial C_L = 0$ for the range of $0.1 < C_L < 0.3$ (Figure 5-19) corresponding to incidence angles ranging from: $2° \leq \alpha \leq 6°$, implying that a neutral point (aerodynamic center) can be maintained at these values of C_L in the absence of AFC. Applying AFC makes the model statically stable since $(\partial C_{LM}/\partial\alpha)C_\mu = \text{const.}<0$. Using only 4 actuators located over the flap (labeled 4TE in Figure 5-19), enabled one to trim the model up to $\alpha \approx 15°$ by varying C_μ but limiting it to $C_\mu \leq 1.7\%$ ([7], see double arrow in Figure 5-19). One may recall, that it is the upstream effect of jet entrainment that that enables the trimming of the SACCON and not the downstream redirection of the flow that increases the pressure downstream of the MRL. Using 5 actuators located at the LE was less efficient than operating the 4TE actuators at approximately the same momentum input. When used in conjunction at an aggregate $C_\mu \approx 1.6\%$ the result was worse than the 4TE actuators by themselves. **Thus disrupting the LE vortex does not necessarily increase the stability of a tailless configuration in pitch**.

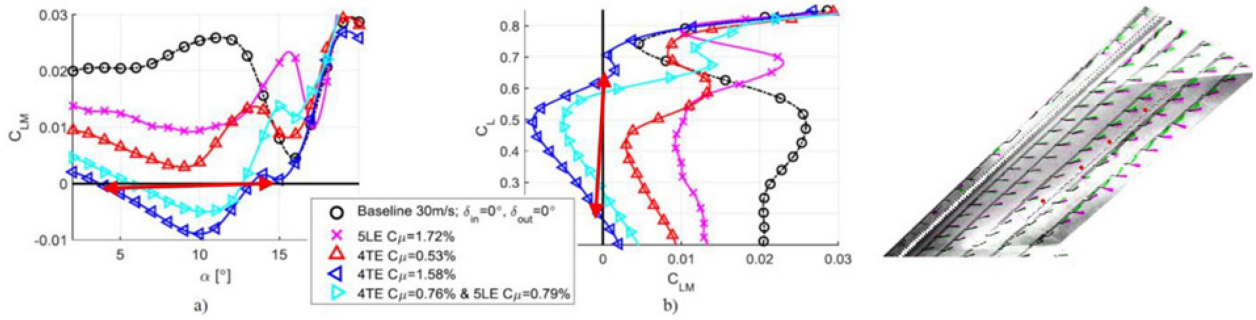

Figure 5-19: The Effects of 4TE Actuators and 5LE Actuators on C_{LM} with MRL Changed to x/c = 0.5505. Tuft Visualization at α = 11°.

5.8 CONTROLLING THE YAW OF SACCON

Spoilers or split flaps are commonly used on tailless aircraft to generate a yawing moment that enables the aircraft to turn. Upper surface spoilers are preferable as they sacrifice less of the airplane's stealthy design [7], thus one assignment given the AVT-239 task group was to explore the generation of yawing moment by AFC. Comparison of the yaw generated by a split flap that was opened at ±20° and ±30° to the yaw resulting from the use of AFC is shown in Figure 5-20. Since a semi-span model was used in these tests, the results measured in absence of flap deflection (baseline) were subtracted from the actuated data or from the deflected (opened) split aileron results. The yawing moment generated by the split aileron deflected at ±20° was $\Delta C_{LN} \approx 0.0045$ and it compares very well to the results of Rein [6] for the same configuration in spite of the differences in Mn and Re (Figure 5-20). The effectiveness of the split flap diminished with α and it became completely ineffective around α = 10°. Increasing the split aileron deflection to ±30° increased the yawing moment to $\Delta C_{LN} \approx 0.014$ but it too was ineffective at higher incidence angles where it is mostly needed.

Using four TE actuators located close to the wing tip provided a $\Delta C_{LN} \approx -0.007$ at all incidence angles considered provided $C_\mu = 1.28\%$. Spacing the actuators equally as shown in Figure 5-5 generated a change in the yawing moment that was nearly linearly increasing in magnitude in the range $0° \leq \alpha \leq 11°$. For $\alpha > 11°$ the $|\Delta C_{LN}|$ started to decline but in a more predictable way compared to the split flap. At incidence corresponding to the range of $6° \leq \alpha \leq 13°$, the evenly distributed actuation outperformed the bunched tip actuation implying that it is not a simple moment-arm calculation that contributes to ΔC_{LN}. Hence, AFC applied close to the trailing edge offers an alternative to common control surface deflection that provides yaw. More significantly, AFC yaw control is still effective at $\alpha > 10°$, where a split flap fails. This might be

important at low speed flight required for loiter, takeoff or landing. Moreover, since the duration for yaw control is short higher levels of C_μ are not necessarily a limiting factor.

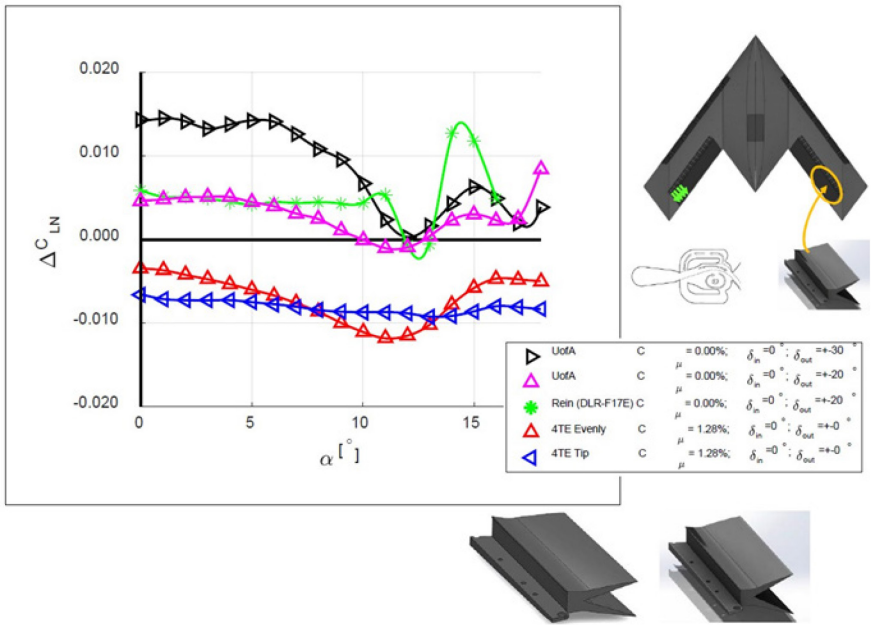

Figure 5-20: Comparison of Yaw Control Provided by a Split Aileron to that Provided by 4 Sweeping Jets in Absence of Surface Deflection.

5.9 INCREASING THE TRIMMED LIFT OF SACCON

Although trimming the SACCON was the primary task of this investigation, a question arose whether one may increase the lift of the model while retaining the trim. AFC was able to trim the model in the absence of control surface deflection up to $C_L = 0.6$ (Figure 5-21, right). By lowering a simple flap to 20° while keeping the same level of AFC input C_{LM} is constant but negative (i.e., the neutral point is maintained up to $C_L = 0.6$), thus trim is required. Assume that one cruises at $C_L = 0.35$ without the use of flaps and one wants to start a landing procedure by lowering flaps and maintaining trim, it can be done by a concomitant decrease of the AFC input, because this condition can be attained by a flap deflection of $\delta = 20°$ and $C_\mu = 0\%$. By adding C_μ as required, on may slow down and increase the trimmed C_L up to $C_L = 0.8$ while around $C_L = 0.75$ very little AFC input is required. One may potentially increase the lift beyond this point by adding a larger AFC input. This proves that one may increase the trimmed lift by combining surface deflections with AFC beyond the currently acceptable level. The above only demonstrates the novel capability and it was not optimized in any manner.

5.10 EVOLUTION OF THE MAGMA MODEL AND THE EFFECT OF AFC ON IT

A good example showing the conventional approach of delaying pitch-break is given in Figure 5-22 where the AR and $\Lambda_{c/4}$ of the 1303 model were reduced by enlarging its trailing-edge surface area. Doing so ameliorated the pitch-break and delayed it from $C_L \approx 0.25$ to $C_L \approx 0.5$ but did not eliminate it. Thickening the LE, a step that is not included among the independent variables used in preliminary design and shown in Figure 5-1, delayed the occurrence of pitch-break further to $C_L \approx 0.68$ and reduced its severity. In this case the thickening representing the "body" in a BWB configuration shifted to the upper surface as shown in grey at the top left in Figure 5-22 while the wing thickening was symmetrical. The normalized maximum thickness of the two airfoil sections taken in the direction of streaming at the rear crank location (Figure 5-22,

top right) differs by approximately ⅓, but the LE radius of the MAGMA is twice as large as the LE radius of the 1303 with the MAGMA planform. The thickening of the wing had a detrimental effect on $\partial C_L/\partial\alpha$ and on C_{Lmax} (Figure 5-22, center). The skin friction drag (i.e., the drag measured at $C_L = 0$) is also higher on the MAGMA model due to the increased wing area, but at the designed cruise attitude its drag is lower yielding $(L/D)_{max} = 15$. The wing thickening is expected to be deleterious at high speeds for which the present model is not designed.

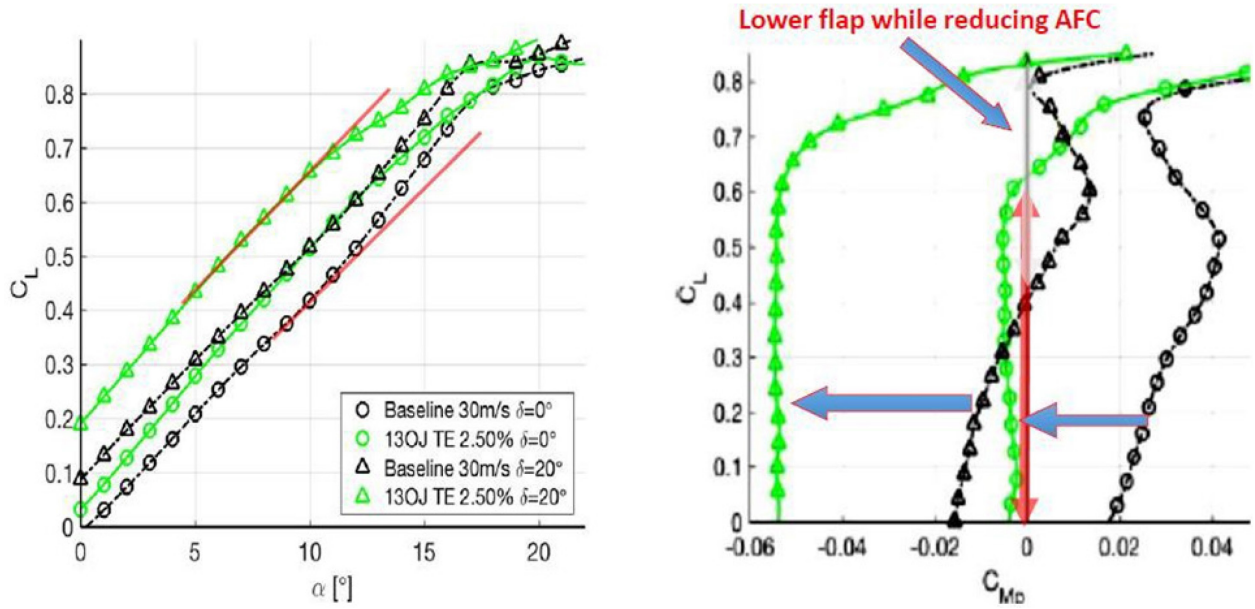

Figure 5-21: Increasing the C_L on the SACCON While Being Trimmed.

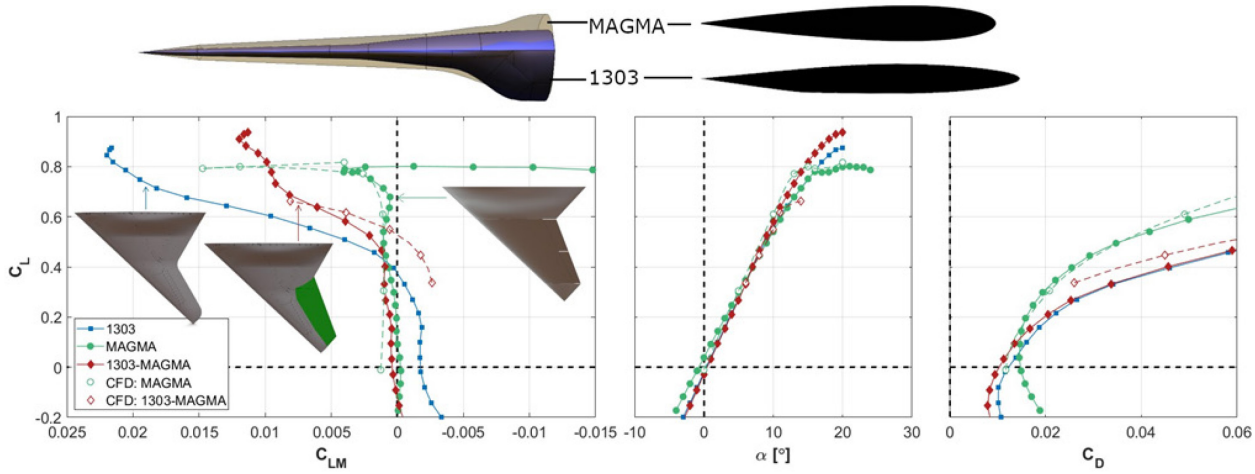

Figure 5-22: The Evolution of the MAGMA Model from its 1303 Predecessor and its Pitch Characteristics.

CFD predicted the dependence of C_L, C_D and C_{LM} on incidence very well as long as there was no major flow separation (Figure 5-22). At higher α, the predicted C_{LM} was much higher than measured, as was the lift prior to the occurrence of complete stall. The tuft-observed flow directions agreed very well with the predicted surface streamline pattern (Figure 5-23, bottom) prior to stall (α = 10°), when approximately 50% of the wing outboard of the crank was stalled (α = 15°) and when the entire outboard wing was stalled (α = 20°).

The calculated pressure distribution pattern agrees very well with the measured one although the measured PSP signature was not calibrated thus providing only a qualitative support for the CFD (Figure 5-23, top).

The large increase in the LE radius of the MAGMA model prevented the creation of a LE vortex resulting in a small separation region at the very tip of the model at $\alpha = 10°$ that progressed inboard and became much larger with increasing incidence, until at $\alpha = 20°$ the separated flow covered the entire surface outboard of the TE crank. Furthermore, there is a good correlation between the measured changes in pressure distribution between the PSP and the calculated pressure contours as marked by the dashed lines in Figure 5-23. Such a good correlation was not expected due to the massive separation that occurred on the outer part of the wing. The computations included wind tunnel wall constraints, because without them the tip flow did not separate at $\alpha = 10°$. This is understandable as in absence of tunnel walls the correct angle of incidence and the pressure field would be different. Since the traditional wind tunnel corrections have not been applied to measured results, the CFD has to include the presence of the tunnel walls.

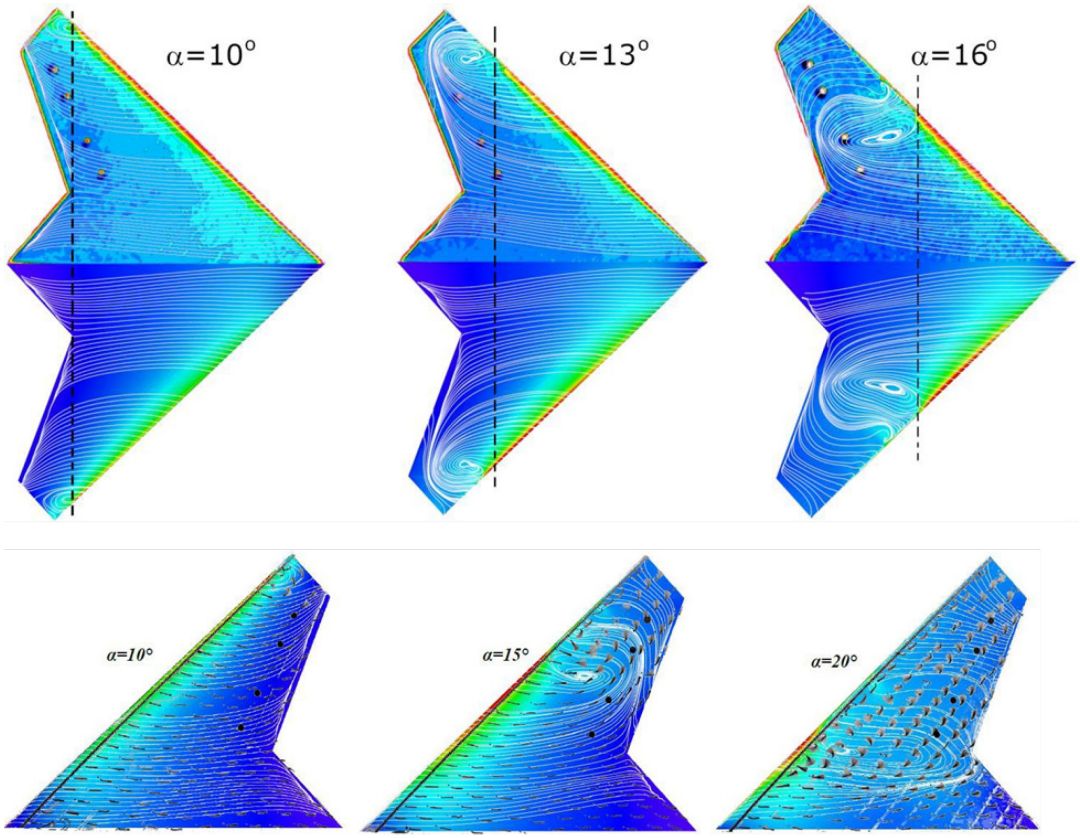

Figure 5-23: Computed and Measured Surface Flow Direction and Pressure Distribution on the MAGMA Model.

The dependence of C_{LM} on incidence prior to stall of the 1303 model was divided into three regions (Figure 5-24, right). For $\alpha < 5°$ the LE flow is attached and $C_{LM} = 0$. Between $5° < \alpha < 10°$ a LE vortex originates near the tip resulting in outboard spanwise flow (Figure 5-24, left). The origin of the LE vortex propagates inboard with increasing α, but its circulation (strength) increases in the outboard direction due to the vortical fluid that is continuously feeding the LE vortex. This lowers the pressure at the tip resulting in the large $\partial C_{LM}/\partial\alpha$. At $\alpha > 10°$ the flow separates at the tip with air rushing inboard along the LE surface. The tip stall may have been initiated by the LE vortex turning in the direction of streaming and lifting off the flow outboard of its path (axis). This creates a situation where the LE surface flow proceeds in opposite directions as seen on the tuft picture at $\alpha = 15°$ (Figure 5-24).

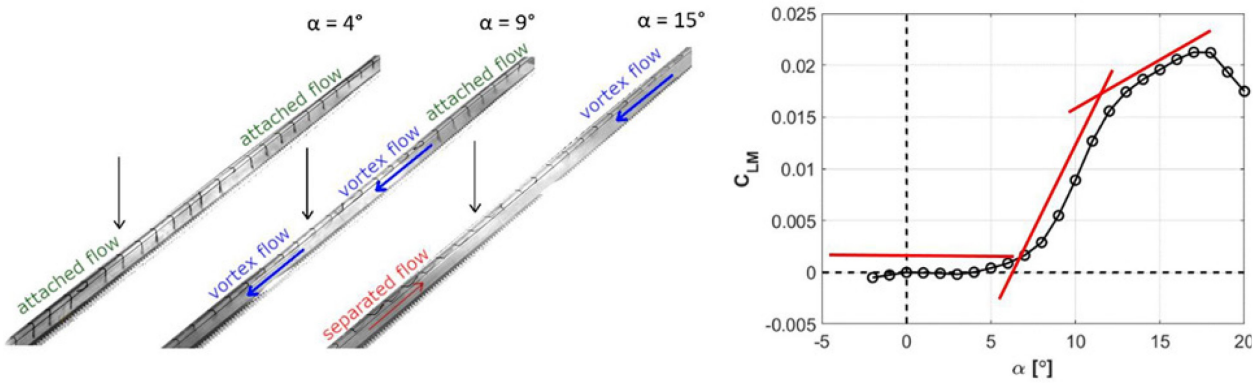

Figure 5-24: LE Tuft Visualization of the 1303 and its Relationship to the Dependence of C_{LM} on α.

Pressure Sensitive Paint (PSP) and CFD reinforced the observations explained above and are used to explain the dependence of C_{LM} on α (Figure 5-24, right). The Boeing Computational Fluid Dynamics (BCFD7 [23]) flow-solver was used to obtain solutions of the Model 1303 configuration. The gas was modelled as calorically perfect air using Sutherland's law for viscosity. Thermal conductivity was determined by assuming a constant Prandtl number of 0.72. Reynolds Averaged Navier-Stokes (RANS) simulations were conducted using the Spalart-Allmaras turbulence model [24] (SA) with Rotation Correction [25] (SA-RC).

The model was simulated both installed in the wind tunnel as well as in a free stream for comparison. Results from the configuration installed within the tunnel are shown in Figure 5-25 to be directly comparable to the measurements. The grid topology in the simulations employed unstructured prismatic cells to resolve the boundary layer near viscous walls and become tetrahedron outside the viscous layer. The grid size for this configuration was near 20M cells and a first cell grid spacing of the wall of .0001" was used to provide a y+ near 5 near the leading edge of the wing.

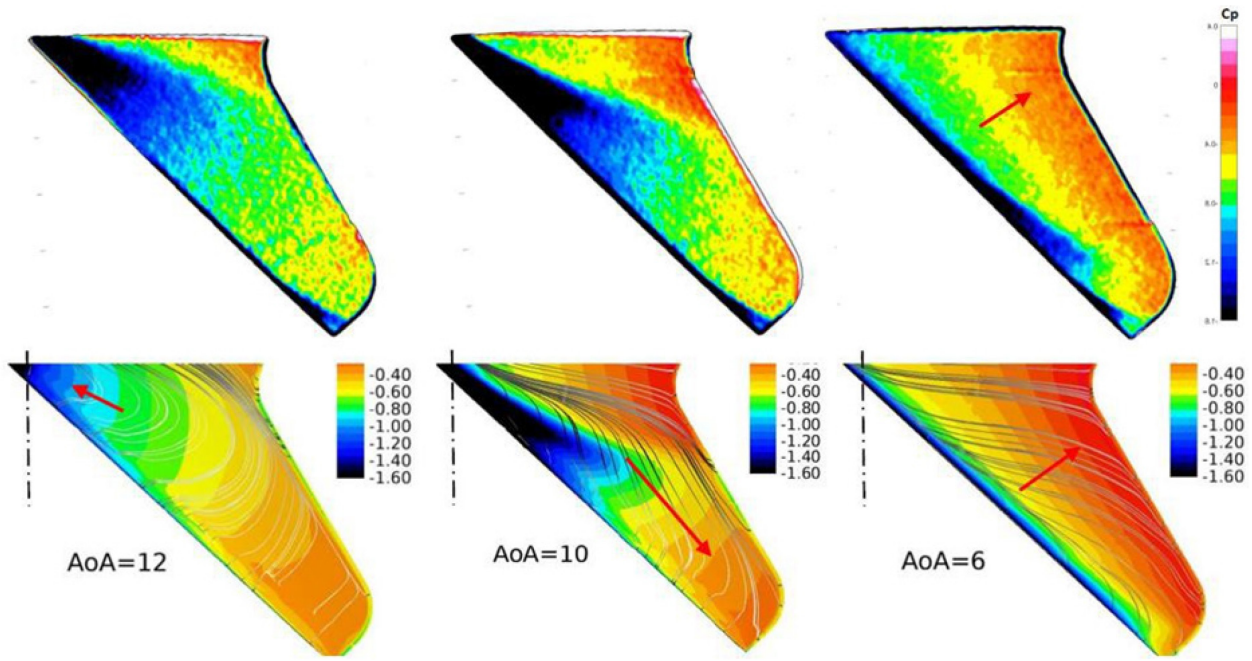

Figure 5-25: Measured and Calculated Pressure Contours and Calculated Surface Streamlines on the Outer Part of the 1303 Model.

The formation of the LE vortex near the wing tip was confirmed by the low surface pressure (colored in blue) that spanned some 30% of the local chord at $\alpha = 6°$ (Figure 5-25, top right). The existence of the LE vortex was also suggested by the computed surface streamlines that are parallel to the leading edge before turning upstream at the tip (Figure 5-25, bottom right). At $\alpha = 10°$, the origin of the LE vortex moved inboard beyond the crank (see Figure 5-33 top right) and the vortex core bent downstream reaching the TE inboard of the tip (Figure 5-25, center). The general migration of the leading-edge vortex from near the tip at $\alpha = 6°$ to near the root at $\alpha = 12°$ is captured by the CFD simulations. There is a hint of the bifurcation of the leading-edge vortex near the tip from the CFD at $\alpha = 6°$ but not as substantial as indicated by the PSP. The CFD does not appear to capture this wing tip expansion effect (dark blue contours) seen in the measurements at $\alpha = 10°$ and 12°. The direction of the vortex core is marked by the surface streamlines that are bunched together. The adverse pressure gradient changed direction from being in the chordwise direction at $\alpha = 6°$ to being mostly in the spanwise direction at $\alpha = 10°$ (see arrows in Figure 5-25). The increase of pressure toward the tip is both measured and calculated as seen in Figure 5-25, center. The footprint of the vortex is substantially weaker at $\alpha = 12°$ since its origin moved inboard with increasing α. The adverse pressure gradient along the span, $\partial p/\partial z$, was also reduced, but the surface streamlines arch toward the LE and turn inboard across from the crank confirming the observation made by the tufts. When the wing begins to have significant reversed flow at $\alpha > 10°$, the CFD solutions do not converge as well as at the lower α indicating some flow unsteadiness not captured in the RANS simulations. Boeing's Research and Technology group is currently exploring the accuracy of predicting these types of unsteady separated flows (with and without AFC) over a variety of wing types at high angles of attack using time-accurate approaches. The recommendations from these studies will benefit future analyses of swept wings like the 1303 that are highly sensitive to angle of attack including guiding placement and estimating effectiveness of AFC for enhanced manoeuvrability.

Since the lift slopes of the 1303 and the 1303-MAGMA model are identical prior to stall and the drag polar hardly differed between these two models (Figure 5-22), the substantial difference in the pitching moment is not well understood as it cannot be attributed to the difference in the reference areas ($C_{LM} = \frac{M}{q_\infty Sc}$ and the root chord is identical for both models). Tuft pictures suggested that the added area in the back of the converted 1303 model did not affect the LE vortex much as long as it remained at the LE (Figure 5-26, bottom). It first appeared around $\alpha \approx 5°$ as it did on the 1303, but after turning downstream at $\alpha = 10°$ it affected a much larger area. At $\alpha = 14°$ the flow separated from the outboard LE region encircled in blue in Figure 5-26, (bottom left). The tuft pictures taken on the 1303 wing show very similar patterns (Figure 5-24, left).

An LE vortex was not observed on the true, thick MAGMA model (Figure 5-26, top). At $\alpha = 10°$, a separated region having a strong inboard velocity component was detected at the wing tip and it increased in size with increasing α. It is therefore the creation of the LE vortex and the change of its path over the wing that causes the nonlinearities in C_{LM} on the SACCON, on the 1303 and on its modified, thin MAGMA planform.

The computed pressure contours and surface streamlines on the 1303 indicate that an adverse chordwise pressure gradient ($\partial p/\partial x>0$) deflects the surface flow outboard prior to pitch-break (Figure 5-25, $\alpha = 6°$). At higher α, the dominant adverse pressure gradient near the wing tip turns in the spanwise direction ($\partial p/\partial z>0$) due to the change in the size and the path of the LE vortex that tends to lift the flow outboard of its path away from the surface. This $\partial p/\partial z$ forces the spanwise flow that was created at lower α, to turn in the upstream chordwise direction toward the LE. It is the latter motion that results in increasing the pressure downstream of the MRL and in pitch-break (Figure 5-25, $\alpha = 10°$).

The results shown in Figure 5-22 indicate that the MAGMA does not have a pitch-break problem since the small pitch-break occurs close to the C_{Lmax} where the wing stalls anyway. Consequently, AFC research on this particular model relevant to the AVT-239 tasks was directed toward yaw control while maintaining the model trimmed in pitch. In the absence of AFC, the maximum L/D of approximately 15 was attained by the model at $\alpha \approx 6°$ corresponding to $C_L = 0.35$, suggesting that the most effective yaw control should be

provided at $C_L \geq 0.35$. The model has two deflectable control surfaces: an aileron on its outboard side and an elevon close to the TE crank. Deflecting the aileron upward, lowers the drag and reduces the lift while deflecting it down does the opposite. Consequently, differential deflection on opposite sides the model provides large bank (rolling moment) and adverse yaw. On a regular airplane the bank generated by the rolling moment enables a turn after the adverse yaw had been counteracted by the rudder and the steepness of the turn, once established, is controlled by pitch and power. On a tailless aircraft roll is undesirable, particularly in the absence of a vertical stabilizer and rudder, so a spoiler or a split flap that generate mostly drag replace the conventional aileron. However, since the currently flying MAGMA model still has a conventional aileron its effect was studied as well (Figure 5-27).

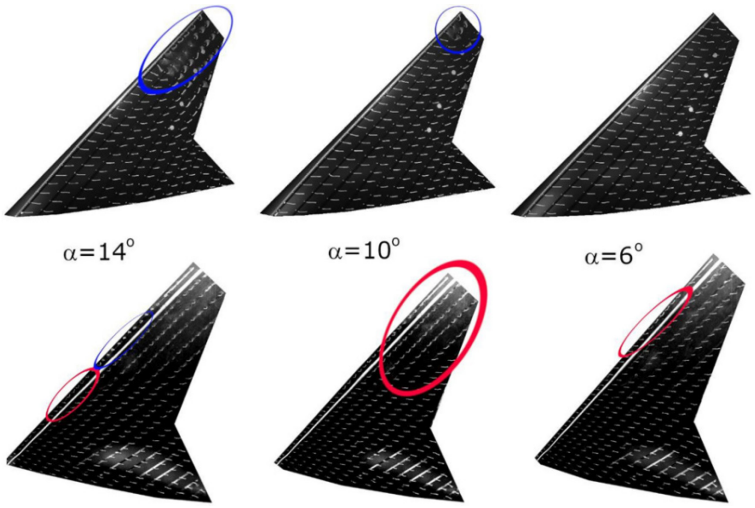

Figure 5-26: Tuft Visualization on the MAGMA Model and its Thin Planform Obtained by Modifying the 1303 Model.

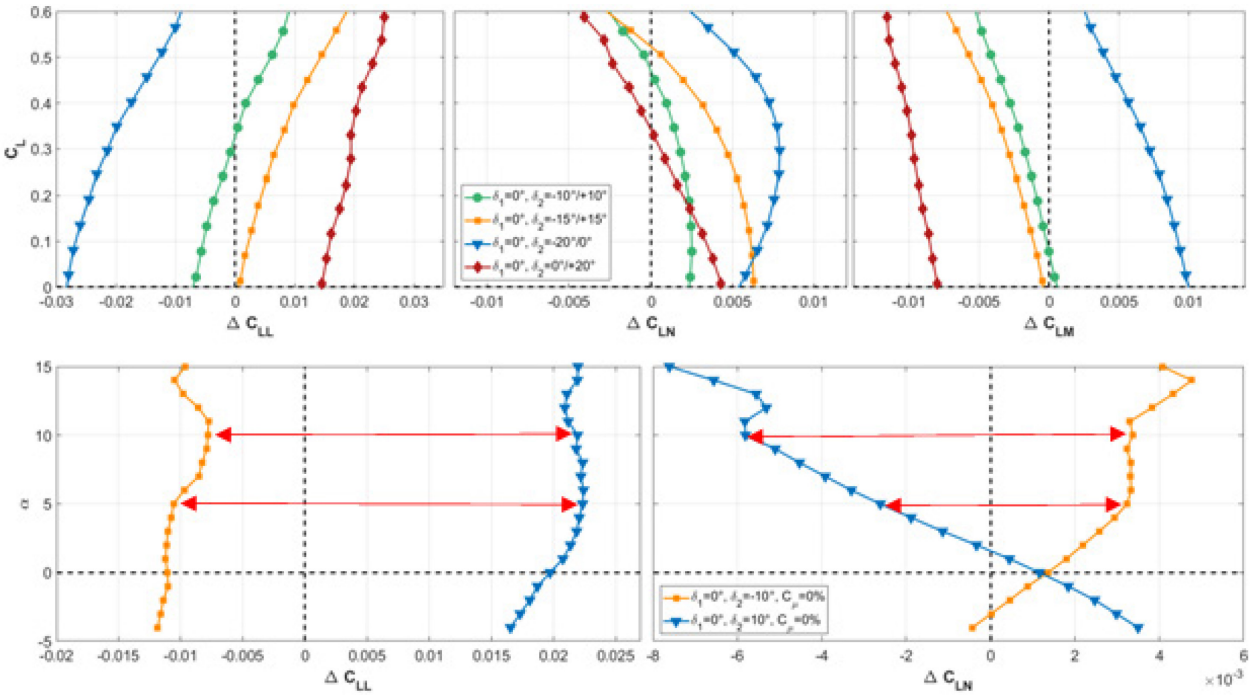

Figure 5-27: Split Flap vs. an Aileron C_{LM}, C_{LN} and C_{LL} Dependence on C_L.

A symmetrically deflected split flap generated a negative C_{LM} that can be overcome by an upward bias of the split flap (Figure 5-27, top right). The maximum yawing moment generated by the current split flap was $\Delta C_{LN} = 0.004$ at best cruise conditions corresponding to $C_L = 0.35$. A flap separation of 30° was required to achieve this yaw, but at $C_L = 0.5$ the split flap was ineffective and at higher C_L it changed the sign of C_{LN} due to the spanwise flow that changes its sign as a consequence of flow separation (Figure 5-27, top-center). The associated rolling moment at best cruise is $\Delta C_{LL} = 0.008$ and it might require a vertical fin to reduce the bank in turn (Figure 5-27, top left). A pair of ailerons deflected in an opposite direction at +/-10° generate a comparable yaw ($\Delta C_{LN} = 0.006$) but a much larger rolling moment of $\Delta C_{LL} = 0.032$ in the opposing direction resulting in side-slip that has to be overcome by a rudder (Figure 5-27, bottom). The big advantage of the aileron is that at $C_L = 0.6$ corresponding to slower flight, its effectiveness increases while the split flap or spoiler are ineffective.

AFC, whose main purpose is to redirect the flow thus resulting in yaw while retaining trimmed conditions in pitch, is effective wherever the spanwise component of the surface velocity is dominant. Since in this case the LE radius of curvature is fairly large, an attempt was made to redirect the flow by a sweeping jet whose plane of sweep is normal to the LE attachment line. The jet emanated from the lower surface of the wing and was oriented forward and downward, thus emulating a fluid vortilon (Figure 5-4). Another option is to deflect the spanwise flow at the rear of the wing near its tip. Therefore, actuator 4 and the "fluid vortilon" were independently tested and these results are shown at the top of Figure 5-28. The effect of a 10° deflection of an aileron is also plotted in this figure, for the sake of comparison. At $C_L = 0.35$ the aileron deflection yields a yaw of $\Delta C_{LN} = -0.0025$ and it attains $\Delta C_{LN} = -0.0055$ at $C_L = 0.6$ while the rolling moment is significantly larger.

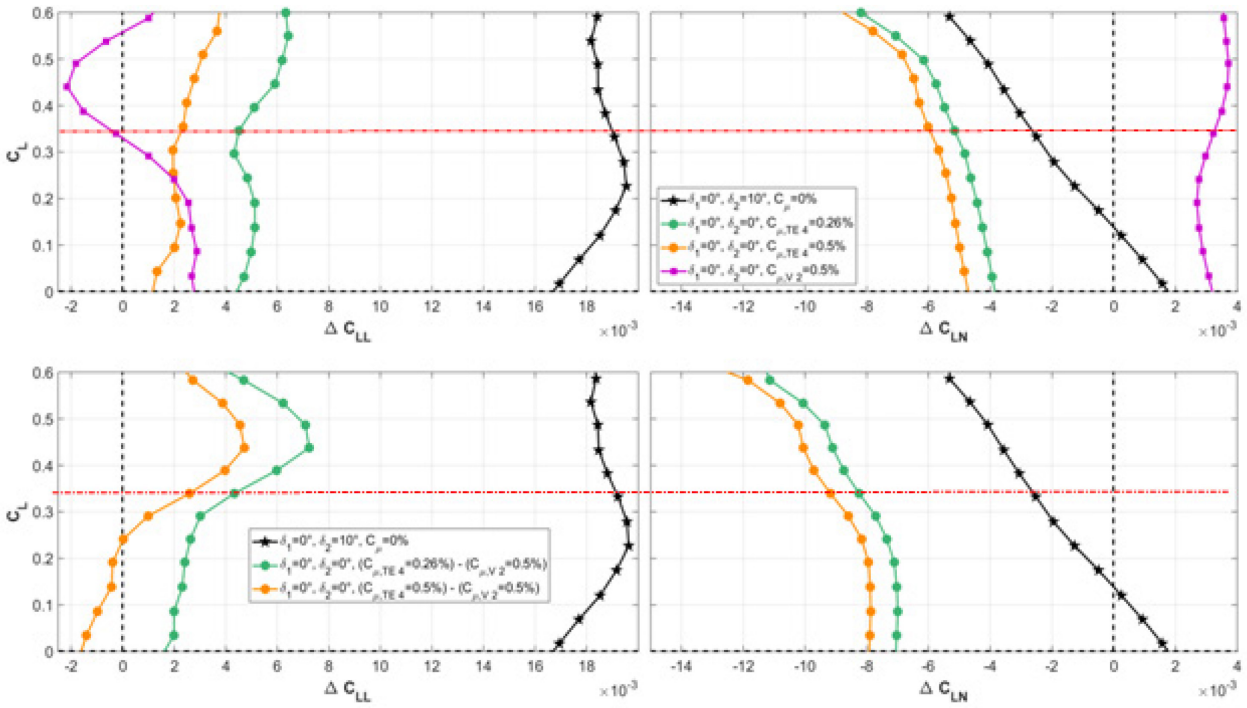

Figure 5-28: The Effect of AFC on C_{LN} (Right) and C_{LL} (Left) and Compared to 10° Deflection of an Aileron. The use of a vortilon on one wing and actuator #4 on the other gives the results shown at the bottom.

Actuator 4 with its jet axis normal to the hinge line at $C_\mu = 0.26\%$ provided yaw that was almost twice as large as the aforementioned aileron deflection attaining $\Delta C_{LN} = -0.005$ at optimal cruising conditions. Its

ΔC_{LL} was approximately the same providing ($\Delta C_{LL}/\Delta C_{LN} \approx 1$). Doubling the C_μ input increased ΔC_{LN} to ΔC_{LN} = -0.006 but it reduced the ratio of $\Delta C_{LL}/\Delta C_{LN} \approx 0.33$ at C_L = 0.35. On the other hand, the fluid vortilon provided ΔC_{LN} = +0.0032 while requiring C_μ = 0.5%. This ΔC_{LN} was independent of the lift. Consequently, using a fluid vortilon on one wing and actuator 4 on the other wing would provide a ΔC_{LN} = 0.009 at an aggregate $C_\mu \approx$ 1% with a vanishingly small ΔC_{LL}. One may note that at this sweeping jet orientation, an increase in C_μ had a very small effect on ΔC_{LN} but a relatively large effect on ΔC_{LL} (Figure 5-28, bottom).

Although it was presumed that the axis of the sweeping jet should be orthogonal to the local streamline the first direction selected was normal to the aileron hinge line. Keeping the C_μ = 0.26% and changing the direction of actuation revealed that by turning the sweeping jet outboard approximately 30° generated a higher yawing moment while maintaining the neutral point and the ratio of ($\Delta C_{LL}/\Delta C_{LN}$) virtually unchanged (Figure 5-29, top). Thus far, there was no attempt at directional optimization but rather at establishing the sensitivity of the flow to actuation direction and hence the angle providing the best yaw result may not be optimal.

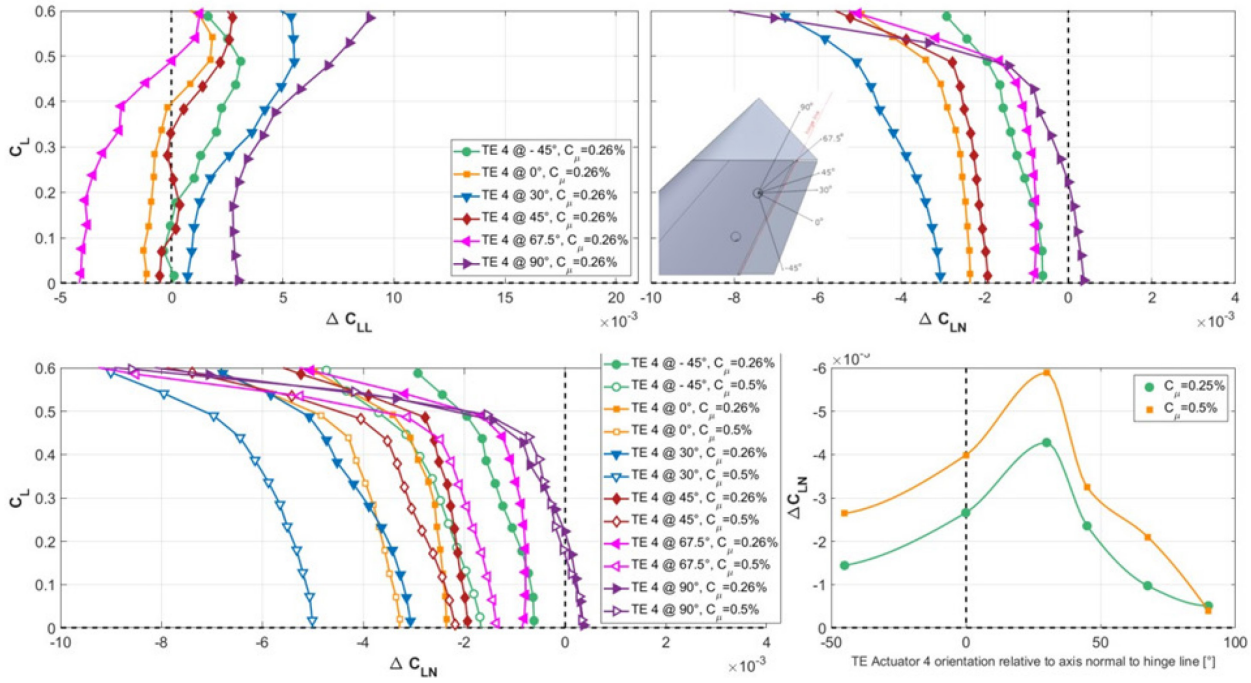

Figure 5-29: The Effect of Orientation of Actuator 4 on C_{LN} (Top Right) and C_{LL} (Top Left) While C_μ = 0.26% (Top) and the Effect of its Increase to C_μ = 0.5% (Bottom).

Doubling the C_μ input of a single actuator could either increase ΔC_{LN} substantially or it had little effect on its value (Figure 5-29, bottom right). At cruise condition of C_L = 0.35 blowing outboard at an angle of 30° to the original orientation (normal to the hinge line) increased the result by almost ΔC_{LN} = -0.002, while rotating the actuator 45° inboard yielded about ΔC_{LN} = -0.001 when doubling the momentum input. The effect is less when orienting actuator 4 so that it blows 45° outboard and is minimal when the jet axis is parallel to the hinge line. It suggests that there is a strong coupling between the jet orientation and its C_μ as far as ΔC_{LN} is concerned.

One may ask whether a single actuator generates a larger C_{LN} than two actuators provided the aggregate momentum input remains unchanged. This increases the volume flow needed by a $\sqrt{2}$. Comparing the two options by using actuators 3 and 4 at C_μ = 0.5% while blowing at 45° outboard revealed an increase in attainable yawing moment of ΔC_{LN} = -0.0021 at cruise condition (C_L = 0.35) that increased to ΔC_{LN} = -0.003 at C_L = 0.5 (Figure 5-30, left). Maintaining a C_μ = 0.5% per actuator thus doubling the volume flow, doubled the

yawing moment capability of the MAGMA increasing it to ΔC_{LN} = -0.0073 at optimal cruise condition and to ΔC_{LN} = -0.012 at C_L = 0.6.

The effectiveness of a single fluid vortilon is substantially lower than that of the rear upper surface actuator (Figure 5-28), however, its advantage is in its different sign that enables using TE actuation on one wing and fluid vortilons on another wing in order to increase the total yawing moment of the model. Doubling the C_μ input into the individual midspan vortilon increases its effectiveness by ΔC_{LN} = 0.0015 at cruise and around C_L = 0.6 (Figure 5-30, right). The result at cruise was independent of the choice between the midspan vortilon and the tip vortilon. However, when the two fluid vortilons were combined at an aggregate momentum input that was equal to the individual vortilon's level (i.e., C_μ = 0.5%) the result was inferior when compared to the value obtained by increasing the C_μ to an individual vortilon. This result applied to an increase in C_μ input from 0.26% to 0.5% but it did not apply to the increase in C_μ from 0.5% to 1%. In the latter case, the effectiveness of the fluid vortilon doubled as a result of doubling momentum input (Figure 5-30, right), thus the ratio between the jet and the free stream velocity might have been of significance whenever the fluid vortilon is considered. Consequently, under some conditions the vortilon's effectiveness was comparable to that of actuator 4 for the same momentum input.

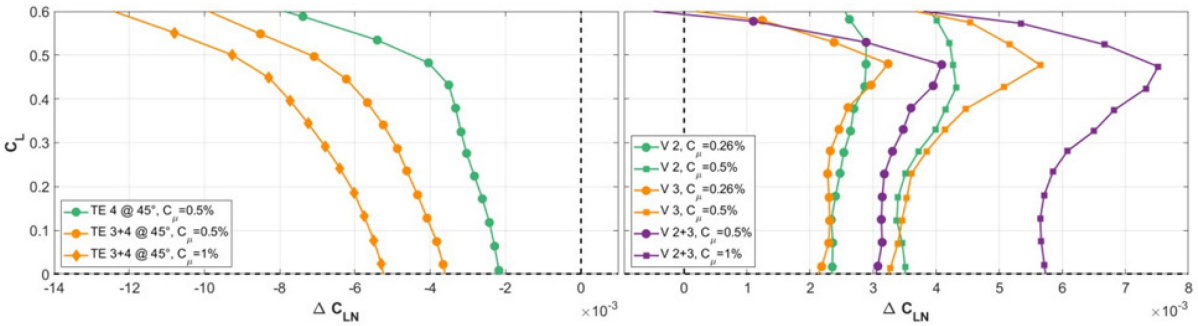

Figure 5-30: The Effect of Increasing the Number of Actuators (Left) or Vortilons (Right) on C_{LN}.

Combining the effect of actuator 4 and fluid vortilon at an aggregate C_μ = 1% generates a ΔC_{LN} = -.01 at cruise. One could use for this purpose either vortilon 2 or 3 and by combining them both and adding momentum at an aggregate C_μ = 1.5% one may attain ΔC_{LN} = -0.012 at cruise and ΔC_{LN} = -0.014 at C_L = 0.5. Since doubling the C_μ of a single actuator is not effective (Figure 5-28, top) a combination of actuators 3 and 4 with one or two vortilons on the opposite wing may provide the best yawing moment (Figure 5-31).

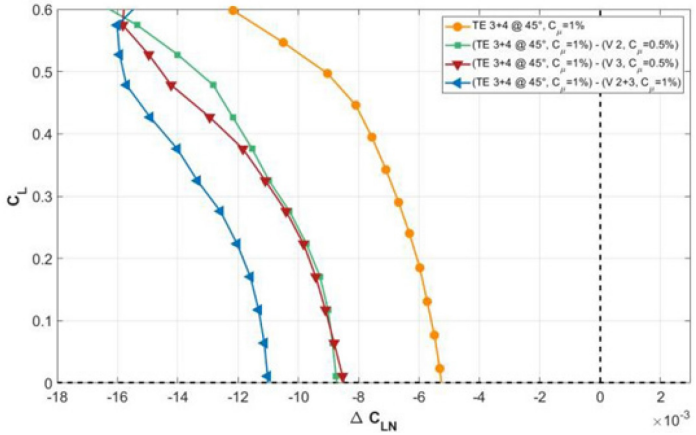

Figure 5-31: The Impact of Trailing-Edge Actuators 3 and 4 in Combination with a Vortilon on the Opposite Wing.

Since the C_L and C_D of the 1303 model and the MAGMA planform derived from it are virtually identical (Figure 5-22), the effects of AFC on the 1303 are considered. For a given wing geometry C_L and C_{LM} are close coupled functions of attitude (α), control surface deflection (δ) and AFC (μ), thus:

$C_L = (\alpha, \delta, \mu)$ & $= (\alpha, \delta, \mu)$ and one may maintain a neutral point provided:

$$\frac{dC_{LM}}{dC_L} = \left[\frac{\partial C_{LM}}{\partial \alpha} + \frac{\partial C_{LM}}{\partial \delta}\frac{d\delta}{d\alpha} + \frac{\partial C_{LM}}{\partial \mu}\frac{d\mu}{d\alpha}\right]\frac{d\alpha}{dC_L} = 0 \tag{5-1}$$

or,

$$\frac{dC_{LM}}{d\alpha} = \frac{\partial C_{LM}}{\partial \mu}\left[\frac{\frac{\partial C_{LM}}{\partial \alpha}}{\frac{\partial C_{LM}}{\partial \mu}} + \frac{\frac{\partial C_{LM}}{\partial \delta}}{\frac{\partial C_{LM}}{\partial \mu}}\frac{d\delta}{d\alpha} + \frac{d\mu}{d\alpha}\right] = 0 \tag{5-2}$$

For this equation to be satisfied while $(\partial C_{LM})/\partial\mu \neq 0$ the term in the square bracket has to vanish yielding after integration the AFC input required to maintain a neutral point on a given wing:

$$\mu = -\int_{\alpha_1}^{\alpha_2} \frac{\partial C_{LM}/\partial \alpha}{\partial C_{LM}/\partial \mu} d\alpha - \int_{\delta_1}^{\delta_2} \frac{\partial C_{LM}/\partial \delta}{\partial C_{LM}/\partial \mu} d\delta + \mu(\alpha_1, \delta_1) \tag{5-3}$$

Where μ is not limited to C_μ but implies variation of actuators, their location and their orientation on the given wing.

The validity of the above equation was tested by adjusting the AFC input and changing incidence while maintaining the model's neutral point and the results are shown in Figure 5-32. AFC delayed the unstable pitch departure by 4.7° thus tripling the usable lift coefficient. This test was carried out without deflecting a control surface although that variable could be added as it was done on the SACCON [7]. The implications of this equation are far reaching as they suggest strong coupling between AFC and inviscidly determined characteristics of a wing implying that the traditional "inviscid limit" obtained by CFD does not hold when AFC is used. The effectiveness of an aileron (i.e., it's ΔC_{LN}) augmented by AFC at its hinge was more than doubled when used on this model (Figure 5-32, right).

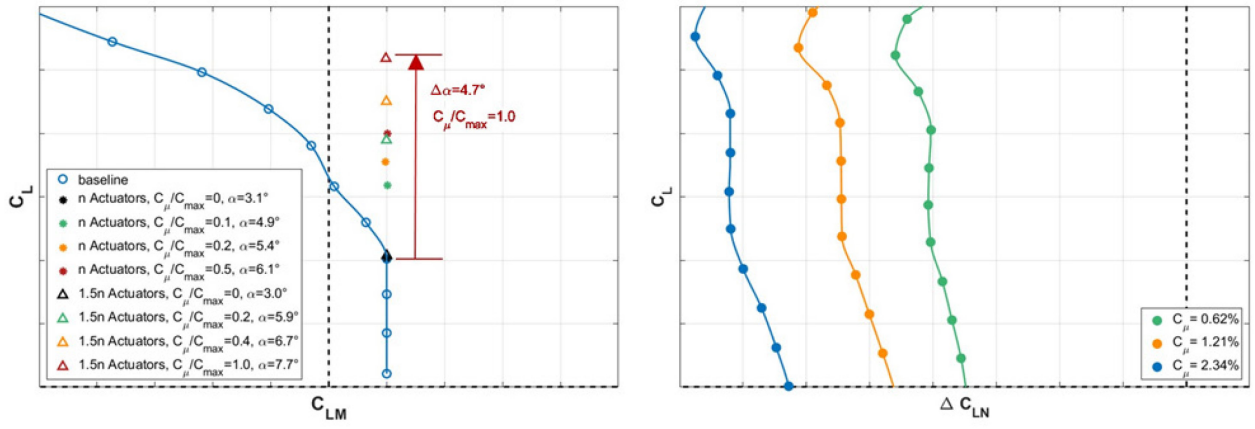

Figure 5-32: Maintaining the Neutral Point and Affecting the Yaw on the 1303 Model.

The application of PSP to the 1303 provided invaluable information about the flow physics on this model that indicated how AFC should be used in conjunction with CFD in the future. Observations focusing on the

significance of the LE radius were discussed in conjunction with Figure 5-25 and they alerted us to the danger of comparing the flow fields on similar planforms of wings (e.g., the flow over the SACCON, the MAGMA and the 1303).

The nose-up pitch-break on the 1303 occurs in the vicinity of $\alpha = 7°$ in the absence of control surface deflection (Figure 5-24, right). So one may examine the effect of AFC on the pressure distribution prior to pitch-break and after its occurrence for the baseline configuration. At $\alpha = 6°$ the low pressure region at the leading edge was confined to a narrow strip except of a small region near the tip where the low pressure widened and it separated from the tip-vortex foot print. Downstream of the mid-chord line (seen as the yellow band where $C_P \approx 0$) there is a region of $C_P > 0$ suggesting that the flow is attached to the surface all the way to the tip (Figure 5-33(a)). The introduction of AFC increased the pressure over the aft portion of the wing (Figure 5-33(b)), preventing the vortex from turning in the free stream direction. Consequently, the difference between these pressure distributions results in an increase of pressure over the aft surface where the aileron is located. Pushing the vortex outboard toward the tip resulted in a narrow band of positive pressure perturbation leaving the LE and being slightly inclined to it (see the encircled zone in Figure 5-33(c)). An increase in C_P behind the axis of rotation (marked by the blue dashed line) implies pitch-up resulting from the actuation seen in this figure – and yet the net effect of AFC that was applied to the entire span of the model was to provide a nose down pitching moment ($\Delta C_{LM} < 0$). Hence, AFC must have changed the flow over the inboard part of the model that overcame the adverse outboard effect.

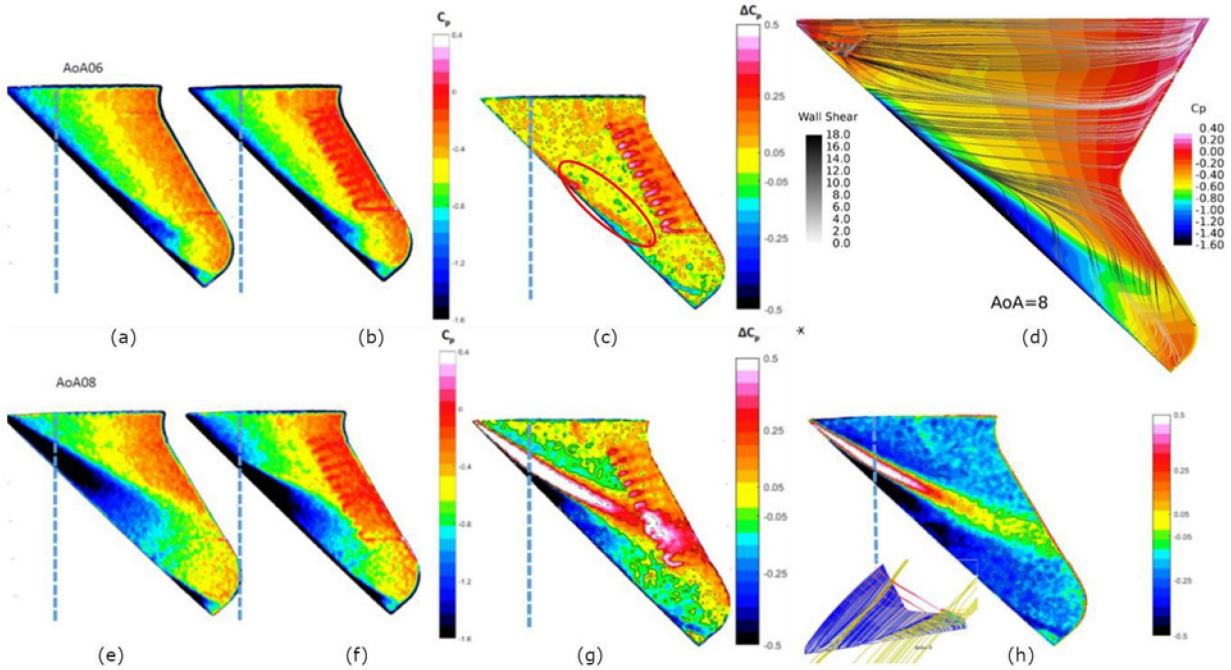

Figure 5-33: Pressure Distributions over the Outer Part of the 1303 Taken at α = 6° and 8°: Baseline PSP (a), (e) and CFD (d); AFC Over the Elevon and Aileron at C_μ = 2% (b), (f), Pressure Difference Between Elevon + Aileron AFC and Baseline (c), (g); Pressure Difference Between Elevon AFC and Baseline (h).

Actuation over the aileron surface at $\alpha = 8°$ generated the most dramatic change in the flow over the painted outer section of the 1303 by preventing the LE vortex to turn downstream and redirecting it toward the tip (Figure 5-33(f)). The jets increased the pressure over the aileron surface, creating an adverse pressure gradient in the chordwise direction affecting the path of the LE vortex. Outboard of the white diagonal strip (Figure 5-33(g)) is a green zone marking a reduced pressure associated with the change in the LE vortex direction, while the green zone inboard of the white strip was caused by jet entrainment.

It was observed that actuation over the hinge of the elevon (located on the inboard part of the 1303 wing) was much more effective than over the aileron for comparable input momentum levels. Inactivating the outboard actuators located over the hinge of the aileron while maintaining actuation over the inboard part of the wing changed the outboard flow field substantially. The difference pressure contours (shown in Figure 5-33(h)) demonstrate the large reduction in pressure achieved by the inboard actuation on the wing section outboard of the crank. It is clear that the LE vortex remained at the LE at $\alpha = 8°$ instead of turning downstream as it did in the absence of AFC (Figure 5-33(e)) because the white band marking an increase in C_P is present on both pressure difference contours plotted in Figure 5-33(g), Figure 5-33(h). The strength of the vortex was probably changed by the inboard actuation that demonstrate the global effect of the actuation that was observed by the tufts on a simple swept-back wing (Figure 5-14). Most significantly, the results shown in Figure 5-33 bottom suggest that actuation outboard of the crank is deleterious. One may conclude that the location, orientation and number of actuators should change with all other parameters that affect the flow over such a configuration.

CFD provided pressure distributions and surface stream lines for the baseline configuration thus providing guidance for AFC applications and enabling comparison with the pressure contours measured. There is a very good agreement between the CFD and the experiment as seen in Figure 5-23 where the continuous, clean, computed contour lines delineate clearly the pressure gradients that are hard to distinguish in an experiment. The surface streamline pattern that changes with incidence also helps in determining the actuation orientation (Figure 5-33(d)).

5.11 CONCLUDING REMARKS

Typical planforms of tailless, BWB aircraft look like the X-47 sketched in Figure 5-34 with varying ratios between the inner and outer areas and their relative sweep. The cranked parallel wing extension increases the AR thus improving the L/D in cruise. It also reduces the average-quarter-chord sweep, $\Lambda_{1/4}$, making the planform more stable (Figure 5-1). The outboard wing may have a small outwash whose negative local C_L may trim such an airplane around its CG that is marked by the dashed line in the sketch. It was observed that a wall-jet and in particular a sweeping wall-jet emanating from the wing surface increases the pressure under its path (e.g., Figure 5-18 and Figure 5-33). The pressure perturbation is larger at the LE because of the low C_P existing there. Thus jets emanating upstream of the dashed line will result in a negative C_{LM} and jets emanating downstream of it result in pitch-up. This concept was used in the past (e.g., A-5 “Vigilante”) and it led to LE slot blowing that covered a large portion of the wing area. Using jet sheets over deflected flaps helped to overcome the adverse pressure gradient caused by the flap deflection thus maintaining attached flow at larger deflection angles, δ, and it is widely referred to as boundary layer control. This use of momentum input applies to two-dimensional flow and it does not require wing sweep.

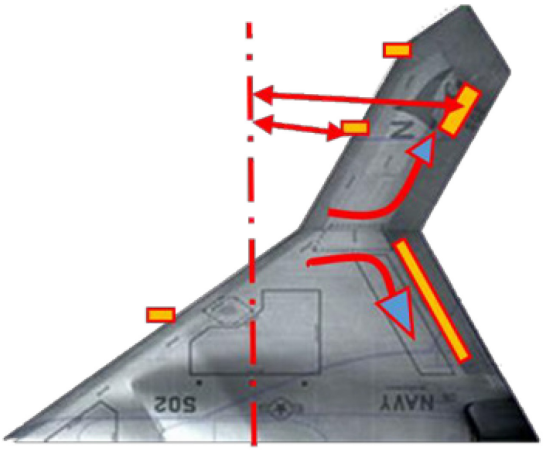

Figure 5-34: The X-47 Planform and Potential Application of AFC on Such a Planform.

However, this is not what AFC is all about as it was demonstrated on the 757 vertical tail experiment in the 40 x 80 wind tunnel at NASA [18], where a single jet emanating from a small nozzle had a large effect on the rudder efficacy while covering a very small area of the rudder's surface. Interference with the spanwise flow over a wing and with its LE vortex (if there is one) provides large control authority for a small input of momentum or mass flow. Spanwise flow dominates the surface velocity on a swept wing near the front attachment line and over the aft portion of the wing. Interfering with it at the LE by using passive devices such as vortilons, fences and snags is common. The use of AFC near the LE met with little success [26] because it was applied to the upper surface of the wing where the chordwise flow was dominant and it covered most of its span as it was done on the "Vigilante". One may create a substantial effect whenever the sweeping jet emanates from a nozzle located close to the attachment line on the lower surface of the LE. Interfering with the spanwise flow over the aft portion of the wing is much easier because it is less sensitive to actuation location as long as the flow remains attached to the surface. It also provides a longer moment-arm for pitch control than actuation at the LE (see Figure 5-34).

On configurations that have a moderate LE sweep (MAGMA 47°, SACCON 53°), the percentage of C_L generated by the LE vortex depends largely on the LE radius of curvature. The MAGMA stalls without a LE vortex being present and hence its $\frac{\partial C_L}{\partial \alpha}$ and C_{Lmax} are smaller than on its thin planform made out of the $\partial\alpha$ 1303 model. However, since a LE vortex increases the drag, the $(L/D)_{max}$ of the MAGMA is 50% larger than its thin planform would provide, its critical Mn is expected to be smaller unless its airfoil becomes supercritical. The absence of a LE vortex delays the pitch-up departure on this model and makes it gentle in comparison to the 1303 or the SACCON, thus AFC can only increase its lift and provide yaw whenever the deflection of control surfaces is undesirable. Using a single actuator located in the aft of the wing's upper surface and a fluid vortilon on the opposite wing provides a $C_{LN} = 0.01$ while requiring an estimated air supply of 1.62 lbs/sec per meter^2 of the wing area at Mn = 0.8 if the MAGMA were ever to fly at that Mn. This is an extrapolated result that assumes constancy of C_μ as being the leading parameter affecting yaw control. The effectiveness of the actuation at high speeds is unknown and there may be other parameters (other than C_μ) affecting the flow control. Increasing the number of actuators or their size and adding an actuator at the LE provides a C_{LN} of 0.014 while requiring an estimated mass flow of 2.42 lbs.

To control the flow over the SACCON or the 1303 and its thin MAGMA derivative is more complicated because a LE vortex is involved. A change in LE radius, a snag or a vortilon affect the vortex direction resulting in non-linear pitch behavior. Thus, the primary task of AFC on thin planforms is to control pitch in order to avoid accidents of the Dark Star type [27]. AFC was able to double the usable (trimmed) lift on the SACCON and even triple it on the 1303 by actuating from the aft part of the wing. Actuation from the LE was mostly deleterious. The LE vortex generated at the apex of the SACCON wing changed its direction due to an abrupt change in its LE radius and adopted an "S" trajectory ending up being parallel to the TE. Thus, the trajectory of the actuation was easy to guess. A linear array of sweeping jets increased the pressure downstream but reduced it upstream due to jet entrainment. The reduction of pressure downstream of the MRL provided the nose down stabilization. However, it also pulled the second LE vortex from the tip creating another adverse effect at high incidence.

The trailing-edge crank often separates the outboard wing from the thick trapezoidal body. The surface streamlines outboard of the TE crank move outboard and the ones inboard of it move inboard (see arrows in Figure 5-34, Figure 5-26 and Figure 5-33). A linear array of sweeping jets located on the inboard part of the wing near the hinge of the elevon has a larger effect on C_{LM} than a similar array outboard of the crank. Actuation on the outboard wing of the 1303 that has a relatively small surface area was deleterious while the actuation on the inboard section generated a very desirable effect on the outboard section as seen in Figure 5-33. Thus, the effect of AFC is global and it is not limited to the region downstream of the actuation. This was observed on numerous occasions on the simple swept-back wing (e.g., Figure 5-14) and on the SACCON. It suggests that lift enhancement should be carried out on the inboard wing where an AFC assisted flap deflection provides high ΔC_L while the control of pitch should be carried out near the wing tip.

Split ailerons or spoiler flaps are widely used on tailless aircraft for yaw control so it was appropriate to compare the efficacy of AFC to these devices (Figure 5-20, Figure 5-27). It turns out that these devices work reasonably well at low C_L providing comparable ΔC_{LN} to AFC's although the rolling moment associated with their deployment is larger. However, they are not effective at higher C_L when they are needed most in order to overcome gusts on landing approach or a takeoff run. This deficiency requires rudders and vertical fins and those are the surfaces one wants to eliminate on stealthy configurations.

A split flap provides large drag by maintaining a trapped vortex between the deflected upper and lower surfaces. At high incidence, the flow near the trailing edge is dominated by spanwise velocity that is parallel to the TE, so the deflected surfaces are parallel to the flow and they provide only skin friction drag and the trapped vortex that generated the required C_{LN} is disgorged. Replacing the TE by a blunt semi-circle in conjunction with the "Coanda Effect" may face similar difficulties because the entire effect is based on the balance between centrifugal force and pressure gradient normal to the curved streamlines. So what will happen when the flow is tangential to the axis of the cylinder forming the TE of the wing?

Limiting ourselves to small AR, highly swept-back delta planforms results in very low L/D that should be avoided (Figure 5-1). Since most of the lift on thin delta wings at low speeds, is derived from the LE vortex, placing control surfaces at the TE of a delta is not effective. For this reason many delta wing combat airplanes have auxiliary control surfaces either behind and above the delta wing (Skyhawk, MiG-21, Mirage 2000) or they have a canard (Kfir, Typhoon, Rafale). Very little is known about AFC augmented surfaces in that region, particularly in the outboard part of the TE where the vortex is. Water tunnel observations at the University of Arizona on a sharp LE delta wing having a 70° sweep back revealed a clear "vortex break down" upstream of the TE at $\alpha = 30°$. In this case, the streamwise velocity in the core of the vortex stagnated spreading the air bubbles trapped in the core in radial directions (Figure 5-35, left). Therefore, the streamwise velocity underneath the burst core is small making TE control surfaces ineffective. Installing 4 hypodermic tubes on both leading edges of the wing (See inset in Figure 5-35, left) and allowing jets of water to emanate from the left wing in the direction that is perpendicular to the LE, spread the LE vortex over the entire left side of the wing's surface (Figure 5-35, right). According to Williams [28], this action does not affect the lift but it affects the drag and the yawing moment. However if the jets emanate upstream of the MRL, they will result in pitch-down. This can be avoided by concentrating the jet emission on or slightly downstream of the MRL if pitch-up correction is desired.

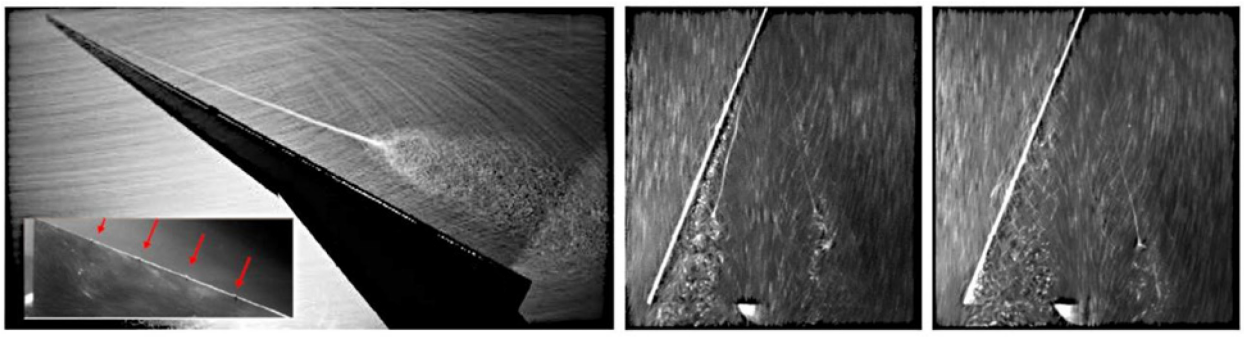

Figure 5-35: Some Observations on a 70° Delta Wing Having a Sharp LE and 4 Steady Jet Nozzles Along its LE.

A low momentum AFC input originating from a small number of actuators can change the direction of flow and pressure distribution on a swept wing, thus affecting its integral forces and moments. The effects of AFC are closely coupled to the model's design parameters and therefore they should be considered in the very earliest stages of the design process. It is particularly imperative to include stability and control considerations during the configuration-development. Otherwise, stability and control "fixes" invoked later

in the design process would introduce suboptimal compromises at best, and devastating intractability at worst. We suggest augmenting the stability/control tool kit with AFC as its utility was demonstrated in this article. Sweeping jet actuation is more effective because these actuators are more forgiving when the flow direction is not precisely known. In addition, these actuators may generate an absolutely unstable flow zone in their vicinity, thus intensifying in the process. The sweeping jets therefore not only add momentum to the flow but they act as large vortex generators.

5.12 ACKNOWLEDGEMENTS

The construction of the SACCON model was supported by Dr. D. Smith while he was at AFOSR while the purchase of the PSP equipment was supported by Dr. J. Milgram from ONR. The investigation pertaining to the simple swept-back wing was sponsored by the Ohio Aerospace Institute in support of the Air Force Research Laboratory (AFRL) contract FA8650-16-C-2644 and Monitored by Dr. G. Dale. This portion of the report has been cleared by 88ABW: Case Number 88ABW-2018-5829.

The construction of the 1303 model and the investigation of its pitch-break were sponsored by the Boeing Research and Technology division of the Boeing Company and the release of some of that information, including CFD was approved.

5.13 REFERENCES

[1] Cummings, R. and Schütte, A., The NATO STO Task Group AVT-201 on 'Extended Assessment of Stability and Control Prediction Methods for NATO Air Vehicles', in 32nd AIAA Applied Aerodynamics Conference, Atlanta, GA, 2014.

[2] Liersch, C. and Huber, K., Conceptual Design and Aerodynamic Analyses of a Generic UCAV Configuration, in 32nd AIAA Applied Aerodynamics Conference, Atlanta, GA, 2014.

[3] Huber, K., Vicroy, D., Schütte, A. and Hübner, A., UCAV Model Design and Static Experimental Investigations to Estimate Control Device Effectiveness and Stability and Control Capabilities, in 32nd AIAA Applied Aerodynamics Conference, Atlanta, GA, 2014.

[4] Zimper, D. and Rein, M., Experimental and Numerical Analysis of the Transonic Vortical Flow Over a Generic Lambda Wing Configuration, in 32nd AIAA Applied Aerodynamics Conference, Atlanta, GA, 2014.

[5] Vicroy, D., Huber, K., Rohlf, D. and Löser, T., Low-Speed Dynamic Wind Tunnel Test Analysis of a Generic 53° Swept UCAV Configuration with Controls, in 32nd AIAA Applied Aerodynamics Conference, Atlanta. GA, 2014.

[6] Rein, M., Irving, J., Rigby, G. and Birch, T., High Speed Static Experimental Investigations to Estimate Control Device Effectiveness and S&C Capabilities, in 32nd AIAA Applied Aerodynamics Conference, Atlanta, GA, 2014.

[7] Jentzsch, M., Taubert, L. and Wygnanski, I., On the Use of Sweeping Jets to Trim and Control a Tailless Aircraft Model, AIAA2017-3042, *AIAA Journal Special Issue on AFC*, 2017, 2018.

[8] Hitzel, S., Perform and Survive, Evolution of Some U(M)CAV Platform Requirements, STO-MP-AVT-2015, 2015.

[9] Furlong, G. and McHugh, J., A Summary and Analysis of the Low Speed Longitudinal Characteristics of Swept Wings at High Reynolds Number, NACA TN 1339, 1957.

[10] ESDU 01005: Effect of Geometry on Low Speed Pitch-Break Characteristics of Swept Wings, IHS ESDU, 2001.

[11] Hirsch, D., An Experimental and Theoretical Study of Active Flow Control, Ph.D Thesis, California Institute of Technology, 2017.

[12] Abott, I., von Doenhoff, A. and Stivers, L., Summary of Airfoil Data, NACA TR 824, 1945.

[13] Hoerner, S., Fluid-Dynamic Drag, Published by the Author, 1965.

[14] Wygnanski, I., Tewes, P. and Taubert, L., Applying the Boundary Layer Independence Principle to Turbulent Flows, *Journal of Aircraft*, vol. 51, no. 1, pp. 175-182, 2014.

[15] Tewes, P., Taubert, L. and Wygnanski, I., On the Effect of Sweep on Separation Control, in 7th AIAA Flow Control Conference, AIAA 2014-2513, 2014.

[16] Tewes P. and Taubert, L., Control of Separation on a Swept Wing Using Fluidic Oscillators, in 53rd AIAA Aerospace Sciences Meeting, AIAA 2015-0783, 2015.

[17] Tewes P., Application of Active Flow Control to a Finite Swept Wing, Ph.D. Thesis, Technische Universität Berlin, 2015.

[18] Andino, M., Lin, J., Washburn, A., Whalen, E., Graff, E. and Wygnanski, I., Flow Separation Control on a Full- Scale Vertical Tail Model using Sweeping Jet Actuators, in 53rd AIAA Aerospace Sciences Meeting, AIAA 2015-0785, 2015.

[19] Cummings, R., Vicroy, D. and Schütte, A., An Integrated Computational/Experimental Approach to UCAV Stability and Control Estimation: Overview of NATO RTO AVT-161, in 28th AIAA Applied Aerodynamics Conference, Chicago, IL, 2010.

[20] Löser, T., Vicroy, D. and Schütte, A., SACCON Static Wind Tunnel Tests at DNW-NWB and 14'x22' NASA LaRC, in 28th AIAA Applied Aerodynamics Conference, Chicago, IL, 2010.

[21] Vallespin, D., Da Ronch, A., Badcock, K. and Boelens, O., Vortical Flow Prediction Validation for an Unmanned Combat Air Vehicle Model, *Journal of Aircraft*, vol. 48, no. 6, Nov. – Dec. 2011.

[22] Schütte, A., Hummel, D. and Hitzel, A., Numerical and Experimental Analyses of the Vortical Flow Around the SACCON Configuration, in 28th AIAA Applied Aerodynamics Conference, AIAA 2010-4690, Chicago, IL, 2010.

[23] Mani, M., Cary, A. and Ramakrishnan, V.S., A Structured and Hybrid Unstructured Grid Euler and Navier- Stokes Solver for General Geometries, AIAA Paper 2004-524, January 2004.

[24] Spalart, P.R. and Allmaras, S.R., A One-Equation Turbulence Model for Aerodynamic Flows, *Recherche Aerospatiale*, no. 1, pp. 5-21, 1994.

[25] Shur, M.L., Strelets, M.K., Travin, A.K. and Spalart, P.R., Turbulence Modeling in Rotating and Curved Channels: Assessing the Spalart-Shur Correction, *AIAA Journal*, vol. 38, no. 5, May 2000.

[26] Parekh, D., Williams, S., Amitay, M., Glezer, A., Washburn, A., Gregory, I. and Scott, R., Active Flow Control on the Stingray UAV: Aerodynamic Forces and Moment, in 33rd AIAA Fluid Dynamic Conference and Exhibit, AlAA 2003-4002, Orlando, FL, 2003.

[27] McDaid, H. and Oliver, D., *Smart Weapons*, NY: Barns and Noble (ISBN 0 -7607-0760-X), 1997.

[28] Williams, D.P., Interviewee, Private Communication. [Interview]. ITT Chicago USA, August, 2018.

Chapter 6 – FLOW CONTROL SYSTEM INTEGRATION INTO THE TAILLESS ICE AND SACCON/MULDICON AIRCRAFT

Brant H. Maines
Lockheed Martin Aero
UNITED STATES

Daniel N. Miller
Lockheed Martin Aero
UNITED STATES

Clyde Warsop
BAE Systems Air
UNITED KINGDOM

6.1 OVERVIEW

This chapter explores the integration of an active flow control effectors into the innovative control effector, ICE-101 and SACCON/MULDICON aircraft configurations. The objective of this study is to size an active flow control effector suite to reduce or eliminate the utilization of the primary control effector suite over select mission phases. The baseline ICE-101 vehicle with a conventional control effector suite is first established to provide a basis of comparison. A first pass conceptual installation design then is evaluated to identify first order integration requirements and compare the impacts to conventional aerodynamic control effectors. The flow control suite is sized to complete M = 0.9 ingress and egress mission segments using only fluidic controls. Key components are identified, and ducts are routed through the aircraft to develop an estimate of the weight and volume impacts to the vehicle. A preferred control effector suite is down selected and design approaches considered to minimize overall system weight and volume. Based on the approach developed for ICE-101 a similar approach was taken to size an AFC system on the SACCON/MULDICON configuration.

6.2 INTRODUCTION AND BACKGROUND

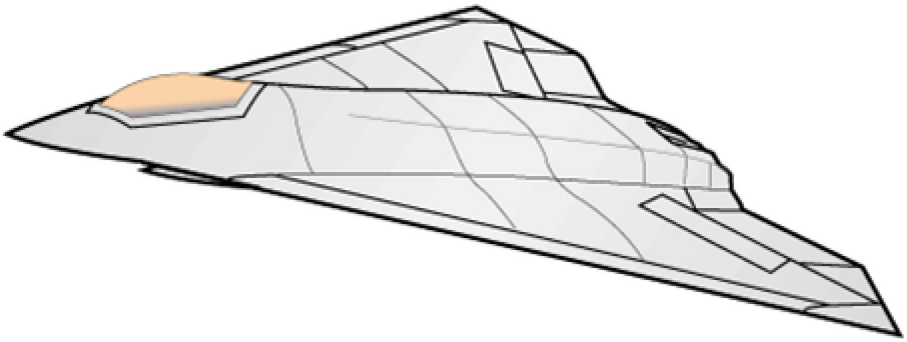

Figure 6-1: ICE Tailless Fighter Research Aircraft.

The integration component of the NATO task group AVT-239 employs best design practices to develop a concept level integration of an active flow control effector suite into the ICE configuration shown in Figure 6-1. The all-wing tailless aircraft can be either inhabited or uninhabited. This configuration was derived from a Lockheed Martin Aeronautics internal research and development program in 1991. The aircraft employs a suite of conventional hinged control effectors that include Leading Edge Flaps (LEF), elevons, Spoiler Slot Deflectors (SSD), pitch flaps and All-Moving Tips (AMT). A description of the configuration and the utilization of this control effector suite is provided in Niestroy et al. [1]. Table 6-1 summarizes the reference data for this configuration. The conceptual design and integration of the flow control system is based on requirements defined in recent papers that define the flow control implementation [2] and flow rate requirements as derived from 6-DOF flight control simulations [3].

Table 6-1: LM Aero Tailless Aircraft Model Reference Data.

Parameter	Value
Reference Wing Area, S_{ref}	808.6 ft^2
Reference Span, b_{ref}	37.5 ft
MAC	345 in
FS LEMAC	160.84 in
MRC	38% MAC
Weight	37,084 lbs

6.3 BASELINE ICE VEHICLE

As a basis for comparison to the integrated flow control system, a basic layout and internal arrangement of the ICE aircraft was established and updated for this effort. While integration of a flow control system onto a vehicle during the conceptual design phase allows the most flexibility in the arrangement, it is important to understand at a high level how the flow control system must integrate with the other interfaces and subsystems on the aircraft. Figure 6-2 highlights the arrangement of the conventional control suite for the baseline ICE configuration. The conventional hinged control effector suite includes pitch flaps, elevons leading edge flaps and a spoiler slot deflector. Included in the figure are the estimated total weights and volumes for each effector that include the structure and actuators. A concept level structural layout also shown in the figure was developed to inform the internal subsystem arrangement.

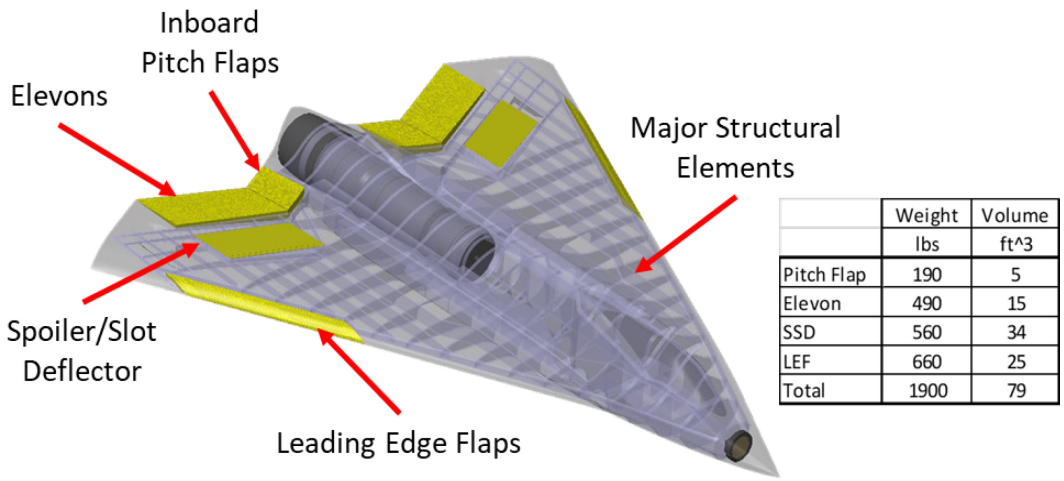

	Weight	Volume
	lbs	ft^3
Pitch Flap	190	5
Elevon	490	15
SSD	560	34
LEF	660	25
Total	1900	79

Figure 6-2: Baseline Control Conventional Effector Suite and Structural Arrangement.

Figure 6-3 highlights the internal arrangement of the basic avionics subsystems, control surface actuators, fuel tanks and landing gear. The objective of this concept level internal arrangement was to capture the volume of the major systems that would impact the integration of the flow control system.

Based on the approach developed for ICE-101 a similar approach was taken to size an AFC system on the SACCON/MULDICON configuration the details of which are presented in Section 6.5.

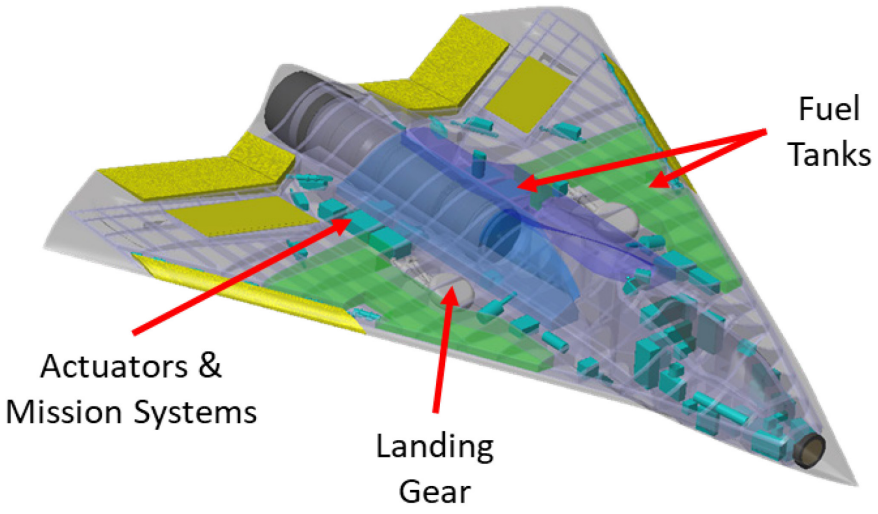

Figure 6-3: Major Subsystems.

6.4 FLOW CONTROL SUITE INTEGRATION

Based on preliminary aerodynamic flow control effector studies [2], a suite of active flow control effectors was integrated into the ICE vehicle (Figure 6-4). The flow control effector suite consists of both forebody and trailing edge controls. Forebody effectors include blowing slot jets at the apex of the vehicle just downstream of the radar and slot jets along the mid-span of the wing leading edge. Trailing edge effectors include fluidic yaw thrust vectoring and outboard wing trailing edge slot jets. The wing trailing edge slot jets on each side are split and controlled separately to generate both positive and negative aerodynamic forces and moments. Nozzle lengths and location requirements were defined by the aerodynamic studies and the function of each is described in recent papers [2], [3].

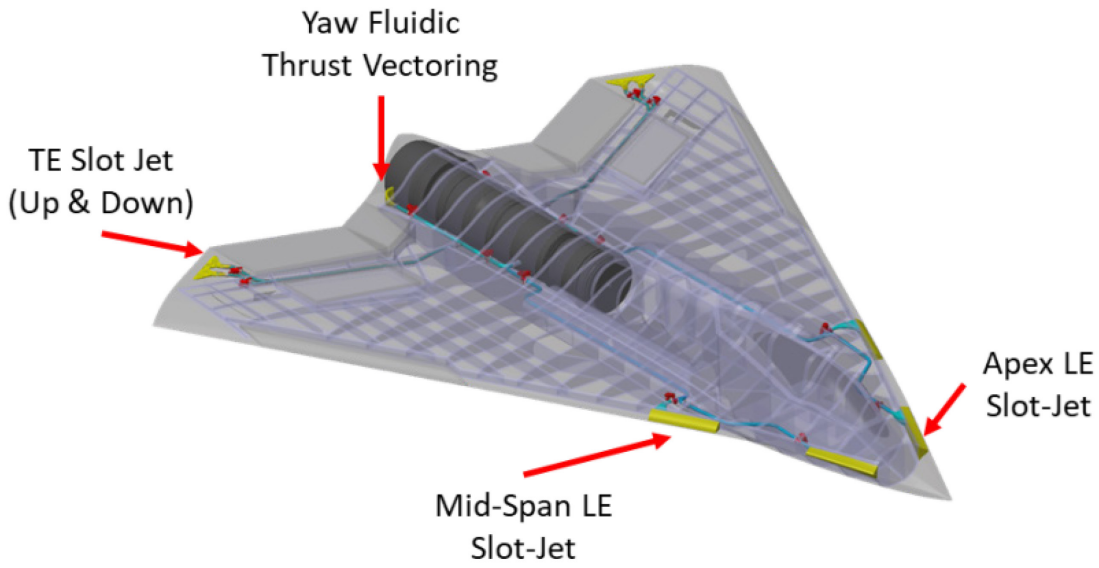

Figure 6-4: Flow Control Effectors Selected for Integration Studies.

With the nozzle size and location defined the internal arrangement of the flow control system was sized based on the primary flow rate requirements defined in the recent flow control paper [3]. Four combinations

of flow control effector suites were considered to complete the up and away portion of the mission at Mach = 0.9, at 30,000 ft. The combinations are described in Table 6-2 and include:

1) All four effectors;
2) The Apex effector with wing trailing edge and thrust vectoring;
3) The LE mid-span effector with wing trailing edge and thrust vectoring; and
4) Only use of the wing trailing edge and thrust vectoring flow control effectors.

Table 6-2 summarizes the mass flow rate requirements for two control conditions. The first is for the mean peak flow rate requirement to reject a gust throughout the cruise mission. The second case is the mean flow rate requirement plus three standard deviations. This flow rate accounts for approximately 99% of the mass flow rate requirements throughout the mission. The difference between these two design approaches will have a significant impact on the size and weight of the overall flow control system.

Table 6-2: Mass Flow Rate Requirements.

		Flow Control Effector			
Flight Control Requirement	**Configuration**	**Apex**	**Mid**	**TE**	**TV**
Mean Peak During Gust (lbs/sec)	1	0.85	0.85	0.95	2.84
	2	0.91		0.99	2.80
	3		1.41	0.99	3.00
	4			1.11	2.98
Mean + 3*std (lbs/sec)	1	0.31	0.50	0.32	0.40
	2	0.40		0.37	0.46
	3		0.51	0.37	0.42
	4			0.48	0.50

For each configuration a flow control system was designed to handle the flow rate requirements for a mean peak gust during the mission. The key design parameters used for this study are summarized in Table 6-3.

Table 6-3: Flow Control Design Parameters.

Design Parameter	Assumption
Air Source	Engine Bleed Air
Air Pressure	50 psia
Air Temperature	440 deg F
Duct/Nozzle Material	Inconel 625
Factor of Safety	2
Duct Mach Number	0.4

The primary air source for this study is assumed to be engine bleed at a pressure of 50 psia and temperature of 440 degrees Fahrenheit. For this conceptual design, no heat exchanger is assumed. Further studies are required to determine if this assumption is valid. To handle the high temperatures, duct and nozzle material is assumed to be Inconel 625 and is sized to have a factor of safety equal to 2 times the operating pressure of 50 psia. To minimize duct losses the Mach number in the duct is assumed to be 0.4 for the peak flow rate values. Figure 6-5 highlights the relevant subsystem components used in the installation. The engine bleed take-off is configured with a ball joint compensator and high temperature bellows to accommodate engine

movement and pipe expansion. Additional bellows are installed in each flow control segment. A master valve enables the flow control system. Air flow ducts are sized appropriately to ensure duct Mach numbers remain below 0.4. The ducts are routed through structure as required to minimize impacts to fuel volumes and mission systems. Marman clamps are used to connect pipes to each component and at pipe joints as required for installation. At this concept level, notional pipe breaks were defined primarily to accommodate bends. Pipe hangers were distributed to secure the air ducts to structure as deemed necessary. Pipe wall thickness was sized with a safety factor of 2. Based on stress calculations, the wall thickness was the greater of 0.02" or the thickness required to achieve the safety factor. Insulation around the pipe was assumed to be 0.375" thick to provide separation from aircraft systems and fluid lines. Flow control valves are assumed to be similar to existing Environmental Control System (ECS) butterfly valves to provide proportional control. Lastly, compact nozzle designs with a rapid spanwise expansion coupled with a streamwise contraction were used. Internal vanes are assumed to uniformly distribute the flow.

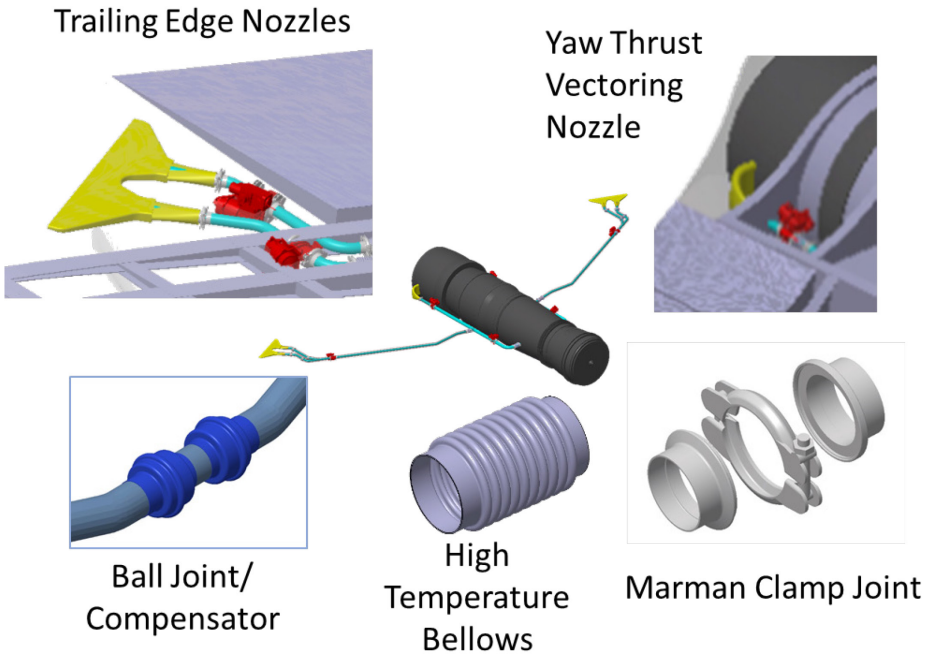

Figure 6-5: Major Flow Control System Components.

As the flow control concept matures, additional factors should be considered primarily due to the high temperature engine bleed air source for the flow control system. During a detailed design phase heat impacts to the external surfaces should be considered. Excessive heating of external surfaces may require the addition of a heat exchanger to cool the air prior to exhaust. While the air ducts are insulated, local steady state temperatures can still reach 200 degrees F or more due to the high temperature engine bleed air flow. This may affect local structural strength or mission systems. To protect against pipe rupture, a dual wall or dry bay design enclosing the air ducts may be required in some regions of the aircraft. A more detailed assessment of the system architecture is also required to develop additional derived requirements. These may include requirements for partitioning the ECS from the flow control system, prevention of backflow through the system, the handoff back to the conventional control effectors in the event of failures, over pressurization and general maintenance and access. In addition, a safety and hazard analysis should be conducted to develop requirements for flight and ground operations. As the design matures, these additional derived requirements may increase system weight and volume. For these reasons, a weight and volume margin of 25% is included in the following assessment [4].

Using the components described in Figure 6-5, flow control systems for each configuration defined in Table 6-2 were developed and sized for the flow rate condition to handle the mean peak during a gust. This approach was selected to ensure that conventional controls could remain fixed for virtually the entire Mach = 0.9 mission segment. The weights and shrink-wrapped volumes for each system are listed in Table 6-4. Results from Niestroy et al. [3] indicate that each system defined in Table 6-4 meets mission requirements. Thus, Configuration 4 is recommended to minimize weight, volume and flow rate requirements (Figure 6-6).

Table 6-4: Flow Control Suite Weight and Volume Comparisons when Sized to Handle the Mean Peak During Gust Requirement.

Flow Control Effectors	Configuration	Weight (lbs)	Volume (ft^3)
Apex + Mid + TE + TV	1	646	8.9
Apex + TE + TV	2	536	7.7
Mid + TE + TV	3	556	7.3
TE + TV	4	390	4.5

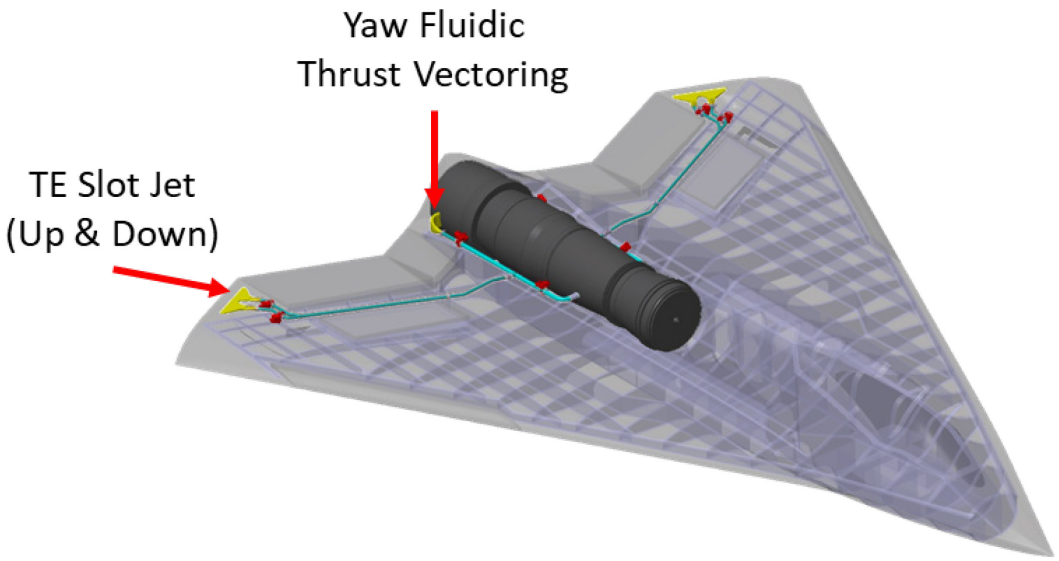

Figure 6-6: Preferred Flow Control Suite Consists of Trailing Edge Slot Jets and Fluidic Thrust Vectoring (Configuration 4).

For this preferred configuration two additional flow control air supply system configurations were considered to further reduce weight. The first approach relaxed the design requirement for the pipe Mach number and the second assumed the system was sized to provide just the mean flow rate plus 3 standard deviations described in Table 6-2. In the first case, the pipe Mach number was relaxed from 0.4 to 0.6. The rationale for this stems from the fact that the mean peak values occur for less than 1% of the duration of the mission. The duct Mach number will be lower for the remainder of the mission. The weight for this system is reduced by 45 lbs and the volume by 0.8 ft^3 as shown in Table 6-5. For the second approach, the system is sized to just provide the mean flow rate plus 3 standard deviations to further reduce both weight and volume. However, the latter system requires utilization of the conventional control effectors during the mission segment. This may not be desirable. Thus, it is recommended to size the system to provide the mass flow rate to accommodate the mean peak during a gust. The design should also consider allowing the peak Mach number in the pipe to rise above the Mach = 0.4 convention at peak flow rates to minimize weight and

volume impacts to the system. The extent of this relaxation in Mach number should be determined through more detailed analysis. Compared to the conventional control suite, the proposed complete flow control suite weighs less than the ICE elevon at a significantly reduced volume.

Table 6-5: Design Considerations Drive Flow Control System Total Weight and Volume (Configuration 4).

Flight Control Requirement	Weight (lbs)	Volume (ft^3)
Mean Peak During Gust - (Mach = 0.4)	390	4.5
Mean Peak During Gust - (Mach = 0.6)	355	3.7
Mean + 3 sigma (Mach = 0.4)	305	2.8

Lastly, the weight and volume fractions of the subsystem components for Configuration 4 are shown in Figure 6-7. For this configuration, the nozzles and flow control valves drive weight, while as expected, the air ducts, insulation and nozzles drive volume.

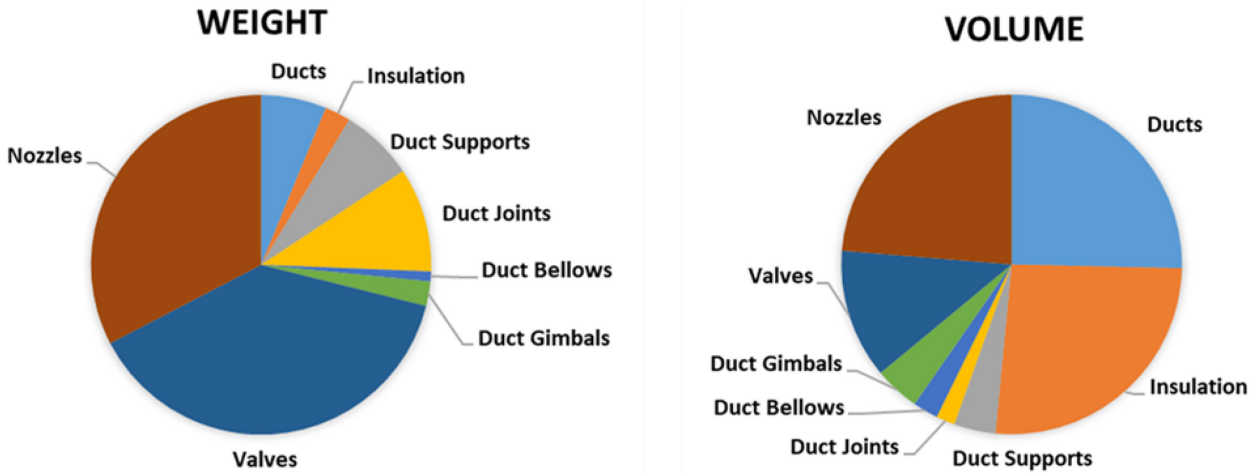

Figure 6-7: Flow Control Subsystem Weight Breakdown for Configuration 4.

6.5 AFC INTEGRATION ON THE SACCON/MULDICON CONFIGURATION

6.5.1 General

The aerodynamic and performance assessments undertaken within the AVT-239 study were carried out on the SACCON configuration since significant aerodynamic data (both wind tunnel and CFD) were freely available for both high- and low-speed flight conditions with and without control effectors. SACCON was originally conceived to represent a geometry possessing a number of complex flow features to challenge existing CFD modelling capabilities. It is therefore not considered as a geometry that would make a practical airframe. Because the QFD integration evaluation required a configuration having the potential to be representative of a practical flying vehicle a decision was made to use the NATO AVT-251 MULDICON configuration as the baseline for these studies [5]. MULDICON has its origins in SACCON (same leading-edge sweep, and wingspan) however it has a leading/trailing edge shape, camber, thickness and twist distribution optimised for a practical aircraft configuration. Previous studies have also developed a preliminary internal layout for primary structure, primary systems (powerplant, landing gear, fuel tanks, avionics, flight control surfaces) and payload for MULDICON (Figure 6-8).

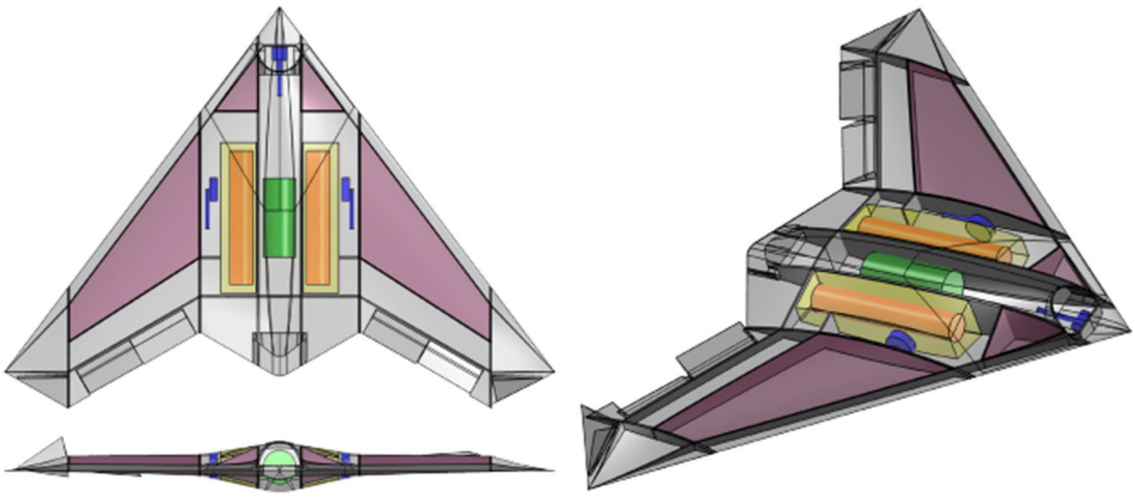

Figure 6-8: Conceptual Layout for the MULDICON Aircraft Showing Primary Structure, Powerplant, Landing Gear, Flight Controls, Fuel Tanks, Avionics and Payload Bays.

6.5.2 AFC Components and System Layout

Based on the AVT-239 performance studies for the SACCON configuration (Chapter 8) the 'preferred' AFC concept (dual blowing trailing edge circulation control applied to both inboard and outboard elevons) was down selected for the 'integration' and 'ilities' QFD study. Using a mainly identical approach to system component sizing used for the ICE configuration a duct, control valve and nozzle sizing and layout exercise was conducted for MULDICON based on the AFC system flowrates determined from the SACCON study. Once the various duct sizes had been determined routing paths were assessed to allow the ducts and other system components to be placed in the aircraft with appropriate consideration for the presence of other major structure and systems elements. The fidelity of the baseline airframe CAD model for MULDICON was more crude that for the ICE configuration so engineering judgement was used to assess the optimal routing paths and placement locations for AFC system components. Care was taken to ensure adequate clearances from primary structure and outer mould lines to account for non-represented structure and system components. The weights sizes and volumes of the AFC system components for MULDICON were generated using the same rules applied for the ICE integration analysis.

Key to the design of the MULDICON CC system is the optimisation and sizing of the trailing edge AFC nozzles themselves to maximise flow quality and operating efficiency while minimizing their volume and mass. The MULDICON AFC nozzle design was based on previous CC nozzle optimisation and manufacturing studies [6]. For the present study the assumption has been made that the AFC system will have to integrate with the conventional control surfaces since the assumption is that the AFC will only be used during ingress mission phases and that conventional controls will be required for other mission phases (manoeuvre, take-off/landing) and as a high reliability backup for the AFC system. Future studies and improvements in AFC reliability may eventually negate the need to have duplicate flight controls but at present duplicated AFC and conventional controls are assumed. Based on this assumption it has been necessary to integrate the AFC nozzles within the elevon structures and to bridge the AFC air supplies across the elevon hinges using rotary duct gimbals. Fortuitously the low peak mass flows mass flows required by the AFC system enable the integration of the air supply and nozzles within the elevons themselves (Figure 6-9). Each elevon contains a full-span dual slot CC nozzle that is divided into 8 spanwise chambers. Each chamber has separate upper and lower plenums that are fed from separate supply pipes from the AFC control valves mounted outside the elevon in the space between the rear of the fuel tank and the mounting spar for the elevon hinges. Pipes from each of the control valves are bridged across the elevon hinge by means of a purpose designed dual flow path rotary gimbal. Once inside the

envelope of the elevon the air in the upper and lower surface supply pipes is both diffused and split into four paths by means of a multi-cell diffuser/splitter (diffusion ratio 1:2, included angle of diffuser 7°). Each flow path is further diffused and split into two (diffusion ratio 1:2, included angle of diffuser 7°) before passing into the CC plenum chambers. Splitting and diffusing the flow by a ratio of 4:1 combined with appropriate internal design of the CC plenum chambers results in minimal pressure losses and high quality slot exit flow (flow uniformity better that 96% and skewness better than 1.7%).

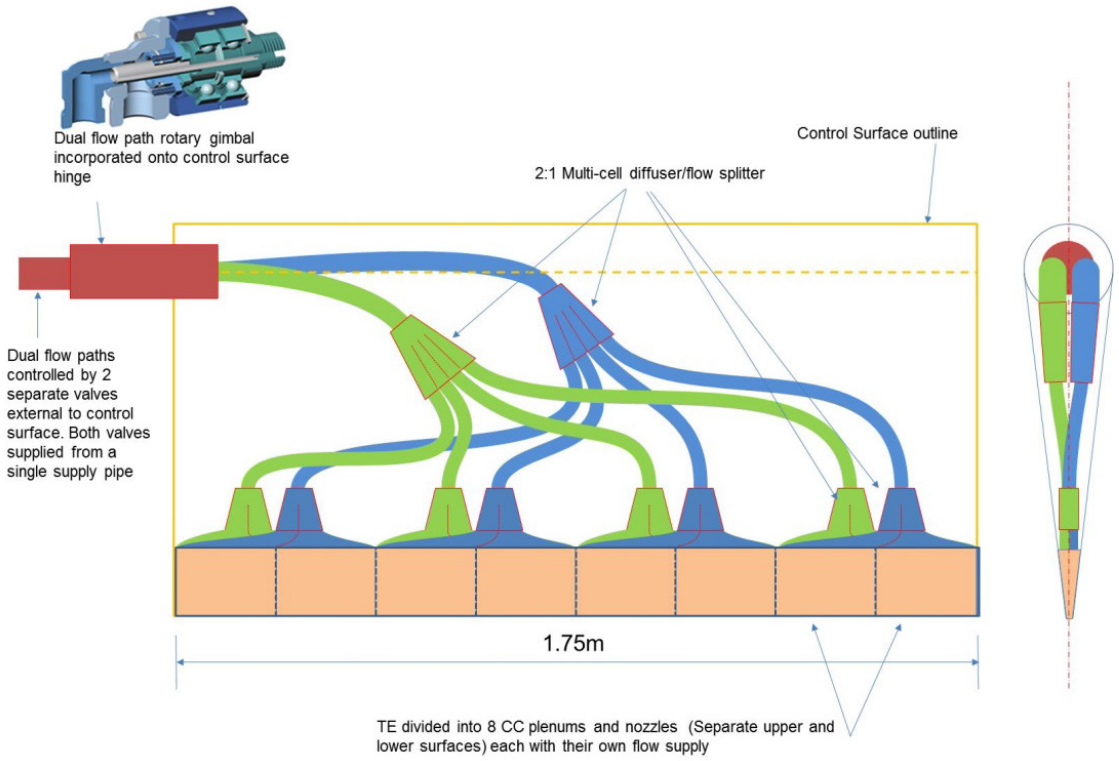

Figure 6-9: Schematic of the TE CC ACF System Integrated in a Single MULDICON Elevon-Components and Mould Lines Drawn to Scale.

An estimated breakdown for the AFC components (from the rotary gimbal to the nozzle inclusive) within a single elevon is presented in Table 6-6. The mass contributions have been calculated assuming that all components are of Inconel. Reduced mass could potentially be achieved by replacing the components with alternative, lighter weight materials such as titanium or aluminium alloy. For a single CC actuator contained within an elevon the CC components total 31.9 lb mass. For the complete aircraft having four CC effectors the calculated actuator mass is 124.8 lb mass.

The layout of the full AFC system within MULDICON is presented in Figure 6-10 and the AFC component mass and volume breakdown in Table 6-6. Similar bleed air supply off-take pressures (51 psia) and temperatures (440 °F) to those used for the ICE integration assessment have been assumed. For the determined AFC sizing mass flow requirement (1.81 lb mass/s) the required bleed air duct internal diameter between the engine and the AFC control valves on each side of the aircraft (duct Seg 1 and Seg 2 in Figure 6-10) is 2.22 in. The internal diameter of the duct that supplies the outboard CC control effector (designed for a sizing mass flow of 0.78 lb mass/s) is 1.46 in. The calculated masses and volumes of the complete AFC components for MULDICON are presented in Table 6-7.

Table 6-6: Mass Breakdown for a Single MULDICON CC Control Effector as Depicted in Figure 6-9 (Full Aircraft System Has Four Effectors).

Component	No. Off	Total mass (lb)
Inlet Gimbal	1	1.65
Upper Inlet Pipe	1	2.07
Lower Inlet Pipe	1	1.53
First Splitter/Diffuser	2	1.10
Secondary Upper Pipe	4	3.06
Secondary Lower Pipe	4	3.00
Second Splitter/Diffuser	8	2.84
Tertiary Upper Pipe	8	0.51
Tertiary Lower Pipe	8	0.51
Trailing Edge Nozzle	1	15.63
TOTAL		**31.9**

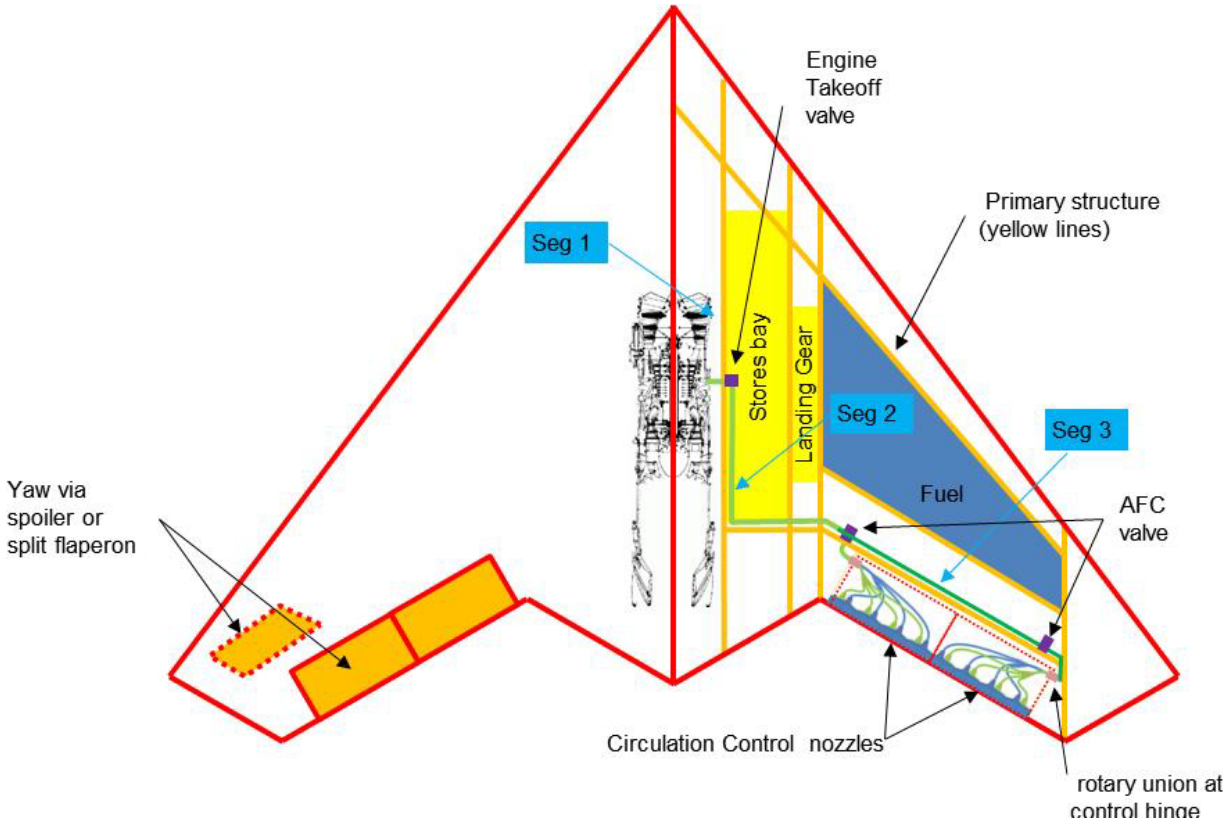

Figure 6-10: Schematic of the MULDICON AFC Duct, Valve and Nozzle Layout (Drawn to Scale).

Table 6-7: Mass and Volume Breakdown for the MULDICON AFC System Components as Depicted in Figure 6-10.

Component	Mass (lb)	Volume (in^3)
Duct Seg 1 (both sides of aircraft)	1.7	161
Duct Seg 2 (both sides of aircraft)	17.7	1660
Duct Seg 3 (both sides of aircraft)	9.4	584
Duct Insulation	11.1	2138
Duct Supports (34 off)	18.8	-
Duct Joints (18 off)	33.2	-
Duct Bellows (8 off)	6.4	-
Duct Gimbal (10 off)	30.9	-
Engine Off-Take Valves (2 off)	10.6	-
AFC Valves (4 off)	67.1	-
AFC Nozzles (4 off)	127.6	2789
TOTAL	**334.5**	**7332**

6.6 SUMMARY AND CONCLUSIONS

An active flow control effector suite was integrated into the tailless ICE air vehicle capable of performing the Mach 0.9 ingress and egress mission phases. The preferred system integration includes only outboard wing trailing edge and yaw thrust vectoring jets. To meet mission requirements without the use of conventional controls, it is recommended to size the active flow control effectors to handle the mean peak flow rates as determined through 6-DOF flight simulations. This ensures that the active flow control effector suite can handle turbulence and all but the most severe gusts. To minimize system weight and volume it is recommend allowing the duct Mach number to increase beyond the Mach 0.4 best practices value at the peak flow rate conditions. The weight of the proposed flow control system is similar to a conventional ICE elevon. A similar flow control system has also been integrated into the MULDICON configuration for the Mach 0.7 ingress mission. Future work should focus on minimizing weight and volume of the proportional actuators and should consider developing alternate form factors for integration into thin wings.

6.7 ACKNOWLEDGEMENTS

The authors would like to acknowledge Bryan Guzzardo and Michael Niestroy from Lockheed Aeronautics, David Williams from the Illinois Institute of Technology, Chris Hutchin from Dstl and Patrick Loechert from DLR for their contributions in system integration and definition.

6.8 REFERENCES

[1] Niestroy, M.A., Dorsett, K.M., and Markstein, K., A Tailless Fighter Aircraft Model for Control-Related Research and Development, AIAA SciTech Conference, AIAA Paper 2017-0757, January 2017.

[2] Williams, D., Osteroos, R., and McLaughlin, T., Flight Control Derivatives Using Active Flow Control Effectors on the ICE/SACCON UCAS Model, AIAA SciTech Conference, AIAA Paper 2019-0043, January 2019.

[3] Niestroy, M.A., Williams, D.R., and Seidel, J., NATO AVT-239 Task Group: Flow Control Simulation of the ICE Aircraft, AIAA SciTech Conference, AIAA Paper 2019-0279, , January 2019.

[4] American National Standard, Mass Properties Control for Space Systems, ANSI/AIAA S-120A-2015, Sponsored by American Institute of Aeronautics and Astronautics and International Society of Allied Weight Engineers, Inc., 2015.

[5] Karakoc, A. and Kaya, H., A Multi-objective Multi-disciplinary Optimization Approach for NATO AVT 251 UCAV – MULDICON, 2018 Applied Aerodynamics Conference, AIAA AVIATION Forum, (AIAA 2018-3001) https://doi.org/10.2514/6.2018-3001.

[6] Llopis-Pascual, A., Supercritical Coanda Jets for Flight Control Effectors, PhD Thesis, Manchester University, Manchester, 2017.

Chapter 7 – ACTIVE FLOW CONTROL SIMULATION OF THE TAILLESS ICE AIRCRAFT

Michael A Niestroy
Lockheed Martin Aero
UNITED STATES

David R Williams
Illinois Institute of Technology
UNITED STATES

Jurgen Seidel
United States Air Force Academy
UNITED STATES

7.1 OVERVIEW

This chapter makes a first pass at simulating, controlling, and assessing requirements for an aircraft that uses only active flow control effectors for specific mission phases. Flight control force and moment data obtained from wind tunnel measurements are used in a flight simulation of the tailless ICE-101 aircraft equipped with active flow control effectors and yaw fluidic thrust vectoring to estimate performance. The nominal flight properties at trim conditions are examined. Active flow control trim conditions are compared to conventional control effector trim. An initial nonlinear dynamic inversion control system and a quadratic programming control allocation module is used to generate simulation results. The mass flow rate requirements for the bleed air system to compensate for light and moderate turbulence on flight at M = 0.9 cruise conditions are documented. The effects of discrete gusts on the aircraft and the ability of the active flow control effectors to compensate for them are investigated. The results show that these effectors, along with fluidic yaw thrust vectoring, are sufficient to reject gusts and turbulence using a reasonable amount of engine bleed for an ingress or egress mission segment.

7.2 INTRODUCTION AND BACKGROUND

The flight simulation component of the NATO task group AVT-239 is an essential element in the evaluation of innovative control effectors for flight control. Wind tunnel and numerical simulations provide information about flight control derivatives, but only full six degree of freedom flight simulations can provide realistic evaluations of the engine bleed air requirements necessary to fly a mission. Combining aircraft design data with aerodynamic derivatives and active flow control derivatives enables the flight simulator to approximate how an actual aircraft will respond to active flow control effector inputs during cruise flight in a turbulent environment.

The ICE aircraft is an all-wing, tailless configuration that can be manned or unmanned. The aircraft, shown in Figure 7-1 with the baseline control effectors indicated, evolved from 1991 Internal Research and Development (IRAD) studies at LM Aero and was subsequently studied in depth under AFRL sponsorship [1], [2]. The configuration and aerodynamic database are documented in [3], which includes a description of the publicly available simulation that has been the basis of several recent research papers. The simulation model incorporated a number of control devices including Leading-Edge Flaps (LEF), All-Moving Wingtip (AMT), Spoiler Slot Deflector (SSD), pitch flaps, and elevons. Table 7-1 summarizes the reference data for this model.

7.3 MASS PROPERTIES

The estimated lightweight and heavyweight mass properties are shown in Table 7-2 and Table 7-3, respectively. These are the two mass properties examined in this study, anticipating that linear interpolation could be used to determine the amount of flow needed at any intermediate mass.

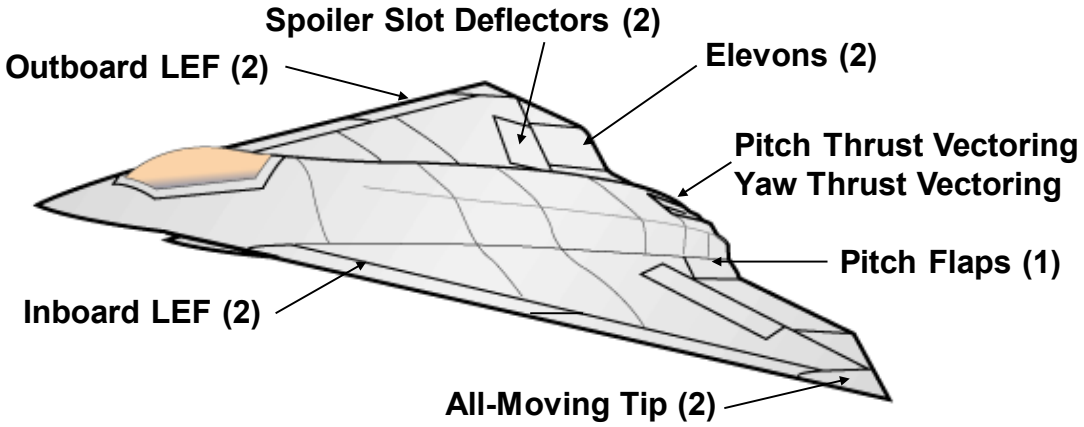

Figure 7-1: The ICE Tailless Fighter Research Aircraft.

Table 7-1: LM Aero Tailless Aircraft Model Reference Data.

Parameter	Value
Reference Wing Area, S_{ref}	808.6 ft^2
Reference Span, b_{ref}	37.5 ft
Mean Aerodynamic Chord	345 in
FS Leading-Edge MAC	160.84 in
Moment Reference Center	38% MAC
WL MRC	100.0 in

Table 7-2: ICE Aircraft Lightweight Mass Properties.

Weight and C.G. Location		Inertias	
Weight	25,989 lb	I_{xx}	35,479 slug-ft^2
x_{cg}	40% cbar	I_{yy}	67,500 slug-ft^2
y_{cg}	0	I_{zz}	83,800 slug-ft^2
z_{cg}	88.97	I_{xz}	-250 slug-ft^2

Table 7-3: ICE Aircraft Heavyweight Mass Properties.

Weight and C.G. Location		Inertias	
Weight	37,084 lb	I_{xx}	42,576 slug-ft^2
x_{cg}	36% cbar	I_{yy}	81,903 slug-ft^2
y_{cg}	0	I_{zz}	118,379 slug-ft^2
z_{cg}	88.97	I_{xz}	-525 slug-ft^2

7.4 SIMULATION MODEL

Ref. [3] gives a significant amount of information about the simulation model, therefore this chapter focuses on the additional fluidic effector data and on an overview of the controller used for the simulation results to follow. The flight condition for all the simulation results is 30,000 ft altitude, Mach 0.9.

The simulator code runs in the MATLAB/Simulink (R2018b) environment. Models for active flow control effectors were added to the simulation that used data from the wind tunnel measurements by Williams et al. [4]. The names and approximate locations of the fluidic control effectors are shown in Figure 7-2. The data is included in look-up table form, and the control derivatives computed from the original data and stored in data tables used in control allocation. The traditional actuator dynamics are described in the earlier paper while the active flow control actuation is assumed to operate at an equivalent sixty degrees per second. A brief study done to specify requirements shows that fifty degrees per second is the minimum actuation rate, while performance did not improve significantly if the effective rate is set higher. Vehicle stability and performance is noticeably worse if the effective rate is lower than 45 deg/sec. Because this effort is a feasibility study, equivalent time delay of either the traditional effectors or of the active flow control effectors was not considered here.

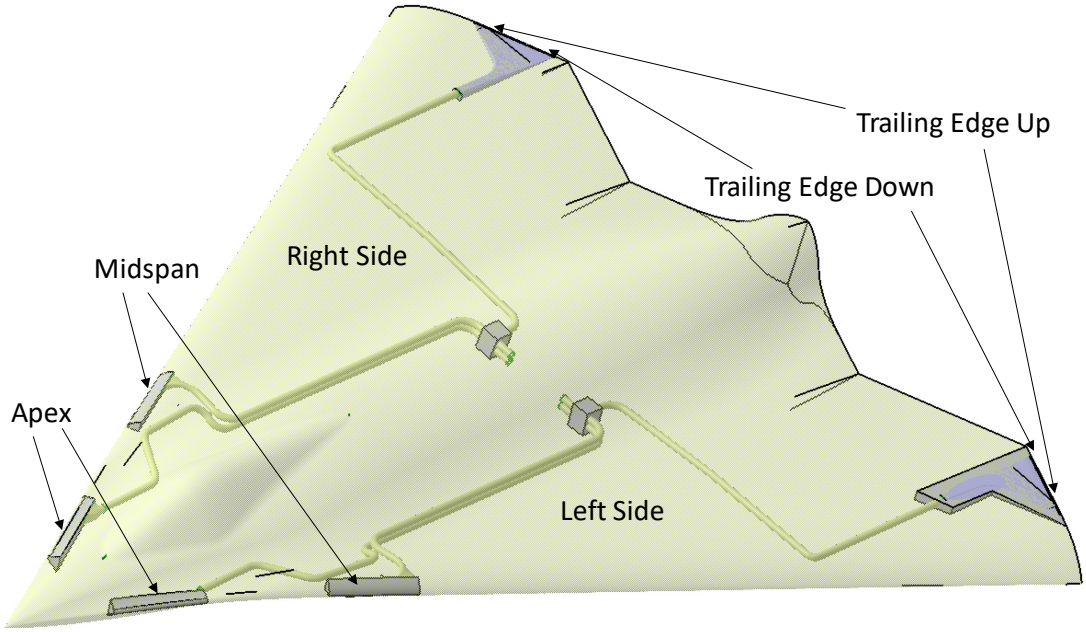

Figure 7-2: The ICE Simulation Model is Expanded to Include Active Flow Control Effectors.

The simulation uses a simplified nonlinear dynamic inversion methodology. The roll channel desired dynamics specified the roll mode time constant of 0.5 seconds. The yaw channel dutch roll frequency is set at 2.75 rad/sec and a damping ratio of 0.95. Finally, the pitch channel seeks a short period frequency of 2 rad/sec and a damping ratio of 0.7 and a numerator time constant of 0.8 sec. The aero model and equations of motion are duplicated and act as the on-board model for acceleration prediction and control effectiveness modelling. A Quadratic Programming (QP) control allocation method from Ref. [5] is used to convert the desired accelerations into physical effector movement or flow commands. Besides specifying rate and position limits, the weighting of the active flow control effectors is set to 0.06 for yaw thrust vectoring and to 0.2 for all the remaining active flow control effectors when operating in the all flow control mode; all the traditional effectors and both pitch and yaw fluidic thrust vectoring has weighting set to one when in traditional effector mode, except as noted below. A basic autopilot is used to maintain pitch attitude and bank angle.

The standard atmosphere models provided in the Simulink Aerospace Blockset are used to provide the turbulence and gust disturbances to the aircraft simulation. The values of the turbulence block are set to English Units, MIL-HDBK-1797 specification, Continuous Dryden (+q -r), 1750 ft scale length, and the reference wing span. The discrete wind gust model is modified to have the gust ramp out over the same gust length as it ramps in. The gust amplitude for a light gust is computed to be 4.5 ft/sec and for a moderate gust to be 9 ft/sec, using the MIL-HDBK-1797 reference tables. For these gust amplitudes, the worst-case distances are determined by running the simulation for varying values. These studies indicate that the worst-case disturbance occurs when the gust length is 750 ft (750 ft gust ramp in, + 750 ft gust ramp out). Similarly, simulation of six gust axes combinations show that a v-axis gust produces the largest magnitude or is very close to the largest magnitude. Therefore, all the simulation results with gust responses which follow have a v-axis gust alone (i.e., no u-axis or w-axis components).

7.5 SIMULATION RESULTS

7.5.1 Traditional Aerodynamic Effectors

Before discussing the results of active flow control effectors alone, the following section presents responses to gust and turbulence when using various combinations of traditional, aerodynamic effectors and in possible combination with yaw thrust vectoring. These offer a comparison of the amount of surface movement needed which might be of interest. The simulation shows the heaviest effector usage, whether traditional or active flow control effectors, for the heavyweight aircraft. Therefore, the simulation results in this section are for the heavy aircraft as a worst-case.

The general philosophy taken for traditional effector usage attempts to minimize the amount of yaw thrust vectoring needed since it is also a fluidic control effector. This minimization occurs through adjustment of the associated weight in the control allocation module, mentioned above. Figure 7-3 shows the control effector activity when hit by the moderate side gust in the presence of light atmospheric turbulence. In this case, the elevons and spoiler slot deflectors are available along with yaw thrust vectoring. Even though yaw fluidic thrust vectoring is available, it is heavily penalized. As such, the control allocation uses a combination of elevons and spoiler slots to reject the gust and turbulence, using at peak approximately 7 deg. of left elevon and 6 deg of left spoiler slot deflector. Therefore, yaw fluidic thrust vectoring is not needed for this mission segment with this combination of traditional aero effectors.

Restricting the control allocation to a different set of aero effectors, Figure 7-4 presents the time histories of control effectors that were limited to elevons, all-moving wing tips, and yaw thrust vectoring. In this case, all the control surfaces were active at some point in the simulation, with magnitudes of 6-8 deg. for most of them. It is assumed that, for this study, fluidic thrust vectoring can achieve 3 deg. of thrust deflection with 1 lb/sec of flow through slots in the engine nozzle. So, in this simulation, a peak of 9 deg. of yaw fluidic thrust vectoring is achieved with 3 lb/sec flow rate. Note the simulation indicated insufficient control power without the yaw fluidic thrust vectoring and the amount used here is the minimum found through a short study of adjusting the weighting penalty on yaw fluidic thrust vectoring.

Finally, if the control allocation was given the elevons, the all-moving wing tips, the spoiler slots, and yaw fluidic thrust vectoring, it sought to use all of the effectors to some extent, as shown in Figure 7-5. All of the effectors are weighted the same in this simulation. The magnitude of the several of the effectors peaked near 10 deg. Similar to the above case, approximately 3 lb/sec of flow was needed to generate the approximate 9 deg of yaw thrust vectoring that was needed at peak times. Note that, in this case, there was some ringing of the right all-moving wing tip which warrants further investigation as to the cause. Recall this control allocator was not tuned for optimal operation with any particular suite of control effectors.

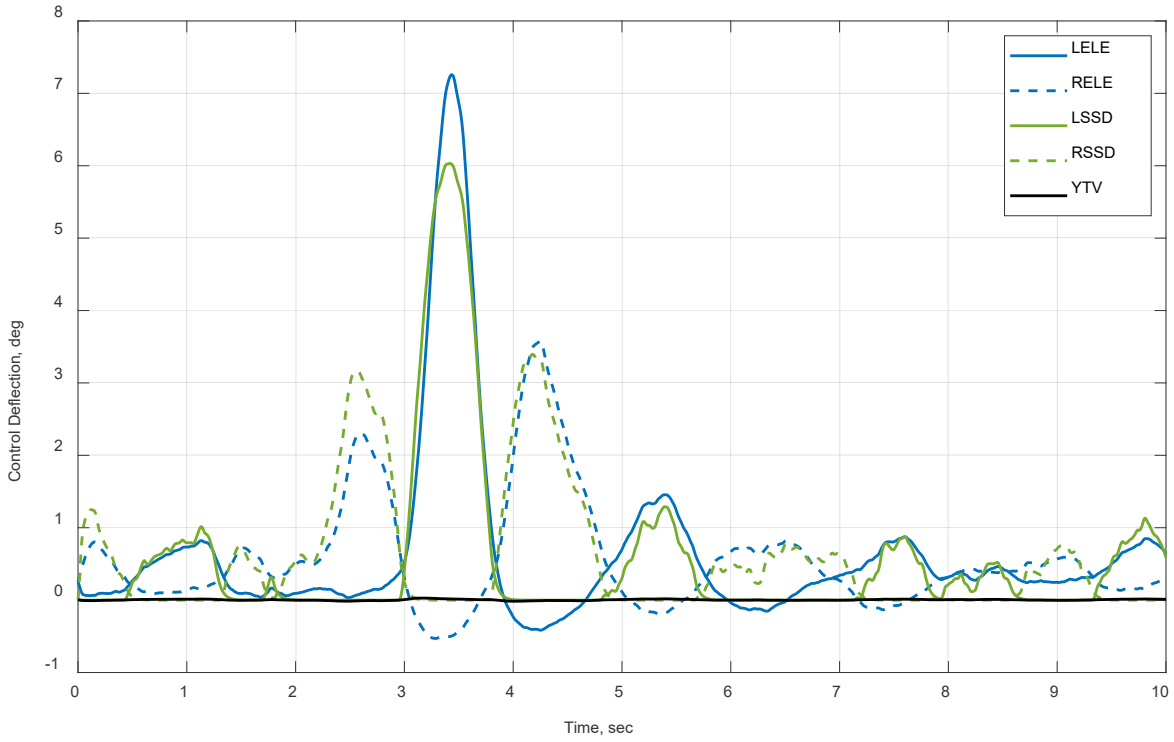

Figure 7-3: Traditional Control Effector Simulation Results Show Sufficient Control Power with Elevons and Spoiler Slot Deflectors Alone During the Ingress and Egress Mission Phases.

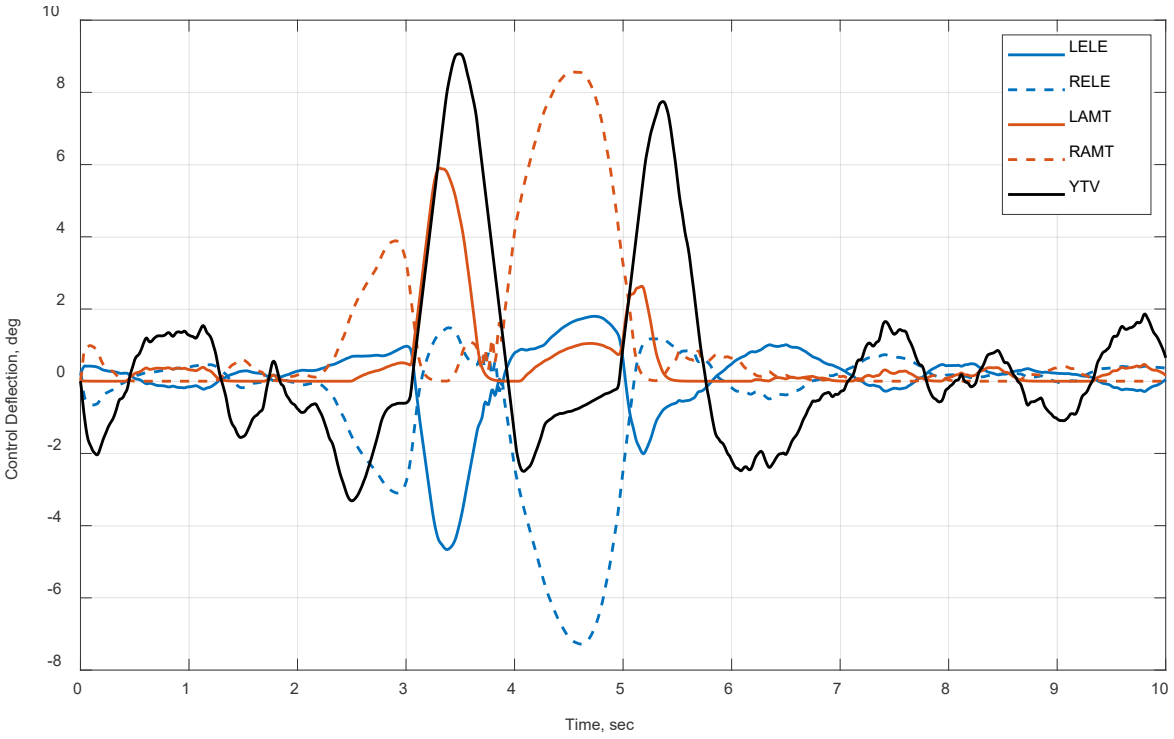

Figure 7-4: Elevons and All-Moving Wingtips Alone Show Insufficient Control Power for the Mission Segments of Interest and Require Yaw Fluidic Thrust Vectoring.

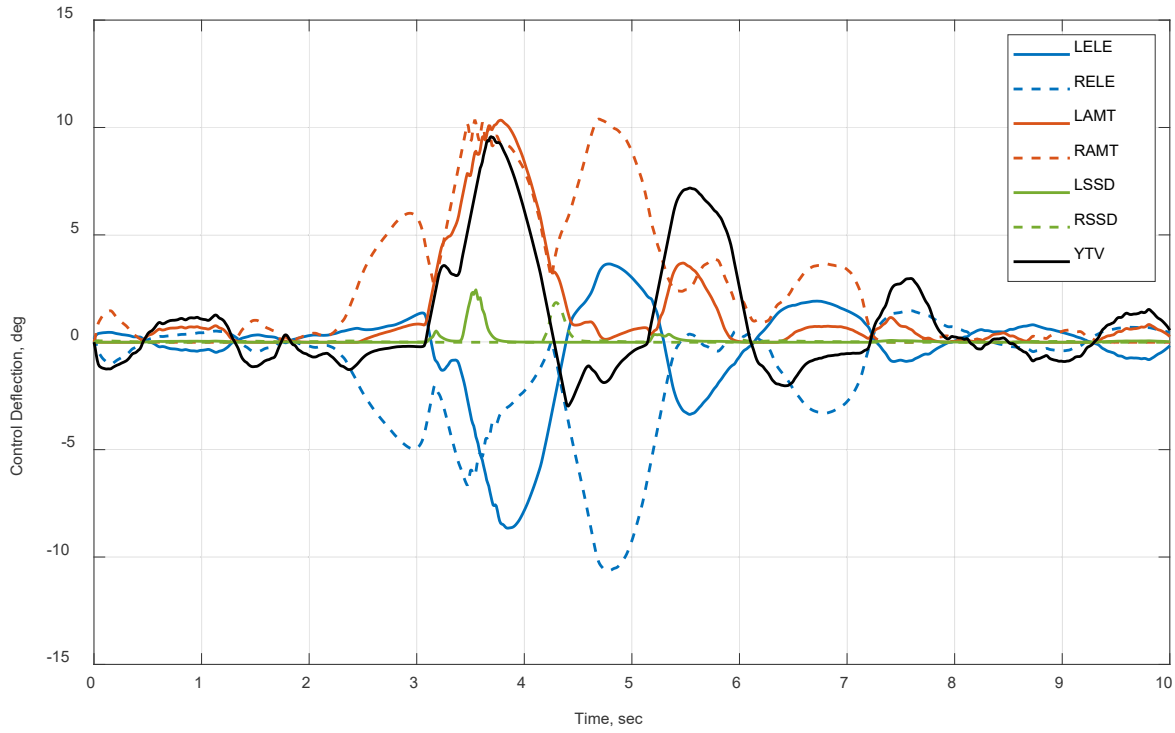

Figure 7-5: When Elevons, Spoiler Slot Deflectors, and All-Moving Wingtips are Available for Control Allocation, Yaw Fluidic Thrust Vectoring is Needed for Stability.

7.5.2 Active Flow Control Effectors

This section presents responses to gust and turbulence when using various combinations of active flow control effectors in combination with yaw fluidic thrust vectoring. The different combinations were explored to determine how specific active flow control effectors may contribute to the effective control of the vehicle in these conditions. All of the traditional aerodynamic effectors are driven from trim to zero in the simulation and the active flow control effectors take over the function of trimming the aircraft before the turbulence is engaged. Again, these results are for the heavyweight aircraft.

Figure 7-6 shows the active flow control effector activity when the aircraft is hit by the moderate side gust in the presence of light atmospheric turbulence, the same conditions for the aerodynamic effector results shown above. Here, all of the flow control effectors, left and right apex, left and right midspan, left and right trailing edge down, left and right trailing edge up, and yaw fluidic thrust vectoring are made available to the control allocation module. The yaw fluidic thrust vectoring used the most flow, approximately 2 lb/sec during the gust. The sum total flow needed for all of these effectors is shown in Figure 7-7. The peak usage was approximately 4 lb/sec during the gust and settled to approximately 0.5 lb/sec average during light turbulence.

Figure 7-8 shows simulation results when the midspan active flow control effectors are removed from allocation. As in the case where all flow control effectors are present, the peak usage was by the yaw fluidic thrust vectoring of 2 lb/sec for a fraction of a second. The total flow needed, shown in Figure 7-9, has a peak of just under 4 lb/sec during the gust and settles to about a half pound per second during the light turbulence.

Figure 7-10 presents the simulation time histories when the apex slots are disabled but the midspan slots are active. A similar trend shows here with the peak yaw thrust vectoring taking 2 lbs/sec peak during the gust and the total flow peak, Figure 7-11, of just over 4 lb/sec.

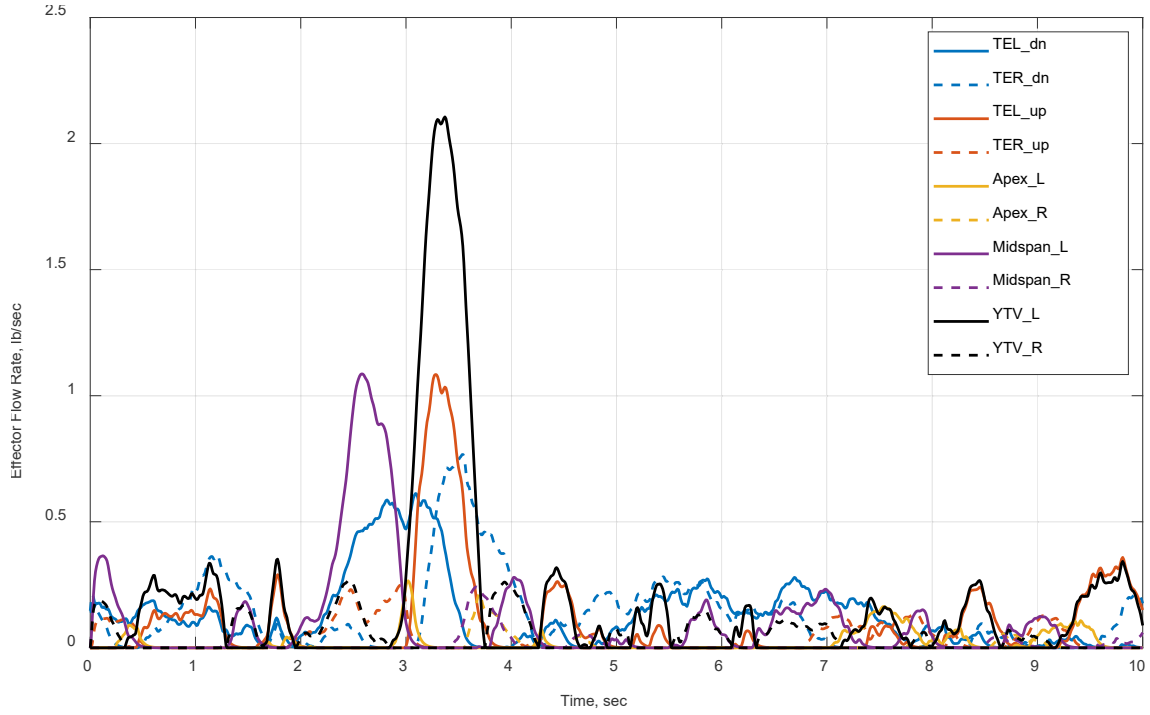

Figure 7-6: With All of the Active Flow Control Effectors Available, the Control Allocation Module Makes Use of Most of the Effectors During Light Turbulence with a Discrete Moderate Gust.

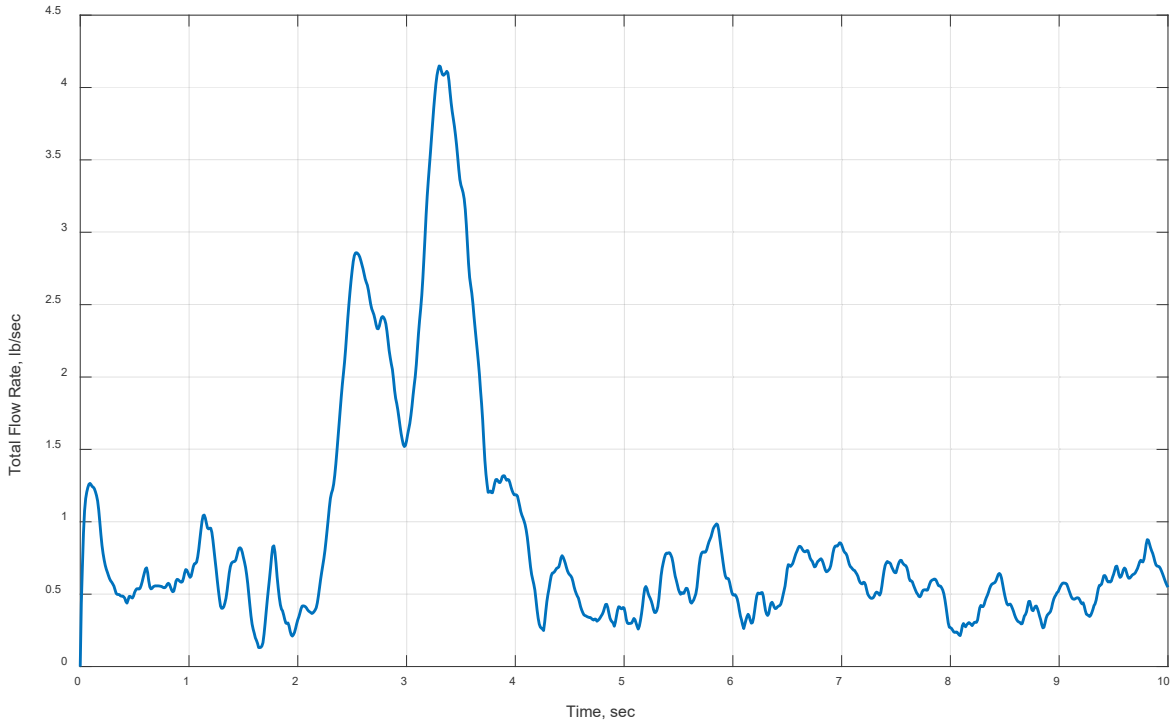

Figure 7-7: The Total Flow Required Peaks Slightly Above 4 lb/s During the Gust and Settles to Approximately One-Half Pounds per Second when in Light Turbulence.

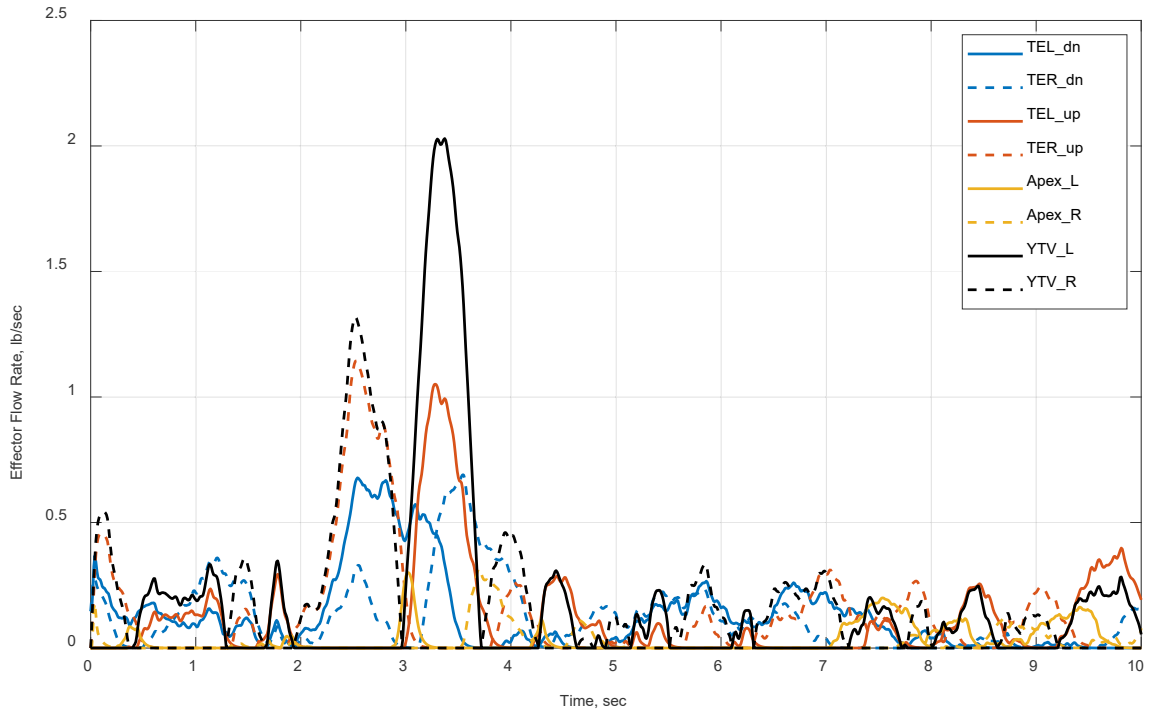

Figure 7-8: With Midspan Slot-Jet Effectors Removed, Much of the Activity Comes from the Trailing Edge Slot-Jet Effectors and Yaw Fluidic Thrust Vectoring with Little Apex Slot-Jet Utilization.

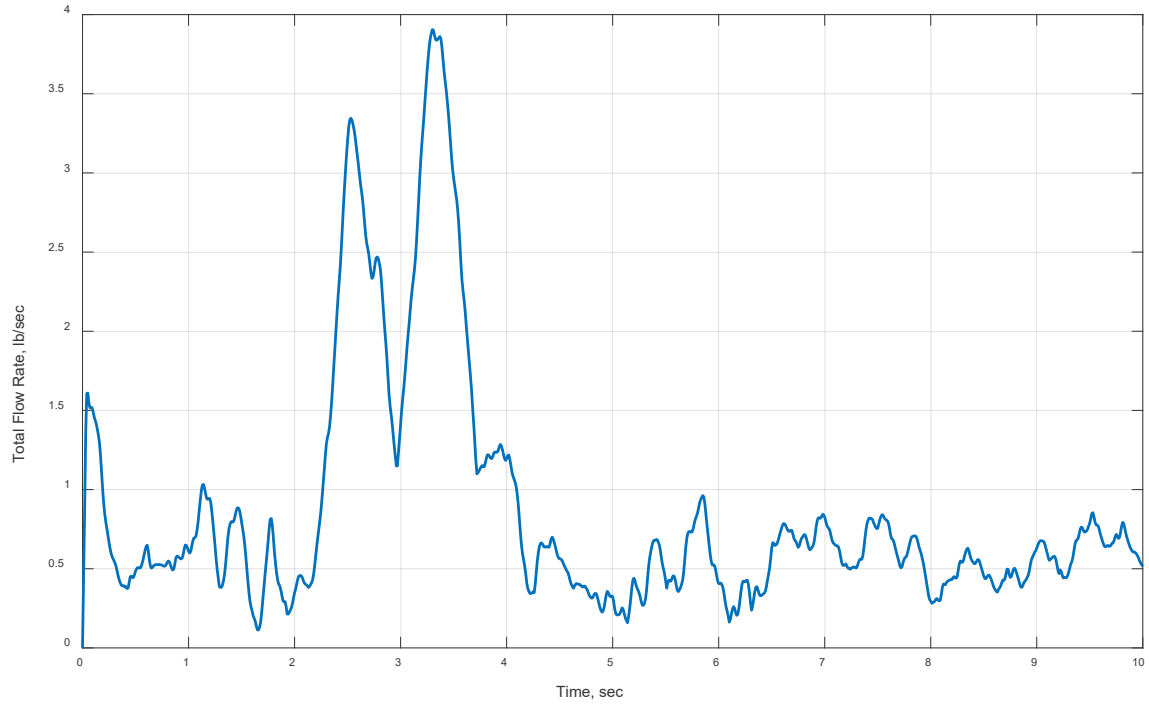

Figure 7-9: Slightly Less Flow is Required when the Midspan Slot-Jet Effectors are Removed but the Peak is Near 4 lb/sec and the Mean During Turbulence Unchanged.

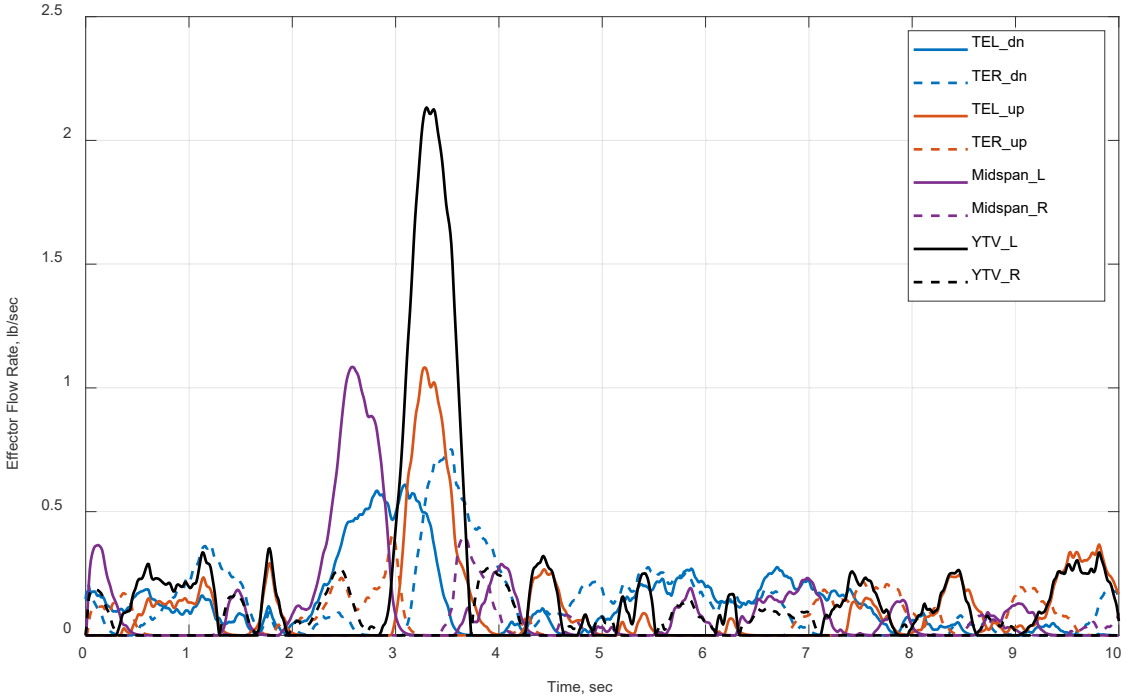

Figure 7-10: With the Apex Slot-Jet Effectors Eliminated, the Simulation Result is Similar to the Case Where All Active Flow Control Effectors are Considered by the Control Allocator.

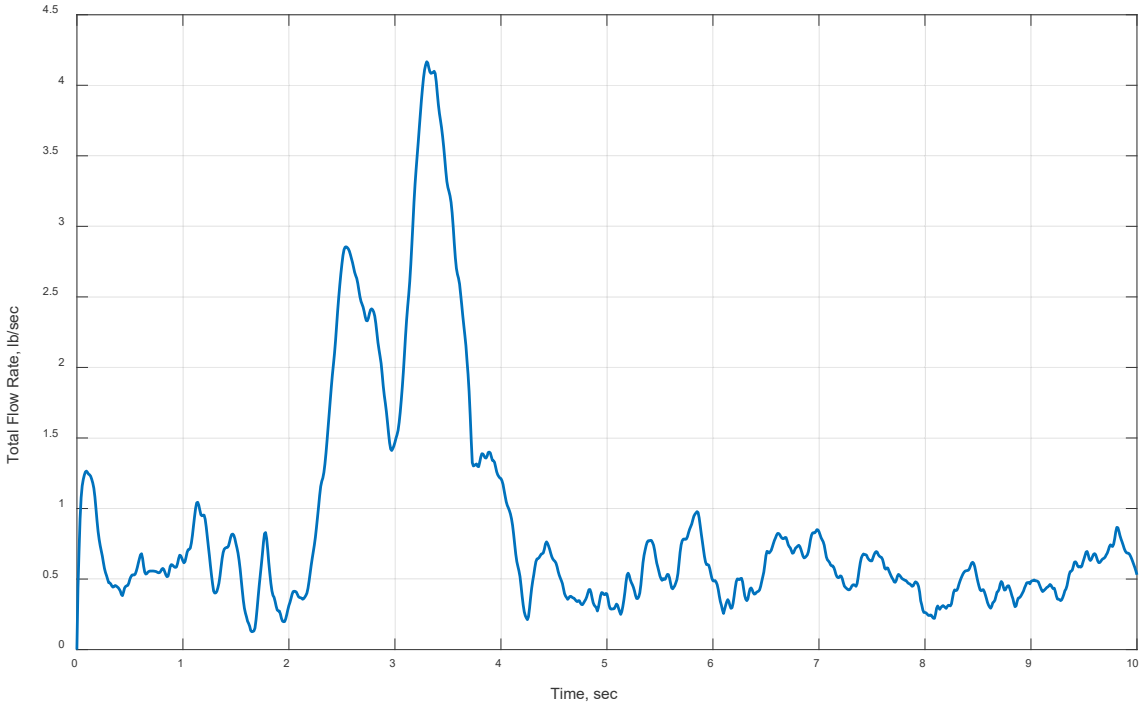

Figure 7-11: The Total Flow Required Without the Apex Slot-Jet Effectors Closely Matches the Case with All Active Flow Control Effectors.

Figure 7-12 presents simulation results with the midspan and apex slot-jet effectors inactive, leaving only the four trailing edge slot-jet effectors and yaw fluidic thrust vectoring. The peak flow of any effector is, again, 2 lb/sec taken by the yaw fluidic thrust vectoring effector and a total peak of just under 4 lb/sec total for all effectors combined (Figure 7-13).

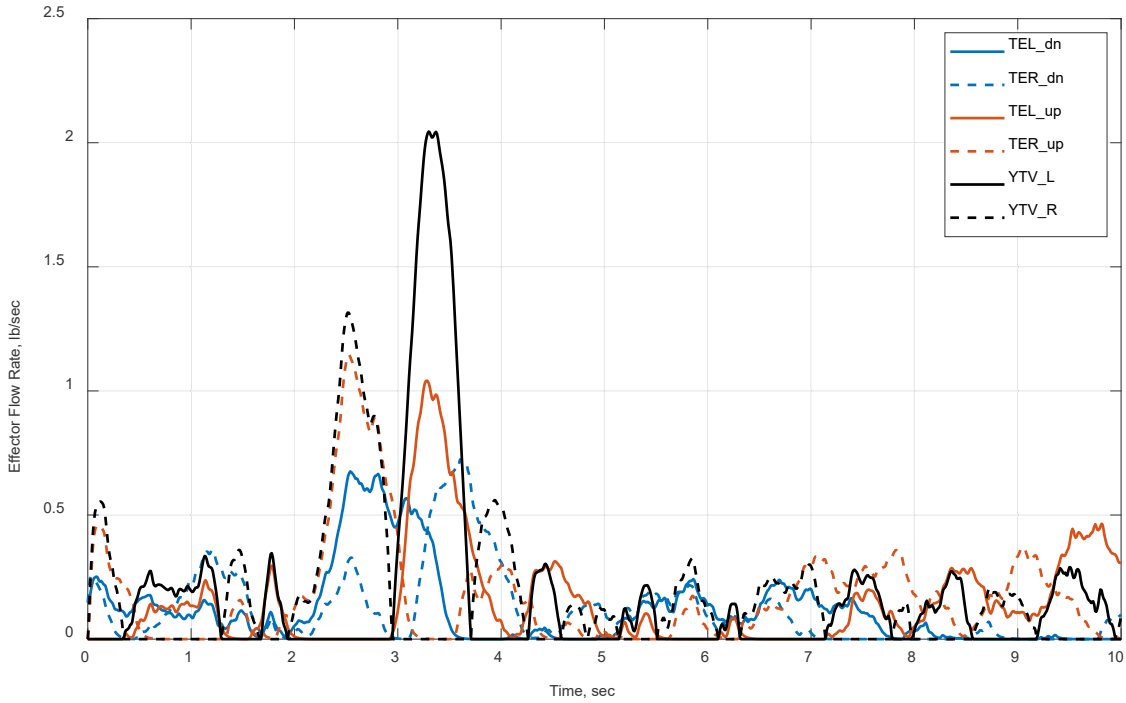

Figure 7-12: With the Leading-Edge Slot-Jet Effectors Removed, the Control Allocation Makes Extensive Use of the Trailing Edge Slot-Jet Effectors and Yaw Fluidic Thrust Vectoring.

These active flow control effector usage cases highlight the better overall effectiveness of the trailing edge slot-jet effectors. When the leading-edge effectors are included in the allocation, they do utilize some flow to maintain stability, but their cross coupling, it is assumed, necessitates some extra flow to balance the moment generation. Adjusting the relative weighting of the various active flow control effectors results in different overall flow requirements, but the trend is always to need more total flow if the yaw fluidic thrust vectoring weight is increased (making the yaw thrust vectoring less preferred). Also note that, as in the case of traditional aero effectors alone where the all-moving wingtips, elevons, and yaw fluidic thrust vectoring are used, the thrust vectoring needs a peak of 3 lb/sec. In comparison, a peak of 4 lb/sec needed by the active flow control system eliminates the need to utilize the elevons and all-moving wing tips and can eliminate the use of the spoiler slot deflectors during this mission phase.

Table 7-4 presents the summary results from a series of simulations with various atmospheric turbulence and gusts, including a representative statistically significant mass flow needed during an hour long mission and the amount of flow needed to trim the aircraft. All these are for both the heavy weight and light weight aircraft properties described in the introductory section. Because the aircraft is near neutrally stable and the zero lift pitching moment is small, the amount of flow needed to trim the aircraft is 0.33 lb/s for the heavyweight aircraft and 1 lb/s for the lightweight aircraft. For light turbulence, the peak total flow needed over a ten second simulation is approximately 1.34 lb/sec for any active flow control effector combinations tested in the heavyweight aircraft case and approximately 1.56 lb/s for the lightweight aircraft. Note this includes the amount of flow needed to trim the aircraft, so it is not surprising that the light aircraft requires slightly more

flow given its higher trim flow rate. Without turbulence, simulations are conducted for light and moderate gusts. In this case, the effector configuration of the trailing edge devices alone coupled with yaw fluidic thrust vectoring shows a lower amount of flow needed for gust rejection, especially in the heavyweight aircraft case.

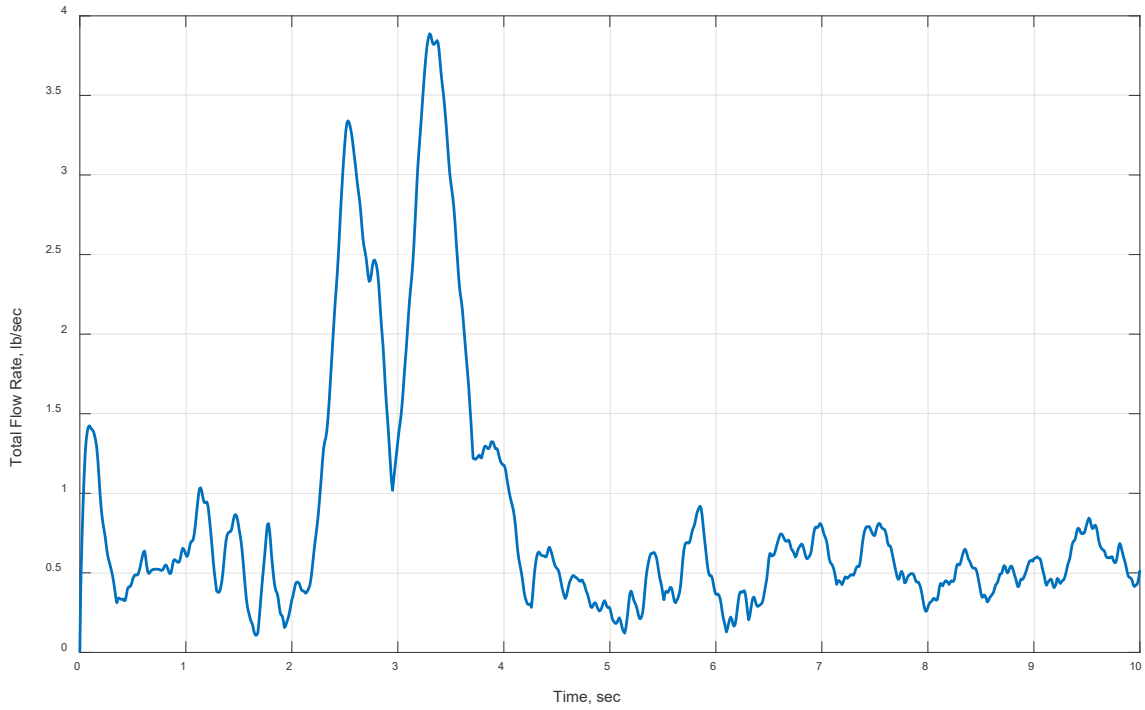

Figure 7-13: The Peak Flow Required When the Leading Edge Effectors are Removed Peaks Below 4 lb/sec.

Table 7-4: Summary of Total Peak and Trim Flow Requirements for Various Active Flow Control Effector Combinations and Mass Properties for the Ingress/Egress Mission Segments.

			Heavy Aircraft, Effector Configuration				Light Aircraft, Effector Configuration			
Atmospheric Condition	Metric	Units	1	2	3	4	1	2	3	4
Reject light turbulence	Peak flow (10s sim)	lb/s	1.36	1.34	1.35	1.31	1.57	1.56	1.57	1.56
Reject light gust	Peak flow (10s sim)	lb/s	1.70	1.60	1.66	1.54	1.31	1.28	1.30	1.28
Reject moderate gust	Peak flow (10s sim)	lb/s	3.44	3.21	3.27	2.90	2.35	2.20	2.34	2.19
Accommodate trim	Flow to Trim	lb/s	0.33	0.33	0.33	0.33	1.00	1.00	1.00	1.00
Effector Configuration										
1	TE_dn+TE_up+Apex+Midspan+YTV									
2	TE_dn+TE_up+Apex+YTV									
3	TE_dn+TE_up+Midspan+YTV									
4	TE_dn+TE_up+YTV									

7.5.3 Impact on Mission Performance and Flow Control System Requirements

The prior section focuses on requirements to handle discrete events or short durations of turbulence. This section focuses on the time averaged flow needed during a nominal mission ingress or egress. Such information helps size the plumbing of the flow control system and the fuel consumption impact because of the engine bleed, presumed to supply the flow for the fluidic effectors, including yaw fluidic thrust vectoring.

The total flow rate needed for the heavyweight aircraft is typically higher than for the lightweight aircraft when considering a longer mission duration. Table 7-5 presents data taken over one hundred simulations of light turbulence with different random number seeds and a moderate gust occurring one percent of the time for the heavy aircraft. Note the v-axis (side) gust always comes in from the right side of the aircraft, resulting in a positive sideslip initially. Therefore, sizing the ducting of any active flow control effector takes the higher value of right or left effector pair. The intent is to determine the average amount of flow through any one particular effector. As in the prior section, differing combinations of active flow control effectors are analyzed to determine the amount of flow needed for that effector suite and presumed selection of the preferred effector suite for this mission.

Table 7-5: Mean Flow Rates Taken from One Hundred Simulation Runs for Each Active Flow Control Effector for the Four Effector Suites, Heavy Aircraft.

	Heavyweight Aircraft, 100 Runs, Light Turbulence, Moderate Gust, Mean Flow Rates, lb/s									
	Apex_L	Apex_R	Midspan_L	Midspan_R	TE_L_dn	TE_R_dn	TE_L_up	TE_R_up	YTV	Sum Total
mean over mission	0.06	0.03	0.10	0.03	0.06	0.06	0.07	0.03	0.11	0.56
std over mission	0.08	0.05	0.13	0.04	0.06	0.07	0.08	0.04	0.10	0.66
mean + 2*std	0.23	0.13	0.37	0.10	0.19	0.20	0.24	0.11	0.31	1.88
mean + 3*std	0.31	0.18	0.50	0.14	0.25	0.27	0.32	0.15	0.40	2.53
	Apex_L	Apex_R	Midspan_L	Midspan_R	TE_L_dn	TE_R_dn	TE_L_up	TE_R_up	YTV	Sum Total
mean over mission	0.10	0.08	-	-	0.05	0.05	0.09	0.08	0.14	0.59
std over mission	0.10	0.10	-	-	0.06	0.05	0.09	0.09	0.11	0.60
mean + 2*std	0.30	0.27	-	-	0.17	0.16	0.28	0.26	0.35	1.78
mean + 3*std	0.40	0.37	-	-	0.22	0.21	0.37	0.34	0.46	2.38
	Apex_L	Apex_R	Midspan_L	Midspan_R	TE_L_dn	TE_R_dn	TE_L_up	TE_R_up	YTV	Sum Total
mean over mission	-	-	0.10	0.05	0.06	0.06	0.10	0.06	0.12	0.56
std over mission	-	-	0.13	0.07	0.06	0.06	0.09	0.06	0.10	0.59
mean + 2*std	-	-	0.37	0.19	0.19	0.19	0.28	0.19	0.32	1.73
mean + 3*std	-	-	0.51	0.27	0.25	0.25	0.37	0.25	0.42	2.32
	Apex_L	Apex_R	Midspan_L	Midspan_R	TE_L_dn	TE_R_dn	TE_L_up	TE_R_up	YTV	Sum Total
mean over mission	-	-	-	-	0.04	0.04	0.15	0.15	0.17	0.55
std over mission	-	-	-	-	0.05	0.05	0.11	0.11	0.11	0.43
mean + 2*std	-	-	-	-	0.14	0.15	0.37	0.37	0.39	1.41
mean + 3*std	-	-	-	-	0.18	0.20	0.47	0.48	0.50	1.84

The first section of the table presents results when all the active flow control effectors are available to the control allocation module. The mean values are computed for a mission segment for light turbulence and a moderate gust occurring one percent of the time. The average flow summed across all effectors is 0.56 lb/sec and the standard deviation, sigma, is 0.66 lb/sec. The mean plus two sigma represents the amount of flow needed to handle 95% of the mission segment and the mean plus three sigma represents the amount of flow needed to handle 99% of the mission. In this last case, a peak flow rate of 2.53 lb/sec is needed to successfully control the aircraft for 99% of the mission.

Considering the 99% coverage cases, discarding the availability of the midspan slot-jet effectors drops the flow requirements to 2.38 lb/sec. Similarly, if the apex slot-jet effectors are inactive, the flow needed is 2.32 lb/sec. However, if all four of the leading-edge active flow control effectors are eliminated from allocation, the trailing edge slot-jet effectors coupled with fluidic thrust vectoring consumes less than 1.84 lb/sec for 99% of the mission.

Repeating the simulations for the light aircraft, Table 7-6 shows results with the same combinations of active flow control effectors. With all active flow control effectors available for the control allocator, the flow rate

of 1.87 lb/sec provides sufficient control for 99% of the mission. Without the apex slot-jet actuation, the needed flow rate declines to 1.75 lb/sec. In the case where only the midspan slot-jet effector is zeroed, the total flow rate needed is 1.63 lb/sec. This trend is different than for the heavy aircraft where apex slot-jet effector elimination required less flow than midspan elimination. But, as in the heavy aircraft case, the lowest flow needed for the light aircraft occurs when all four leading-edge slot-jet effectors are eliminated from allocation, needing only 1.42 lb/sec total flow rate.

Table 7-6: Mean Flow Rates Taken from One Hundred Simulation Runs for Each Active Flow Control Effector for the Four Effector Suites, Light Aircraft.

	Lightweight Aircraft, 100 Runs, Light Turbulence, Moderate Gust, Mean Flow Rates, lb/s									
	Apex_L	Apex_R	Midspan_L	Midspan_R	TE_L_dn	TE_R_dn	TE_L_up	TE_R_up	YTV	Sum Total
mean over mission	0.06	0.03	0.10	0.03	0.06	0.06	0.07	0.03	0.10	0.55
std over mission	0.03	0.02	0.10	0.03	0.07	0.08	0.05	0.02	0.07	0.47
mean + 2*std	0.07	0.05	0.27	0.07	0.26	0.27	0.14	0.04	0.25	1.41
mean + 3*std	0.09	0.07	0.37	0.09	0.33	0.35	0.19	0.06	0.32	1.87
	Apex_L	Apex_R	Midspan_L	Midspan_R	TE_L_dn	TE_R_dn	TE_L_up	TE_R_up	YTV	Sum Total
mean over mission	0.02	0.02	-	-	0.10	0.10	0.04	0.04	0.12	0.43
std over mission	0.04	0.04	-	-	0.07	0.07	0.05	0.05	0.08	0.40
mean + 2*std	0.09	0.09	-	-	0.23	0.24	0.15	0.14	0.28	1.23
mean + 3*std	0.13	0.13	-	-	0.30	0.32	0.20	0.19	0.36	1.63
	Apex_L	Apex_R	Midspan_L	Midspan_R	TE_L_dn	TE_R_dn	TE_L_up	TE_R_up	YTV	Sum Total
mean over mission	-	-	0.07	0.02	0.11	0.12	0.04	0.01	0.10	0.47
std over mission	-	-	0.10	0.04	0.07	0.08	0.05	0.02	0.07	0.43
mean + 2*std	-	-	0.27	0.09	0.26	0.27	0.13	0.06	0.24	1.32
mean + 3*std	-	-	0.37	0.13	0.33	0.35	0.18	0.09	0.31	1.75
	Apex_L	Apex_R	Midspan_L	Midspan_R	TE_L_dn	TE_R_dn	TE_L_up	TE_R_up	YTV	Sum Total
mean over mission	-	-	-	-	0.09	0.09	0.06	0.06	0.12	0.41
std over mission	-	-	-	-	0.06	0.07	0.06	0.06	0.08	0.34
mean + 2*std	-	-	-	-	0.22	0.22	0.18	0.18	0.28	1.08
mean + 3*std	-	-	-	-	0.28	0.29	0.25	0.24	0.36	1.42

When using traditional effectors, the combination of spoiler slot deflectors and elevons are sufficient to handle the gust and turbulence studied in this chapter for ingress and egress missions. If all-moving wingtips are combined with elevons, though, yaw fluidic thrust vectoring must also be used, and the peak flow rate needed is approximately 3 lb/sec. Similarly, if elevons, spoiler slot deflectors, and all-moving wingtips are used, yaw fluidic thrust vectoring must also be used and requires a peak of approximately 3 lb/sec. An all-fluidic control effector suite can perform the same mission without the need for any external surface movement using approximately 4.5 lb/sec peak flow rate, at most, during a moderate gust. However, 99% of an ingress/egress mission can be performed with active flow control effectors alone and for total flow rates of under 2 lb/sec.

7.6 SUMMARY AND CONCLUSIONS

The ICE study conducted in the 1990's generated a significant amount of information concerning the development of a tailless fighter aircraft configuration, including aerodynamic and mass properties information. Much of the data in report format was publicly released in 1998 by AFRL and in simulation format by Lockheed Martin Aero in 2017. A NATO research group studying the potential uses of flow control on such aircraft has integrated flow control data into a nonlinear, six degree of freedom simulation of the ICE aircraft along with a simplified nonlinear dynamic inversion controller and a quadratic programming-based control allocation module. During a simulated ingress or egress mission segment, simulations are conducted of the

vehicle in light turbulence and discrete light and moderate gusts. Baseline simulations of the aircraft with traditional aerodynamic effectors suites that included yaw fluidic thrust vectoring are presented for comparison to active flow control effectors-only simulations in the same conditions.

Should an aircraft designer choose to eliminate traditional control surface deflection or movement during the ingress or egress mission phases, for an aircraft similar to the ICE configuration, active flow control effectors offer such a capability utilizing a reasonable amount of engine bleed. These control effectors provide stabilizing forces and moments during periods of light or moderate turbulence or periods of light turbulence in combination with light or moderate discrete gusts. The impact on overall mission performance, airframe integration, or reliability and maintainability are addressed in complementary papers presented in this special session.

For future work, many issues need addressing. The ability to scale low speed wind tunnel data for use at high speed/high altitude conditions needs examination. The amount of nonlinearity in the active flow control effector data needs refinement as control reversals are noted in the wind tunnel data. The control allocation function needs improvement to optimally transition between all traditional effectors to all active flow control effectors. Saturation protection and optimization are two areas of particular interest. With some of these issues addressed, additional mission phases such as high angle of attack maneuvering and crosswind landing should be examined in more detail to gauge the overall effectiveness of active flow control effectors along the path to potentially remove traditional effectors completely from an aircraft.

7.7 ACKNOWLEDGEMENTS

The flow control model development was sponsored, in part, by the U.S. Air Force Office of Scientific Research under grant FA9550-16-1-0098 with program manager Dr. Douglas Smith and his support is gratefully acknowledged. The collaboration with Dr. Christopher Hutchin and Dr. Clyde Warsop was very fruitful and is sincerely appreciated.

This material is based in part on research sponsored by the US Air Force Academy under agreement number FA7000-13-2-0009. The U.S. Government is authorized to reproduce and distribute reprints for Governmental purposes notwithstanding any copyright notation thereon.

The views and conclusions contained herein are those of the authors and should not be interpreted as necessarily representing the official policies or endorsements, either expressed or implied, of the US Air Force Academy or the U.S. Government.

7.8 REFERENCES

[1] Dorsett, K.M., and Mehl, D.R., Innovative Control Effectors (ICE), Phase 1 Final Report, WL-TR-96-3043, January 1996.

[2] Dorsett, K.M., Fears, S.P., and Houlden, H.P., Innovative Control Effectors (ICE) Phase II, Phase II Final Report, WL-TR-97-3059, August 1997.

[3] Niestroy, M.A., Dorsett, K.M., and Markstein, K., A Tailless Fighter Aircraft Model for Control-Related Research and Development, AIAA SciTech Conference, Paper 1757, January 2017.

[4] Williams, D., Osteroos, R., and McLaughlin, T., Flight Control Derivatives Using Active Flow Control Effectors on the ICE/SACCON UCAS Model, AIAA SciTech Conference, January 2019.

[5] Matamoros, I., and de Visser, C.C., Incremental Nonlinear Control Allocation for a Tailless Aircraft with Innovative Control Effectors, AIAA SciTech Conference, Paper 1116, January 2018.

CHAPTER 8 – ACTIVE FLOW CONTROL SIMULATION OF THE SACCON AIRCRAFT

Chris Hutchin
Defence Science and Technology Laboratory
UNITED KINGDOM

8.0 NOMENCLATURE

C_L	Lift coefficient	C_m	Pitch moment coefficient
C_n	Yaw moment coefficient	$\underline{u}$	Vector of control effector inputs
C_l	Roll moment coefficient	u_n	n^{th} control effector input…….

8.1 OVERVIEW

Task Group AVT-239 "Innovative Control Effectors for Manoeuvring Aircraft", was formed under the auspices of the NATO Science and Technology Organization Applied Vehicle Technologies panel. Within this Task Group, researchers and engineers assessed potential for active flow control effectors to be incorporated into combat aircraft configurations. The methodology reported in this chapter was used to develop aerodynamic effectiveness data into quantified requirements for control system size, weight and complexity in order to meet a defined system performance requirement. Active flow control technologies studied included trailing-edge circulation control, active flow control using sweeping jet effectors, and fluid thrust vectoring. Evaluations required control system capability to reject gusts and turbulence at a high-level, transonic flight condition, although the approach taken could be applied to different, more stressing conditions. Results indicated that configurations using active flow control effectors could have sufficient capability to fulfil this requirement. The outputs of the performance assessment reported within this chapter have informed integration assessments performed elsewhere within the AVT-239 activity.

8.2 INTRODUCTION

8.2.1 NATO STO AVT-239 "Innovative Control Effectors for Manoeuvring Aircraft"

Conventional controls – movable aerodynamic surfaces including rudders, elevators, ailerons, leading and trailing edge flaps, spoilers, and others – are well-proven technologies for primary and secondary flight control of fixed-wing aircraft. Nevertheless, there have been efforts in recent decades to investigate new types of control effectors for combat aircraft (see Refs. [1], [2]), motivated by such factors as changes in aircraft configuration (e.g., removal of empennage surfaces), stressing manoeuvre requirements (e.g., post-stall manoeuvre) and low-observable integration. Within the collaborative framework provided by the NATO Science and Technology Organization (STO) Applied Vehicle Technology (AVT) panel, a number of contributors from industry and academia have proposed applications of active flow control technologies as flight control effectors, exploiting local flow injection, suction or oscillation to manipulate global aerodynamic flows around the air vehicle. Under appropriate conditions, the authority of these effectors is comparable to that of conventional control surfaces.

For these technologies to be considered feasible for incorporation into future air vehicles, though, it is necessary to look beyond their aerodynamic effectiveness and consider the wider challenges and opportunities in design and integration. Some of the challenges may be obvious: the flow effects which are being exploited need to be robust across a range of operating conditions; there must be means to manufacture

and install actuators at the appropriate scale; there must be means to generate the required energy (pressurised air) and to route it around the aircraft as required; accommodation of system degradation should be considered. For the candidate technologies within the scope of the present activity, this means that the impacts on integration with the engine and other vehicle systems, the mass and packaging of the system, and the overall range/payload performance of the aircraft must be justifiable in terms of the net benefit that is realised. This benefit might include improved maintainability and reliability through reduced part count, saving in weight, accommodation of unconventional configuration features or reduced numbers of outer mould line breaks and excrescences.

The NATO AVT-239 "Innovative Control Effectors for Manoeuvring Aircraft" Task Group was convened to develop a structured, multi-disciplinary trade study considering aspects of system effectiveness, design integration, impacts on reliability and maintainability, and maturity.

8.2.2 Control Performance Assessment and Sizing in the Context of the AVT-239 Study

In the context of this report, "performance assessment" tested the capability and efficiency of each active flow control system against a given mission requirement, by determining the energy (expressed as engine bleed air mass flow) necessary to provide the required control authority. In turn, this informed the size, weight and complexity of candidate systems and reflected across multiple aspects of the trade study. A process of Quality Function Deployment (QFD) unified the assessment strands. The relationships between contributing study tasks are depicted in Figure 8-1.

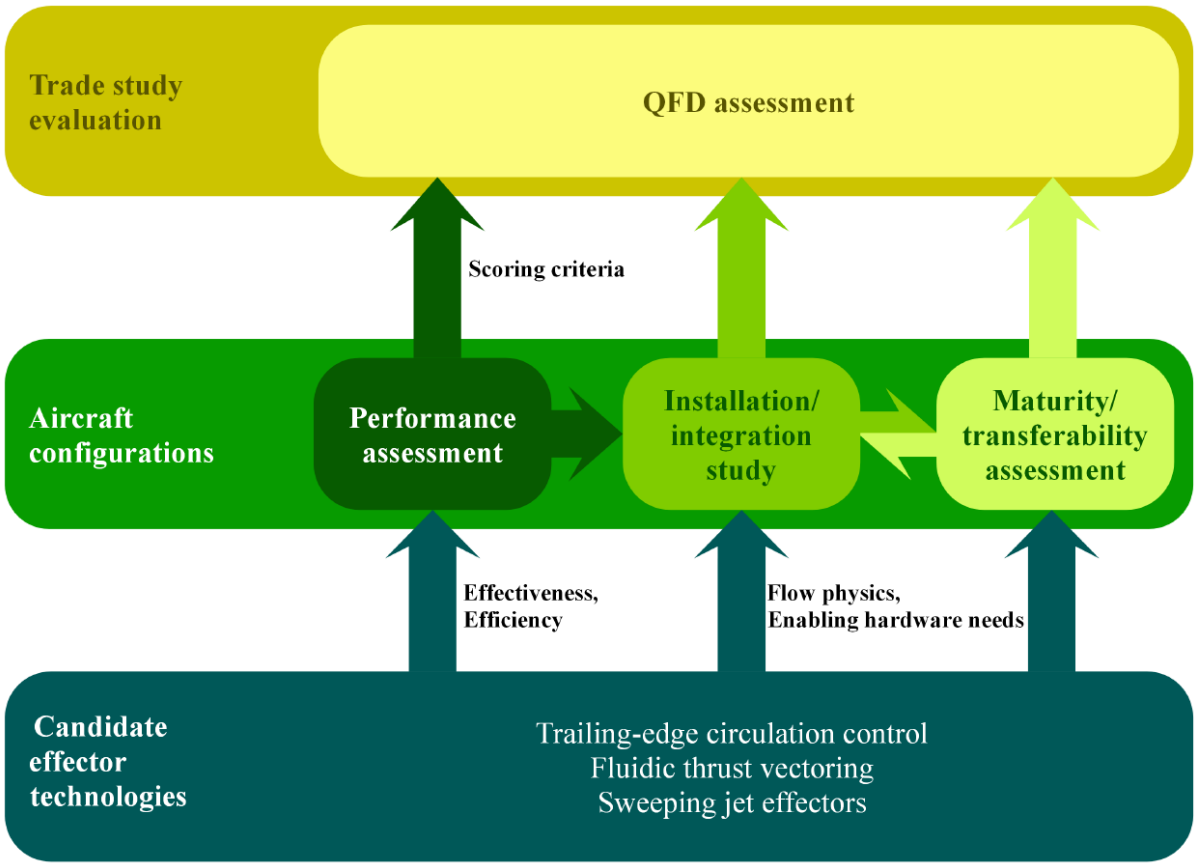

Figure 8-1: Contribution of Studies to AVT-239 Activity.

Within AVT-239, two strands of performance assessment activity were undertaken, considering different airframes and candidate effector technologies for application on those airframes. This chapter is concerned with application of trailing-edge circulation control, fluidic thrust vectoring, and a boundary layer control scheme utilizing sweeping jet actuators, to the "Stability and Control CONfiguration" (SACCON). A parallel activity, reported separately, assessed applications of leading-edge vortex control and trailing-edge circulation control on a tailless fighter configuration developed at Lockheed Martin – the "ICE" configuration previously reported by Dorsett [1].

The next section of the report describes the SACCON airframe and the candidate effector technologies. The methodology for performance assessment is then outlined in Section 8.5. Combination of effectors into aircraft configurations, and resulting performance scores are addressed in Section 8.6.

8.3 SACCON AIRFRAME AND CANDIDATE CONTROL EFFECTORS

8.3.1 Surrogate Airframe: "Stability and Control CONfiguration" or "SACCON"

SACCON is a tailless, lambda-wing configuration representative of a class of unmanned combat air vehicles (UCAVs) with constrained geometry for low observability. This configuration has been used within a number of NATO activities, both to validate aerodynamic predictive capability [3] and as a surrogate airframe in multi-disciplinary studies on design optimisation and technology integration [4]. Through these activities, a body of aerodynamic data for this configuration has been obtained experimentally at subsonic and transonic speeds.

The availability of the geometry and of datasets assembled from Computational Fluid Dynamics (CFD) and experiment has resulted in its adoption, by contributors to the AVT-239 activity, for demonstration of active flow control ideas.

8.3.2 Effector Technology: Active Flow Control Using Sweeping Jets

Jentzsch, Taubert and Wygnanski [5] have demonstrated at model scale the use of sweeping jet actuators – directing an oscillating flow across a wing area – for boundary layer control on the SACCON wing geometry. The results, obtained for a half-span model at approximately Mach 0.1, demonstrated that arrays of sweeping jet actuators could provide comparable pitch trim authority to conventional Trailing-Edge Flaps (TEFs) for this aircraft configuration, and discussed a range of possible applications. The model installation considered an array of 13 actuators spread along the parallel section of the wing, although experiment showed that similar effectiveness could be achieved with only subsets of these actuated.

The sweeping jet effector schemes carried forward into the AVT-239 performance assessment comprised three different modes of actuation: the full 13-actuator array operated concurrently; actuation of only 4 of these actuators located near the wing tip; and actuation of an alternative subset comprising 4 sweeping jet actuators distributed evenly along the wing. It was assumed that, subject to suitable piping, these three modes of actuation could all be realised by the same installation, but that the effects could not be combined by superposition.

8.3.3 Effector Technology: Trailing-Edge Circulation Control

Forster [6], at University of Liverpool, UK, conducted computational study and geometry optimisation to refine a scheme for Trailing-Edge Circulation Control (TECC). The resulting scheme included slotted jet nozzles on the upper and lower trailing edge, with a profiled Coanda surface located in between. High-speed blowing through either slotted nozzle entrained slower fluid from the surrounding freestream and turned it around the Coanda surface, providing a change in sectional lift. Effectiveness was limited by onset of flow separation as blowing rates are increased.

CFD data were supplied for simulations performed at wind-tunnel scale and Mach 0.7. Control moments for single-slot blowing were compared [6] to those generated by a conventional TEF at that same spanwise location. There was reasonable linearity of control power with blowing momentum coefficient, generating similar control power to a TEF deflected more than 10° before flow separation was predicted.

Additionally, a second mode of actuation was modelled where both the upper and lower surface slot jets were blown simultaneously at the same pressure ratio, giving rise to separated flow and providing a different characteristic: a yawing moment which weakly coupled into the pitch and roll axes.

8.3.4 Effector Technology: Fluidic Thrust Vectoring

Active flow control in engine exhausts is of interest (see Refs. [7], [8], [9]) as a potential enabler for use of fixed-geometry nozzles, with potential advantages in reduced system weight and mechanical complexity as well as signature control. As well as providing for the necessary variation in nozzle exit area, fluidics have been considered as means of providing thrust vectoring, which may be attractive in regimes where aerodynamic control effectiveness is limited by low dynamic pressure or gross flow disturbance.

University of Manchester, UK, contributed abstracted data for a pitch-axis Fluidic Thrust Vectoring (FTV) concept to the AVT-239 Task Group. In this case the control power that could be achieved was directly related to the current engine gross thrust, and the secondary mass flow requirement for FTV was proportional to the vector angle and primary jet momentum. A maximum of 15° upward or downward vector angle could be achieved, requiring secondary mass flow of 1.7% the primary jet mass flow. The authority and the efficiency of the FTV were therefore more directly dependent on the engine characteristic and trim condition than was the case for the other effectors. A generic engine model, used in foregoing NATO collaboration with similar vehicle configuration and size, was selected for the purposes of the AVT-239 study.

8.4 ASSESSMENT METHOD

Evaluation of control capability (and of associated mass flow rate “cost”) was applied as a two-step process. In the first step, a requirements model was constructed, and exercised to determine control power necessary for disturbance rejection. Reconciliation of these demands with the control power available was undertaken as a subsequent activity. This decoupled approach was employed as it generalised easily to effector models with different structures and dependencies, which could be addressed without modification of the requirements model. It also allowed for alternative control allocation algorithms to be quickly implemented and evaluated. This was particularly relevant since the configurations studied comprised different numbers of effectors and since control allocation had an important secondary objective (minimisation of mass flow demands) in addition to obtaining the demanded control moment. Importantly, this approach allowed for a straightforward treatment of those effectors which had multiple, distinct, modes of actuation (as for TECC and sweeping jet effectors, described earlier).

8.4.1 Requirements Model

The requirements model was implemented as a time-domain simulation, combining models of the basic airframe, atmospheric disturbance environment and a prototyping control law to achieve desired dynamics. The intent was to determine the forces and moments required of a set of effectors, without requiring detailed models of these effectors or control allocation schemes to be included in the simulation. Figure 8-2, illustrates the approach taken.

Overall vehicle size and associated mass properties (see Table 8-1) were derived from work published by Liersch [10].

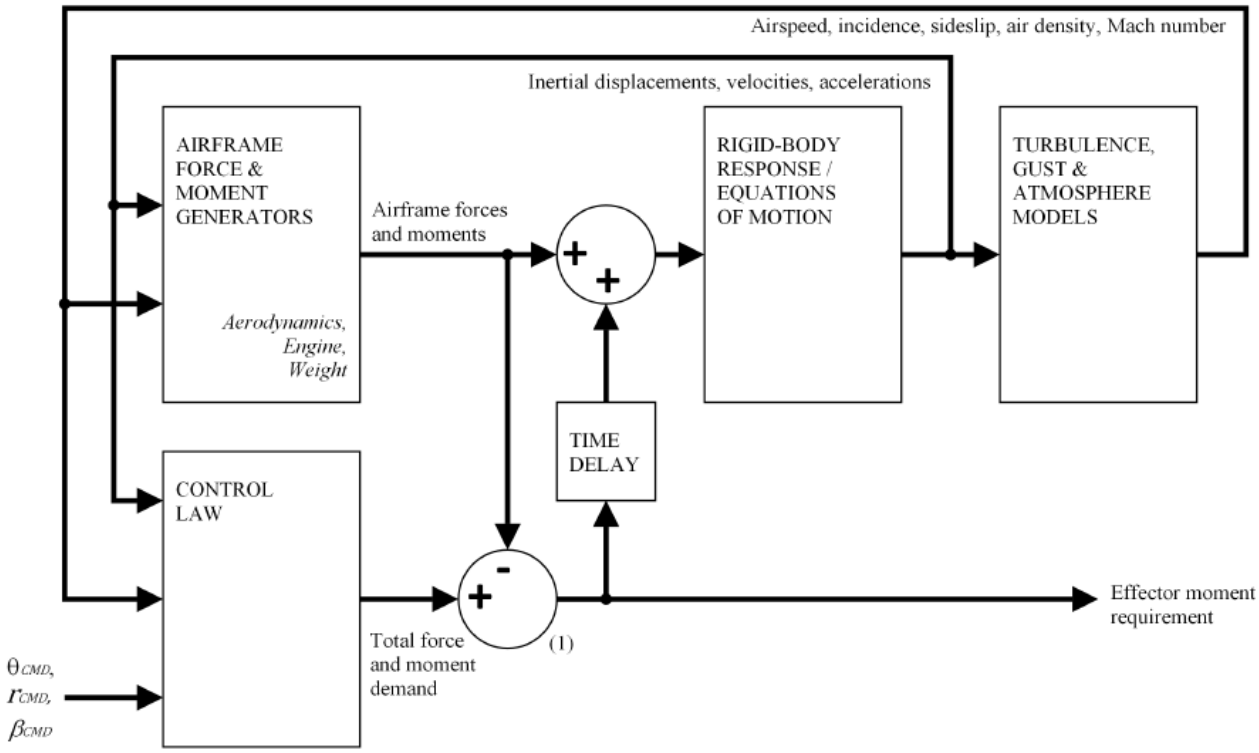

Figure 8-2: Structure of Control Moment Requirements Model.

Table 8-1: Aircraft Parameters at Evaluation Conditions.

Parameter	At 90% Fuel Load	At 60% Fuel Load
Span	15.36 m	
Reference chord	4.79 m	
Reference area	77 m^2	
Mass	13.7 t	12.1 t
Longitudinal CG	5.57 m	5.57 m
Moment reference point	6.0 m	
I_{xx}	8.79 x 10^4 kg.m^2	7.12 x 10^4 kg.m^2
I_{yy}	3.07 x 10^4 kg.m^2	2.49 x 10^4 kg.m^2
I_{zz}	1.19 x 10^5 kg.m^2	9.61 x 10^4 kg.m^2

Foregoing work described by Irving [11] combined experimental data into a Simulink®[1] model representing the build-up of aerodynamic force and moment coefficients on the air vehicle. This was incorporated within the "Airframe Force and Moment Generators" subsystem, along with the effects of weight and engine thrust. Whilst these datasets provided for terms due to TEF deflections, for the purposes of the present study these flap deflections were all hard-coded to zero. Engine thrust, acting through the aircraft centreline, was fixed at a nominal trimmed condition.

[1] Simulink is a registered trademark of The Mathworks, Inc., Natick, Massachusetts, USA.

The outputs from the "Airframe Force and Moment Generators" subsystem were the forces and moments generated by the airframe and propulsion at a specified aerodynamic condition. This condition was described in terms of airspeed, incidence and sideslip angles, and angular rates. Euler angles and angular rates were obtained from solution of the equations of motion, with additional airspeed terms where discrete gusts or random turbulence inputs were specified.

The "Control Law" subsystem took as inputs a set of demanded motions (pitch attitude, roll rate and sideslip angle were selected for the purposes of demonstration) and the rates and accelerations computed by the "Rigid-Body Response" subsystem. Its outputs were the required total moments about the aircraft moment reference point, in order to provide assigned dynamics, specified by roll, pitch and yaw bandwidths.

The use of direct feedbacks of accelerations, velocities and displacements into the control law represented a simplified, idealised situation without sensor dynamics or noise. Further, the structure described in Figure 8-2, with airframe loads provided into the summing junction at (1) effectively provided an on-board model perfectly representing the vehicle behaviour.

Whilst the requirements model did not represent a practical control application on a flight vehicle, it fulfilled its purpose within the context of the study, determining control moment requirements on the assumption that these were achievable without effector saturation. The next step of the evaluation process – control allocation – was intended to test the validity of this assumption.

8.4.2 Assessment Flight Conditions

As introduced earlier at Figure 8-1, the performance assessment studies fulfilled two, related, roles in the context of the overall AVT-239 effort. The first of these was to determine whether the candidate effectors possessed sufficient authority to achieve the defined set of performance objectives, and to identify the corresponding mass flow requirements. The second objective was to provide suitable data to size elements of a potential installation. As a result, partners within AVT-239 were able to assess the mass and volume impacts of incorporating fluidic actuation systems into an airframe, as well as resulting effects on reliability and maintainability. Integration assessments addressing these attributes are reported separately, by other AVT-239 contributors.

The activity was initially planned to assess the potential for air vehicle manoeuvrability without employment of conventional control surfaces. This aim was not fully realised. Assessment activity instead centred on a spot point in the flight envelope – an ingress condition at moderately high altitude and transonic speed – substituting use of fluidic effectors in place of TEFs for trim and disturbance rejection. Dubbed "Mission One", this might be considered to be a "screening" condition, with the expectation that resulting control requirements should be less demanding than for gross manoeuvre or terminal flight phases and should therefore be achievable by smaller, lighter installations. Additionally, this emphasis placed a less onerous requirement for development of effector aerodynamic data at high angles of attack or with significant body rates applied.

During the course of the study, it was apparent that the pitching-moment-to-trim inherent in the aerodynamic dataset could be a dominant influence on the effector demands, particularly in the case of the sweeping jet effector configuration. For the "Mission One" evaluation conditions, the study team agreed that the pitching moment characteristics for SACCON could be re-baselined to trim without use of active flow control at 30,000 ft, Mach 0.8 and 90% fuel load. In a practical sense, this might be achieved by scheduling some other kind of trim surface in a manner consistent with the mission goals.

Performance criteria directly attracting scoring within the AVT-239 QFD process were agreed with the AVT-239 technical team, and were defined as in Table 8-2.

Table 8-2: Scoring Criteria Used Within AVT-239 Performance Assessment Task.

Condition	Measure	Unit	Intent to	Score 9	Score 3	Score 1
Reject light turbulence	Peak flow	lb/s	Minimise	$\dot{m}_{pk} < 3$	$3 < \dot{m}_{pk} < 6$	$\dot{m}_{pk} > 6$
Reject light gust	Peak flow	lb/s	Minimise	$\dot{m}_{pk} < 3$	$3 < \dot{m}_{pk} < 6$	$\dot{m}_{pk} > 6$
Reject moderate gust	Peak flow	lb/s	Minimise	$\dot{m}_{pk} < 3$	$3 < \dot{m}_{pk} < 6$	$\dot{m}_{pk} > 6$
Reject light turbulence + moderate gust 1% of mission	Mean flow + 2 standard deviations	lb/s	Minimise	$\dot{m}_{2\sigma} < 3$	$3 < \dot{m}_{2\sigma} < 6$	$\dot{m}_{2\sigma} > 6$
Accommodate re-trim due to fuel burn	Flow to re-trim from 90 – 60% fuel weight	lb/s	Minimise	$\dot{m} < 3$	$3 < \dot{m} < 6$	$\dot{m} > 6$

Light turbulence conditions were specified according to the Dryden form stated in MIL-HDBK-1797 [12], at the required 30,000ft altitude condition. For these cases, multiple simulations were aggregated with the random seed varied, and statistical measures extracted.

Double-sided discrete gusts were applied simultaneously in multiple axes with “Light” and “Moderate” amplitudes scaled according to altitude and gust length as directed by MIL-HDBK-1797. Parametric study determined the most critical gust lengths and directions for application.

In all cases, the figure of merit chosen is the mass flow rate of pressurised air through the system of fluidic effectors, and the intent is that this should be minimised. Threshold values of 3 lb/s and 6 lb/s system mass flow rate were selected within the study group, as indicative of engine / bleed air off-take availability at this flight condition

8.4.3 Control Allocation

The outputs of the requirement modelling activity described earlier were time histories of control moment about three axes. Having developed these time histories, a process of optimal control allocation was applied to identify effector commands that provided these control moments whilst minimising consumption of pressurised air across the system.

Control allocation was therefore posed as a constrained, weighted least squares problem to compute a framewise increment $\Delta\underline{u}$ in control demand $\underline{u}$:

$$\min \left\| [P].\Delta\underline{u} - \underline{q} \right\|^2, \underline{u}_{min} - \underline{u} \leq \Delta\underline{u} \leq \underline{u}_{max} - \underline{u} \tag{8-1}$$

with:

$$[P] = \begin{bmatrix} W_{mom}\frac{\partial C_l}{\partial u_1} & W_{mom}\frac{\partial C_l}{\partial u_2} & \cdots & W_{mom}\frac{\partial C_l}{\partial u_n} \\ W_{mom}\frac{\partial C_m}{\partial u_1} & W_{mom}\frac{\partial C_m}{\partial u_2} & \cdots & W_{mom}\frac{\partial C_m}{\partial u_n} \\ W_{mom}\frac{\partial C_n}{\partial u_1} & W_{mom}\frac{\partial C_n}{\partial u_2} & \cdots & W_{mom}\frac{\partial C_n}{\partial u_n} \\ W_{\dot{m}}\frac{\partial \dot{m}}{\partial u_1} & W_{\dot{m}}\frac{\partial \dot{m}}{\partial u_2} & \cdots & W_{\dot{m}}\frac{\partial \dot{m}}{\partial u_n} \\ \frac{\partial \dot{m}}{\partial u_1} & 0 & \cdots & 0 \\ 0 & \frac{\partial \dot{m}}{\partial u_2} & \cdots & 0 \\ 0 & \vdots & \ddots & 0 \\ 0 & 0 & 0 & \frac{\partial \dot{m}}{\partial u_n} \end{bmatrix}, \underline{q} = \begin{pmatrix} W_{mom}\Delta C_{l,req} \\ W_{mom}\Delta C_{m,req} \\ W_{mom}\Delta C_{n,req} \\ W_{\dot{m}}\,\dot{m} \\ \frac{\partial \dot{m}}{\partial u_1}.u_1 \\ \frac{\partial \dot{m}}{\partial u_2}.u_2 \\ \vdots \\ \frac{\partial \dot{m}}{\partial u_n}.u_n \end{pmatrix} \quad (8\text{-}2)$$

The fixed weights $W(\cdot)$ in $[P]$ and $\underline{q}$ were chosen to prioritise minimisation of moment errors, and were fixed throughout the simulation. The partial derivatives of mass flow rate with respect to each control input were computed at each solution time step, to prioritise use of the most efficient effectors.

As discussed earlier, there were multiple modes of actuation for the trailing-edge circulation control and for the sweeping jet effectors. For the purposes of this study, these multiple modes were treated separately and so generated a number of distinct solutions of varying acceptability (tracking accuracy) and efficiency. Post-processing discarded solutions which did not track demand within a prescribed tolerance band. The most efficient (minimum mass flow rate) solution achieving acceptable tracking of the control moment demand at each time step was retained.

8.5 ASSESSMENT RESULTS

8.5.1 Twin TECC Installations on Outboard Wing Sections

The effectiveness data supplied by Forster were extrapolated, using ratios of lever arms about the moment reference point, in order to represent wing installations with two trailing-edge circulation control effectors on the outboard section of each wing (Figure 8-3).

As expected, control allocation preferred usage of the furthest-outboard effectors, which were more effective in all axes due to the longer moment arms (Table 8-3). This was clearly apparent for trim and symmetric disturbances, but generalised throughout the range of simulations performed. Capability to effect bi-directional control by blowing through the upper or lower slots appears useful, allowing all four wing effectors to be used simultaneous irrespective of the direction of roll or yaw. In this configuration, the redundant installation provides the opportunity for optimal allocation to actively minimise the system mass flow rates. Overall mass flow requirements were well within the 3lb/s high-scoring band for all performance criteria.

The twin-slot blowing mode, which was proposed as a possible yaw control, was used a small proportion of the time in rejecting the turbulence and gust inputs, where its relatively weak coupling to pitch and roll moments appears to have been useful; generally it was the case that the redundant combination of four effectors each using the upper or lower slot exclusively provided sufficient authority to track the moment demand within the prescribed tolerance in all axes.

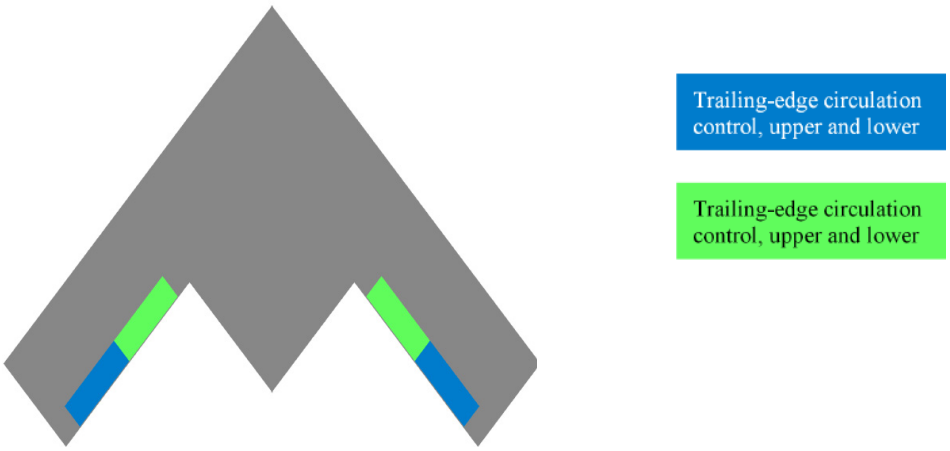

Figure 8-3: Schematic View of Trailing-Edge Circulation Control Configuration.

Table 8-3: Performance Assessment Scores for Configuration with TECC.

Condition	Measure	Unit	Intent to	Measured Result	Performance Score
Reject light turbulence	Peak flow	lb/s	Minimise	1.41	9
Reject light gust	Peak flow	lb/s	Minimise	1.55	9
Reject moderate gust	Peak flow	lb/s	Minimise	1.90	9
Reject light turbulence + moderate gust 1% of mission	Mean flow + 2 * standard deviations	lb/s	Minimise	0.90	9
Accommodate re-trim due to fuel burn	Flow to re-trim from 90 – 60% fuel weight	lb/s	Minimise	0.09	9

8.5.2 TECC Installations on Inboard and Outboard Wing Combined with Pitch-Axis FTV

Results for the configuration with combined CC and pitch-axis FTV (Figure 8-4) are presented in. Table 8-4 Comparison of Table 8-4 and Table 8-3 indicates that the addition of pitch-axis fluidic thrust vectoring to the effector set does not provide significant value in these assessment cases. This may be understood by realising that the lateral and directional moments were significant drivers of demand to the trailing-edge circulation control actuators and could not be affected by the thrust vectoring scheme considered.

The swept, edge-aligned wing planform of the SACCON configuration afforded fairly long moment arms about the aircraft pitch axis for the trailing-edge circulation control effectors. By comparison, the aft displacement of the engine nozzle from the centre of gravity was small. This geometric effect directly, and adversely, influences both the authority (moment coefficient at limit of vectoring effect) and efficiency (pitching moment per unit mass flow input) of the pitch-axis FTV on SACCON.

Moreover, the CFD data for the TECC effectors indicated that these were more efficient at higher mass flow rates. Through combination of these factors, at the ingress condition selected for the AVT-239 study there was only a very limited range of pitching moments where use of fluidic thrust vectoring would be preferential to trailing-edge circulation control.

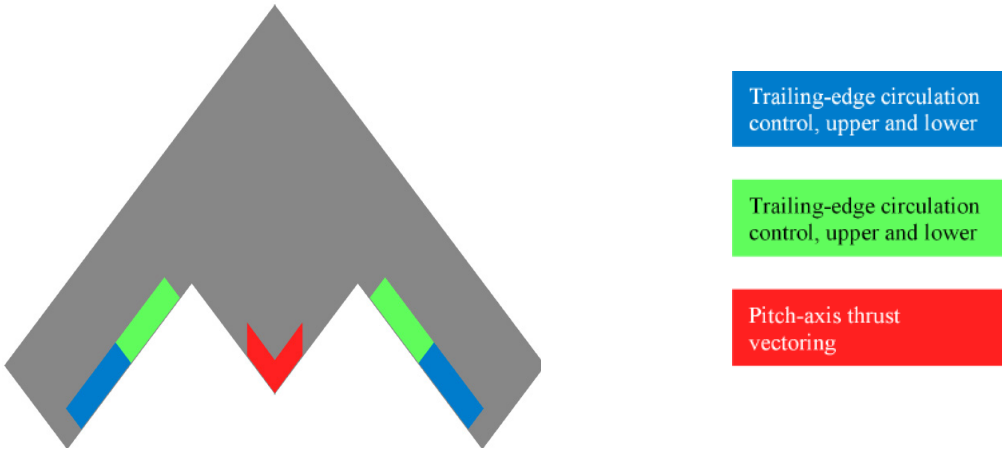

Figure 8-4: Schematic View of Trailing-Edge Circulation Control and Pitch-Axis Thrust Vectoring Configuration.

Table 8-4: Performance Assessment Scores for Configuration with TECC, Pitch-Axis FTV.

Condition	Measure	Unit	Intent to	Measured Result	Performance Score
Reject light turbulence	Peak flow	lb/s	Minimise	1.44	9
Reject light gust	Peak flow	lb/s	Minimise	1.55	9
Reject moderate gust	Peak flow	lb/s	Minimise	1.88	9
Reject light turbulence + moderate gust 1% of mission	Mean flow + 2 * standard deviations	lb/s	Minimise	1.29	9
Accommodate re-trim due to fuel burn	Flow to re-trim from 90 – 60% fuel weight	lb/s	Minimise	0.09	9

8.5.3 Sweeping Jet Arrays on Outboard Wing Section Combined with Pitch-Axis FTV

A study configuration (Figure 8-5) was evaluated employing one sweeping jet effector on each wing. This configuration reflected in part the model configuration of University of Arizona, where an array of sweeping jet actuators was addressed to the whole constant-chord section of the wing. Addition of FTV provided the minimum number of effectors for resolving moment demands about three axes, but no redundancy.

It is not clear that the use cases and configuration chosen for this phase of AVT-239 study were the most suitable application of the sweeping jet effectors. On the one hand, comparison of the moment coefficients achievable from a single sweeping jet effector shows authority in roll and pitch of comparable magnitude to that obtained from a single trailing-edge circulation control effector. In yaw, the sweeping jet effector may have higher authority. However, when the dimensional mass flows required to achieve these control moments were computed at the Mach 0.8 study condition, they were orders of magnitude higher than for the TECC installations (Table 8-5). It is acknowledged also that these study conditions are far from those (relatively low-speed) conditions at which experimental effectiveness data were obtained.

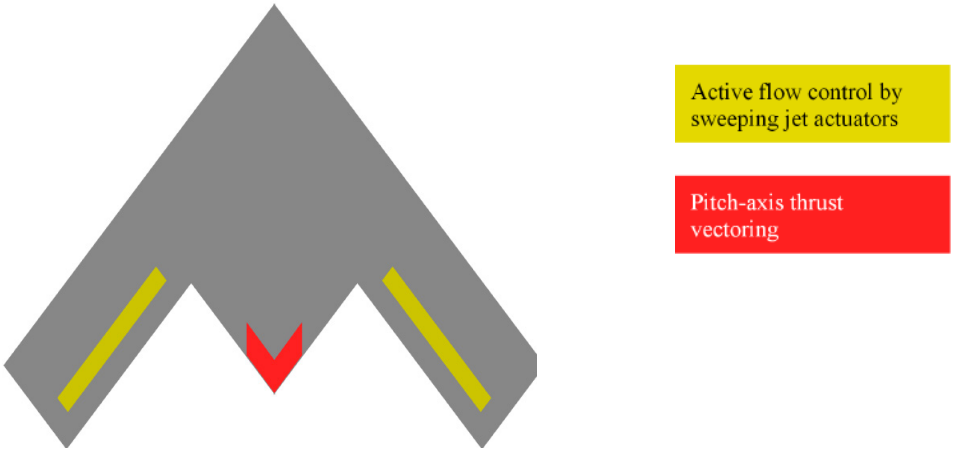

Figure 8-5: Schematic View of Sweeping Jet Effector and Pitch-Axis Thrust Vectoring Installation.

Table 8-5: Performance Assessment Scores for Configuration with Sweeping Jet Effectors, Pitch-Axis FTV.

Condition	Measure	Unit	Intent to	Measured Result	Performance Score
Reject light turbulence	Peak flow	lb/s	Minimise	5.93	3
Reject light gust	Peak flow	lb/s	Minimise	13.18	1
Reject moderate gust	Peak flow	lb/s	Minimise	18.55	1
Reject light turbulence + moderate gust 1% of mission	Mean flow + 2 * standard deviations	lb/s	Minimise	5.25	3
Accommodate re-trim due to fuel burn	Flow to re-trim from 90 – 60% fuel weight	lb/s	Minimise	0.11	9

The experimental data obtained for the sweeping jet effectors showed capability to generate nose-down pitching moment only. As highlighted in Section 8.4.2, the basic airframe aerodynamic data compiled in the requirements model tended to result in nose-down pitching moment at the trim conditions selected for the AVT-239 “Mission One” study, but achieving this with sweeping jet effectors required excessive mass flow rates. The TECC effectors discussed above were much less sensitive to this, being generally more efficient.

In the case of the sweeping jet effectors, re-baselining the airframe pitching moment characteristic provided only partial mitigation. The sweeping jets’ effect on the wing tip flows results in strong roll-pitch-yaw coupling (Figure 8-6). Therefore, gust and turbulence cases always required another effector with nose-up pitching moment capability to compensate; pitch-axis thrust vectoring in this case, at the cost of further mass flow. This may be a significant result in application of active flow control to a wider range of missions and flight conditions, implying a trade-off between required flow rates in different flight phases.

In the case of re-trimming due to fuel burn (90% fuel load to 60% fuel load), control allocation used the pitch-axis fluidic thrust vectoring only.

The results obtained for this sweeping jet-effected configuration, therefore, may highlight a number of key points. It is important that discussion differentiates properly between effector technology, effector installation and overall configuration.

The premise of this type of active flow control is to influence gross flow features by providing small, targeted flow injection. The results already published in Ref. [5] demonstrated the possibility to optimise the installation of sweeping jet actuators to provide greater efficiency (in that case, 4 suitably-situated actuators could generate comparable effect to 13 actuators, for less effort). However, where the flow control mechanisms are optimised around specific flow features, there is inherently larger uncertainty in extrapolating effectiveness. This may be the case in applying cost and effectiveness data obtained for sweeping jet effectors at low Mach number to the transonic condition proposed by the study.

Incorporation of control effectors into complimentary or redundant configurations provides greater opportunity for control allocation to affect a secondary characteristic or cost function. This is not purely down to increasing overall moment capability in any one axis – there were few instances where saturation of the wing effectors affected the solution, and in fact the characteristics of both the sweeping jet effectors and trailing-edge circulation control effectors show increasing efficiency at higher mass throughput (corresponding to higher nozzle velocities). In the case of the sweeping jet effector configuration studied, the most efficient solutions for turbulence and gust rejection regularly employed different modes of actuation on the port and starboard wings to exploit the differences in roll-yaw coupling.

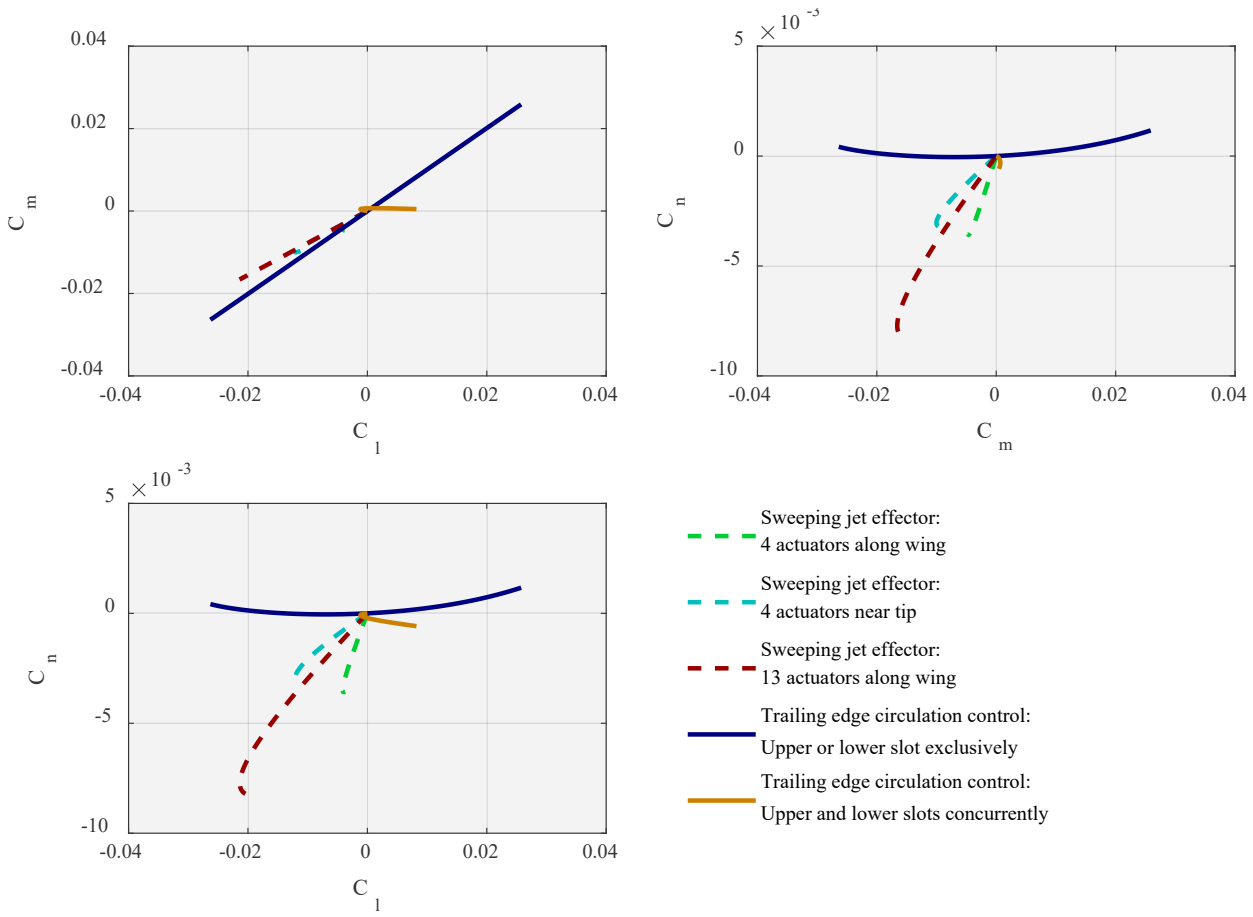

Figure 8-6: Illustration of Control Moment Coupling for Candidate Control Effectors.

8.6 CONCLUSIONS

This task contributed to the technology assessment proposed by NATO AVT-239, and in particular demonstrated the role of a performance assessment phase to reconcile predictions of aerodynamic effectiveness and more detailed integration studies.

A methodology for system sizing was applied to assess combinations of candidate aerodynamic technologies. Key outputs were quantified requirements for pressurised air through different elements of the fluidic control systems, which data were used elsewhere within the AVT-239 technical team to determine size and weight of installations and to assess impacts associated with taking this pressurised air as bleed from the aircraft engine.

The focus of the activity reported in this chapter has been to assess whole-aircraft configurations of control effectors, in order to address issues of integration. It is important therefore that the lessons learned are properly attributed to characteristics of the effector installations and constituent actuation technologies or to the constraints imposed by the overall configuration.

Although limited, the performance assessments have indicated some of the potential trades that designers may have to consider if the benefits of active flow control technologies appear attractive. Whilst focused on particular aircraft configurations and a small range of evaluation conditions, the results demonstrated that the effectiveness and efficiency of active flow controls as flight control effectors could be particularly sensitive to the concept of system employment, the flight condition, control redundancy and the behaviours of the un-effected airframe.

8.7 REFERENCES

[1] Dorsett, K.M., and Mehl, D.R., Innovative Control Effectors (ICE), Wright Laboratory, Rept. WL-TR-96-3043, Wright-Patterson Air Force Base, OH, Jan 1996.

[2] Engelbeck, R.M., Investigation into the Impact of Agility in Conceptual Fighter Design, NASA Contractor Report 195079, Boeing Defense and Space Group, Seattle, WA, Jun 1995.

[3] Cummings, R.M., and Schűtte, A., An Integrated Computational/Experimental Approach to UCAV Stability and Control Estimation: Overview of NATO RTO AVT-161, Applied Aerodynamics; 28th; 28 Jun -1 Jul. 2010, AIAA Paper 2010-4392.

[4] Cummings, R.M., and Schűtte, A., The NATO STO Task Group AVT-201 on 'Extended Assessment of Stability and Control Prediction Methods for NATO Air Vehicles', Applied Aerodynamics; 32nd; 16-20 Jun. 2014, AIAA Paper 2014-2000.

[5] Jentzsch, M.P., Taubert, L., and Wygnanski, I.J., On the Use of Sweeping Jets to Trim and Control a Tailless Aircraft Model, Applied Aerodynamics; 35th; 5-9 Jun. 2017, AIAA Paper 2017-3042.

[6] Forster, M, and Stejil, R., Circulation Control for High-Speed Unmanned Combat Air Vehicles, RAeS Applied Aerodynamics Conference, Bristol, UK, 2016.

[7] Deere, K.A., Summary of Fluidic Thrust Vectoring Research Conducted at NASA Langley Research Center, Applied Aerodynamics; 21st; 23-26 Jun. 2003, AIAA Paper 2003-3800.

[8] Crowther, W.J., Towards Integrated Design of Fluidic Flight Controls for a Flapless Aircraft, *The Aeronautical Journal,* Vol. 113, No. 1149, 2009, pp. 699-713.

[9] Miller, D.N., and Flamm, J.D., Air-breathing Propulsion Flowpath Applications, *Fundamentals and Applications of Modern Flow Control*, edited by R. Joslin and D.N. Miller, Progress in Astronautics and Aeronautics Volume 231, AIAA, Reston, 2009.

[10] Liersch, C.M., Huber, K.C., Schütte, A., Zimper, D., and Siggel, M., Multidisciplinary Design and Aerodynamic Assessment of an Agile and Highly Swept Aircraft Configuration, *CEAS Aeronautical Journal,* Sept. 2016.

[11] Irving, J.P., Vicroy, D.D, Farcy, D., and Rizzi, A., Development of an Aerodynamic Simulation Model of a Generic Configuration for S&C Analyses, Applied Aerodynamics; 32nd; 16-20 Jun. 2014, AIAA Paper 2014-2393.

[12] Flying Qualities of Piloted Aircraft, MIL-HDBK-1797, US Department of Defense, Dec 1997.

Chapter 9 – ASSESSMENT OF PROSPECTS OF AFC ON A NEXT-GENERATION TAILLESS AIRCRAFT

Daniel N. Miller, Brant H. Maines, and Michael A. Niestroy
Norwegian Defence Research Establishment (FFI)
NORWAY

David R Williams
Illinois Institute of Technology
UNITED STATES

Clyde Warsop
BAE Systems
UNITED KINGDOM

Douglas R Smith
United States Air Force (USAF)
UNITED STATES

9.1 OVERVIEW

Results of a trade study are presented to evaluate modern flow control technology integrated on a representative future military tailless aircraft configuration. A North Atlantic Treaty Organization technical task group was commissioned to investigate the feasibility of active flow control for providing disturbance rejection during ingress/egress flight conditions. A design of experiments trade study approach is employed to assess the feasibility of integrating a suite of active flow control technologies for this application relative to a conventional mechanical flap-based control suite. The trade study employs four categorical metric groups including:

1) Flight control performance;
2) Aircraft integration;
3) Technology "ilities" including reliability, maintainability, scalability, and affordability; and
4) Technology maturity.

The overall process of the trade study approach is discussed including supporting engineering modeling and simulation, conceptual design, and analyses. AFC is found to be feasible and reasonable for incorporation on the ICE platform for providing control power needs during ingress/egress.

9.2 INTRODUCTION AND BACKGROUND

Next generation military Unmanned Aerial System (UAS) aircraft will confront an increasingly contested and more sophisticated threat environment. UAS aircraft will require an unprecedented level of flight performance while simultaneously becoming more affordable. To meet these future challenges, the North Atlantic Treaty Organization (NATO) launched an Applied Vehicle Technology (AVT) technical task group AVT-239 to evaluate and flight test scaled versions of conceptual next generation UAS platforms. These platforms will be equipped with modern Active Flow Control (AFC) technologies that might eliminate the need for complex, moving flight control surfaces which constrain current UAS performance. The goals for the AFC technologies under investigation are to enable reduced weight, size, complexity and cost, with increased availability and agility during enhanced, evasive tactics.

The task group identified two candidate conceptual aircraft platforms to conduct this study – (1) The innovative control effector (a.k.a. ICE) [1], [2] and the stability and control (a.k.a. SACCON) [3] configurations, both shown in Figure 9-1. The scope of this chapter is confined to the trade study conducted on the ICE platform. The ICE aircraft is an all-wing, tailless configuration that can be manned or unmanned. The aircraft with the baseline conventional control effectors indicated, evolved from 1991 Internal Research And Development (IRAD) studies at Lockheed Martin Aeronautics and was subsequently studied in depth under AFRL sponsorship [1], [2].

9.3 NATO AVT-239 TASK GROUP OVERVIEW

New control effector strategies are desired for future UAS configurations. Approaches that minimize 'seams', 'gaps' or moving surfaces have been studied in the past and continue to evolve toward ever improving efficiency and ease of integration. The need to be seamless invokes a very critical characteristic – in general because control power for any one control effector is limited, a suite of control effectors are required to provide all-envelope control of a vehicle. This is true even for a vehicle that only requires mild maneuvering. Control effectors for take-off and landing requirements have particularly difficult integration issues. There are many approaches that involve seamless geometry movement including morphing leading and trailing edges, morphable wings and wing tips, and continuous mould line technology. [4].

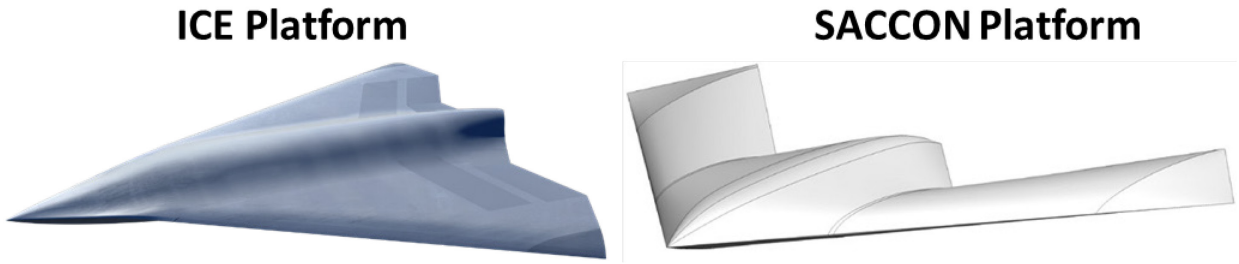

Figure 9-1: ICE and SACCON Tailless Platforms Selected for Investigation.

Likewise, there are many AFC approaches to create 'virtual geometry changes' that involve blowing or suction to increase the effectiveness of (or even replace) conventional aerodynamic control surfaces. Successfully implemented AFC technologies have the potential to revolutionize the performance and maneuver characteristics of modern air and maritime platforms. Flow control technologies have a wide range of uses from separation control for improving high alpha performance, to lift augmentation and full 3-axis flight control. However, to date, implementation on production platforms has been limited, often due to the complexity, power requirements and impact on cruise performance [5]. A STO workshop (May 2013, AVT-215, Novel Control Effectors for Military Vehicles) explored innovative control effector technologies including AFC techniques for providing control power. The conclusion of the workshop was that the application of novel AFC technologies to the maneuvering of a future UAS offers the most promising route to raising the Technology Readiness Level (TRL) sufficiently to allow exploitation onto future NATO UAS platforms. The AVT-215 workshop set the stage for the AVT-239 working group study.

NATO AVT-239 was launched to investigate AFC technologies to provide flight control power for next-gen tailless UAS platforms. The AFC technology feasibility would be assessed by assessing their feasibility against platform integration criteria. The goal is to minimize reliance on conventional control surfaces during select portions of the UAS mission profile. Three flight regimes of interest include mission ingress/egress, maneuver, and take-off/landing. For the Phase I of the NATO study, the scope was confined to an ingress/egress mission profile, with tentative plans to address the other two regimes in a subsequent Phase. To accomplish this objective, the AVT-239 task group was organized into three sub-groups that to focus on principal topic areas and collaborate together including:

1) Flow Control Technology;
2) Vehicle Performance; and
3) Trade Study/Requirements (Figure 9-2).

Initial UAS platform requirements were defined by sub-group #3. These requirements were used to direct computational and experimental research being conducted by group #1. The requirements and data resulting from these tasks were used in a flight control simulation under sub-group #2 to conduct vehicle performance

assessments. Details on the AVT-239 organization are provided in a companion paper [6]. This chapter addresses the trade study approach conducted under sub-group #3.

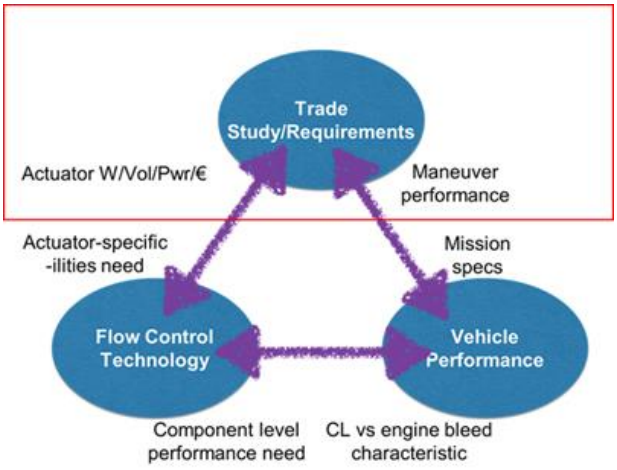

Figure 9-2: NATO AVT-239 Task Group Organization.

9.4 TRADE STUDY APPROACH OVERVIEW

9.4.1 Overview

The objective of the trade study is to assess the feasibility of AFC technology for future tailless UAS platforms. Consistent with the scope for this Phase I trade study, the scope is confined to implementation of an AFC suite on the ICE platform to manage turbulence and gust disturbance rejection and to trim the aircraft for a representative ingress/egress mission. As such, the goal is to provide sufficient control power for this regime at an acceptable 'opportunity cost'. Flight conditions are defined as 30Kft altitude and Mach 0.9 speed for a one hour ingress/egress flight duration.

As a basis for evaluating an integrated AFC system, a basic layout and internal arrangement of the ICE platform was updated for this effort. While integration of an AFC system onto a vehicle during the conceptual design phase allows the most flexibility in the arrangement, it is important to understand at a high level how the AFC system must integrate with the other interfaces and subsystems on the aircraft. Figure 9-3 highlights the basic arrangement of the conventional and AFC effector flight control suites for the baseline ICE configuration. The conventional hinged control effector suite includes pitch flaps, elevons leading-edge flaps and a spoiler slot deflector.

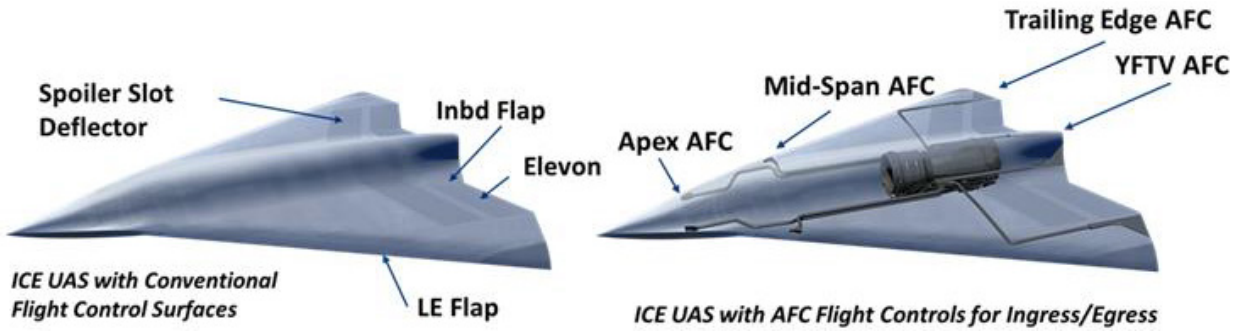

Figure 9-3: ICE with Conventional Control Suite (Left) and AFC Flow Control Suite (Right).

The AFC effector suite includes a bilaterally symmetric installation of control effectors positioned at four principal locations on the aircraft:

1) Leading-Edge (LE) apex;
2) LE mid-span;
3) Trailing-Edge (TE) outboard; and
4) Nozzle wall using Yaw-plane Fluidic Thrust Vectoring (YFTV).

The AFC effector suite is distributed to provide multiple options for control power in aircraft pitch, roll, and yaw axes. Each AFC effector is supplied with bleed air extracted from the inter-stage port of a representative modern military turbofan engine. The bleed air is transported to each AFC location via a valve and duct assembly.

The AFC effector suite uses an array of surface-integrated slot-jets at each of the four locations, as shown in Figure 9-4. The AFC suite injects high-pressure air that interacts with the boundary or shear layer to modify the local pressure distribution on the aircraft and therefore provide control power. The YFTV AFC creates a virtual aero-surface on the internal nozzle wall that emulates the function of a moving mechanical flap, but with no hinges or variable geometry [7]. The TE AFC modifies the local airfoil circulation and pressure distribution using a tangential wall-jet [8]. The LE Apex and Mid-Span AFC also modify the local lift distribution along the airfoil [9].

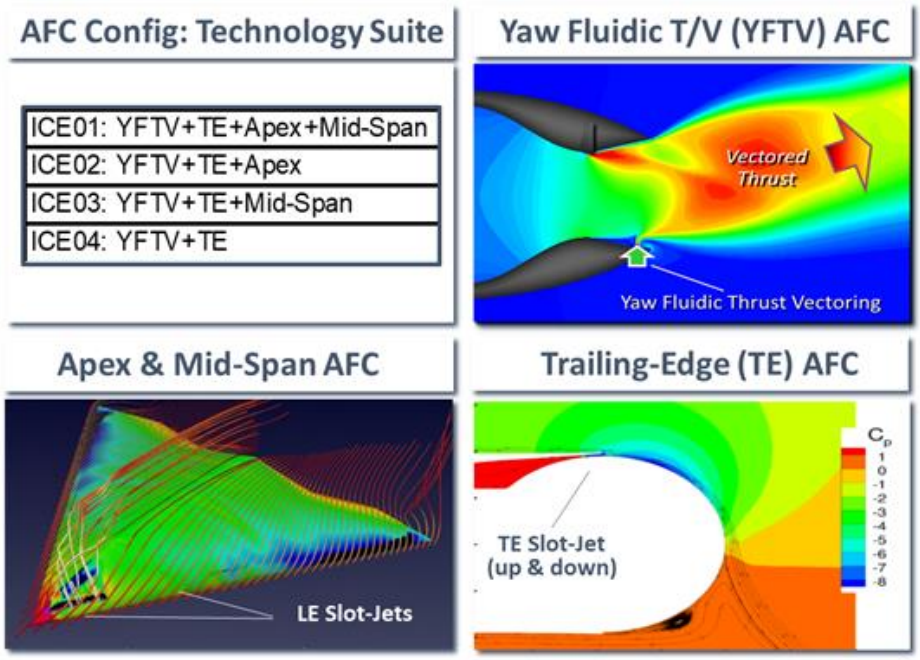

Figure 9-4: ICE AFC Technology Suite and Configurations ICE01-04.

9.4.2 Trade Study Matrix

A relatively simple 'house of quality' or Quality Function Deployment (QFD) experimental design [10] matrix was developed to conduct the trade study, as shown in Figure 9-5. Architecturally, the trade matrix features 4 configuration combinations (dubbed ICE01-04) of the AFC effector suite evaluated on the ICE platform, shown Figure 9-4. The AFC configurations employ the entire suite in ICE01 (forward and rear) and sequentially remove AFC effectors/locations until ICE04 (rear only).

Four groups of trade study metrics each with four Key Performance Parameters (KPPs) are employed to represent the AFC performance and platform integration 'opportunity cost'. Group I (or G-I) measures AFC flight control performance on the ICE platform, G-II measures the integration impacts, G-III measures the so-called 'ilities' impacts, and G-IV measures the technology maturity. The aim of the matrix is to provide a structured tool to compile and compare relative qualitative and quantitative measures of the metric groups / KPPs. An overview of the trade study process including metric groups, their respective KPPs, and the scoring criteria are described below.

9.4.3 Trade Study Process

The QFD process is a powerful technique to make more objective (or at least less subjective) assessments and design decisions. An overview of the QFD trade study process is illustrated in Figure 9-5. Generally, engineering analysis and design is conducted across the four metric groups to define values for the KPPs and their consequent scores that feed into the QFD matrix. Weights are defined across the metric groups and KPPs to reflect relative importance in the overall assessment. The trade study results are used to generate KPP response plots (or bar graphs) across the four AFC configurations to permit side-by-side relative comparisons. The resultant KPP scores for each configuration also permit assessment of AFC feasibility against defined criteria. More specifically, the overall process work flow (Figure 9-5) for the AVT-239 trade study initiates sequential tasks to define data for metric groups G-I to G-IV. A flight control model is developed under the vehicle performance sub-group to define performance characteristics of each AFC effector and combination of effectors on the ICE platform. The flight control model is calibrated with experimental and computational flow control data provided by researchers in the AVT-239 flow control sub-group and the literature (cited prior). Mission simulations are run using this flight control model to define required AFC flow rate profiles that provide the basis data for G-I performance KPPs. The required AFC flow rate profiles are then provided to the trade study sub-group to define the subsequent AFC architecture, component sizing, and design integration into the ICE platform. With the integration concepts completed, the basis data is available for the G-II integration, G-III 'ilities', and G-IV maturity KPPs. A QFD score of 9, 3, or 1 is applied based on pre-defined grading criteria that are associated respectively with the preferred target value, an acceptable value, or an unacceptable value. Details on the trade study approach are provided in a companion paper [11].

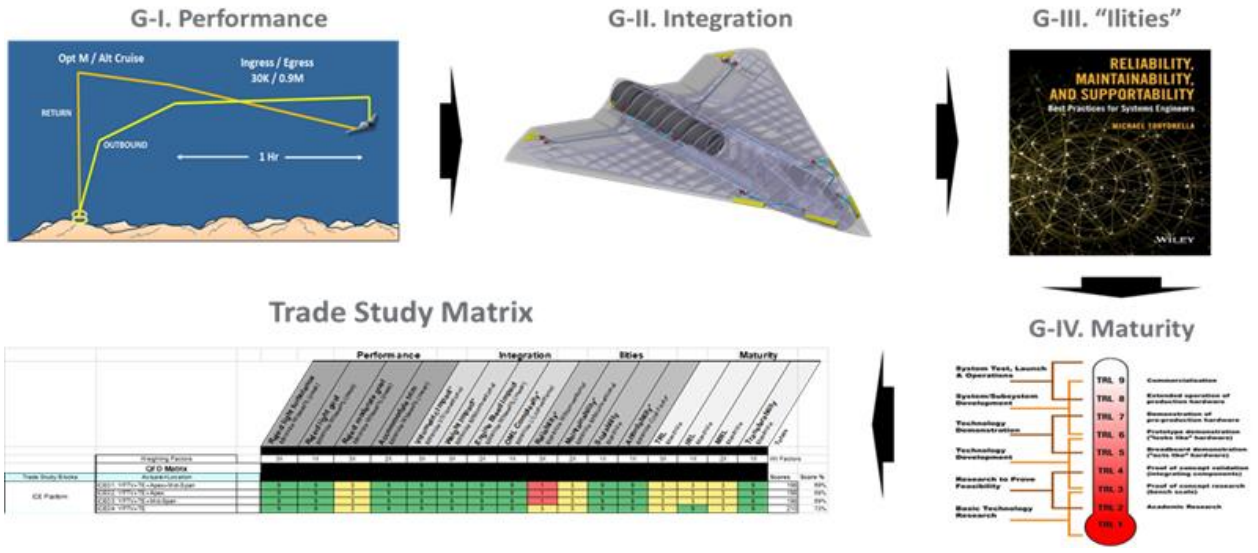

Figure 9-5: Trade Study Process Incorporates Analysis and Design Task Across 4 Groups of Metrics.

9.5 TRADE STUDY RESULTS

9.5.1 G-I (Performance) Summary Results

A summary of trade study results for performance metric group G-I is provided. A series of 100 mission simulations are run using the ICE platform flight control [12], [13], [14] model with random light turbulence and both light and moderate gust intensity levels. Prior work has shown that this approach provides a near-Gaussian probability distribution in the results. These results define the required AFC bleed mass flow rate profiles that provide the basis data for the G-I performance KPPs. The required AFC mass flow rate profiles are then provided to the trade study sub-group to define the subsequent AFC architecture, component sizing, and design integration into the ICE platform [15].

An example of the ICE flight control simulation results is shown in Figure 9-6 for the 1 hr mission profile with 99% duration light turbulence and a 1% moderate gust superimposed randomly. The required engine bleed flow rate (lb/s) is plotted vs. time for the 10 second sample specified in the G-I trade study approach (over which the 1% mission duration moderate gust is imposed). The dynamic characteristics of each individual AFC effector are plotted for aircraft left (L) and right (R) sides:

1) LE Apex;
2) LE Mid-Span;
3) TE outboard for up and down (dn) pitch-plane directions; and
4) Nozzle wall using YFTV (designated YTV in the plot).

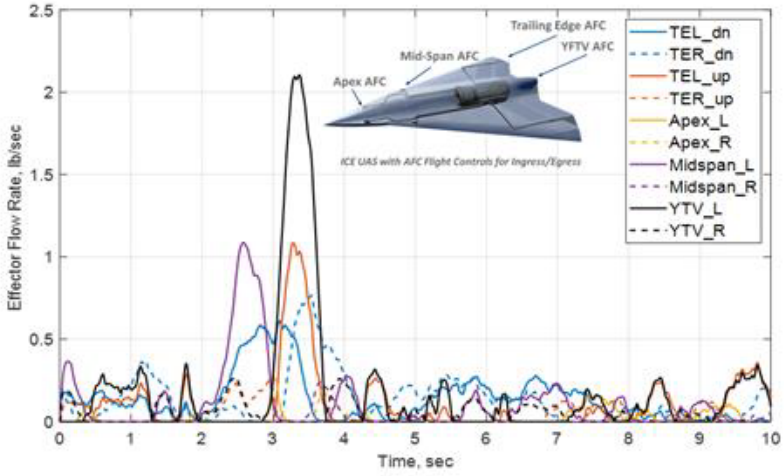

Flight Control Requirement	AFC Config/Tech Suite	AFC Tech/Location			
		TV	TE	Apex	Mid
Mean Peak During Gust (lbs/sec)	CE01: YFTV+TE+Apex+Mid-Span	2.84	0.95	0.85	0.85
	CE02: YFTV+TE+Apex	2.80	0.99	0.91	
	CE03: YFTV+TE+Mid-Span	3.00	0.99		1.41
	CE04: YFTV+TE	2.98	1.11		
Mean + 3*std (lbs/sec)	CE01: YFTV+TE+Apex+Mid-Span	0.40	0.32	0.31	0.50
	CE02: YFTV+TE+Apex	0.46	0.37	0.40	
	CE03: YFTV+TE+Mid-Span	0.42	0.37		0.51
	CE04: YFTV+TE	0.50	0.48		

Figure 9-6: Example G-I Results: Simulation / KPP Metric Values.

Several observations regarding the simulation results are evident from the plot:

- For the light turbulence condition (99% mission duration), all AFC effectors require comparable levels of flow rate (< 0.5 lb/s).
- For the moderate guest condition (1% mission duration), YFTV AFC requires the most flow rate (and provides most of the control power for the yaw plane) [12].
- The nominal flow rates < 0.5 lb/s (with exception of the high peaks during the gust).
- Most of the dynamics suggest a < 1 sec period for the peak flow rates encountered.

The flight simulation results are reduced to provide multiple averaged metric quantities including the guest peak ensemble average and the time-averaged mean (both used for the KPP metrics), and the mean+3*standard deviation which is used to size the AFC system architecture [15]. Values of these metrics are summarized in Figure 9-6. Similar to the simulation results, the 'mean peak during gust' metric shows YFTV dominating the AFC flight control followed by a balance of the other AFC effectors.

A summary of G-I performance metric sensitivities is provided in Figure 9-7 (metric details are found in Ref. [11]).

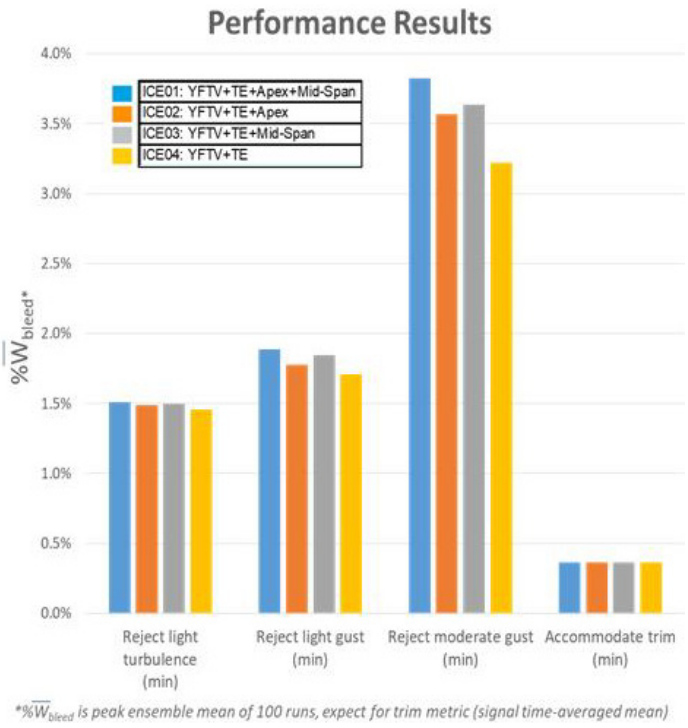

Figure 9-7: Summary G-I Results (Performance Metric Sensitivities).

The averaged bleed flow rates (all of which are to be minimized from a design standpoint) from the simulations are normalized by the total engine airflow to obtain a percent bleed flow (% $\overline{W}$ bleed) metric. This metric is computed for the 4 G-I KPP metrics and plotted for each of the ICE01-04 AFC configurations. Key observations include:

- All configurations perform similar (require comparable levels of the % bleed flow metric) for accommodating trim (< 0.5%) and rejecting light turbulence (~1.5%).

- For the light and moderate gust conditions (more stressing condition requires nominally 1.75% – 3.5%), configuration ICE01 requires the highest and ICE04 requires the lowest % bleed flow metric.
- Overall, given that the simulation results show that sufficient control power can be generated across all KPPs and at a peak flow rate for a modern turbofan engine, the G-I results suggest AFC is feasible from a performance standpoint.
- The results also show a slight preference for configuration ICE04 (lowest KPP 'cost' levels).

9.5.2 G-II (Integration) Summary Results

A summary of trade study results for integration metric group G-II is provided. Figure 9-8 summarizes conceptual design results from the ICE configuration equipped with a conventional hinge-based control suite and the AFC flight control suite (component and design integration details are available in [15]). The design results were used to compute system volumes, weights, and seam lengths for the G-II integration KPP metrics. The conventional system is used as the reference to normalize the AFC integration KPPs to provide a measure of 'reasonableness' in assessing the results. Several observations from the integration results include:

- The conventional system weighs 1900 lbs and occupies 79 ft^3 in volume.
- The ICE AFC system layout appears reasonable from a general size and routing perspective relative to the platform. Prior concerns that an AFC system may overwhelm the available space in a UAS – this does not appear to be the case for ICE.
- The AFC volume is dominated (~75%) by the high-pressure bleed air ducts (shown in blue), insulation, and slot-jet nozzles (shown in yellow).
- The AFC weight is dominated (~75%) by the AFC control valves (shown in red) and slot-jet nozzles.

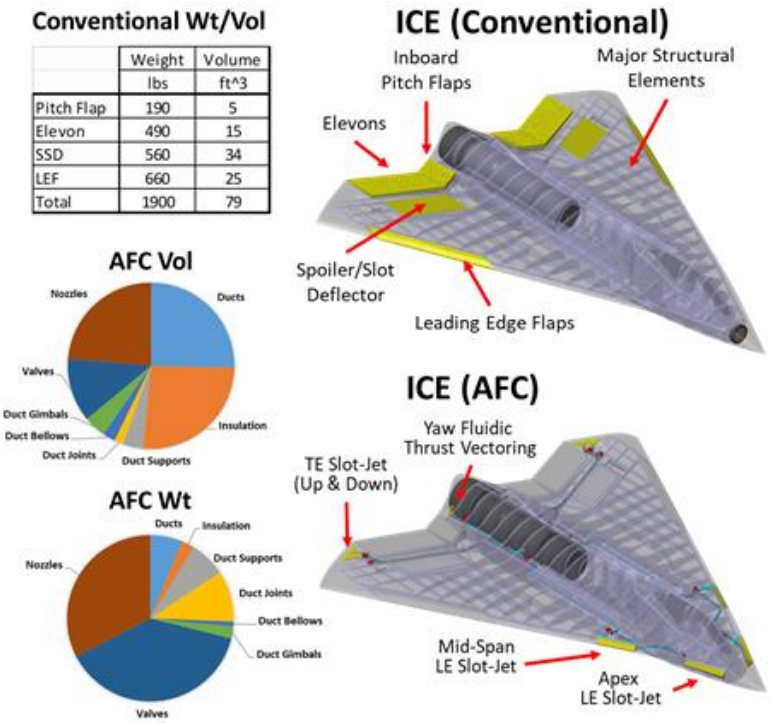

Figure 9-8: Example G-II Results: Integration Concepts / KPP Metrics.

A summary of G-II integration metric sensitivities is provided in Figure 9-9 (metric details are found in Ref. [11]). The G-II KPP metrics (all of which are to be minimized from a design standpoint) for volume impact, weight impact, Outer Mould Line complexity (OML), and engine bleed flow impact are computed from the conceptual design specifications. Key observations include:

- The nominal AFC system volume impact KPP is ~5 – 10% of the conventional system.
- The nominal AFC system weight impact KPP is ~25% of the conventional system.
- The OML complexity factor KPP is a measure of surface discontinuities (e.g., seams, gaps) that generally drive up platform complexity and cost. The nominal AFC system OML metric is 15% of the conventional system.
- These size, weight, and OML results suggests very reasonable levels for AFC and the possibility to integrate alongside a conventional system (as a redundant control to permit safe developmental and operational testing).
- The nominal AFC engine bleed impact KPP is ~0.5%. This level of bleed flow is acceptable to most modern turbofan engines and suggests a 1% impact to aircraft range.
- Overall, the G-II results suggest AFC is feasible from a platform integration standpoint.
- The results show a preference for configuration ICE04 (lowest KPP levels).

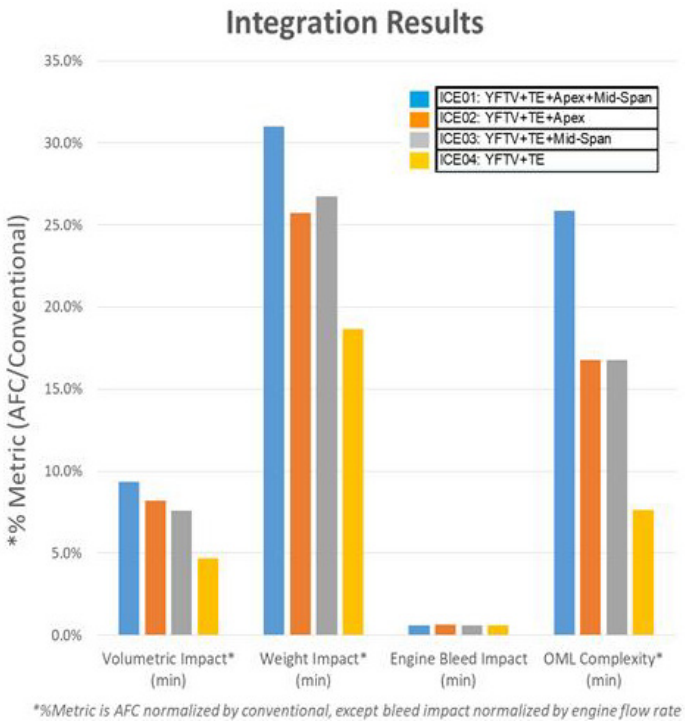

Figure 9-9: Summary G-II Results (Integration Metric Sensitivities).

9.5.3 G-III ('Ilities') Summary Results

A summary of trade study results for 'ilities' metric group G-III is provided. Figure 9-10 summarizes the results of the 'ilities' KPP metrics for reliability (maximize), maintainability (minimize – relates to maintenance hours), affordability (minimize – relates to cost impact), and scalability (maximize, metric details are found in Ref. [11]).

Key observations include:

- The nominal AFC system reliability KPP is ~50% of the conventional system. This represents a future challenge and need to integrate AFC onto UAS platforms. This 50% metric is being dominated by the AFC control valve reliability. If AFC control valves can be improved in their Mean Time Between Failure (MTBF) by roughly a factor of 2X (threshold) to 2.5X (objective), the AFC system will see comparable reliability as the conventional suite.
- The nominal maintainability KPP is comparable to the conventional system.
- The affordability (cost impact) KPP is ~20% of the conventional system. This suggests a distinct possible advantage to AFC from a cost standpoint.
- The scalability KPP is ~90-100%. This metric is based on the AFC system architecture being proven to be scalable from a Mach Number, Reynolds Number, and manufacturing standpoint. This result suggests AFC is generally scalable to full-scale from the scaled test conditions that researchers have been investigating.
- Overall, the G-III results suggest AFC is feasible from an 'ilities' standpoint. The only exception is in the reliability. This issue can be mitigated in the near term with scheduled AFC control valve replacement and in the mid-term with future research conducted to improve control valve reliability 2X-2.5X.
- The results show a slight preference for configuration ICE04 (best KPP levels).

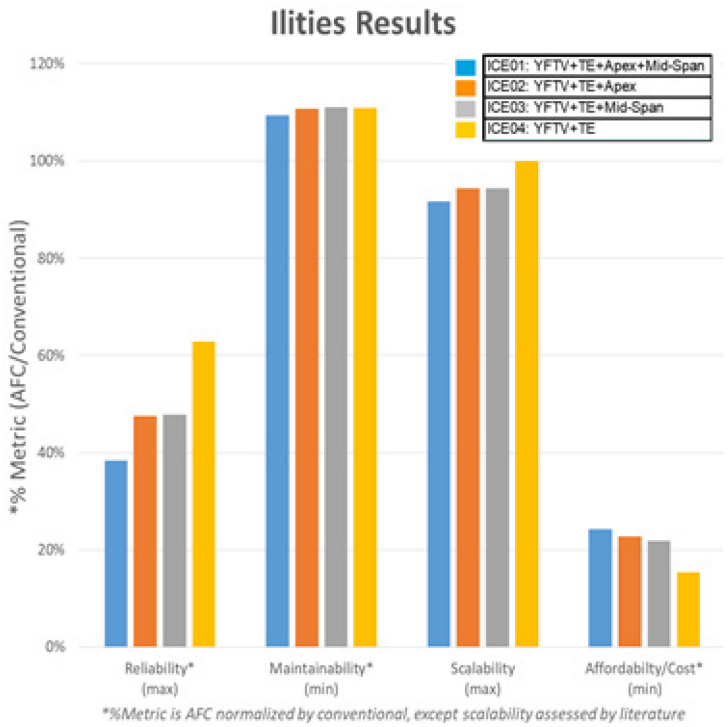

Figure 9-10: Summary G-III Results ('Ilities' Metric Sensitivities).

9.5.4 G-IV (Maturity) Summary Results

A summary of trade study results for the maturity metric group G-IV is provided. Figure 9-11 summarizes the results of the maturity KPP metrics (all are to be maximized) for Technology Readiness Level (TRL), Integration Readiness Level (IRL), Manufacturing Readiness Level (MRL), and transferability (measured by

the number of platforms to which the AFC technology suite can be "cross-decked" based on platform leading-edge sweep angle).

Metric details are found in [11]. Key observations include:

- All standard DoD readiness levels KPPs are 3-4 overall for the configurations ICE01-04.
- IRL KPPs identify an area of focus for the near term and could be addressed in reduced-scale flight tests currently in planning for the AVT-295 group.
- The transferability KPP (6) suggests that all ICE01-04 configurations are excellent. A level 6 suggests the technology can be hypothetically developed on one UAS platform and then "cross-decked" or transferred readily with no major developmental obstacles from an aerodynamic standpoint.
- Overall, the G-IV results suggest AFC is feasible from a maturity standpoint. The readiness levels are adequate, but more R&D investment is needed to increase readiness levels to at least 5 to be ready for a major flight demo that would help transition the technology.
- The results show a slight preference for configuration ICE04 (best KPP levels).

Figure 9-11: Summary G-IV Results (Maturity Metric Sensitivities).

9.5.5 QFD Results

The QFD trade study matrix is completed across all ICE AFC configurations ICE01-04 using a pre-defined scoring approach. Generally, a QFD score of 9, 3, or 1 are applied based on pre-defined grading criteria that are associated respectively with the preferred target value, an acceptable value, or an unacceptable value. A separate weighting factor is applied to each metric section to reflect a priority of 3 (high), 2 (medium), or 1 (low). Details on the trade study approach are provided in a companion paper [11]. The resulting QFD matrix and total score are summarized in Figure 9-12. Key observations include:

- All ICE AFC configurations yield a comparable overall score with a significant number of nines suggesting AFC meets/exceeds the preferred target KPP values for performance (except for

moderate gust which scores acceptable), integration, 'ilities' for scalability and affordability, and maturity for transferability.

- The most challenging area for incorporating AFC is in reliability as noted in the KPP sensitivities.
- Areas for future investment (based on scores of 1 and 3) include:

  1) AFC valve reliability;

  2) AFC maintainability;

  3) reducing bleed flow for moderate gusts;

  4) maturing technology, integration, and manufacturing readiness to 5+.

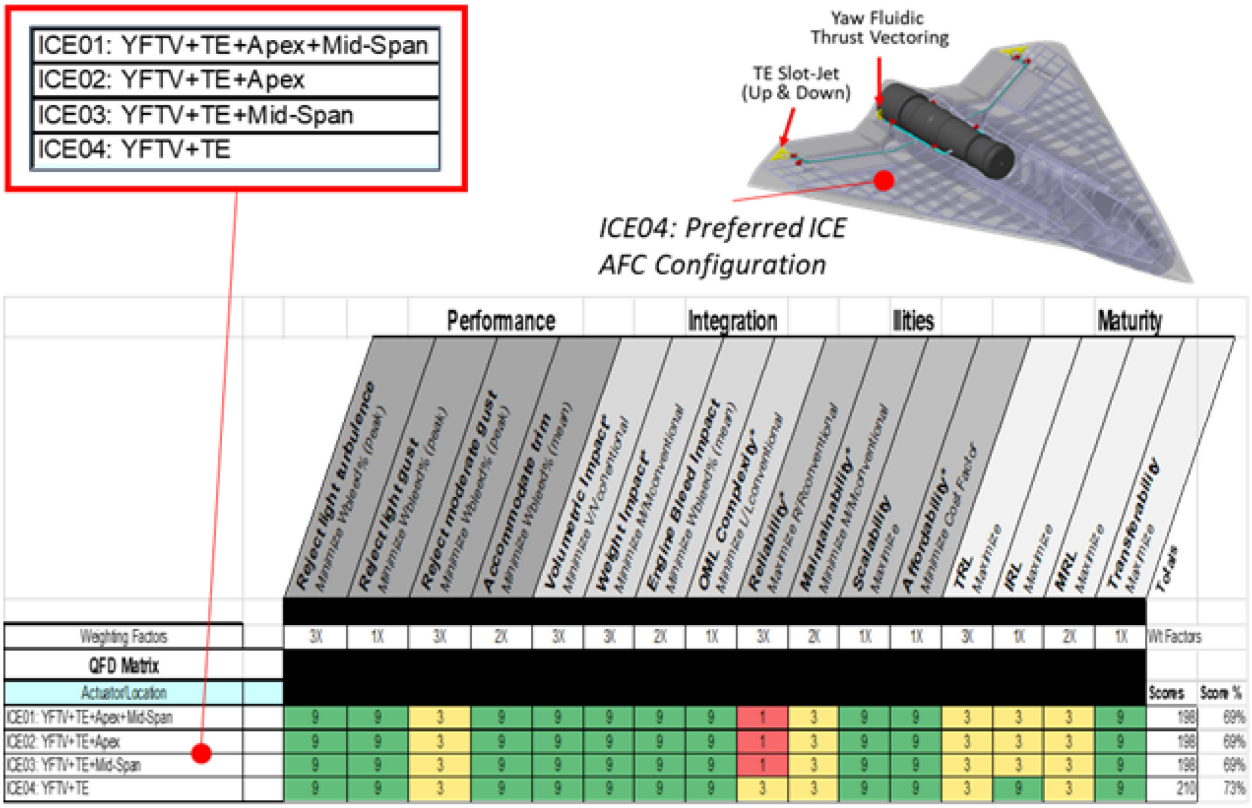

Figure 9-12: QFD Results: ICE01-04 Feasible; ICE04 Preferred Based on KPP Sensitivities (Figure 9-7 to Figure 9-11).

In summary, Figure 9-12 reveals that ICE04 has the highest QFD score percentage at 73% (slightly higher than ICE01-03 at 69%) for the ingress/egress mission use case. This QFD study result is consistent with the GI-IV KPP sensitivity results (summarized in Figure 9-7, Figure 9-8, Figure 9-9, Figure 9-10 and Figure 9-11) that generally showed more significant gains across many of the KPP metrics for ICE04.

9.6 CONCLUSIONS AND RECOMMENDATIONS

The trade study results described in this chapter suggest that AFC technology is both feasible and reasonable for application to the ICE platform. The approach is based on 16 KPPs that address AFC technology performance, integration, 'ilities', and maturity.

Key conclusions include:

- The flight control simulation results show that sufficient control power can be generated across all KPPs and at a peak flow rate for a modern turbofan engine, the G-I results suggest AFC is feasible from a performance standpoint.
- The nominal AFC system volume impact KPP is ~5 – 10% of the conventional system.
- The nominal AFC system weight impact KPP is ~25% of the conventional system.
- The OML complexity factor KPP is a measure of surface discontinuities (e.g., seams, gaps) that generally drive up platform complexity and cost. The nominal AFC system OML metric is 15% of the conventional system.
- These size, weight, and OML results suggests very reasonable levels for AFC and the possibility to integrate alongside a conventional system (as a redundant control to permit safe developmental and operational testing).
- The nominal AFC engine bleed impact KPP is ~0.5%. This level of bleed flow is acceptable to most modern turbofan engines and suggests a 1% impact to aircraft range.
- All standard DoD readiness levels KPPs are 3 – 4 overall for the configurations ICE01-04.
- The transferability KPP (6) suggest that all ICE01-04 configurations are excellent. A level 6 suggests the technology can be hypothetically developed on one UAS platform and then "cross-decked" or transferred readily with no major developmental obstacles from an aerodynamic standpoint.
- Overall, ICE04 is the preferred configuration considering all 16 KPPs across four groups.
- Areas for future R&D investment include:
  1) AFC valve reliability;
  2) AFC maintainability;
  3) Reducing engine bleed peak mass flow rate for moderate gusts; and
  4) Maturing technology, integration, and manufacturing readiness to 5+.
- Further investigation of AFC should be done on the ICE and SACCON platforms for the maneuver and take-off/landing flight regimes to determine if conventional controls could eventually be significantly reduced in size or ultimately eliminated.

This trade study approach [11] can be used on future phases of the AVT task group to investigate other critical flight regimes and platforms. Additional conclusions and next steps are found in a companion paper [6].

9.7 ACKNOWLEDGEMENTS

The authors are indebted to the following supporting contributors from LM Skunk Works to this chapter including: Dan Baruzzini, Derek Bye, Ken Dorsett, Bryan Guzzardo, and Andrew Ross, as well as Gary Dale (AFRL), Jurgen Seidel (USAFA), and Chris Hutchins (UK NATO AVT-239 representative).

9.8 REFERENCES

[1] Dorsett, K.M., and Mehl, D.R., Innovative Control Effectors (ICE), Phase 1 Final Report, WL-TR-96-3043, January 1996.

[2] Dorsett, K.M., Fears, S.P., and Houlden, H.P., Innovative Control Effectors (ICE) Phase II, Phase II Final Report, WL-TR-97-3059, August 1997.

[3] Cummings, R.M., Introduction: SACCON Uninhabited Combat Aerial Vehicle Experimental and Numerical Simulations, *Journal of Aircraft*, Vol. 49, No. 6, November – December 2012.

[4] Wu, C.R., Soutis, C., Zhong, S. and Filippone, A., A Morphing Aerofoil with Highly Controllable Aerodynamic Performance, The Aeronautical Journal, Volume 121, Issue 1235, January 2017, pp. 54-72.

[5] Joslin, R.D. and Miller, D.N., Fundamentals and Applications of Modern Flow Control, *Progress in Astronautics and Aeronautics*, 1st edition, AIAA, 2009.

[6] Warsop, C., Smith, D.R., and Miller, D.N., NATO AVT-239: Innovative Control Effectors for Manoeuvring of Air Vehicles - Conclusions and Next Steps, AIAA SciTech Conference, January 2019.

[7] Miller, D.N. and McCallum, B.N., Prospects for Fluidic Thrust Vectoring Technology on a Next-Generation Air Vehicle, NATO STO Workshop, Session 4, Paper #10, May 2013.

[8] Hoholis, M.G., Steijl, R., and Badcock, K., Circulation Control as a Roll Effector for Unmanned Combat Aerial Vehicles, *Journal of Aircraft*, Vol. 53, No. 6, November-December 2016.

[9] Williams, D.R. and Seidel, J., Crossed-Actuation AFC for Lateral-Directional Control of an ICE-101/Saccon UCAV, AIAA 2016-3167, 8th Annual Flow Control Conference, 2016.

[10] Box, G.E.P., Hunter, W.G., and Hunter, J.S., *Statistics for Experimenters*, Wiley, 1978.

[11] Miller, D.N., Williams, D., Warsop, C., and Smith, D.R., NATO AVT-239 Task Group: Approach to Assess Prospects of Active Flow Control on a Next-Gen Tailless Aircraft, AIAA SciTech Conference, January 2019.

[12] Niestroy, M.A., Dorsett, K. M., and Markstein, K., A Tailless Fighter Aircraft Model for Control-Related Research and Development, AIAA SciTech Conference, Paper 1757, January 2017.

[13] Williams, D., Osteroos, R., and McLaughlin, T., Flight Control Derivatives using Active Flow Control Effectors on the ICE/SACCON UCAS Model, AIAA SciTech Conference, January 2019.

[14] Niestroy, M.A., Williams, D, and Seidel, J., NATO AVT-239 Task Group: Flow Control Simulation of the Tailless ICE Aircraft, AIAA SciTech Conference, January 2019.

[15] Maines, B.H. and Miller, D.N., NATO AVT-239 Task Group: Flow Control System Integration into the Tailless ICE Aircraft, AIAA SciTech Conference, January 2019.

Chapter 10 – FLIGHT DEMONSTRATION OF AFC ON THE MAGMA DEMONSTRATOR AIRCRAFT

Clyde Warsop
BAE Systems AIR
UNITED KINGDOM

William J. Crowther and Thomas Shearwood
The University of Manchester
UNITED KINGDOM

10.0 NOMENCLATURE

C_μ	Momentum coefficient = $\dot{m}V_j/q_\infty S$
C_l	Lift coefficient
C_m	Pitching moment coefficient
Cn	Yawing moment coefficient
C_Z	Normal force coefficient
c	Chord (m)
h	Height of blowing slot (m)
h^*	Throat height of convergent-divergent nozzle (m)
r	Radius (m)
δ	Deflection angle of control surface or vector angle of a jet (deg.) or boundary layer thickness (m)

10.1 OVERVIEW

MAGMA is large model-scale technology demonstrator aircraft developed under a collaborative project between BAE Systems and the University of Manchester to explore the application of novel fluidic flight controls on a planform representative of future tailless aircraft. The two main control effectors of interest are Supercritical Circulation Control and Fluidic Thrust Vectoring. This chapter presents the design philosophy and layout of the aircraft together with a description of the systems engineering required to allow the novel control technologies to be successfully implemented. Performance data from ground and flight trials are presented. The chapter concludes with a reflection on the benefits and challenges of using sub-scale flight test vehicles for progressing new technologies.

10.2 INTRODUCTION

A principal driver for Fluidic Control Effectors (FCEs) such at Circulation Control (CC) [1] and Fluidic Thrust Vectoring (FTV) [2] for military aircraft is signature reduction. Conventional moving control surfaces create changes in aircraft external geometry during flight and are the sources of additional edges and gaps that must be carefully treated to minimise radar reflection. FCE's also provide opportunities for lower maintenance requirements since they have fewer, highly-loaded, moving parts compared to conventional control surfaces and are therefore less prone to wear and mechanical failure. FCE's may also be more volumetrically efficient compared with conventional trailing edge control surfaces – allowing for additional fuel or improved structural layout.

The research presented in this chapter builds upon that demonstrated in the successful flight trials of circulation control on the DEMON UAV in 2012 undertaken under the BAE Systems/EPSRC FLAVIIR project [3]. Since that time advances in the understanding of the behaviour of Coanda flows have been achieved to enable supersonic Coanda wall jets (pressure ratios up to 7 and beyond) to remain attached and effective as aerodynamic control motivators [4]. The ability to achieve the controlled attachment of high pressure ratio Coanda wall jets opens up the possibility for effective operation of circulation control at transonic flight speeds and also their use in the vectoring of high pressure ratio exhaust jets. Operating the Coanda jets at high pressure ratio also maximises their efficiency in terms of achieving maximum blowing momentum coefficient for a minimum mass flow bleed requirement from the engine. Reduced mass flow

also has a beneficial impact on the sizing requirements for the valves and ducting used to distribute the bleed flow around the airframe.

Much has been achieved in developing and demonstrating these technologies in the laboratory and by simulation [5]. The main purpose of a sub-scale flight demonstration of the technology is to provide a means of communicating the benefits and achievements of the research to a diverse audience and to provide a means of arousing and maintaining interest from sponsors who are often detached from the language of the science. They also provide data that can be used to extrapolate system performance to full-scale flight conditions and can often highlight some of the complex system integration issues that can be overlooked in simple laboratory tests. Examples of such issues include the manufacturability of components; the impact of thermal effects on geometry and performance, and the complex interactions that occur between propulsion system and flight control system behaviour and performance. While such demonstrators can provide science and engineering benefit; the engineer has to be realistic in assessing what this benefit is and how it extrapolates to full-scale flight conditions.

The chapter is divided into four main sections. The first covers the background science and technology to the fluidic control effectors that represent the primary technology payload of the demonstration activity. The second covers the development of the MAGMA vehicle itself, looking at the choices that defined the requirements and the processes through which the aircraft was designed and built. The third section looks at the process of flight testing and allows reflection on how choices in the design of the technology payload and vehicle itself faired against the reality of flight. Lastly, the fourth section overviews the key technical achievements of the project to date. There is inevitably significant cross over between the sections as there must be for an integrated solution in which all parts have to work as intended at the same time. The chapter ends with wider reflections on the technologies being demonstrated and the process by which this demonstration has taken place.

10.3 FLUIDIC TECHNOLOGIES

10.3.1 Overview

The principal demonstration technologies for the current phase of the MAGMA programme are so-called fluidic effectors that create aerodynamic forces and moments for flight control purposes. The fluidic effectors are distinct from conventional moving surface effectors in that their geometry is fixed and the control input is via strategic injection of high pressure air. The elimination of external moving parts on flight controls has the potential to reduce vehicle signature and the weight of the associated structure and mechanical actuation system. Fluidic systems require actuated valves, but if well designed can by lighter than equivalent moving control surface systems.

The two fluidic technologies of interest are Circulation Control (CC) and Fluidic Thrust Vectoring (FTV).

10.3.2 Circulation Control

The fundamental principles and implementation of CC is shown schematically in Figure 10-1, with a CFD visualisation on a trailing edge geometry used for the present project shown in Figure 10-2. The basic principle of circulation control on an aerofoil using a tangential air jet goes back almost a century [6]. The challenge has always been in the associated systems and performance costs of implementing CC due to impact on engine performance, additional airframe drag and weight and volume of necessary plumbing. The key innovation in the MAGMA implementation of CC is that the devices are run at supercritical pressure ratios of the order of 3 such that the resulting jet is supersonic. This greatly increases the power density of the actuators over subsonic devices such that the same effectiveness can be obtained with a much smaller device [4], [5]. This helps address many of the previous disadvantages.

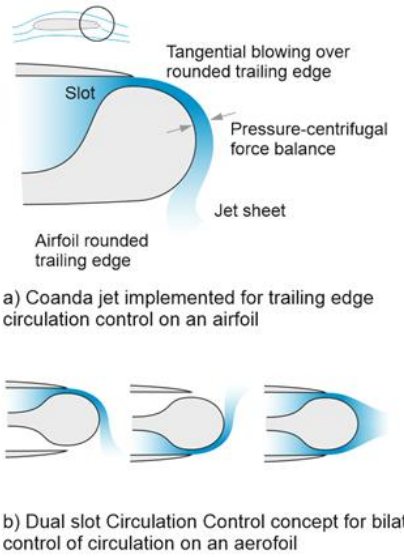

Figure 10-1: Trailing Edge Circulation Control Concept.

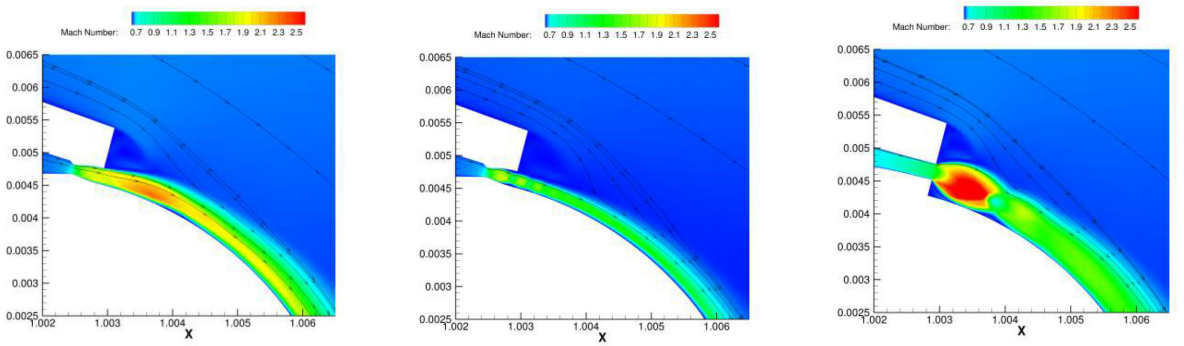

Figure 10-2: CFD Visualisation of Tangential Blowing from Convergent and Stepped Nozzles onto a Curved Surface. 2d compressible unsteady RANS. Colours by velocity magnitude [8].

An implementation of an initial test CC unit is shown in Figure 10-3. Previous work at Manchester University evaluated the use of convergent-divergent nozzles for supersonic Coanda devices [7]. However, the available manufacturing capability does not allow fabrication at the small scales needed as the required blowing slot heights are typically between 0.1 and 0.5 mm. To address this, the concept of a convergent-step nozzle was developed in which the expansion part for the supersonic flow takes place downstream of a backward facing step rather than in an enclosed nozzle [1], [8]. This greatly reduces the requirement for manufacturing precision because the convergent part of the nozzle can be an arbitrary taper with little loss in efficiency and the performance of the expansion side is relatively insensitive to the exact geometry of the step.

The aerodynamic performance of these supersonic CC devices has been shown experimentally in the laboratory to be highly robust. For a single sided device (one slot) the flow will routinely turn through 90 degrees before separation, with strong entrainment of the surrounding fluid (see tape visualisation in Figure 10-3c)). Figure 10-4 shows a schlieren visualisation of the flow from a double sided CC actuator used in both single slot and double slot mode. Note that in Figure 10-4 the slot height is nominally 0.2 mm and the trailing edge radius is just 2 mm.

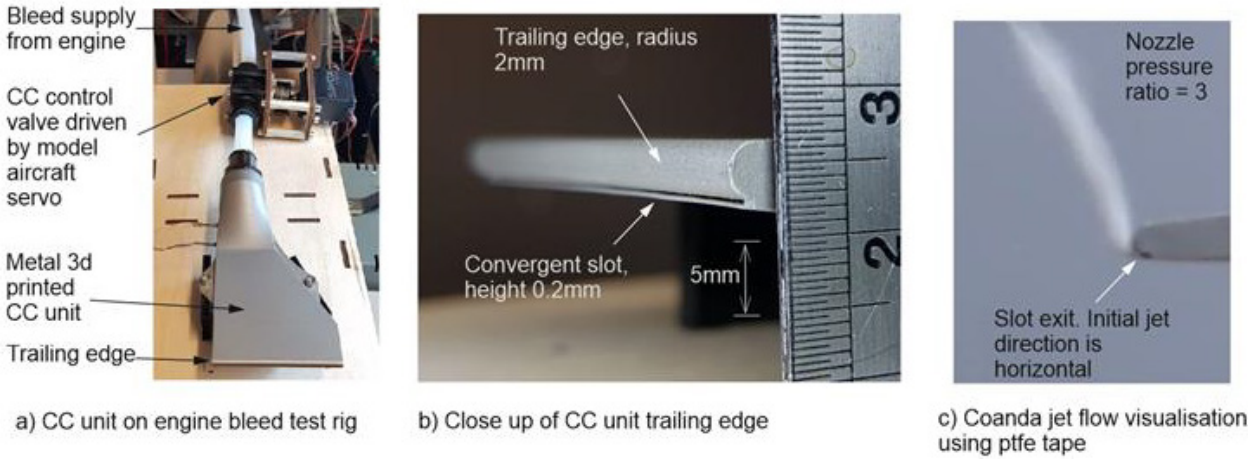

Figure 10-3: Circulation Control Unit Single Slot Test Piece Manufactured in Stainless Steel Using Additive Layer Manufacturing.

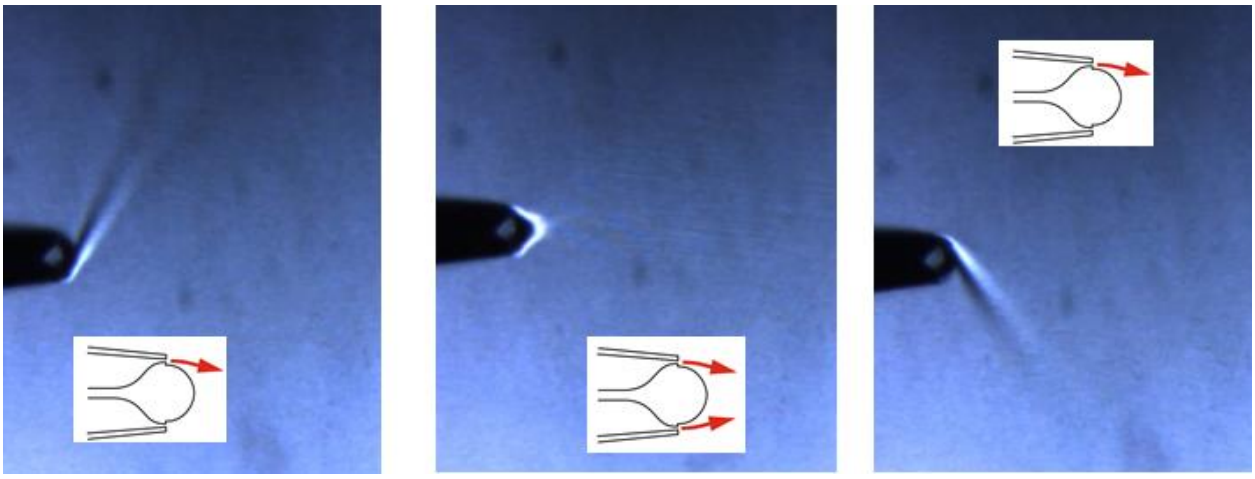

(a) Lower Slot Blowing. **(b) Dual Slot Blowing.** **(c) Upper Slot Blowing.**

Figure 10-4: Schlieren Visualisation of a Circulation Control Flight Unit. Plenum supply pressure ~3 bar, 200° C from engine bleed. Quiescent surroundings.

The geometry of the complete actuator developed for use on the MAGMA demonstrator aircraft is shown in Figure 10-5. Note that at a pressure ratio of 3, the jet is initially under expanded when it exits the convergent nozzle and expands to a Mach number of approximately 1.4 within a few slot heights downstream. The interaction between the supersonic jet and curved surface is complex and a series of shock expansion cells form that ultimately determine the separation point of the jet [1]. These cells are not resolved in the schlieren images in Figure 10-4 due to both small scale and the fact that the image is an integrated 2d view of a 3d flow field. The laterally asymmetric arrangement of the CC upper and lower plenums shown in Figure 10-5 is due to the fact that there is insufficient space within the wing to stack the air inlets on top of each other. The CC unit is fabricated from titanium using Additive Layer Manufacturing (ALM). The 0.2 mm slot size is the smallest gap that can be reliably resolved with the current process. Internal grit blasting in the flow direction after manufacture significantly improves internal surface finish and results in improved maximum angle of attachment. Other than grit blasting there is no other machining post-print. Note that the wing trailing edge thickness is approximately 4 mm so that the CC unit surface is seamless with the wing. The plenums contain strategically placed flow straightening ribs and spacers that both

improve the flow uniformity along the trailing edge slots and provide structural support against 'ballooning' under pressure. The ALM processes employed are again allow such complex structures to maintain high levels of geometric tolerance to be achieved and maintained when operation at both high pressure and temperature is required. The resulting structures have also been shown to be highly resistant to distortion and bucking under these operating conditions.

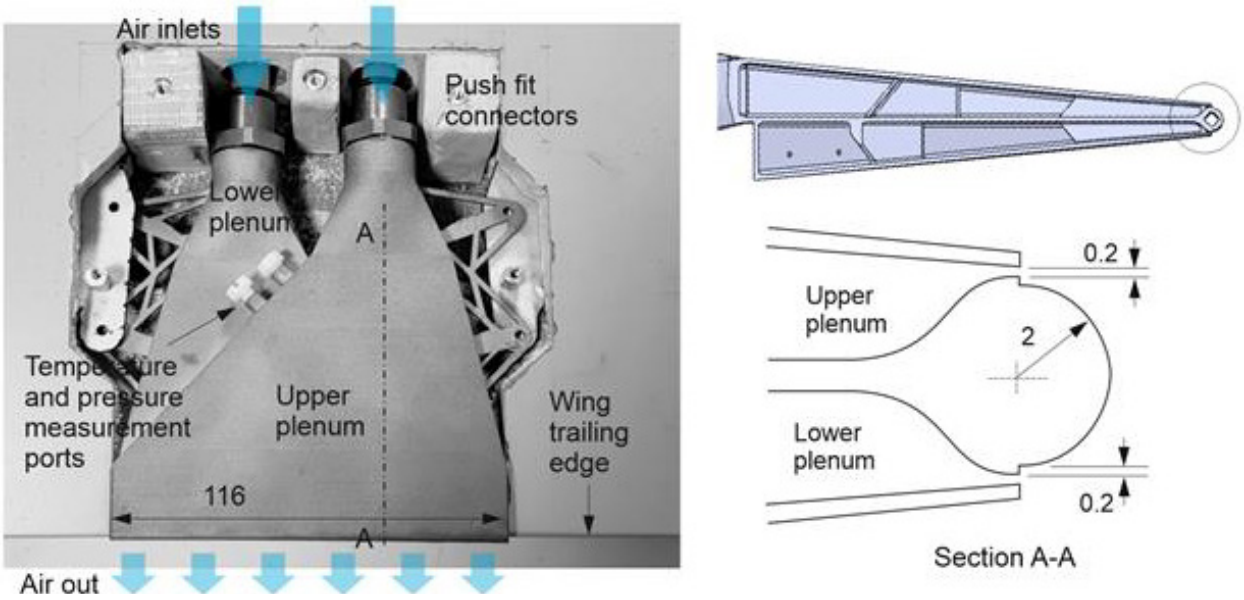

Figure 10-5: Circulation Control Unit Installation and Trailing Edge Geometry. Dimensions in mm. Part fabricated at the Additive Manufacture New Product and Process Development Centre, BAE Systems Samlesbury.

10.3.3 Fluidic Thrust Vectoring

The Fluidic Thrust Vectoring (FTV) nozzle implemented for the MAGMA aircraft is shown in Figure 10-6. Experimental control response, flow schematic, and flow visualisations are shown in Figure 10-7.

The pitch vectoring nozzle is designed for a subsonic primary jet flow velocity (the MAGMA exhaust jet velocity achieves a peak Mach number of approximately 0.8) and is actuated via normal blowing through a spanwise row of holes downstream of a step. Similarly functioning nozzles will operate for supersonic primary flows with appropriately designed reaction surface and nozzle geometries [7], [9], [10], [11]. Without a step, this type of subsonic FTV nozzle tends to exhibit bi-stable behaviour in which the jet is either fully attached to one surface or the other and there is significant hysteresis in the control response. Introduction of the step eliminates hysteresis and bi-stability at the cost of reduced control gain (ratio of the change in vertical momentum of the primary jet to the injected momentum). The efficiency of this class of FTV nozzle is improved by increasing the aspect ratio of the nozzle in a direction normal to the vectoring plane. Thus for pitch vectoring the nozzle should be short in the vertical axis and wide in the lateral axis.

The use of an elliptic rather than rectangular letterbox cross section of the nozzle is primarily driven by the need to integrate upstream with a circular exhaust from the engine via a simple sheet metal jet pipe with minimal engineering complexity and cost. The selection of an elliptic geometry also assists in providing structural stability at minimal nozzle mass which is a key consideration for achieving the desired CG location for the MAGMA configuration. The blend between circular and elliptic is achieved by deforming an initially circular jet pipe with pre-shaped formers. To keep a constant jet pipe cross sectional area as the tube goes from circle to ellipse it is necessary to start with a circular cone whose area increases downstream. The key design choices for

the nozzle were the reaction surface radius to nozzle height ratio (sets the overall system gain), the ratio of step height to nozzle height (sets control response characteristic) and the reaction surface termination angle (sets maximum achievable effectiveness). These ratios were initially determined from 2d RANS CFD studies, and a choice made on a suitable design compromise. For the present nozzle, the priority was for a benign control response rather than a high gain, high authority system. The nozzle 3d geometry was obtained by simply sweeping the centre line 2d geometry around the perimeter of the ellipse keeping the geometric ratios constant with respect to the local nozzle height such that the nozzle is self-similar. The nozzle is manufactured in titanium using Additive Layer Manufacturing with a default wall thickness of 0.5 mm. The shell structure of the curved reaction surfaces produces a high degree of rigidity for its weight. The central splitter plate is a structural component to react bending forces due to thrust vector loads.

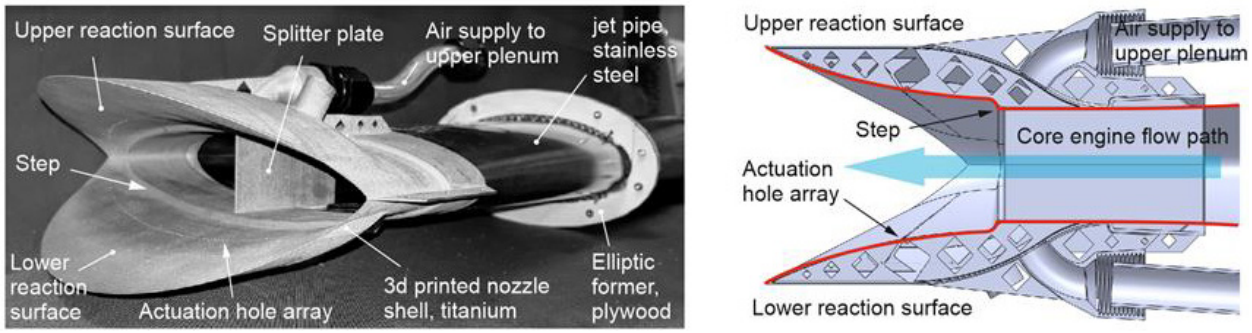

Figure 10-6: Fluidic Thrust Vectoring Nozzle Assembly and Key Features. Part fabricated at the Additive Manufacture New Product and Process Development Centre, BAE Systems Samlesbury.

The thrust vector control response shown in Figure 10-7a) indicates that the nozzle meets its primary requirement of providing a benign control response. Note that it is not unusual for this type of nozzle, implemented using tangential actuation, to have a highly non-monotonic control response, and for it to be necessary to control the pressure difference between the actuation plenums rather than just the absolute pressure. The use of normal blowing greatly simplifies this and makes manufacturing easier. The dead-band in the centre of the response is removed as part of the control logic so that the pilot experiences the thrust vector control in a manner similar to that of a conventional elevator. The maximum vectoring angle is approximately 10 degrees and the actuation input requires approximately 2% of the engine core flow. Other research studies [7], [9], [10], [11] have shown that this type FTV implementation can achieve much higher gains and vector angles (up to an order of magnitude higher) with greater geometric optimisation and attention to manufacturing tolerance. However, the prime consideration for the MAGMA FTV nozzle has been robustness and insensitivity to manufacturing tolerances and operating conditions purely from a reliability and flight safety perspective.

10.4 MAGMA FLIGHT VEHICLE DESIGN

10.4.1 Engine Choice

The starting point for the design was the requirement for a model-scale gas turbine engine that had a suitably high pressure and high flow rate bleed capability. Appraisal of the market showed that this capability did not exist in COTS form. Previously, the DEMON demonstrator aircraft [2], [3] had used an existing large model gas turbine engine that had been modified in-house to obtain a bleed air supply. However, while successful had given rise to significant engineering effort to achieve a successful outcome. To avoid this additional in-house engineering development effort, for MAGMA HAWK Turbine of Sweden was approached to develop a variant of their existing HAWK 240R engine modified with a new radial compressor. This new

engine variant was designed to produce a bleed offtake of 0.035 kg/s (9% of primary flow) at approximately 4.2 bar at a max power thrust of 180 N. As with all these types of modification to fundamentally simple engines there are consequences. For the HAWK engine used for MAGMA the stability of engine operation and hence safety, demands that the engine is operated with a continuous bleed output that varies with engine rpm. This is discussed more fully in Chapter 10.5.6

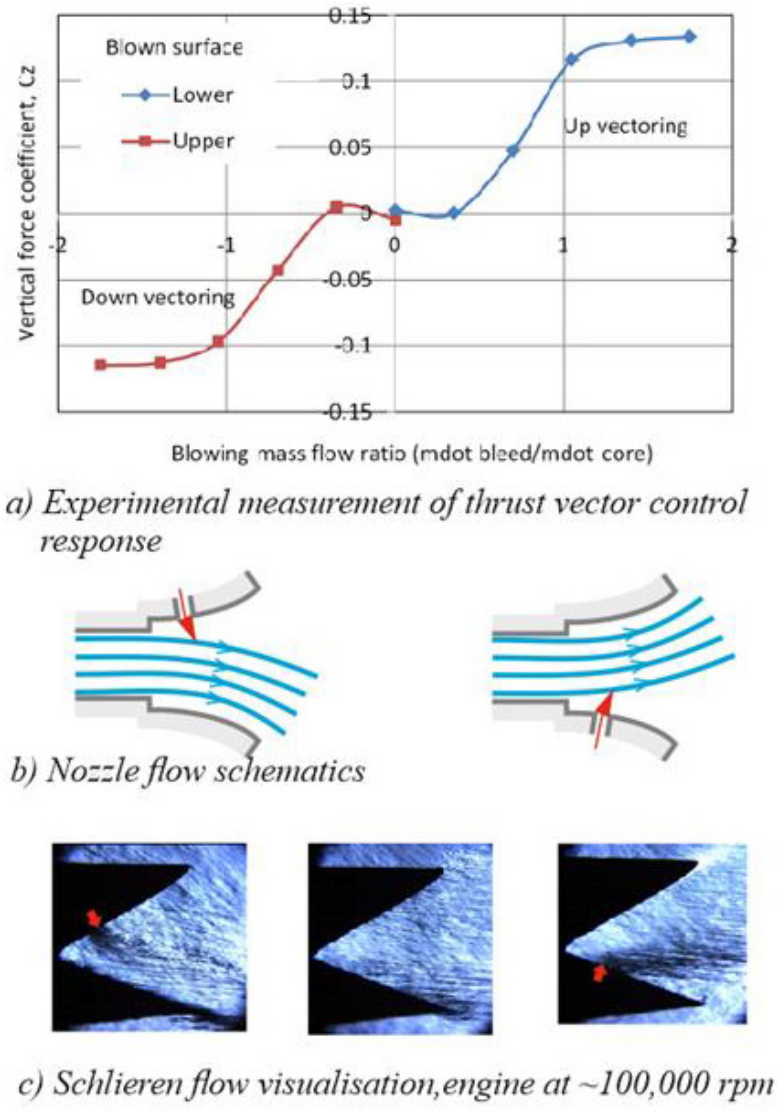

Figure 10-7: Fluidic Thrust Vectoring Experimental Evaluation.

10.4.2 Vehicle Sizing

Given an engine solution, the next step was to choose the target size (wing area) and weight of the vehicle. From previous experience with large-model-scale demonstrator aircraft, a primary requirement was set that the aircraft should have good handling qualities and sufficiently low flight speed that it could be flown line of sight by a remote pilot without excessive workload [4]. This led to an initial choice of design thrust to weight ratio of 0.5 and a stall speed of 20 m/s. The estimated maximum engine thrust of 200 N then set the all-up mass of the aircraft to 40 kg. A target wing loading of around 120 N/m^2 was then identified based on an expectation of a relatively low usable maximum lift coefficient of 0.5 consistent with a tailless low

observable planform. This gave a required wing area of approximately 3 m^2, and a wing span of approximately 4 m based on an aspect ratio of 5. Practicality requirements dictated that the vehicle fuselage should be transportable in a horizontal arrangement in a Transit size of van thus the wings had to be removable from the fuselage.

10.4.3 Planform Choice

The planform needed to set the right context for a low observable class of vehicle, however the validity of the demonstration outcomes were not critically dependent on planform choice as the effectiveness of the flow control technologies being demonstrated are only weakly dependent on planform (unlike other separation control type of flow control applications). More important was an aircraft that would have good pitch/yaw stability and benign handling characteristics to make it easy to fly without the need for auto-stabilisation and minimise the risk of the airframe due to uncontrollable departure. A choice was made to use a modified version of the public domain Boeing 1303 UCAV (Figure 10-8(a)) which was designed by Boeing Phantom Works under contract to the Vehicles Directorate of the AFRL [12]. There were two principal modifications. The first was to reduce the aspect ratio, by adding surface area, to move the design point further towards the stable side of the pitch-up boundary as identified in Figure 10-9. The leading edge sweep angle was kept the same at 47 degrees. The other modification was to move the location of the trailing edge crank. From an ease of manufacture point of view it was essential to place the wing joint at the location of the trailing edge crank. The 1303 planform has the crank relatively far outboard and this would have meant that centre section would not meet the transport constraint. Hence the crank position was moved inboard to give a centre fuselage section width of approximately 1.1 m. A comparison of the geometry of the original 1303 and MAGMA planforms and the effect on the pitching moment with angle of attack characteristics are shown in Figure 10-10. Figure 10-10 shows that simply adapting the 1303 configuration by modification of the trailing edge geometry alone (blue diamond symbols representing measurements on a wind tunnel model where a trailing edge extension was added to a baseline model of the 1303 configuration) was insufficient to achieve complete elimination of the extreme pitch-up behaviour. It was not until the wing section was also modified (NACA 0015) with considerably greater thickness and leading edge radius that a truly benign stall and pitch behaviour was achieved (red Square symbols on Figure 10-10).

In addition to validation of the stall behaviour by CFD assessment, early studies on the pitch/directional stability of the modified planform were undertaken by testing of geometrically representative ‘foam wing’ glider models and then by the use of a 1/3 scale, geometrically representative electric ducted fan powered model (Figure 10-11). This simplified model testing approached proved invaluable in determining the final design for MAGMA and could be undertaken at low cost and in a very short timeframe (a day or two in the case of foam gliders and a week or two in the case of the electric powered foam-built sub-scale model).

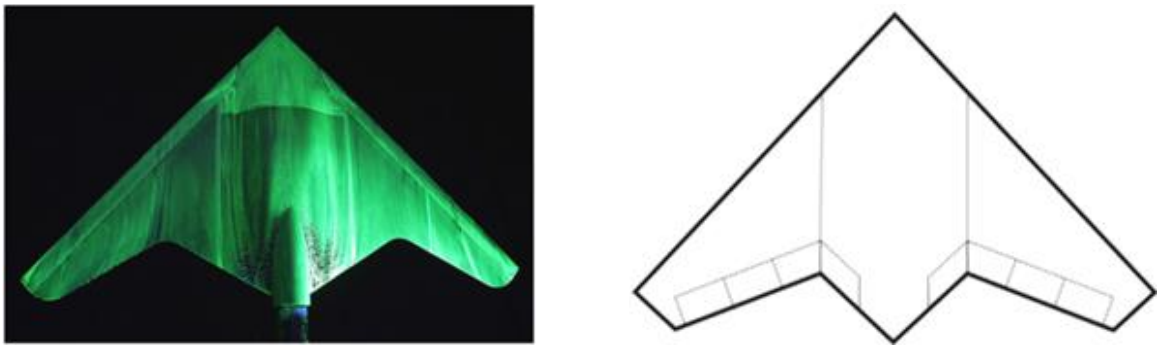

(a) Boeing 1303 UCAV Planform. **(b) MAGMA Planform.**

Figure 10-8: Comparison of the Original 1303 Planform and the Derived MAGMA Planform. The Leading Edge Sweep is the Same but the MAGMA Planform has a Lower Aspect Ratio and the Trailing Crank is Moved Inboard.

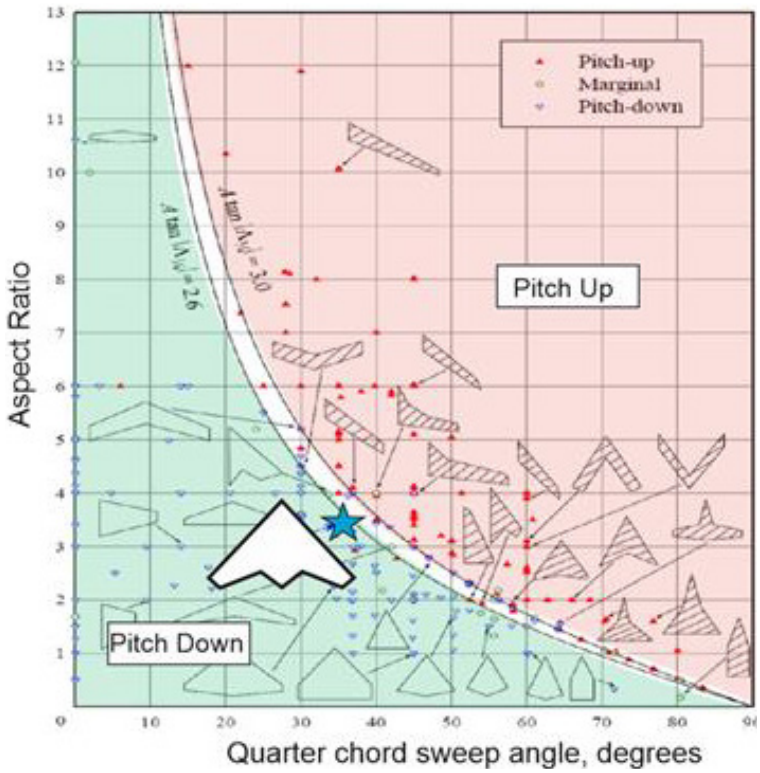

Figure 10-9: Pitch Boundary for Flying Wings as a Function of Wing Sweep Angle and Aspect Ratio. The MAGMA Planform is just Inside the Stable Region. Figure modified from [13].

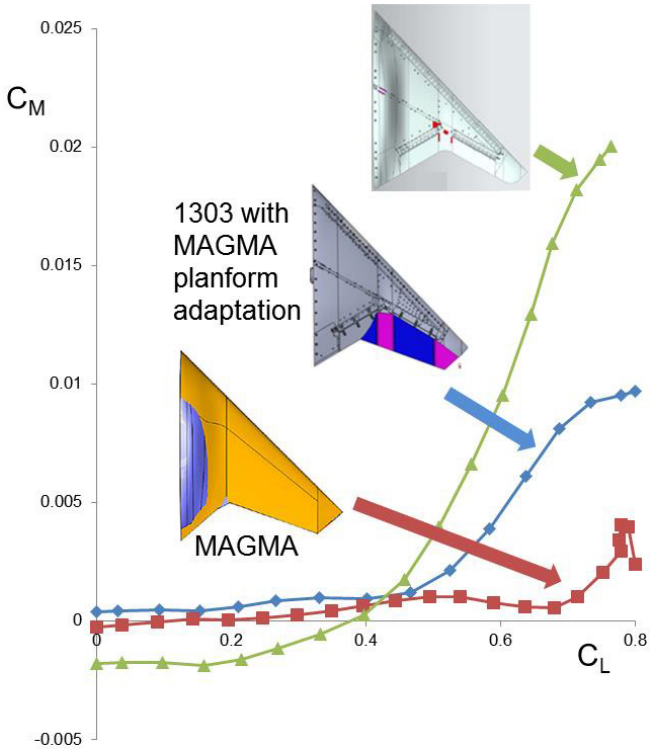

Figure 10-10: Pitching Moment Variation with Lift for 1303 and MAGMA Planforms [14].

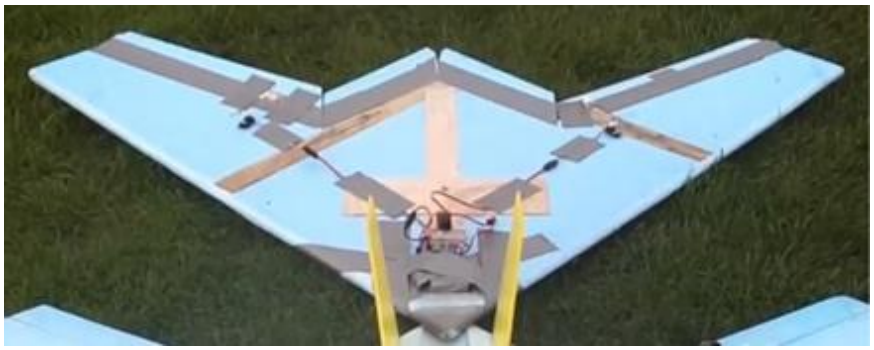

Bungee Launched 1/3 Scale, Flat Plate Model Glider.

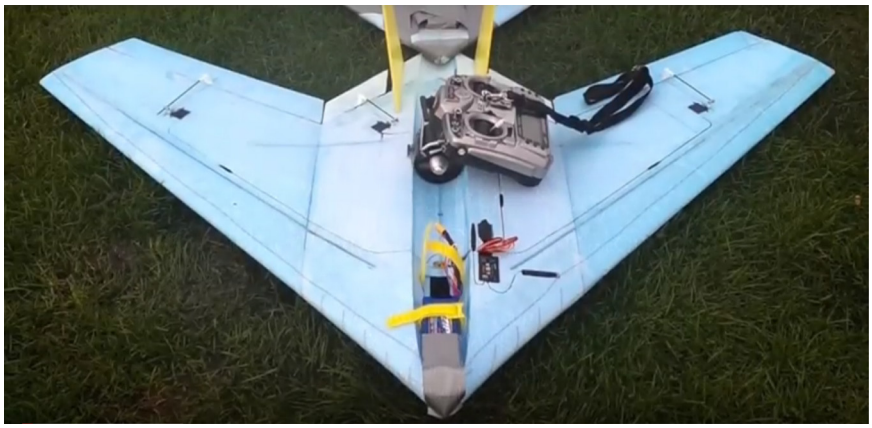

Electric Ducted Fan Powered 1/3 Scale Flying Model.

Figure 10-11: Simple Foam Models Used to Assess Effects of Planform and Aerofoil Section on MAGMA Flight Handling Qualities (Both Configurations had Removable Tail Fins).

10.4.4 Overall Geometry Choice

In order to simplify mould design and reduce the number and complexity of jigs, it was decided to use a symmetric aerofoil section for the wings (NACA0012). The fuselage section was a blend between an approximate NACA0018 with sharpened nose and slight positive camber on the centreline to the NACA0012 at the wing root. It is normal to introduce a few degrees of washout on flying wings of this configuration to reduce tip aerodynamic loads and to facilitate trim at positive lift coefficient without the need for excessive trailing edge control deflection. However, this was not implemented here so that both wings could be made from a single symmetric mould.

A general arrangement drawing of the MAGMA vehicle is shown in Figure 10-12. Flight control surfaces on the trailing edge of the wing are constant absolute chord with the hinge line parallel to the trailing edge. As a fail-safe, backup trailing edge CC effectors are only installed in the mid-span region of the wing on the fluidic aircraft. Therefore in the event of failure of the CC or FTV system (either no control or hard-over control) the pilot still has the ability to control the aircraft via the inboard and outboard conventional control surfaces. The conventional controls have been designed to have sufficient authority to overcome the maximum hard-over failure mode of the fluidic controls to allow the aircraft to be flown to a safe recovery. Two vertical tail surfaces provide for good positive directional stability for early flight tests. These surfaces have been designed to be removable to allow for fin size to be reduced or eliminated in order that advanced trials of directional control using the CC trailing edge controls can be explored.

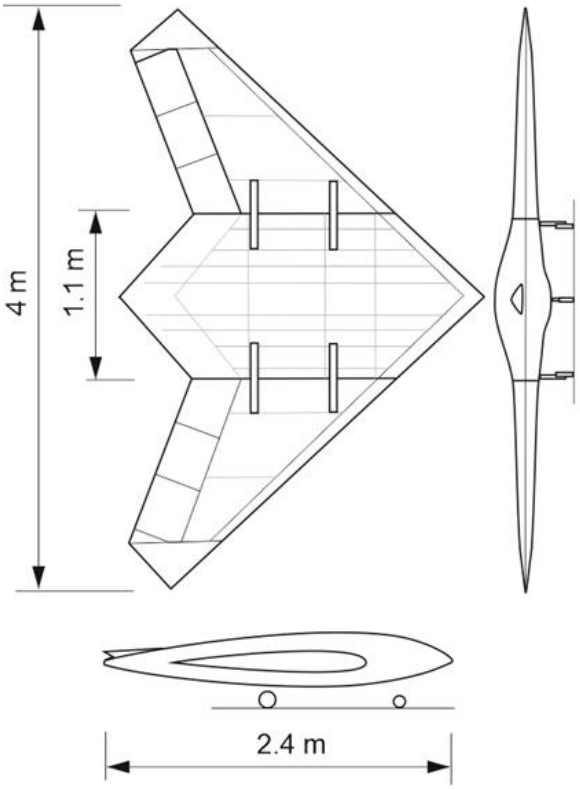

Figure 10-12: MAGMA 3 View Drawing and Key Dimensions, Fins Off.

10.4.5 Structural Design

The original structural design for the aircraft was based on a conventional plywood built-up structure, however the adoption of a stressed skin composite approach yielded a much better overall solution with regard to parts count, weight and the ability to manufacture duplicate copies of the airframe from a set of master moulds (Figure 10-13). For reasons of cost the majority of the structure is of wet-layup glass fibre skinned foam core sandwich construction. All components were laid-up in NC machined model board tooling which allowed good tolerance control of parts, the ability to use the tooling as assembly aids and the ability to manufacture multiple parts from a single mould. A photograph of the wing during manufacture is shown in Figure 10-14.

10.4.6 Fluidic Systems Architecture

The fluidic systems architecture for MAGMA is shown in Figure 10-15. The control valves are comprised of COTS manually operated aluminium ball valves (originally intended for racing car fuel systems) connected to model aircraft servos. The valve ball compression fittings were loosened slightly to reduce friction and hence reduce servo load. The pressure and temperature within the plenum chambers of the fluidic actuators is measured and recorded and can be used as part of closed loop control if needed. The engine bleed system requires active control of the bleed flow rate so that it is kept between manufacture-defined upper and lower limits at all times. Excursion from these limits for any significant time will lead to destruction of the engine through either over heating (too much bleed) or over speeding (not enough bleed).

Annotated photographs of the propulsion and fluidic systems implementation are shown in Figure 10-16. Bleed flow rate is measured with a custom made venturi system (Figure 10-16(a)). Bleed air is distributed via a manifold block to the various fluidic actuators and to a dump port at the rear of the aircraft (Figure 10-16(b)).

The bleed air at the engine offtake is at a maximum pressure of 4 bar and a temperature of around 200°C. The manifold block is machined from PTFE. Pipe work throughout the aircraft is standardised on 15 mm outside diameter tubing (13 mm I.D.). For the hottest parts immediately downstream of the engine and next to the jet tube, aluminium pipes are used. Everywhere else the pipes are PTFE primarily because its flexible nature makes it easier to route through the aircraft (minimum bend radius approximately 20 cm).

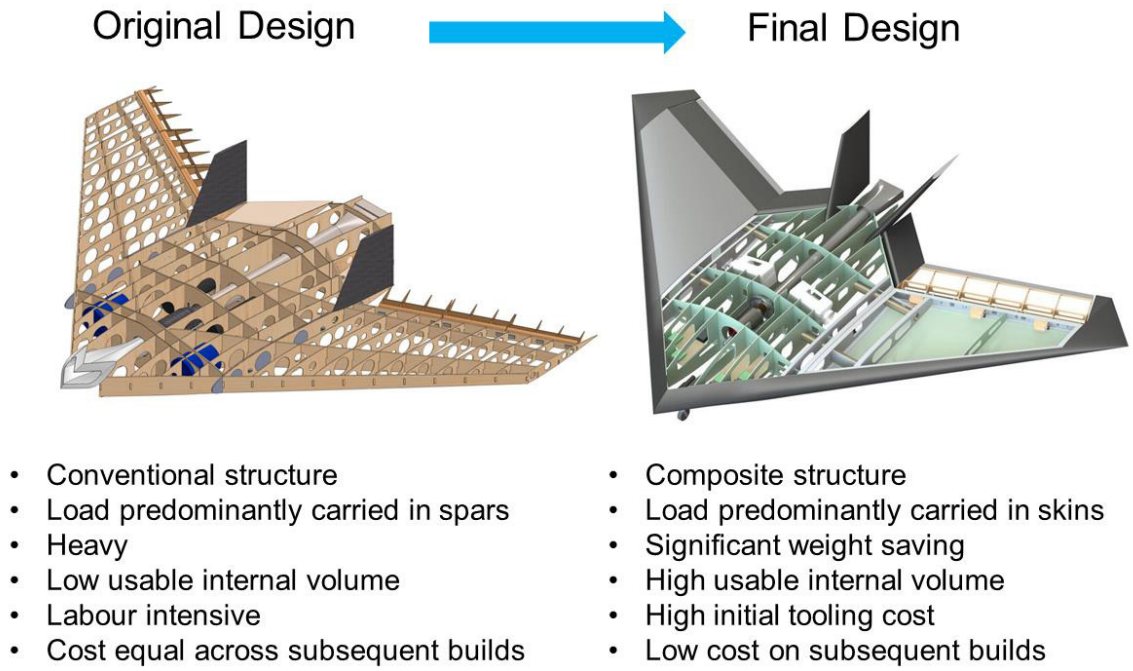

Figure 10-13: Comparison Between Conventional and Composite Stressed Skin Structural Approach.

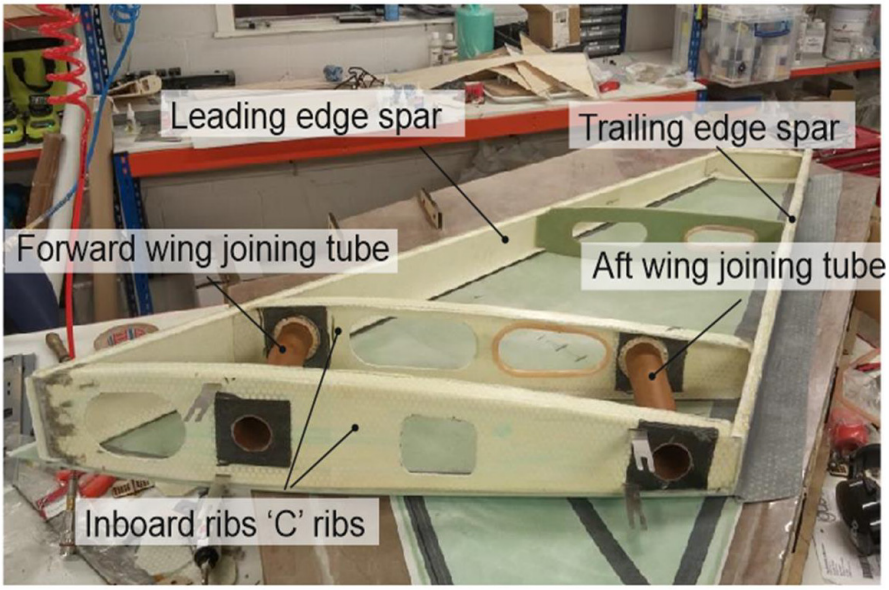

Figure 10-14: Semi-Monocoque Wing Construction. Wing shown prior to bonding of wing upper skin.

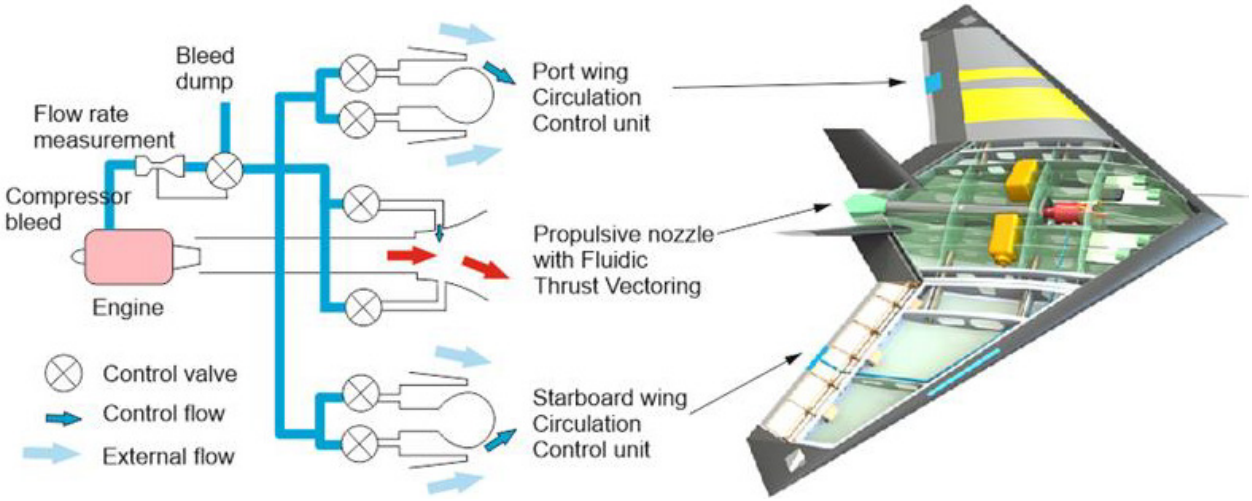

Figure 10-15: MAGMA Fluidic Systems Architecture.

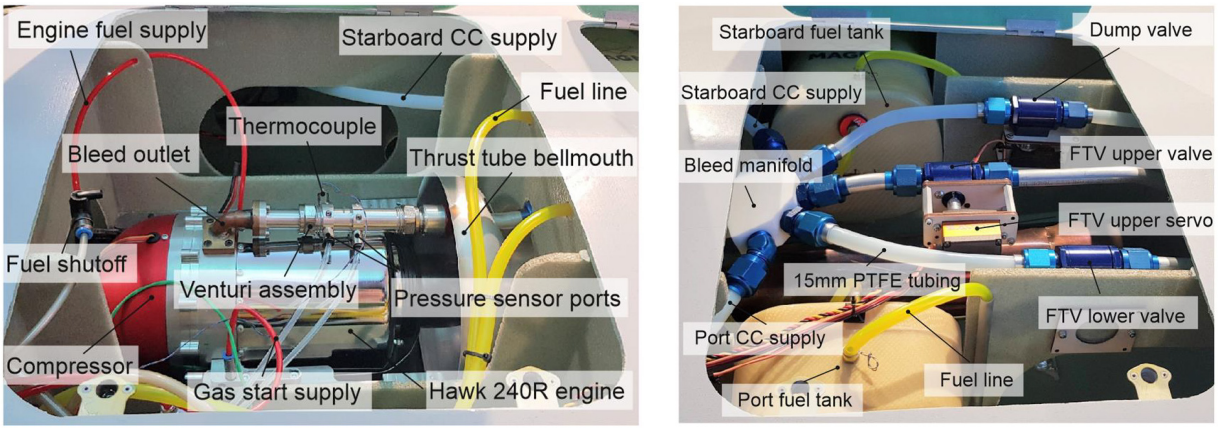

(a) Engine Bay. **(b) Fluidic Systems Bay.**

Figure 10-16: Vehicle Propulsion, Fuel and Bleed Systems Implementation.

Each fluid actuator control valve servo is operated through the flight control computer via PWM signals as though it were a conventional control surface. No-linearities in control response can be dealt with through the 'exponential' functions within the pilot's transmitter handset. The pilot handset allows programming of functionality to allow switching on and off of the fluidic controls during flight. In fluidic system 'off' mode the inboard and outboard elevons provide all flight control functions. In the event of a fluidic system 'hard-over' failure the elevons have sufficient control authority to overcome the fluidic control forces (both CC and FTV) with sufficient margin to allow recovery of the aircraft.

10.4.7 Weight Breakdown

An approximate weight breakdown of the MAGMA aircraft at its certified maximum take-off weight (60 kg) is shown in Figure 10-17. Note that the standard take-off weight of the baseline fluidic aircraft with 8 kg fuel is nominally 48 kg. Approximately half the empty weight of the aircraft is the airframe structure. Whilst this is relatively large compared to production vehicles, it is competitive compared to similar jet model aircraft. The structure is in many areas stronger and stiffer than in needs to be, however this was typically due to working at minimum material handling constraints rather than by design. The fluidic and electronic systems

may be considered the 'payload' for this aircraft and for the fluidic version (48 kg MTOW) comprise approximately 16% of the empty weight. Ballast at 10% is a reflection of the challenge in balancing tailless vehicles of this sort – the lack of a forward fuselage makes it very difficult to place components far enough forward to avoid adding ballast. The aircraft can carry a maximum fuel volume of approximately 10 litres. Maximum flight duration at max fuel is estimated to be approximately 1 hour. Typical test flights are undertaken with a take-off fuel load of 4 kg and landing load of 2 kg to allow for contingency. The aircraft is flown with a positive static margin of between 5 and 10% MAC. A nominal static margin of 7% MAC is considered a good compromise based on the aircraft having acceptable stability and handling qualities (as determined by pilot opinion) while still achieving adequate pitch control authority for take-off rotation and manoeuvre. At this level of static margin nominal cruise speeds require less than 2° of up-elevon deflection. The CG location can be adjusted both fore and aft by modification of the nose ballast weights between flights while variation in CG location during flight is minimised through the fuel tanks being located at the nominal CG position. In laying out the basic internal systems a key consideration was the difference between the conventional and fluidic control variants of the aircraft. The FTV and CC nozzles add significant mass at the rear of the configuration and have a significant impact on CG location whereas other elements of the fluidic system (valves, venturi meters, controllers, etc.) can only be located in the region of the nominal CG meaning they cannot be used to offset the impact of the fluidic nozzles on CG position. It was therefore very important to account for these issues at the conceptual design phase of the aircraft.

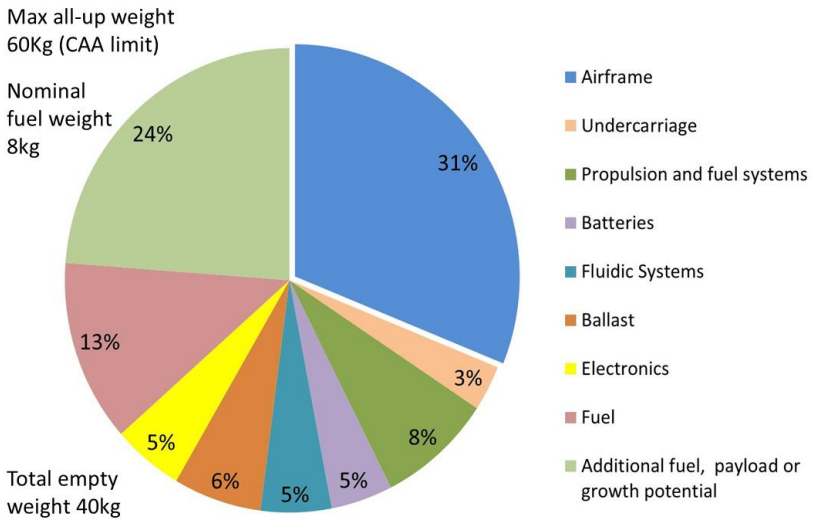

Figure 10-17: Approximate Weight Breakdown for MAGMA at 60 kg Certified Take-Off Weight.

10.5 FLIGHT TESTING

10.5.1 Safety Case

UK Civil Aviation Authority (CAA) permission was obtained for flight testing the MAGMA aircraft up to 60 kg take-off weight under extended visual line of sight operations in a controlled environment. The chosen test site was at Snowdonia Aerospace Centre, Llanbedr, in North Wales. This site provides approximately 1 km x 2 km of usable range area and a conventional three runway layout. The immediate area outside of the designated range is sparsely populated featuring mainly agricultural fields, sand dunes and sea. Flight operations were undertaken below 120^{m} (400 ft). The safety case was based on the ability to maintain the aircraft within the range test area at all times. The critical failure case was loss of radio control link. Fail safes were set up such that following loss of link for more than 2 seconds the aircraft automatically

performed a bunt manoeuvre into the ground. Additionally, if aircraft control was impaired and the aircraft was on a trajectory that would take it out of the flight zone, the pilot could initiate flight termination through turning off the transmitter. The bunt manoeuvre is initiated by a pre-programmed trailing edge down deflection of all trailing edge control surfaces. The cut-down sequence is controlled by the hardware implemented switch built into the fail-safe management system linked directly to the radio receiver on-board the aircraft. The flight and termination zones are defined in Figure 10-18.

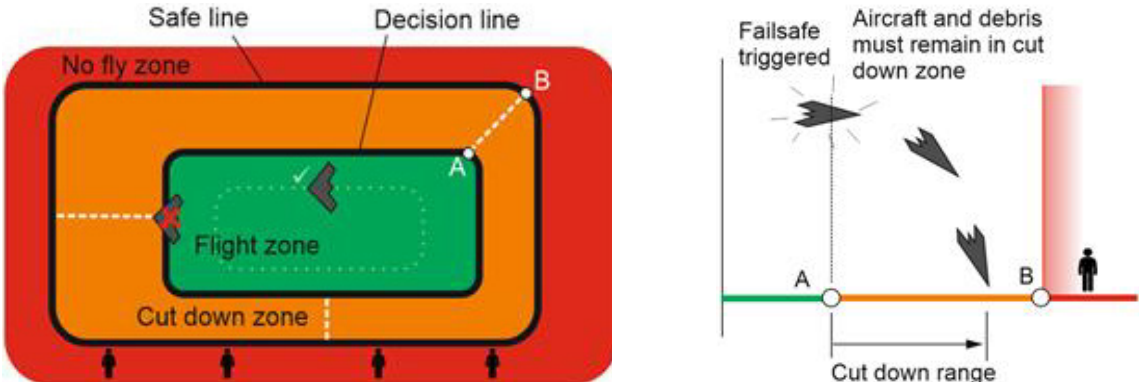

(a) Definition of Flight, Cut-Down and No Fly Zones.

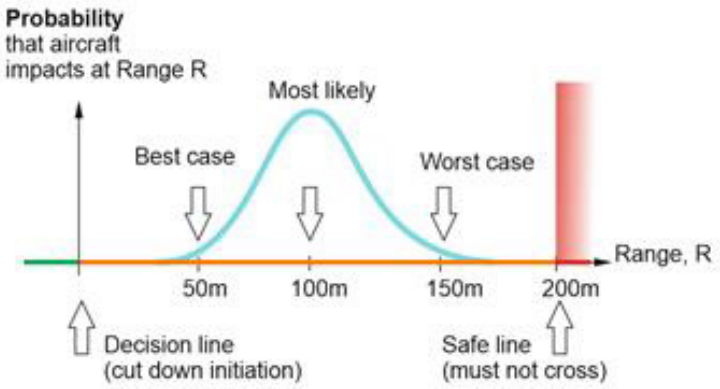

Cut-Down Zone for MAGMA Extends Beyond the Calculated Worst Case Cut-Down Distance

Figure 10-18: Definition of Flight and Cut-Down Zones for Safety Case.

Cut-down distances are defined by a Monte-Carlo type analysis using a simplified numerical model of the aircraft trajectory performance assuming a variety of initial conditions. This model incorporates allowances for decision times (nominally 2 s) and an allowance for a debris zone based on kinetic energy of impact. Cases are simulated for a wide range of initial conditions and the 'cut-down zone' defined by taking a 'worst case' assumption.

The key parameters affecting the required size of the cut-down zone were the flight speed, altitude wind speed and direction. It was found by analysis that at flight speeds much above 35 m/s and altitudes above 120 m, the available flight zone within the airfield boundary became increasing compact, with the aircraft required to be permanently turning in order to remain within the boundary. The analysis has to take into account the wind speed and direction (which adds to the ground speed) and the direction at which the boundary is approached (worst case when the approach is normal to the boundary). Ultimately, the decision line has to be decided on a flight by flight basis, dependent of prevailing wind conditions. An example flight trajectory is shown in Figure 10-19.

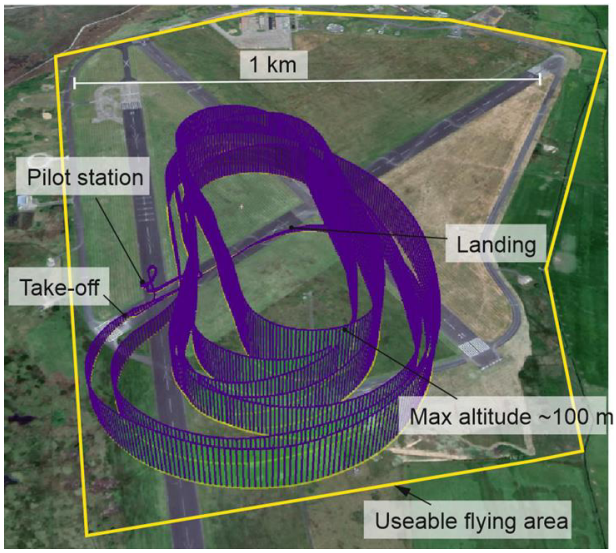

Figure 10-19: Test Range Useable Area and Typical Flight Trajectory, Snowdonia Aerospace Centre, Llanbedr. Typical values: flight speed 30 m/s, typical flight duration 8 minutes, air range 15 km.

10.5.2 Data Acquisition

The aircraft is instrumented with air data (barometric altitude, air speed and 5 hole probe data for Alpha and Beta), 3 axis IMU, GPS, servo positions, fluidic device pressure and temperature, and fuel flow. This data is recorded and stored on SD memory cards on-board the aircraft for post-flight analysis. Real-time flight data is also transmitted to a ground station during flight to allow flight trajectory (superimposed on a map) and airspeed to be monitored by the flight engineer/pilot. Sports cameras were attached to strategic parts of the airframe in order to provide visual record of control deflections, undercarriage deployment, etc., and deformation of structure under load. A tail mounted camera was also used to record in-flight data on the external aerodynamic flow via wool tufts on the wing outer panels (Figure 10-20).

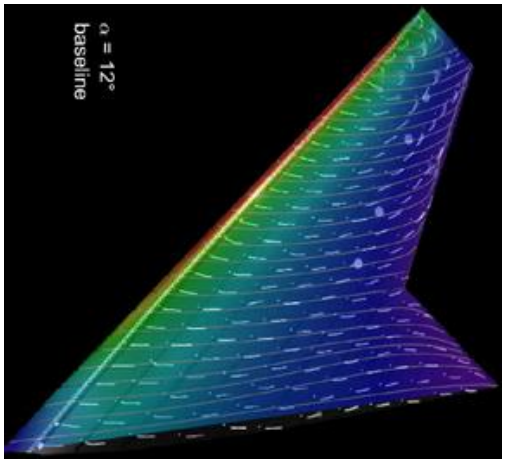

(a) Pressure and Surface Streamline from CFD, with Wool Tufts from Wind Tunnel Experiments, Alpha = 15° [6].

(b) Wool Tuft Measurements in-Flight at Approximately 5 Degrees Angle of Attack.

Figure 10-20: Initial Comparison of in-Flight Wool Tuft Measurements with Wind Tunnel and CFD Results.

10.6 FLIGHT TEST RESULTS

The MAGMA aircraft with conventional controls successfully first flew in September 2017 [15] and has subsequently flown a total of nine times over three flight campaigns. The stability and trim characteristics of the aircraft were in good agreement with the predicted values and the ground and flight handling qualities were consistent with other successful large model aircraft of similar configuration.

At the time of writing the fluidic version of MAGMA has undergone ground test trials to explore ground handling of the aircraft at higher weight and to check potential thermal issues associated with the integration of the modified jet-pipe and fluidic system components (heat-soak trials). The aircraft is expected to have its maiden flight in December 2018. Initial flights will be used to confirm aircraft performance and handling while still in conventional control mode. Subsequently, the fluidic control effectors will be tested in an incremental manner (to minimise risk). Initial fluidic tests will explore the roll effectiveness of the CC system which will then be followed by exploration of their pitch authority. Once the CC system has been successfully proven attention will then switch to exploring the pitch authority of the FTV system. Initial fluidic flights will use conventional controls for take-off, landing and turns with the fluidic systems only being switched on during straight and level flight passes. Once confidence in the fluidic control performance is gained then their use will be extended to other flight phases. The ultimate objective will be to attempt a complete flight under fluidic controls from take-off through to landing.

10.7 OVERVIEW OF TECHNICAL ACHIEVEMENTS

MAGMA has already successfully achieved many of its original objectives and is a good example of how previous experience with flight demonstrators of this type has led to a successful formula that can be applied in the future:

- The vehicle design was uniquely defined by previous experience of model-scale testing [4] which led to a design that had a low wing loading/low stall speed for ease of flight operations, had significant usable and accessible volume in the fuselage to facilitate installation of experimental flight control payloads, and freedom to flexibly locate control payloads through careful attention to mass and balance at the outset.
- Use of advanced metal ALM parts for hot and pressurised fluidic control components has increased the performance of these parts over previous conventional metal manufacture due to the ability to control very tight tolerances on slots, and has significantly reduced the weight and their impact on aircraft weight and balance.
- A key design philosophy was to only innovate when absolutely necessary. As a result the MAGMA aircraft use mainly COTS parts apart from the fluidic systems and the structure. It would have been preferable to use a conventional model engineering manufacturing processes for the structure however this did not deliver an airframe with any payload capability. Development of bespoke composite methods took considerable engineering effort and talent but delivered a uniquely useful airframe concept that can be easily reproduced and extended.
- The safety case development hinged on the reliability of radio links to the aircraft rather than the reliability of the aircraft and its systems. This approach is a key enabler for the achievement of low development costs for demonstration platforms of this type.
- The ability to take high resolution, high framerate video from very compact cameras means that in-flight recording of on- and off- surface flow visualisation is now technically feasible for a vehicle of this class.
- Line of sight testing below 120 m altitude for this class of vehicle is realistic for establishing basic handling qualities, but the need to be constantly manoeuvring and inability to recover from stall ultimately limit the scientific evaluation that can be undertaken. The next step is beyond visual line of sight testing, but this requires significant logistic and safety case development.

10.8 REFLECTIONS ON TEAM WORK AND ENGINEERING TALENT

The MAGMA project is based on an Industry – Academia collaboration that started around 15 years ago and is primarily based on Industry funded PhD projects. Success has to been down to trust on both sides – Industry lets Academia explore new ideas and run risky projects that excite and motivate people. In return, academia delivers knowledge and know-how back into Industry. The PR value of the work has been high to both Industry and Academia because the story is strong and reflects well on both stakeholders. A key element of cost reduction is that academia is able to take on much higher levels of technical risk than Industry without risk of reputational damage. Failure is an option for high risk university-based research.

Over the last three years, the MAGMA project has involved many tens of people, of which most have been PhD students working on the project in their spare time. Support from both BAE Systems and the NATO Applied Vehicle Technology panel has provided for components, materials and manufacturing, and range testing expenses, but the engineering talent largely came from individuals who worked the project because they were inspired to do so. A visual summary of the people, planes and places involved in the MAGMA project to date is shown in Figure 10-21.

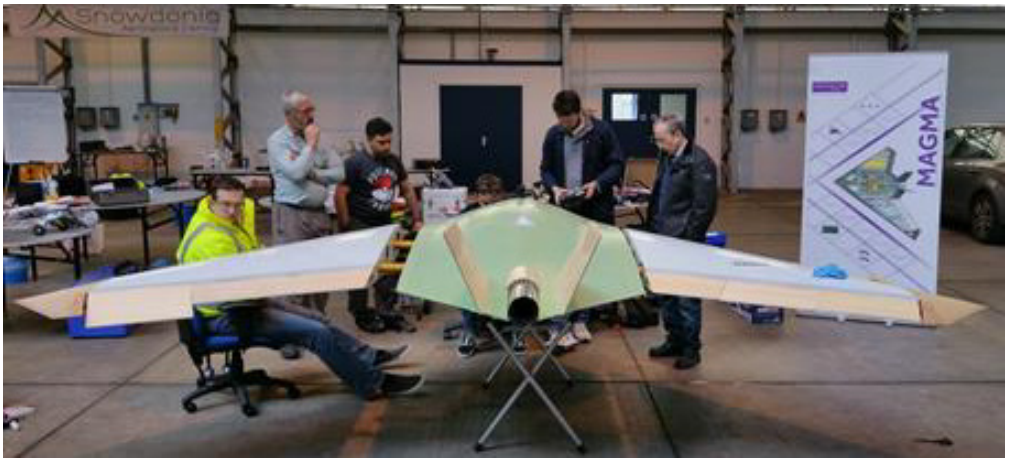

(a) MAGMA Conventional Preparation for Flight, Llanbedr, September 2017.

(b) Flight Test Team, MAGMA Conventional First Flight September 2017.

Figure 10-21: The MAGMA Project: People, Planes and Places.

(c) MAGMA Conventional Variant. Low Pass, Gear Up. Llanbedr, May 2018.

(d) MAGMA Conventional (Left) and MAGMA Fluidic (Right).

(e) Flight Testing June 2018.

Figure 10-21 cont'd: The MAGMA Project: People, Planes and Places.

(f) MAGMA, Farnborough Air Show 2018.

(g) MAGMA Conventional Topping Out Ceremony.

(h) MAGMA Fluidic Final Assembly.

Figure 10-21 cont'd: The MAGMA Project: People, Planes and Places.

10.9 CONCLUSIONS

A large-model-scale flying demonstrator has been successfully developed to apply fluidic flight control effectors (circulation control and fluidic thrust vectoring to a flying wing aircraft having a planform representative of a low observable configuration). Sub-scale flight demonstration of the technology provide a means of communicating the benefits and achievements of scientific research to a diverse audience and to provide a means of arousing and maintaining interest from sponsors who are often detached from the language of the science. They also provide data that can be used to extrapolate system performance to full-scale flight conditions and can often highlight some of the complex system integration issues that can be overlooked in simple laboratory tests.

10.10 ACKNOWLEDGEMENTS

The authors would like to acknowledge the contributions of their co-workers and of the numerous PhD students and technical staff at Manchester a University who contributions over the years made the work described in this chapter possible. They would also like to acknowledge the significant financial contribution made to the various research projects discussed herein made by BAE Systems, the University of Manchester and the NATO Collaborative Support Office.

10.11 REFERENCES

[1] Llopis-Pascual, A., Supercritical Coanda Jets for Flight Control Effectors, PhD Thesis, Manchester University, Manchester, UK, 2016.

[2] Warsop, C., and Crowther, W.J., Fluidic Thrust Vectoring and the FLAVIIR DEMON Flight Demonstration Airvehicle, in *NATO STO Symposium, Innovative Control Effectors for Military Vehicles*, STO-MP-AVT-215, Paper No 11, Stockholm, Sweden, May, 2013.

[3] Fielding, J.P., Lawson, C.P., Pires, R. and Monterzino, G., Development of the DEMON Technology Demonstrator UAV, 27th ICAS Conference, Nice, 2010.

[4] Warsop, C., and Crowther, W.J., Fluidic Flow Control Effectors for Flight Control, *AIAA Journal*, Vol. 56, No. 10, pp. 3808-3824, 2018. doi: 10.2514/1.J056787.

[5] Warsop, C., Forster, M. and Crowther, W.J., NATO AVT-239: Supercritical Coanda Based Circulation Control and Fluidic Thrust Vectoring, 2019 AIAA Aerospace Sciences Meeting, San Diego, CA, 2019.

[6] Davidson, I.M., Aerofoil Boundary Layer Control Systems, US patent office patent number US3062483 A, 1962.

[7] Chippindall, J., Geometric Optimisation of Nozzles for Supersonic Fluidic Thrust Vectoring, PhD Thesis, Manchester University, Manchester, 2010.

[8] Forster, M.J., Computational Modelling of Transonic Circulation Control, PhD Thesis, Liverpool University, Liverpool, 2017.

[9] Afilaka, O., Normal Blowing Fluidic Thrust Vectoring for Supercritical Aft-deck Convergent-Divergent Nozzles, PhD Thesis, Manchester University, Manchester, 2017.

[10] Ashley, J., Aft Deck Supersonic Thrust Vectoring, PhD Thesis, Manchester University, Manchester, 2011.

[11] Jegede, O., Dual-Axis Fluidic Thrust Vectoring of High Aspect-Ratio Supersonic Jets, PhD Thesis, Manchester University, Manchester, 2016.

[12] McParlin, S.C., Bruce, R.J., Hepworth, A.G., and Rae, A.J., Low Speed Wind Tunnel Tests on the 1303 UCAV Concept, AIAA-2006-2985, 2006.

[13] ESDU 01005: Effect of Geometry on Low Speed Pitch-Break Characteristics of Swept Wings, IHS ESDU, 2001.

[14] Phillips, E., Jentzsch, M., Menge M., Forster, M., Taubert, L., and Wygnanski, I., On the Use of Active Flow Control to Change the Spanwise Flow on Tailless Aircraft Models, Thus Affecting their Trim and Control, paper submitted to AIAA 2019 Scitech, January, 2019.

[15] Crowther, W.J., First Flight Video online at https://www.youtube.com/watch?v=q2XjZobD_Qg. 23 October 2017.

Chapter 11 – FLIGHT DEMONSTRATION OF AFC ON THE ICE/SACCON DEMONSTRATOR AIRCRAFT

Steven S. Brandt and Thomas E. McLaughlin
United States Air Force Academy
UNITED STATES

David R. Williams
Illinois Institute of Technology
UNITED STATES

Brock H. Crawford and Jason A. Holmes
United States Air Force Academy
UNITED STATES

11.0 NOMENCLATURE

B	Span	Re_c	Reynolds number based on mean aerodynamic chord
C_μ	Momentum coefficient, $\frac{\dot{m}_{jet} \cdot V_{jet}}{q.S}$	$\bar{c}$	Mean aerodynamic chord
$C_{l,m,n}$	Roll, pitch, yaw moment coefficients	S	Planform area
$C_{L,D,Y}$	Lift, drag, side force coefficients	V	Freestream speed
C_{L0}	Lift coefficient at $\alpha = 0$	V_{jet}	Velocity of actuator jet
$\dot{m}_{jet}$	Mass flow rate through actuator	α	Angle of attack
q	Dynamic pressure, $0.5\rho V^2$	β	Side slip angle

11.1 OVERVIEW

The Innovative Control Effector (ICE) program was designed to expand the capability and survivability of modern stealth aircraft. Aircraft survivability can be jeopardized by actuation of control surfaces. The ICE program was executed to incorporate blown air actuators into an aircraft design, enhancing survivability in future aircraft. ICE uses bleed air from the aircraft's turbofan or turbojet engine to supply strategically placed actuators along the length of the aircraft. Through differential blowing, moments can be generated about the aircraft similar in manner to conventional controls. ICE is a new system and proving its validity on an actual aircraft design requires many steps. First, suitable test platform foam aircraft were constructed through the USAFA Department of Aeronautics. Secondly, the aircraft stability and control characteristics were understood and refined through a subscale flight test program using both foam and carbon fiber variants with conventional elevon controls. Blown actuation was tested on a single aircraft using a compressed air system to validate predictions of roll and yaw control power and basic controllability of the ICE system. Thirdly, a subscale Hawk 240R jet engine powered aircraft was built in order to incorporate the ICE system of two apex (yaw) actuators and two trailing-edge (roll and pitch) actuators sourced with engine bleed air. This aircraft was the same scale as the foam test aircraft and was rigorously ground tested. Flight tests of the jet aircraft were not completed due to safety of flight issues discovered during the build-up flights with a jet powered conventionally controlled aircraft. The focus of the remaining flight tests, therefore, was on determining from the foam aircraft and compressed air blowing if control power derivatives could be derived. Control power derivatives for roll and pitch were not able to be calculated using a mapping scheme from conventional elevon control power derivatives identified during captive aircraft mobile ground tests due to the excessive instability of the ICE aircraft in the roll axis. Yaw control through the apex actuators was not attempted. The static and captive test results demonstrate there is measurable and effective control power in all axes, but although validation of this assertion and control power derivative calculations from flight test with compressed air actuations were attempted, definitive results were not achieved.

11.2 INTRODUCTION

The flight test component of the NATO task group AVT-239 investigating the application of innovative control effectors to the ICE/SACCON unmanned aircraft is discussed. Flight test data was acquired from two different platforms; namely, the MAGMA and the ICE/SACCON hybrid, for the purpose of assessing the validity of wind tunnel measurements and numerical simulation results of the active flow control effector control derivatives. The MAGMA aircraft developed by BAE Systems and the University of Manchester uses thrust vectoring and supersonic circulation control effectors for pitch, roll, and yaw control on the UAS. The ICE aircraft built by the US Air Force Academy (USAFA) and the Illinois Institute of Technology (IIT) uses adjustable strength slotted jets at the apex and trailing edges for AFC flight control effectors. This flight vehicle has the 65° sweep planform taken from the Lockheed Martin ICE-101 [1] with profiles taken from the NATO SACCON design [2]. Both aircraft are designed to use the Hawk Turbine 240R gas turbine engine for propulsion and bleed air supply.

The Active Flow Control (AFC) system consists of pairs of slotted jets located near the nose (apex) of the aircraft and at the trailing edges. Bleed air from the aircraft engine compressor supplies the slot jets with compressed air. The apex control effectors are used primarily for yaw control, while the trailing edge control effectors are used for roll and pitch control.

The aerodynamic and control derivative data were acquired with a static model in the USAFA subsonic wind tunnel and in the numerical simulations [3]. In reality, the aircraft are required to maneuver and compensate for external disturbances during flight, and the associated unsteady aerodynamic effects can change the performance of the active flow control effectors. The unsteady aerodynamic effects appear in different ways, such as, time delays in the aircraft response to control input, and large deviations of transient forces relative to by dynamic stall vortices. Flight tests provide the next level of validation for a new control effector approach to the flight control system by introducing realistic aircraft dynamics into the program. The challenge is to obtain accurate quantitative measurements of the control derivatives from the flight test data that can be compared with the wind tunnel and numerical simulation results.

The primary goal of the flight test program is to acquire the stability and control data from a 1:7 scale ICE aircraft using AFC pneumatic control effectors. The flight test data will be compared to the wind tunnel data presented by Williams, et al. [3] to assess the level of accuracy in the wind tunnel tests. The control derivatives for the comparison are reproduced in Table 11-1.

Table 11-1: Stability and Control Derivatives at α = 4° [3].

	$C_{x,\beta}$	$C_{x,C_{\mu_{apex}}}$	$C_{x,C_{\mu}}$	$C_{x,TEup}$
Roll Cl	-0.049	-0.205	-0.429	-0.44
Yaw Cn	-0.0115	0.624	0.214	-0.463
Side CY	-0.019	1.57	2.14	-0.735
Pitch Cm		-0.220	-0.026	1.56

Section 11.3 describes the details of the extensive and diverse experimental methods. The measurements obtained in experiment are presented in Section 11.4. The conclusions are reviewed in Section 11.5.

11.3 TEST PLATFORMS

An incremental approach to increasing the level of aircraft complexity was used for risk management throughout the flight test program. Foam models 1:10 and 1:7 scale of the ICE aircraft were built with

conventional elevon control effectors, and used to learn basic aircraft control and the performance and flying qualities of the aircraft with conventional controls. Initially the models were mounted on an instrumentation sting on the top of a pickup truck, and driven down the runway under controlled conditions. The pitch and roll moments produced by both conventional and active flow control effectors were measured.

The foam models and one carbon fiber model were powered with electric ducted fan motors, which are low cost, light weight, and safer initially than the heavier jet powered aircraft. Two jet engine powered aircraft have carbon fiber skins, and one has conventional controls only for jet powered flight training, and the other has both conventional and active flow control effectors. The 1/7th scale carbon fiber, fully configured ICE model on the runway at the USAFA Aardvark UAS facility is shown in Figure 11-1. Dimensions of the 1/7th scale models are a centerline chord c = 1.75 m (69 in.) and the span is b = 1.52 m (60 in.). Note that although the NATO task group was concerned with tailless aircraft, two vertical stabilizers were installed for directional stability in the initial part of the flight test program. The rudders will be used to measure yaw moments produced by the active flow control effectors.

Figure 11-1: 1/7th Scale Carbon Fiber ICE Vehicle with AFC and Conventional Control Effectors.

The ICE aircraft uses the 3DR Pixhawk mini autopilot and data acquisition system with Ardupilot software for flight control.

In addition to the multiple aircraft, a captive carry sting instrumented with an ATI Industries Axia80[4] six DOF force and torque sensor with dynamic range switching, shown in Figure 11-2 [4] below, was designed and fabricated to support the ICE system test under both static and dynamic conditions. The system was mounted on top of a Ford F350 pickup truck. A variable angle of attack interface plate was designed for mounting the ICE aircraft to the fixed sting at zero degrees of sideslip, at the C.G., and at five unique angles of attack depending on the shape of the interface plate. The interface system is show in Figure 11-3.

The system was used both statically on thrust checks for the initial aircraft designs and for static ICE forces and moment quantification with the HAWK 240R powered ICE aircraft. The truck mounted system was also used for captive carry dynamic measurements of the roll and pitch axis control power. Figure 11-4 shows the output of the Axia80 in the phase check record at 125 Hz sample rate. Each axis is represented by the force and torque measurements delineated in the boxes. This entire mobile test system is further explained in Crawford and Berson et al. [5]

(a)

Loading Characteristics	Fxy	Fz	Txy	Tz
Rated Range 0	500 N	900 N	20 Nm	20 Nm
Rated Range 1	200 N	360 N	8 Nm	8 Nm
Overload Rating	2500 N	4500 N	100 Nm	100 Nm
Effective Resolution	0.1 N	0.1 N	0.005 Nm	0.005 Nm

(b)

Figure 11-2: (a) Axia80 Force/Torque Sensor and (b) Rated Ranges [4].

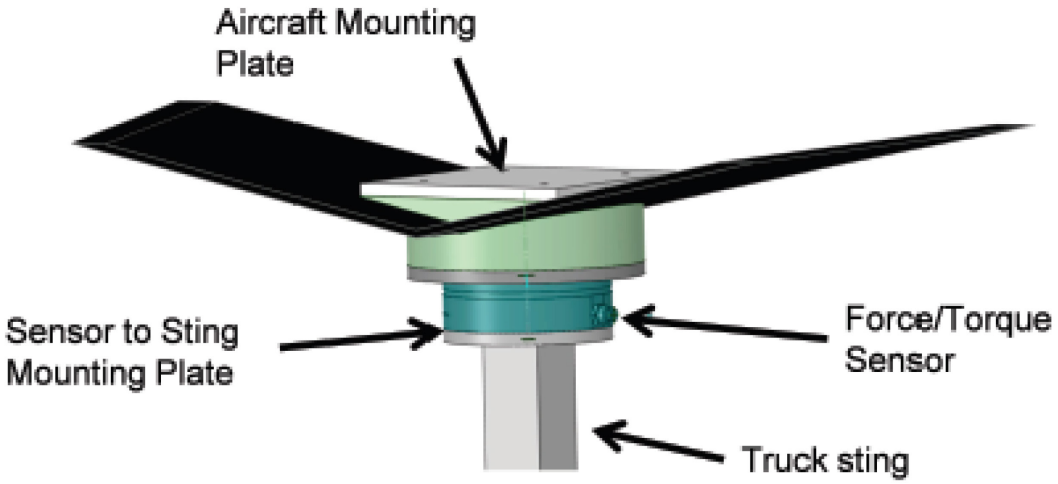

Figure 11-3: Aircraft to Test Sting Interface Design.

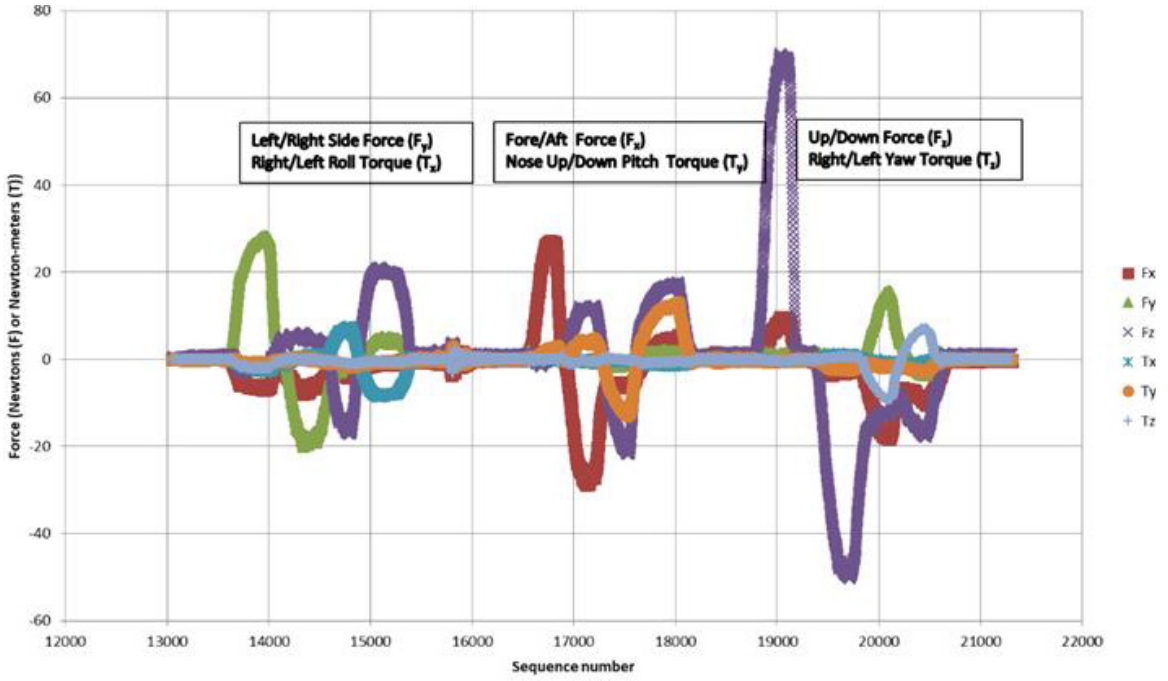

Figure 11-4: Axia80 Force/Torque Sensor Phase Plot All Axes.

11.3.1 AFC System Development

Experiments were done at IIT in 2017 to design, build, and test the active flow control effector and bleed air system for flight control. High pressure bleed air was provided by a Hawk Turbine 240R gas turbine. The Hawk Turbine provides up to 10 percent of the core mass flow for bleed air. The bleed air pressure ratio is 4.3 when the engine operates with 198 N of thrust at 128,000 RPM.

Variable strength slotted blowing actuators are used as the control effectors. Two pairs of actuators are installed in the aircraft. One actuator pair was positioned at the apex of the model, noted as Apex Right (AR) or Apex Left (AL), for yaw control, and a second pair at the outboard trailing edge, noted as Trailing Edge Left (TEL) or Trailing Edge Right (TER), are used for roll and pitch control as shown in Figure 11-5(a). Internal high temperature tubing connected the actuators to the bleed air supply line from the engine can be seen in Figure 11-5(b). The airflow rate was controlled by two radio-controlled sleeve valves as shown in Figure 11-5(c).

Measurements of the AFC effector system gage pressure and its dependence on engine rpm are shown in Figure 11-6(a). In wind tunnel experiments the maximum actuator supply pressure was 15 psig (103 kPa gage). The engine provides that pressure at 100,000 rpm. The flow rate from Figure 11-6(b) corresponding to the absolute pressure 26 psia (179 kPa) is approximately 0.02 kg/s.

11.3.2 Control Derivative Identification

The planned approach to measuring the control derivatives is to first establish steady, level flight, and then balance AFC control input with ‘calibrated’ elevon and rudder control effectors. For example, the right wing trailing-edge AFC control effector will be activated. The flight controller (in FBW-A mode) will use the elevons to compensate for the roll disturbance. The amount of elevon deflection will be an indirect measure of the AFC control authority. In Figure 11-7 the roll moment produced by the trailing-edge AFC effector is shown by the blue line. Positive C_μ corresponds to right side actuation and negative C_μ is left side actuation. The AFC control derivative is $dC_l/dC_\mu = -0.44$. Roll moment data obtained from an ICE-101 flight simulator

are also plotted for four different left elevon deflection angles. The conventional elevon control derivative is $dC_l/d\delta_e = -0.0002 deg^{-1}$. Therefore, the expected left elevon deflection required to compensate for right side AFC $C_\mu = 0.005$ will be approximately 10 deg.

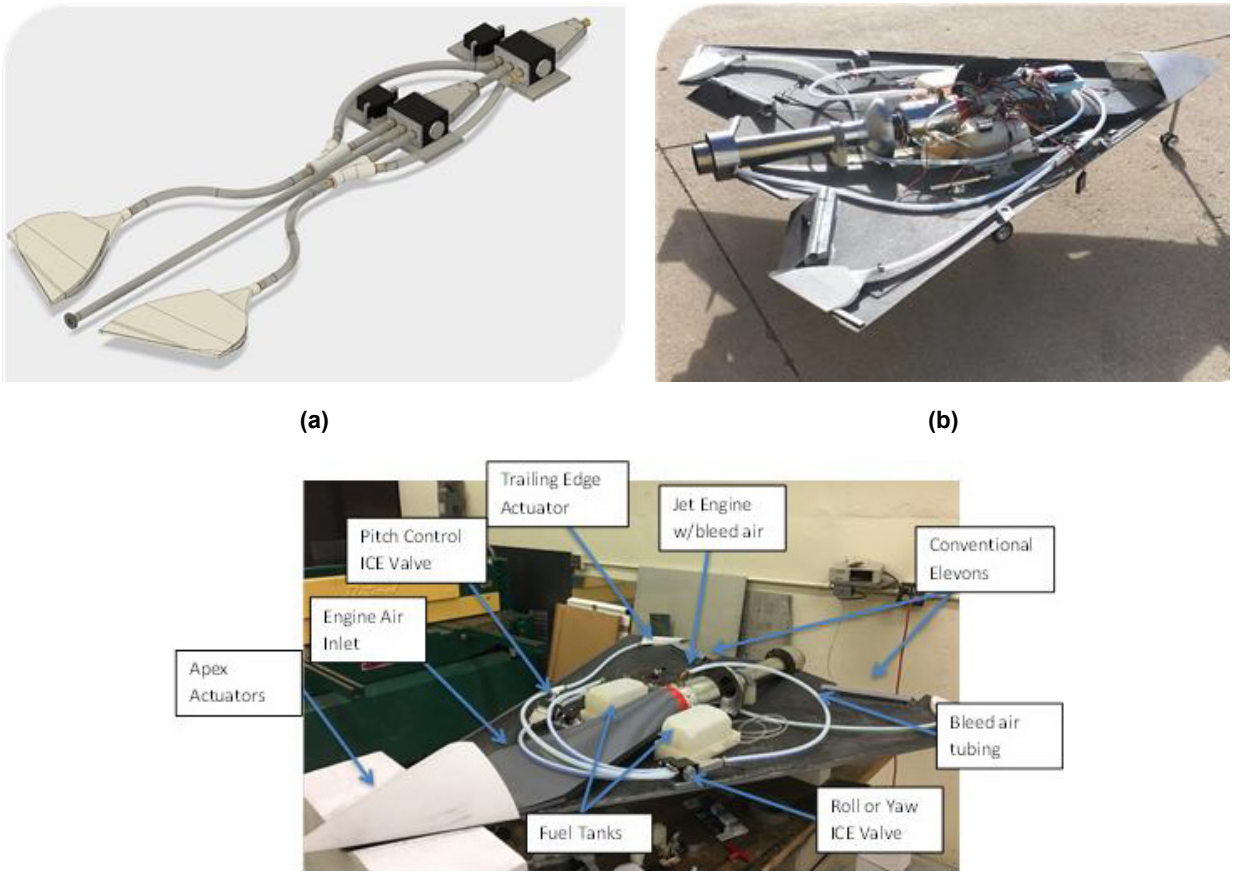

Figure 11-5: ICE (a) Trailing-Edge Control Effector System; (b) Interior View of Components (c) Component Detail.

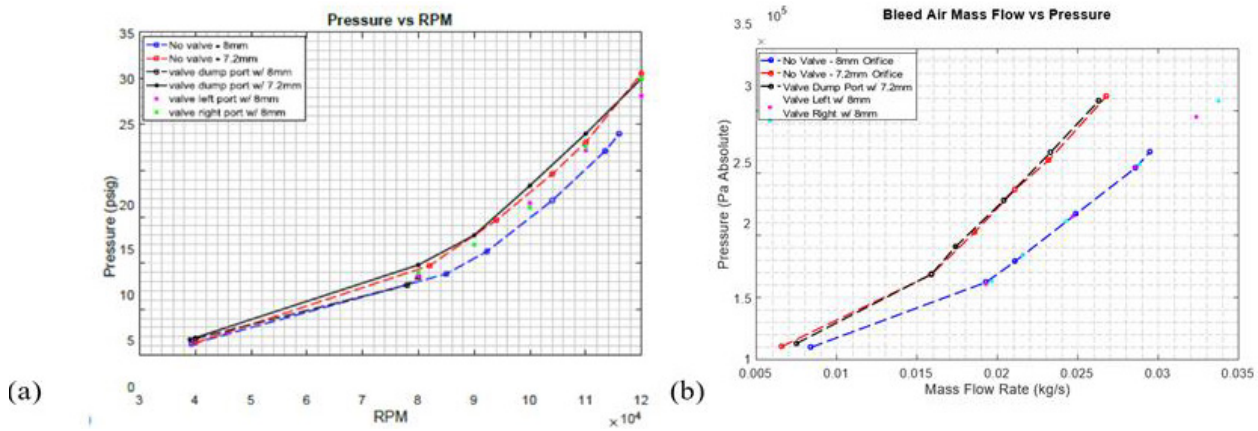

Figure 11-6: Hawk 240R (a) Bleed Air Gage Pressure vs. Engine rpm and (b) Bleed Air Flow Rate vs. Pressure.

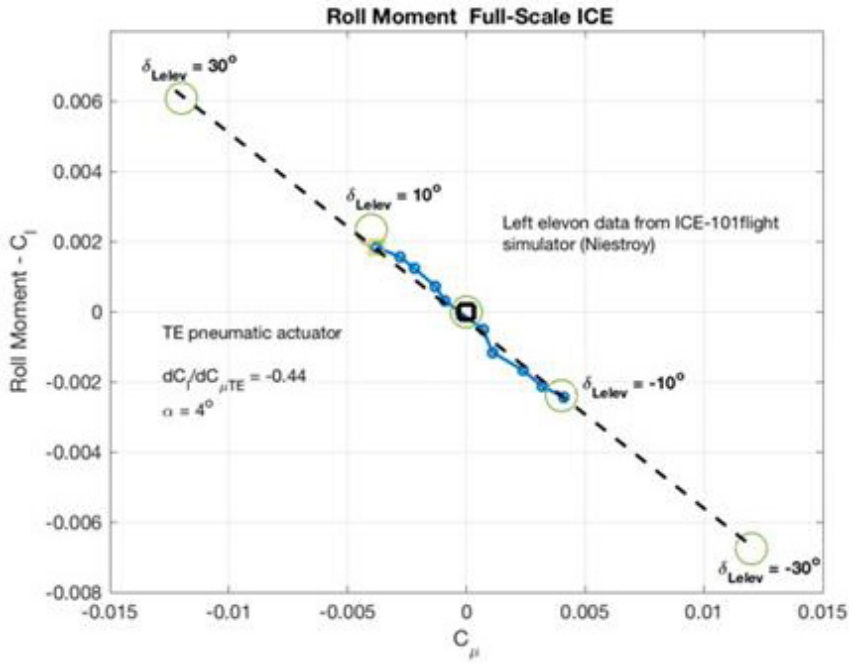

Figure 11-7: Rolling Moment Comparison Between AFC and Conventional Elevons.

11.4 RESULTS

The results of the investigation into innovative control effectors effectiveness for aircraft control are multifaceted. First, the captive carry measurements of the conventional control effectors control power will be presented which were to serve as the baseline for the calculation of the control power of the air jet actuators. Secondly, the captive carry measurements from compressed air actuated innovative control effectors will be presented to provide an initial assessment of air jet actuated control power. Static forces and moments generated by the jet bleed air powered ICE will also be presented for comparison and lastly, ICE aircraft flight test observations and data with both and conventional elevon control and compressed air actuated control attempts will be presented.

11.4.1 Conventional Control Effectors

The roll and pitching moments generated by the conventional control effectors were measured on a carbon fiber ICE aircraft on an instrumented sting above a pickup truck at 5 deg AoA, and at three different stabilized airspeeds of 25, 33 and 41 knots (approximately 30, 40 and 50 mph). Measurements of the roll moment produced by the ICE model using conventional differential elevon control are shown in Figure 11-8. Three time-series plots are shown for three different speeds. The maximum elevon deflection is δ_e = + 25°. A roll right command was followed by a roll left command. The magnitude of the roll moment scales reasonably well with the dynamic pressure and span of the aircraft.

Measurements of the pitching moment produced by the ICE model using conventional elevon controls are shown in Figure 11-9. The time-series plot of full nose up then nose down pitching moment coefficient for 40 mph is shown. This data show the change in pitching moment, C_m, with elevator angle, δ_e, is +0.0024 deg^{-1}. With no control deflections, shown in the baseline moments versus time in Figure 11-10, as the aircraft accelerates on the truck sting to the target speed, an increasing nose down pitching moment in developed since the AoA is fixed until the aircraft speed stabilizes at approximately the 80 second mark. Increasing value in the T_y (pitch) moment is a pitch down. This plot also clearly shows the roll

sensitivity and coupling of the aircraft to any yaw deviations. A small sideslip generated yaw moment, T_z, of just up to 0.5 N-m created a nearly 3.0 N-m roll moment as shown in the boxed area. This effect will create significant flight test complexities. Additional all axis moment captive data at different velocities are presented in Figure 11-11, Figure 11-12 and Figure 11-13.

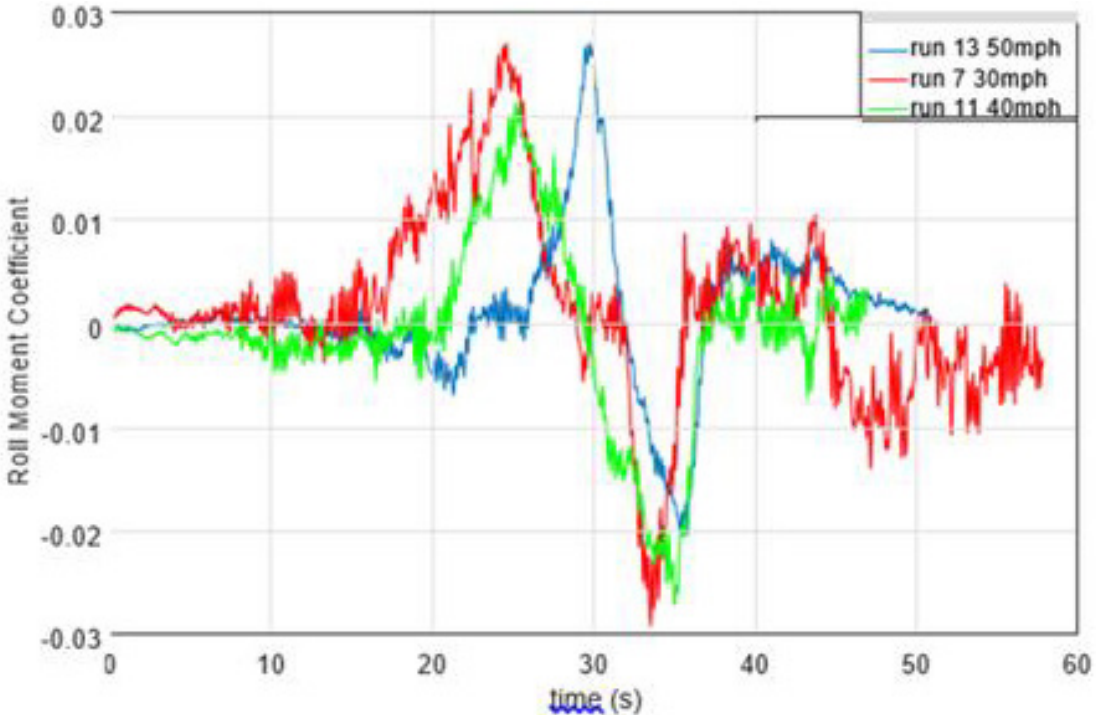

Figure 11-8: Rolling Moment Variation with Conventional Elevons at 5 deg AoA.

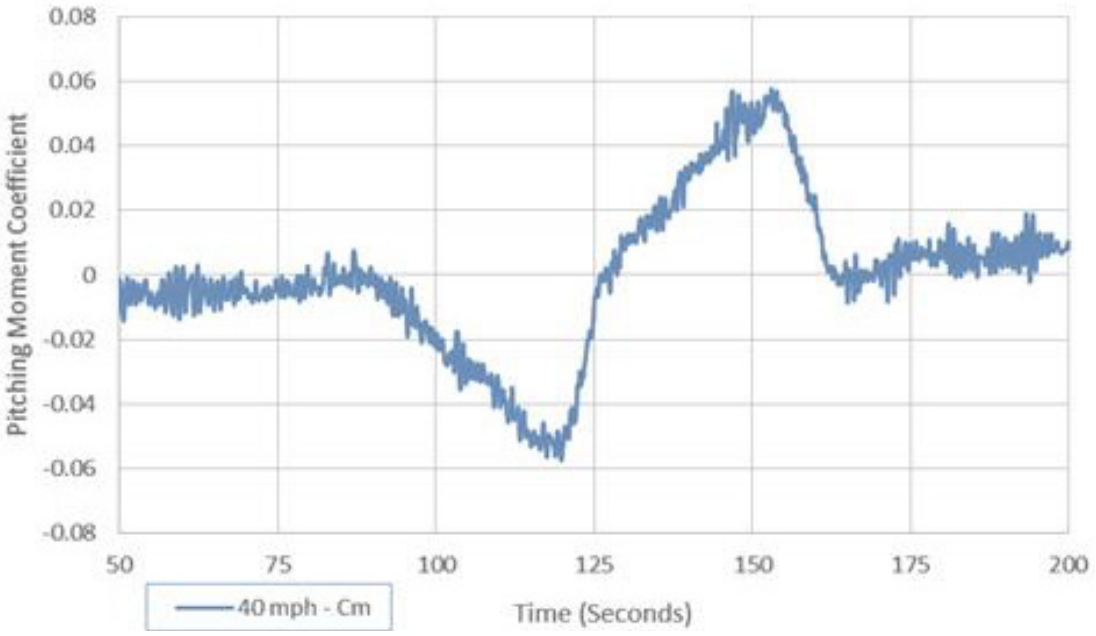

Figure 11-9: Pitching Moment Coefficient, C_m, Variation with Conventional Elevons at 5 deg AoA.

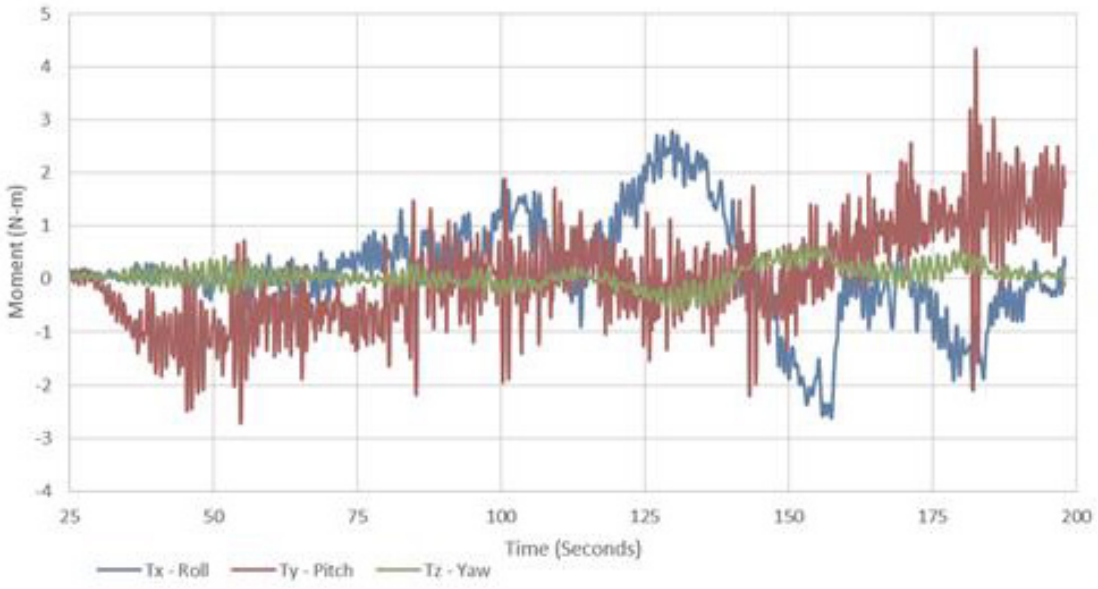

Figure 11-10: Baseline Aircraft Moments with No Control Actuations – 40 mph, 5 deg AoA.

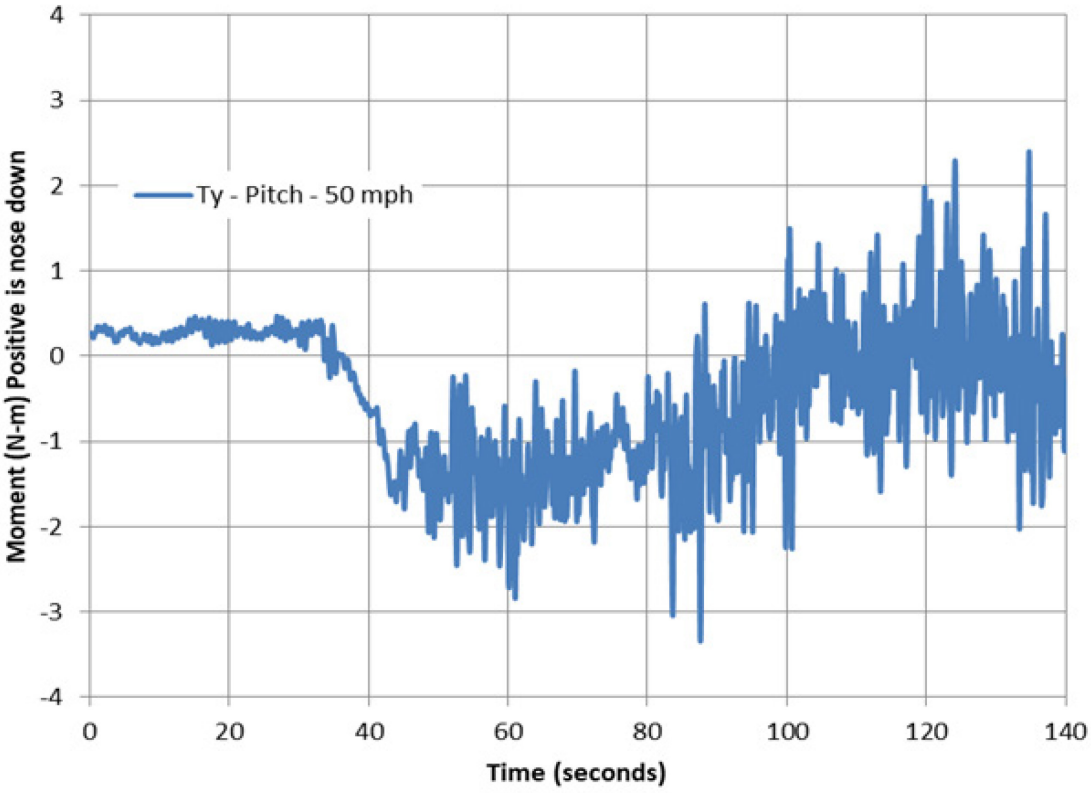

Figure 11-11: Rolling Moment Variation with Conventional Elevons at 50 mph.

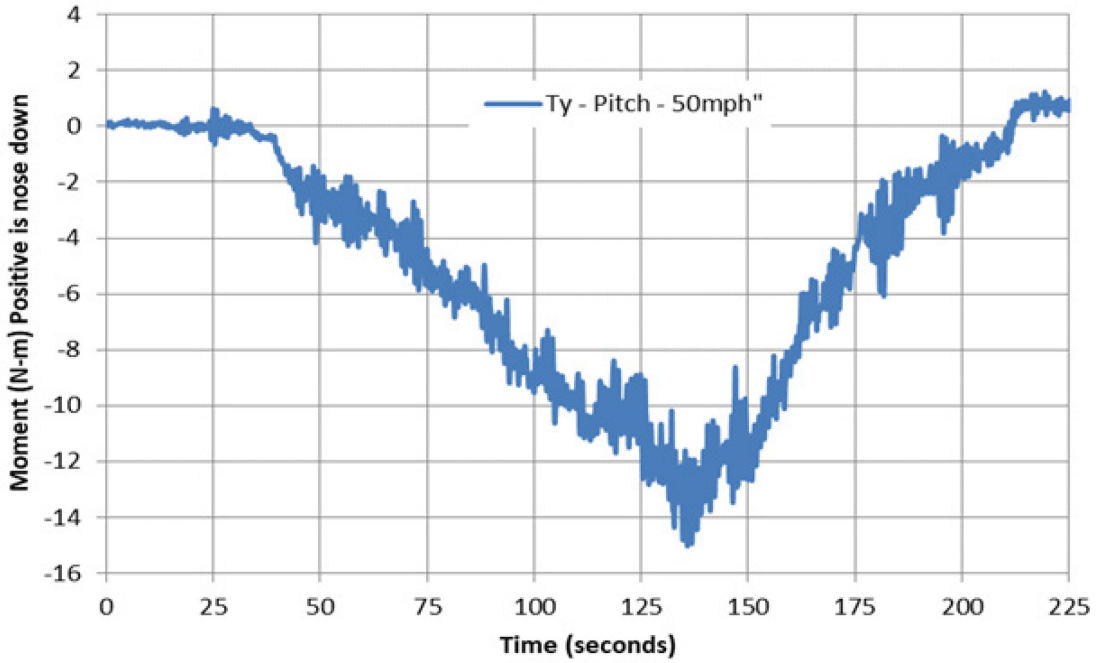

Figure 11-12: Pitching Moment Variation with Speed Accel to 50 mph.

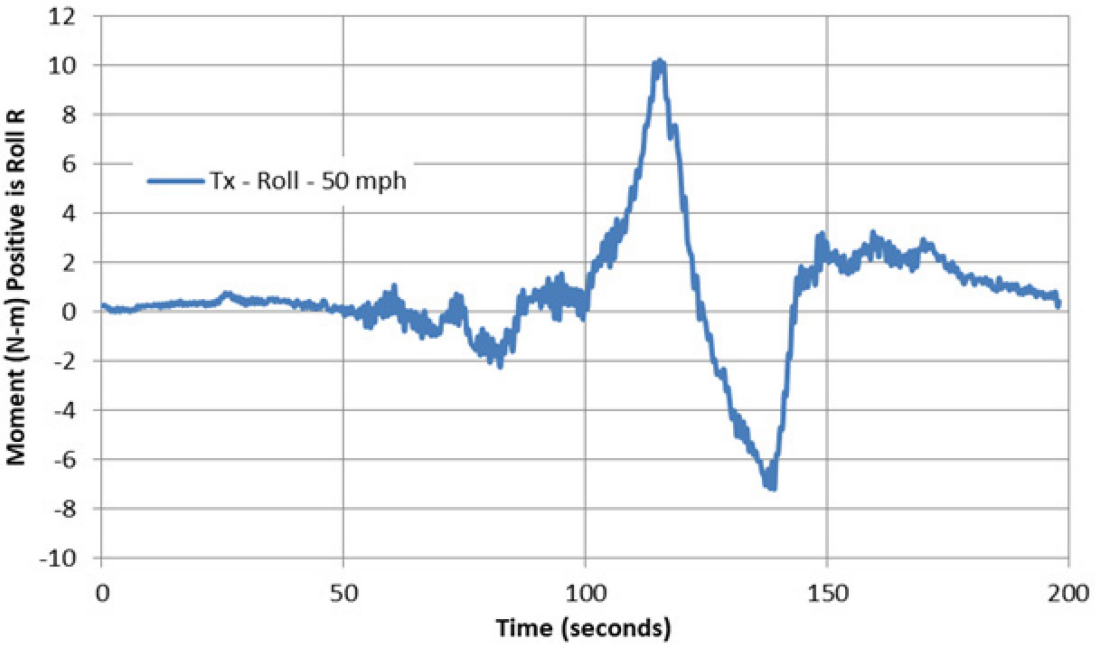

Figure 11-13: Pitching Moment Variation with Full Nose up Elevon Deflection and Hold – Accel to 50 mph.

11.4.2 Compressed Air ICE

The roll, pitch and yaw forces and moments generated by the apex and trailing-edge actuators were measured using the same captive carry experimental setup as the conventional controls, but with the addition

of a compressed air source to feed the air to the ICE. Similar speeds of approximately 22, 27 and 31 knots were driven, but for the ICE data, five different angles of attack were used by mounting the ICE aircraft at each of the fixed angles. This was achieved through an angled mounting plate on the top of the test sting, as shown in Figure 11-3 previously. AoAs of 0, 2.5, 5, 10 and 15 degrees were tested to investigate the effect of AoA on ICE effectiveness. The mass flow rate of air was limited by the size of the air compressor, however adequate air flow was achieved to provide measurable yaw and rolling moments. Pitching moments by blowing both trailing-edge actuators were not measureable, directly due to inadequate air mass flow rate and pressure to feed both actuators simultaneously. This data was presented by Crawford and Berson et al [5], at USAFA. The series of plots below in Figure 11-14 and Figure 11-15 depict baseline yaw and roll moments with no jet actuations, and apex right and trailing-edge left actuations at two angles of attack. These data clearly show there is measurable moment generation by the ICE in roll and yaw. Figure 11-14(c) and Figure 11-15(c) also show the coupling of yaw-to-roll with an AR actuation. These data provided the initial control power measurements which would be used to predict free flight behaviour of the aircraft during an ICE actuation. Actuation times of the ICE are highlighted in the boxes on the right two charts.

Crawford and Berson et al [5], also expound on the relationship between control power and mass flow rate through the ICE. There was a measurable difference between the moments generated by two air mass flow rates through the actuators. This directly correlates to the control power variation of a conventional controller as it sweeps through its full deflection angle as discussed previously. The calculated coefficients of roll, pitch and yaw moments as a function of air volume flow rate (SCFM) and angle of attack are depicted in the Figure 11-16.

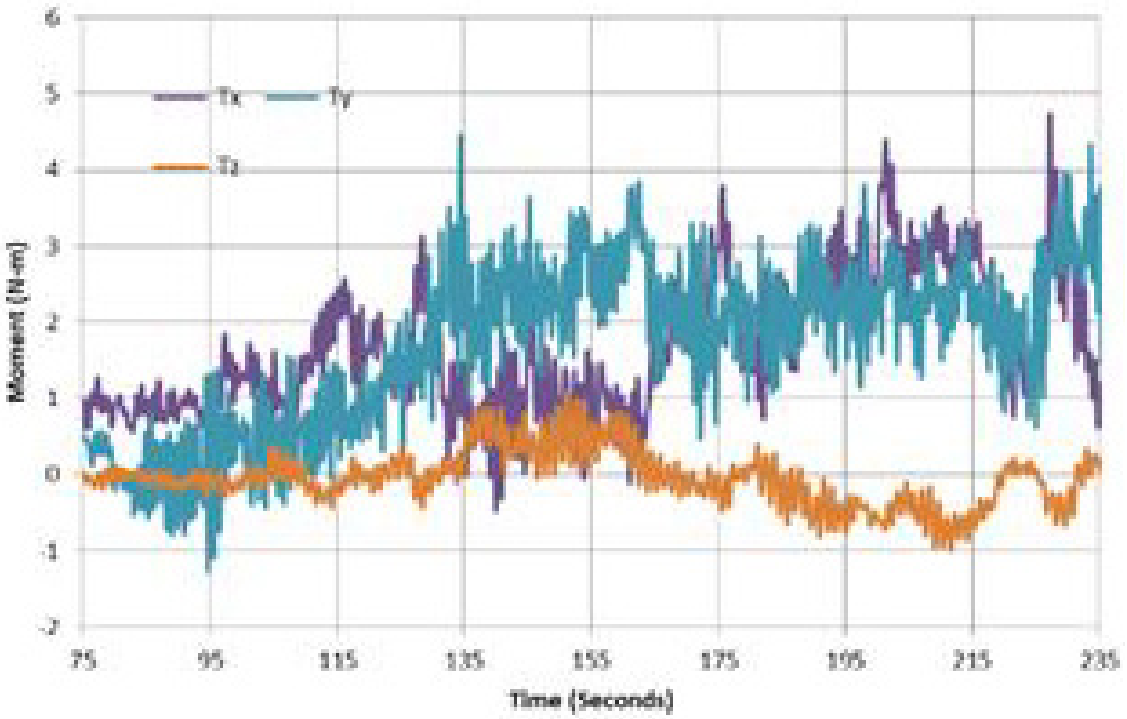

(a)

Figure 11-14: (a) Captive Baseline and Compressed Air (b) TEL and (c) AR ICE Actuation Moment Data 2.5 deg AoA, 31 kts.

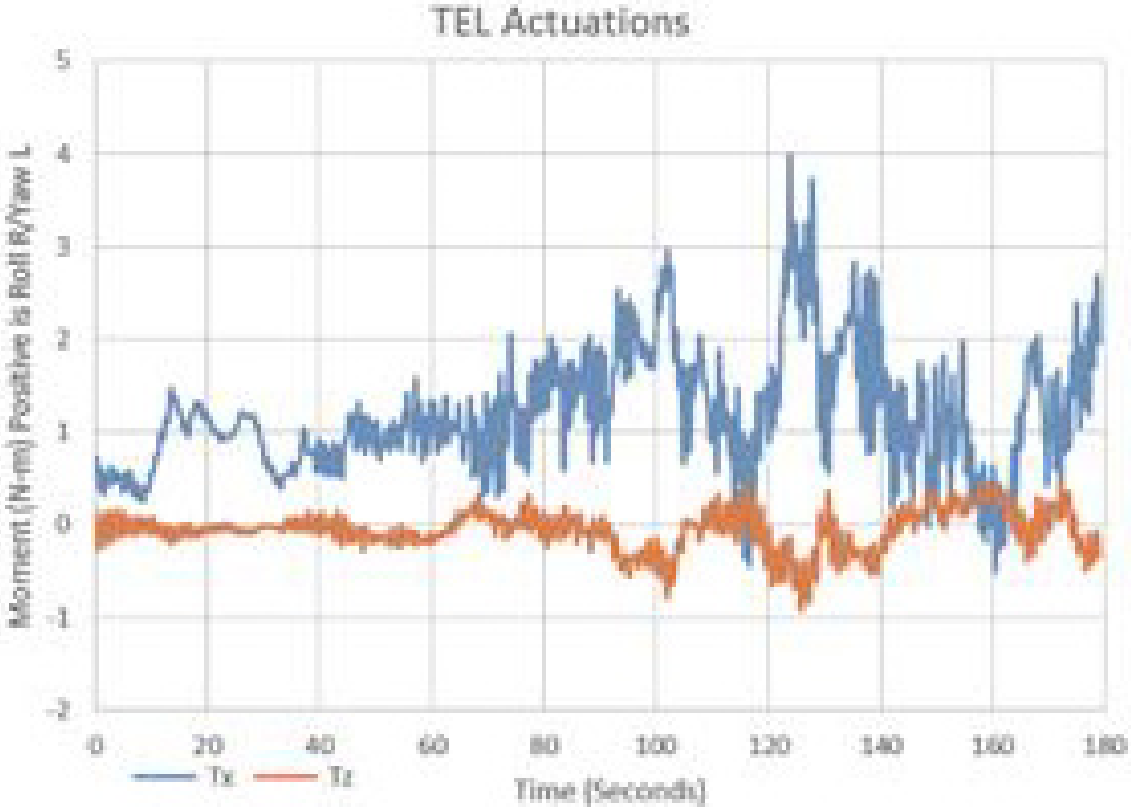

(b)

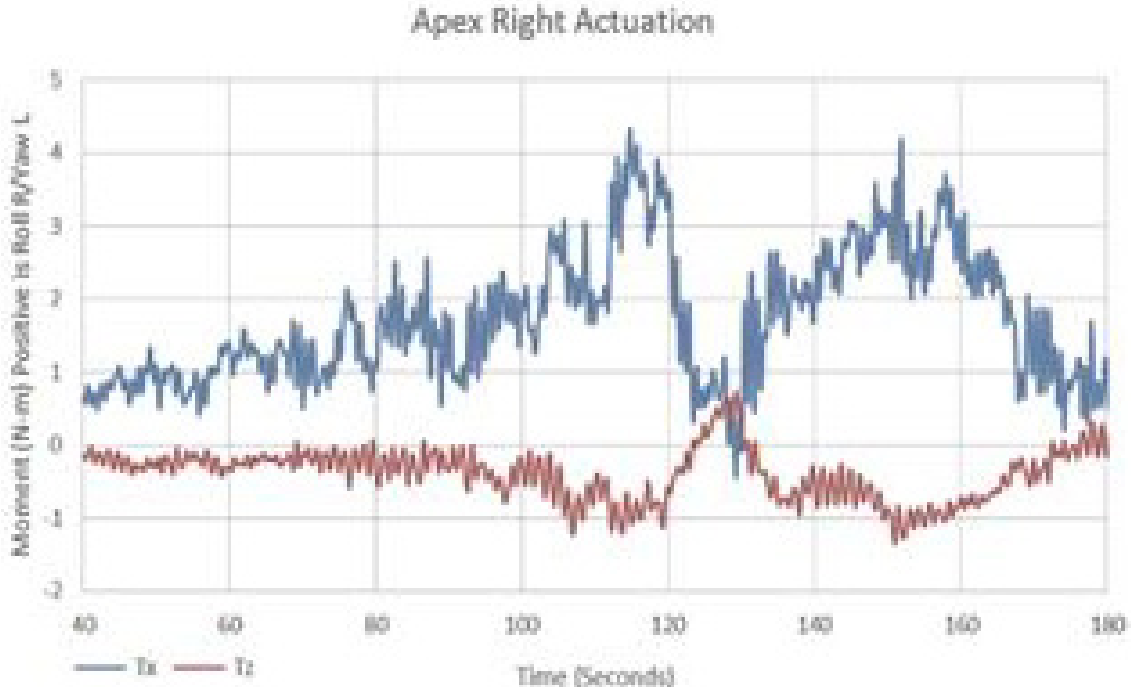

(c)

Figure 11-14 cont'd: (b) TEL and (c) AR ICE Actuation Moment Data 2.5 deg AoA, 31 kts.

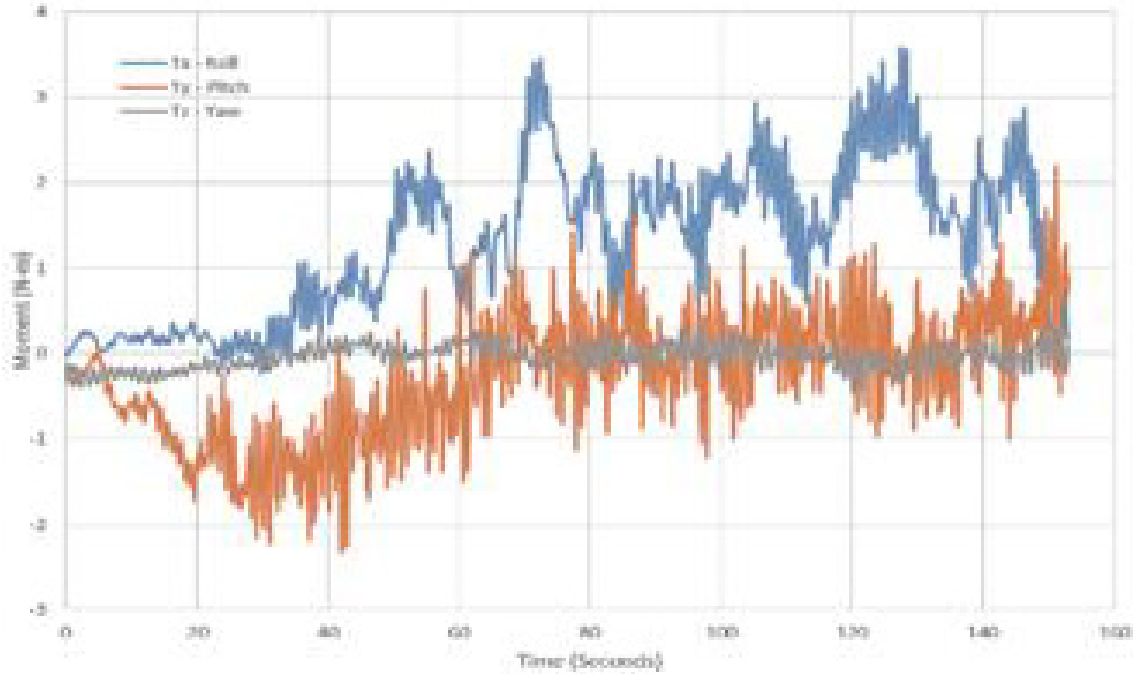

(a)

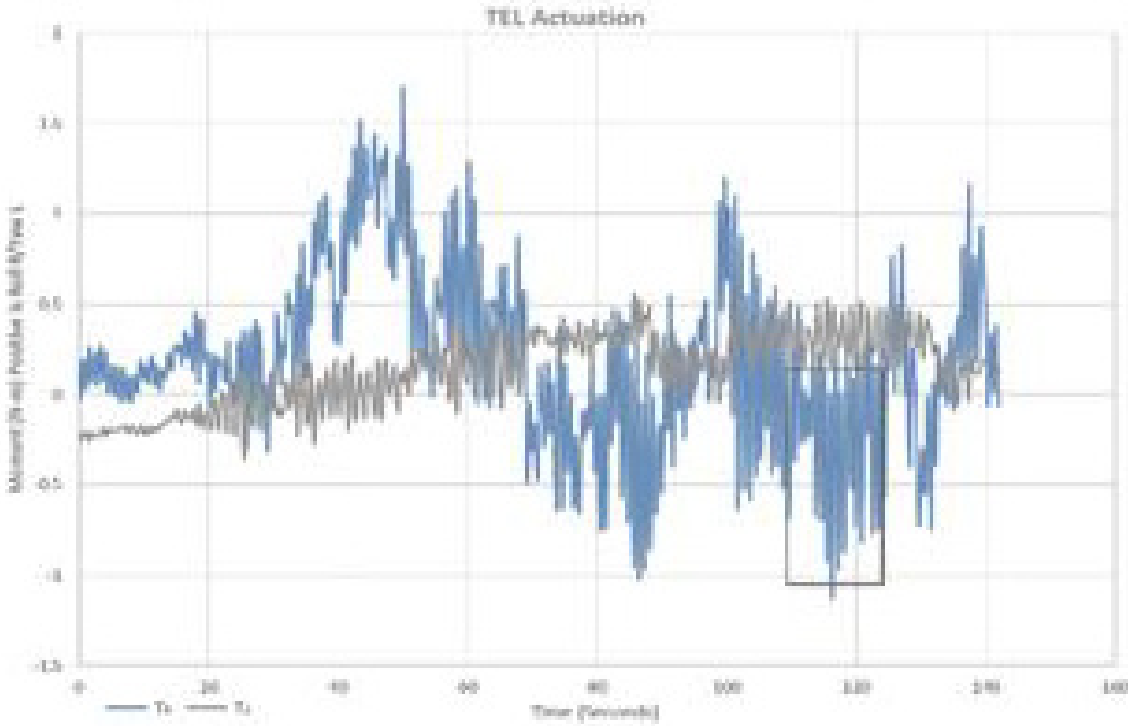

(b)

Figure 11-15: (a) Captive Baseline and Compressed Air (b) TEL and c) AR ICE Actuation Moment Data 5 deg AoA, 31 kts.

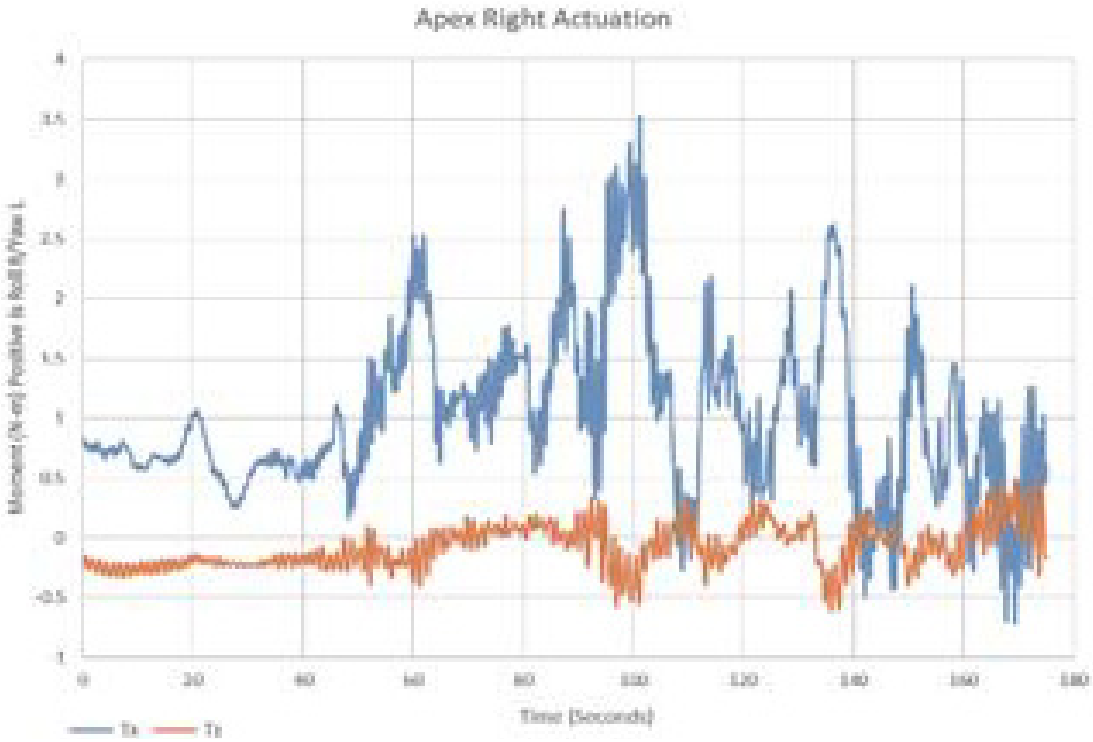

(c)

Figure 11-15 cont'd: c) AR ICE Actuation Moment Data 5 deg AoA, 31 kts.

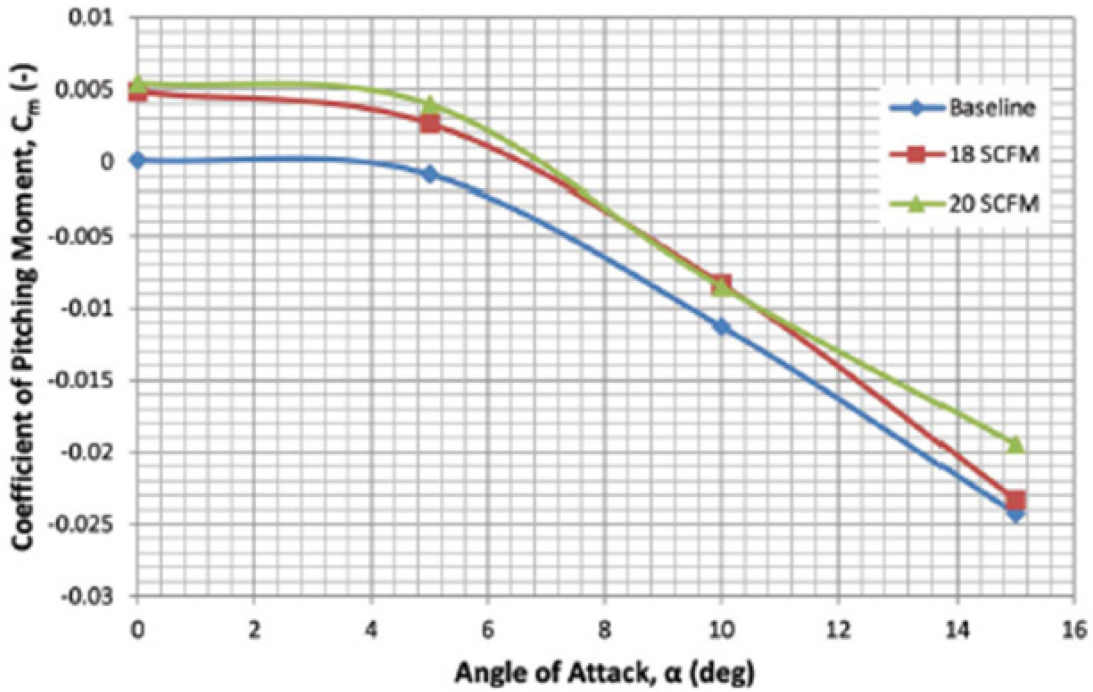

(a) Pitching Moment.

Figure 11-16: Moment Coefficient Variation with One Trailing-Edge Effector with 2 Air Flow Rates [5].

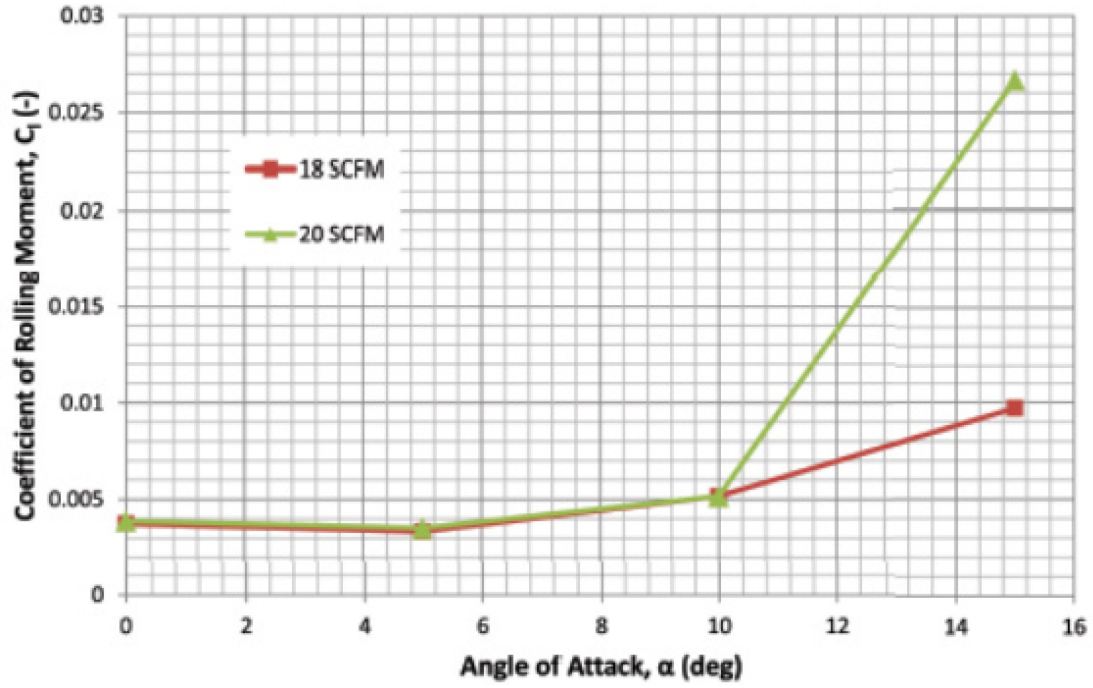

p

(b) Rolling Moment.

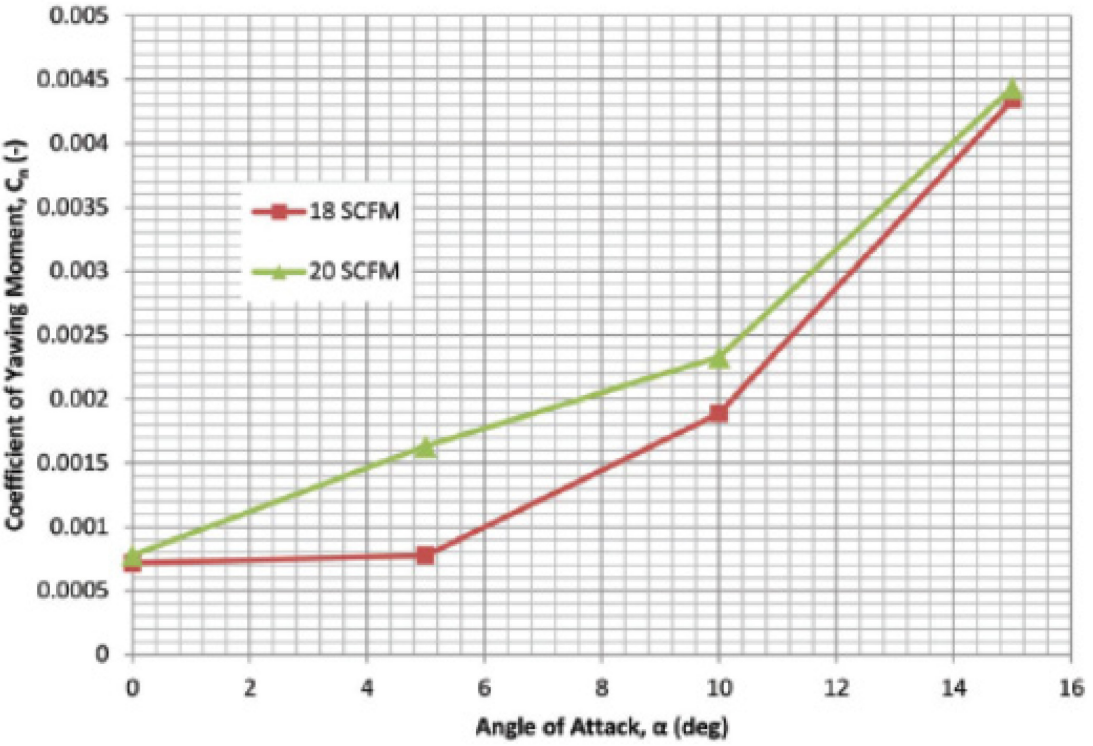

(c) Yawing Moment.

Figure 11-16 cont'd: Moment Coefficient Variation with One Trailing-Edge Effector with 2 Air Flow Rates [5].

11.4.3 Static Jet Bleed Air ICE

The roll and pitch forces and moments generated by the trailing-edge actuators were measured using the fully flight ready Hawk 240R jet engine bleed air system as depicted above in Figure 11-5. Static yaw forces and moments through the apex actuators were not measured. These measurements were taken using the same sting mount as the captive carry data discussed previously. Static ICE actuations were made at three different RPM settings on the Hawk 240R, 80,000, 100,000 and 120,000 RPM. These increased engine settings provide increased mass flow to the actuators, thus higher jet exit velocities. Measured moments in the roll and pitch axes are presented below in Figure 11-17 and Figure 11-18 for 80,000 RPM and 120,000 RPM. The data clearly depicts the importance of mass flow levels in generating the forces through the actuators which translate to the roll and pitch moments. The pitching moment shows a nose down moment due to the elevated offset of the thrust line from the force sensor. Thrust is measured as the force in the x-axis. Actuations of the ICE are noted by boxes on the plots. The order of actuations is TEL, both TE, and TEL.

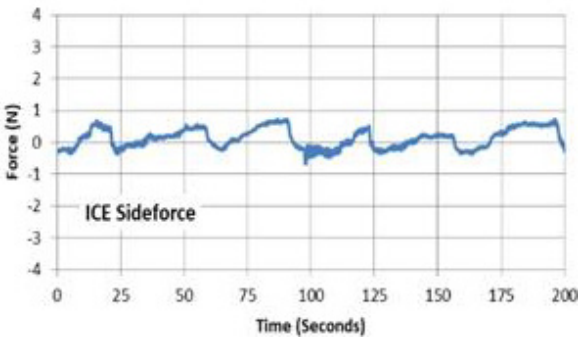

(a) Sideforce.

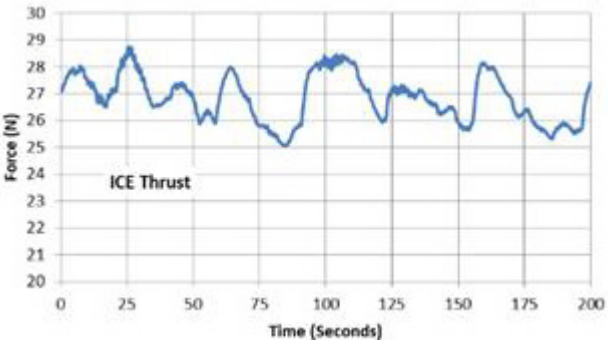

(b) Thrust.

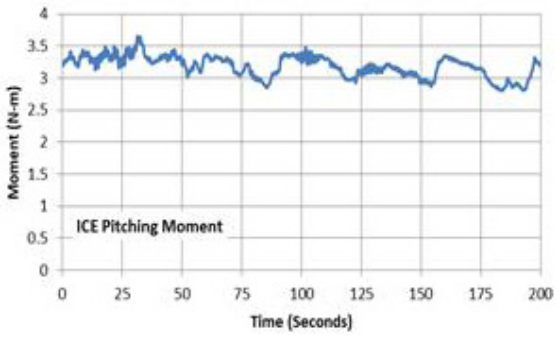

(c) Pitching Moment.

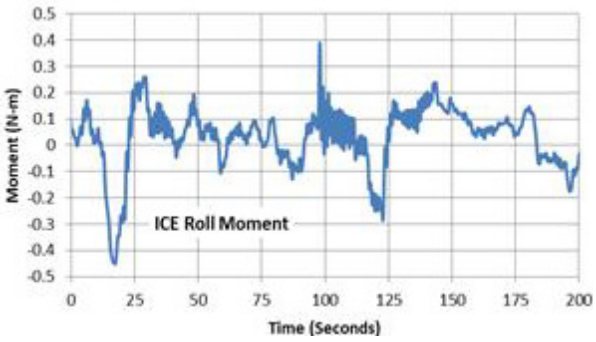

(d) Roll Moment.

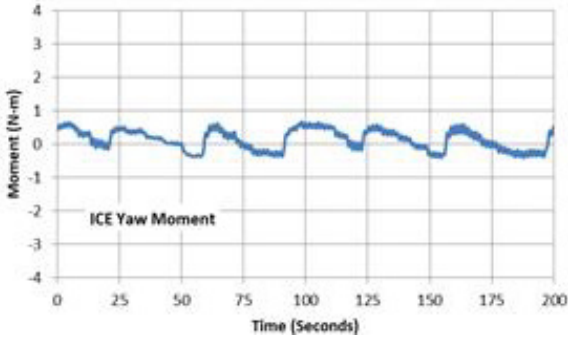

(e) Yaw Moment.

Figure 11-17: Static Hawk 240R Jet Engine at 80,000 RPM; Moments with TEL and TEB ICE.

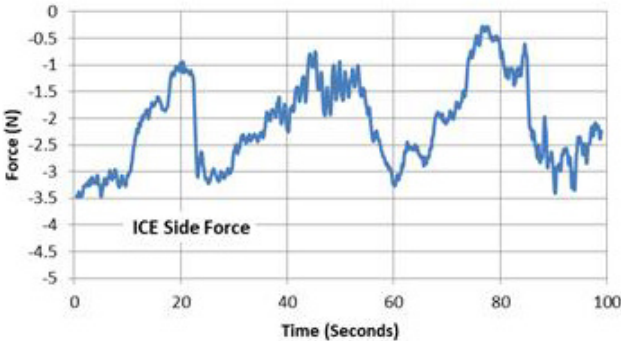

(a) Sideforce.

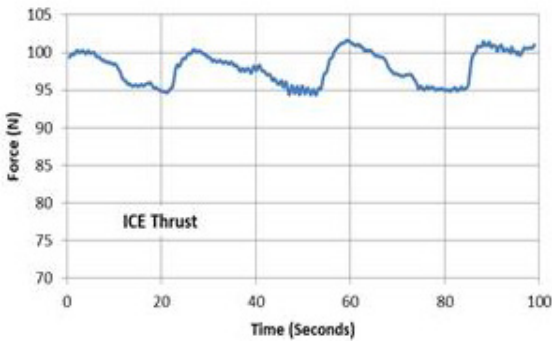

(b) Thrust.

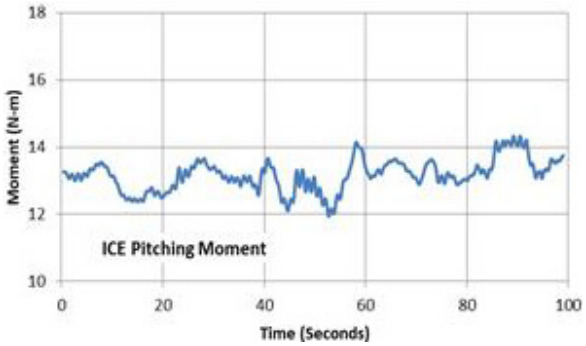

(c) Pitching Moment.

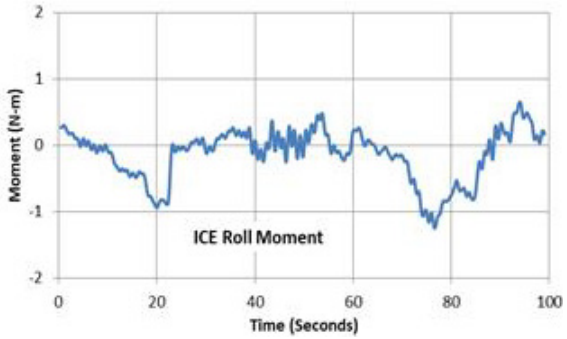

(d) Roll Moment.

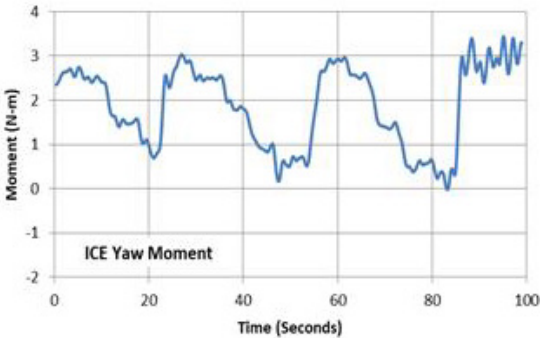

(e) Yaw Moment.

Figure 11-18: Static Hawk 240R Jet Engine at 120,000 RPM; Moments with TEL and TEB ICE.

The effects can be seen clearly in the 120,000 RPM plots to include yaw and sideforce effects even in static conditions. The effect of the actuators at the low RPM setting are nearly unmeasurable except in the roll axis.

11.4.4 ICE Flight Test

The first test aircraft models were 1/10th scale and constructed from a composite of 3D printed plastic and foam. The aircraft were powered by a small electric ducted fan. Launch was conducted via an elastic bungee similar to a catapult on an aircraft carrier. These initial aircraft were used to determine basic stability and control under conventional flight control. A simple, nonprogrammable, attitude stabilization autopilot was used to aid in the flight test of these aircraft. These aircraft were also used to determine the initial vertical tail sizing and number. Additionally, initial elevon location and sizing were determined. A picture representative of these aircraft is shown in Figure 11-19.

Figure 11-19: ICE 1/10th Scale Foam Test Aircraft.

From the initial flights test of the 1/10th scale aircraft, vertical tail sizing and number were defined, elevon sizing and location were finalized and the stable center of gravity range was determined. Thus, the 1/7th scale foam aircraft were built with two vertical tails sized to the lowest dimension while still maintaining adequate directional stability, elevons on the inboard trailing edges to accommodate the outboard ICE actuators, and the target C.G. location was at 56% of the central cord length of the aircraft. These foam aircraft were flown with Pixhawk mini autopilots with a tunable PID controller. Multiple flights over several months were flown to tune the flight control gains and mixing ratio of the elevon conventional controls. The aircraft with its 65 degree wing sweep is very roll sensitive and deeply cross coupled to the yaw axis. Flight path trajectory repeatability and consistency has not yet reached the level for accurate aircraft system identification. A picture of the 1:7 scale foam aircraft in flight is shown in Figure 11-20.

Figure 11-20: ICE 1/7th Scale Foam Test Aircraft in Flight.

Flight data of a relatively stable flight is shown in Figure 11-21, Figure 11-22 and Figure 11-23. The first details the radio control input to the autopilot and Fly By Wire A (FBW-A) output from the Pixhawk. RC1 is roll, RC2 is pitch, RC3 is throttle, and RC4 is rudder/yaw. The FBW-A autopilot setting is an attitude control mode in which if the pitch and roll RC controls are centered the aircraft is to fly in a trimmed, straight and level flight attitude. Additionally, pitch and bank angle limits can be established. Figure 11-21(a) and Figure 11-21(b) show the commanded pitch or roll angle desired by the pilot and the commanded output to the roll and pitch axis through the FBW-A autopilot. This plot shows that the elevons are trimmed near the center of the deflection PWM band at about 1550 PWM, however, the elevons were mechanically trimmed trailing edge up 10 deg from streamline to maintain a stable pitch attitude. Aileron trim was at zero for the elevons. Very little nose down elevator deflection was required to allow the aircraft to pitch nose down. This situation because of the elevon design minimized the amount roll control power available through the servo travel as shown in Figure 11-22(b). This issue translates to the flight conditions shown in Figure 11-22 of roll and pitch attitude. Though pitch is constrained quite well as called out in the plot, the aircraft demonstrates a constant roll oscillation of + 5-15 degrees often times exceeding the 40 deg. bank limit programmed to the autopilot. This effect causes the autopilot to limit its roll output commands to avoid overshooting the roll limit. This command is shown in the magenta line in Figure 11-22. This will prove to be a constant issue throughout the flight test campaign as trimming the aircraft to a steady-state, non-oscillatory condition is required for the actuation of the ICE. Finally, GPS speed is shown in Figure 11-23. The aircraft in these plots weighs about 14 pounds and had a thrust to weight ratio of 0.45. This is adequate at the operations altitude of 7000 ft MSL at USAFA in Colorado. The required nose up trim of the elevons and the roll oscillations also cause a significant drag penalty, which would cause thrust deficiencies as weight is added by the ICE control system being installed in the aircraft. Additional data is included in Figure 11-24 and Figure 11-25 to include flight data from a roll departure from controlled flight due to the extreme roll-to-yaw coupling.

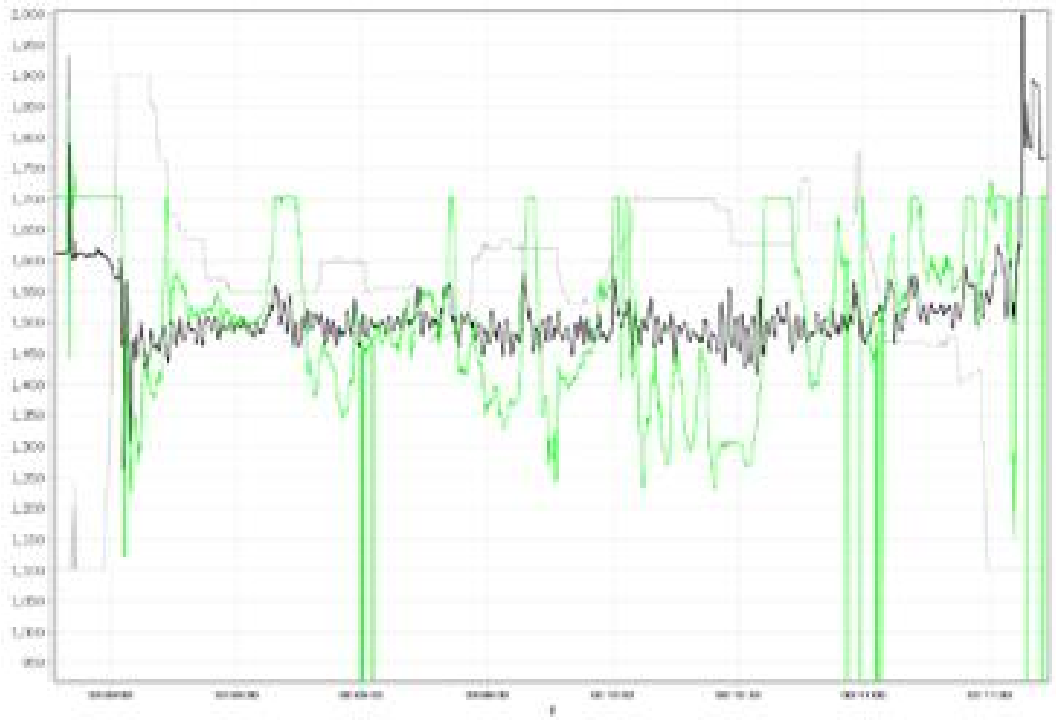

(a) Pitch.

Figure 11-21: 1/7th Scale ICE RC Control Input and Output in FBW.

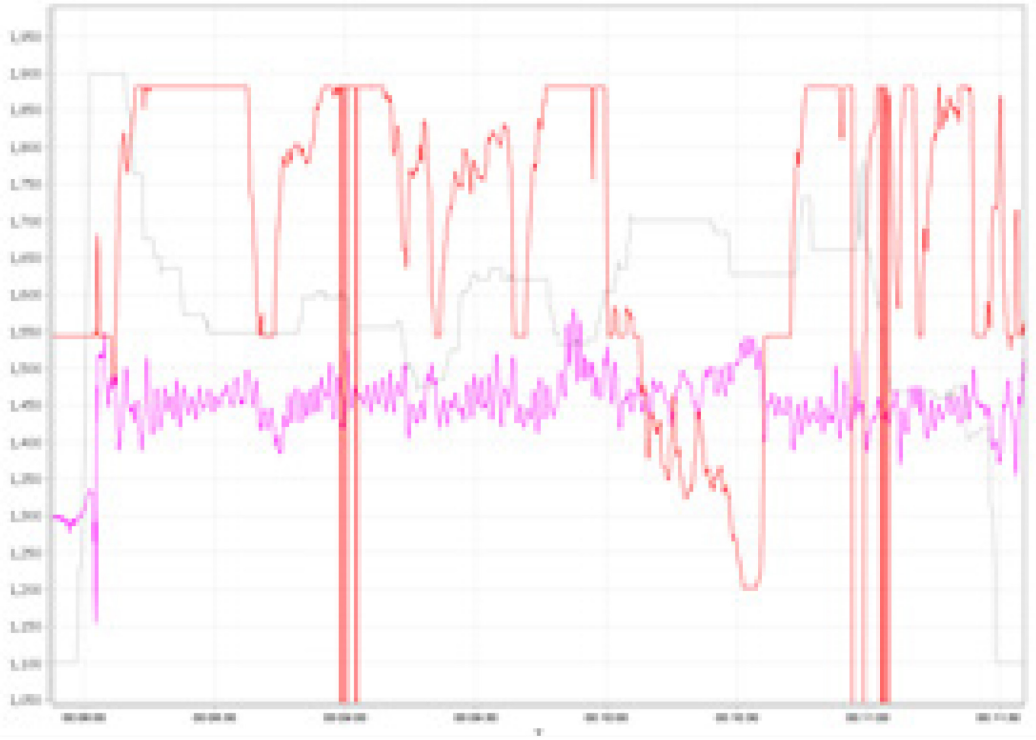

(b) Roll.

Figure 11-21 cont'd: 1/7th Scale ICE RC Control Input and Output in FBW.

Figure 11-22: 1/7th Scale ICE Pitch and Roll Attitude Actual vs. Commanded.

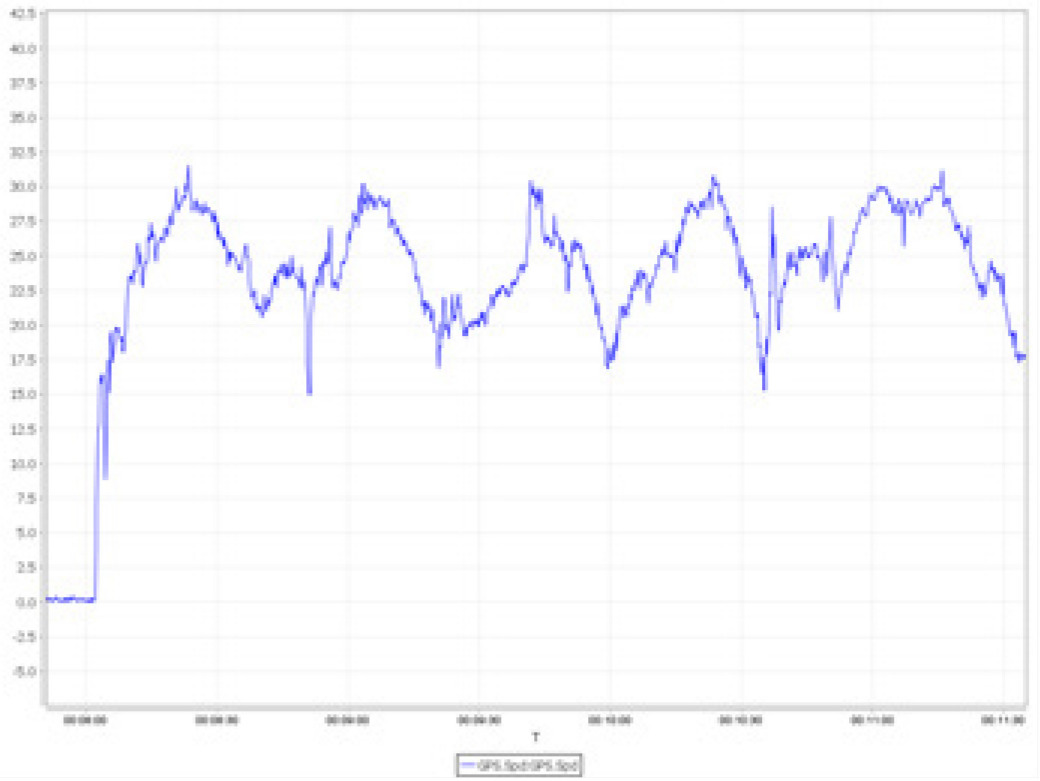

Figure 11-23: ICE 1/7th Scale ICE GPS Speed.

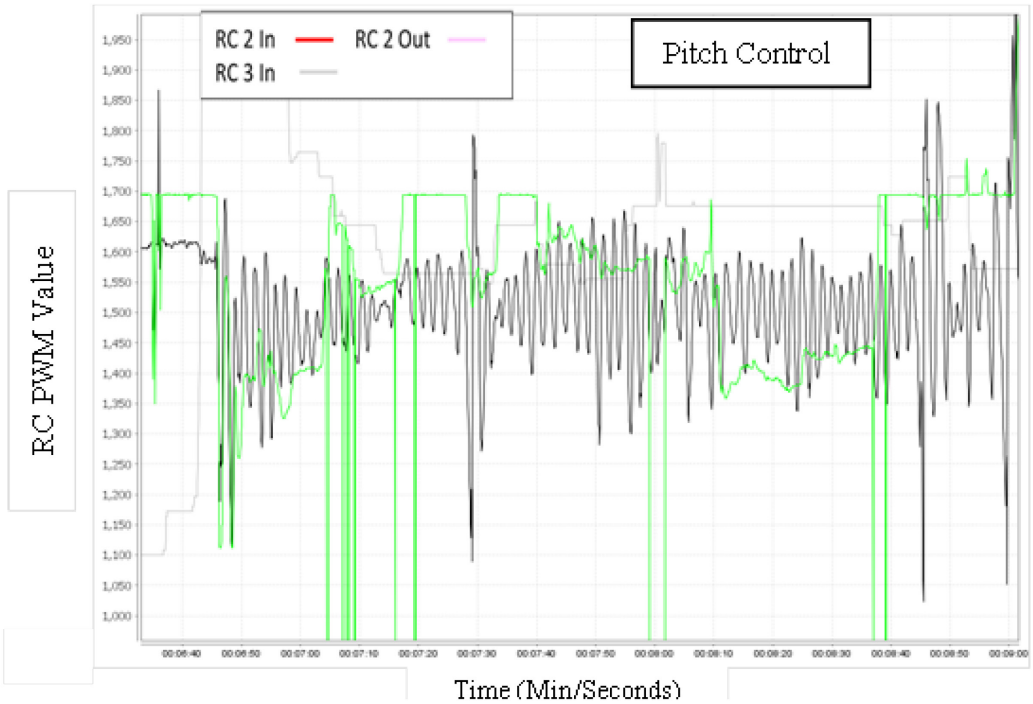

(a) Pitch.

Figure 11-24: 1/7th Scale ICE RC Control Input and Output in FBWA Roll Departure Flight.

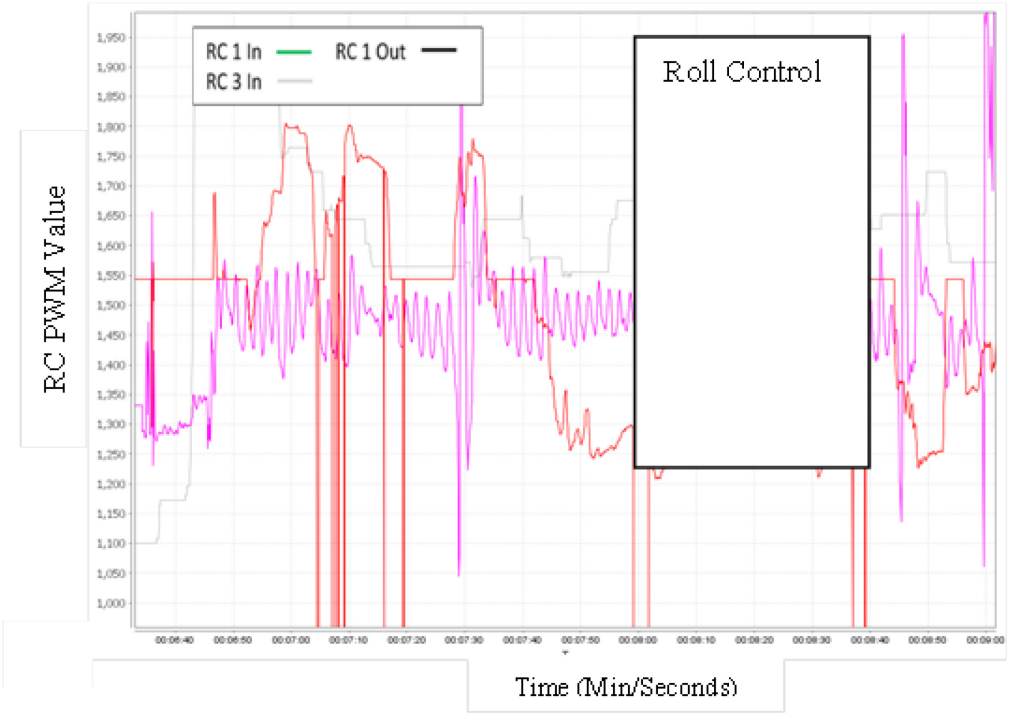

(b) Roll.

Figure 11-24 cont'd: 1/7th Scale ICE RC Control Input and Output in FBWA Roll Departure Flight.

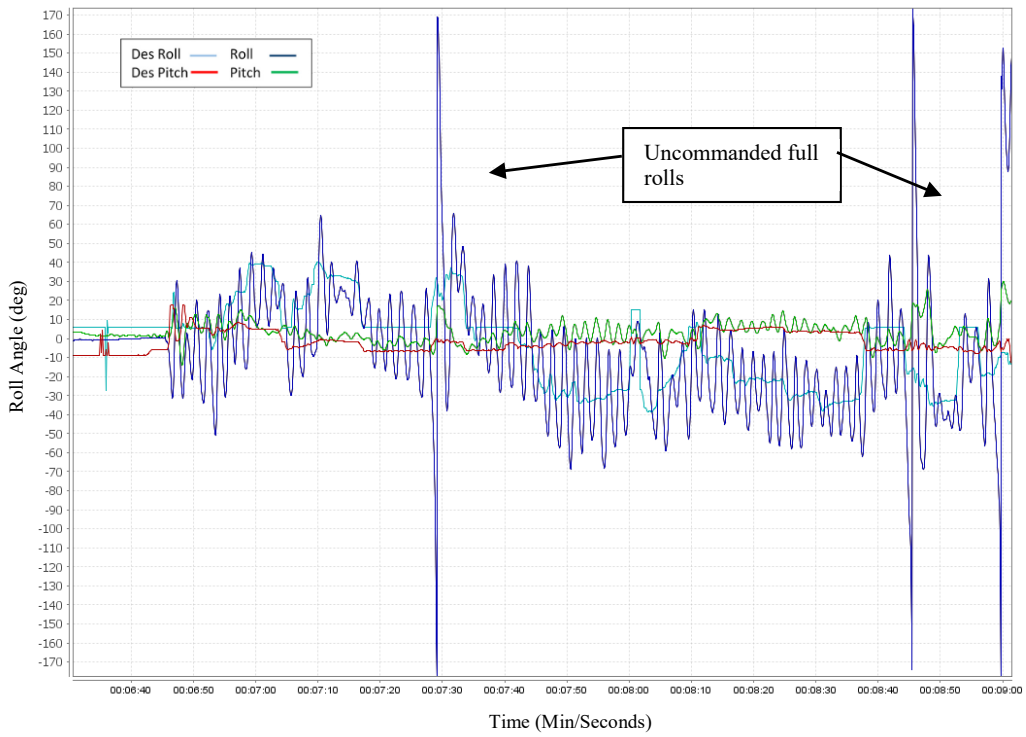

Figure 11-25: 1/7th Scale ICE Pitch and Roll Attitude Actual vs. Commanded – Roll Departure Flight.

Simultaneously to the flight test of the foam 1/7th scale aircraft to tune the autopilot gains and achieve repeatable flying qualities, the two carbon fiber jet powered ICE aircraft were fabricated and constructed. The two jet powered aircraft were built, one with the full ICE control system installed with bleed air and one as a training aircraft to fly at higher speeds and great wing loading. The jet powered trainer was powered by a Jet Rabbit 25 gas turbine engine rated at 25 lbs of thrust at 125,000 RPM at sea level. This aircraft weighed 27 lbs fully fuelled, and it was designed to fly for 7 – 10 minutes. This aircraft had the same vertical tails, rudders, and conventional elevon controls as the foam aircraft and was also configured with apex and trailing-edge ICE. It is shown here in Figure 11-26.

Figure 11-26: 1/7th Scale ICE Jet Powered Trainer.

Two flights were attempted after several taxi tests. The aircraft has a fixed, tricycle landing gear. On both attempts the aircraft nearly immediately after take-off began a left rolling and yawing motion which was unrecoverable. Both flights ended in ground impact. The aircraft design tends to great susceptibility to roll instability if there are any leading edge discontinuities. Additionally, the wing loading on this aircraft was approximately 30% greater than the previous aircraft flown. A combination of these effects is the driving factor to the departures occurring shortly after take-off. These issues drove the decision to not fly the Hawk 240R powered carbon fiber ICE until these issues were solved.

Thus, in order to achieve some free flight data with ICE actuation, the foam ICE models became the only viable option until the flying qualities and possible aircraft manufacturing or construction issues could be resolved. One foam ICE model was constructed with integrated 3D printed trailing-edge and apex ICE. Additionally, a servo controlled air control valve was designed to allow air to flow from a 3000 psi regulated compressed air bottle to one ICE. With the added control elements this aircraft weighed 18 – 19 lbs depending on battery weight. The thrust to weight ratio was on the order of 0.3. This aircraft was aggressively bungee launched to reach necessary flying speed and belly landed off the tiered athletic fields at USAFA. This tiered field layout allowed on average for 15 – 25 seconds of electric ducted fan powered flight time. The aircraft with the ICE actuation system is shown in Figure 11-27.

Several flight attempts were made with the ICE system operative using the compressed air bottle flowed to the TEL or TER actuator. Though six flights were accomplished where the ICE was actuated, the time to establish the aircraft in a stable condition, actuate with the air, and then see a measurable and stable response was not sufficient. The pitch axis control is precise and well understood. The issues associated with the significant yaw-to-roll coupling of this aircraft design leading to excessive roll oscillations have been identified. Resolution of these issues is currently in work and involves elevon and vertical tail sizing design changes and continued autopilot PID controller refinement. Flight test continues.

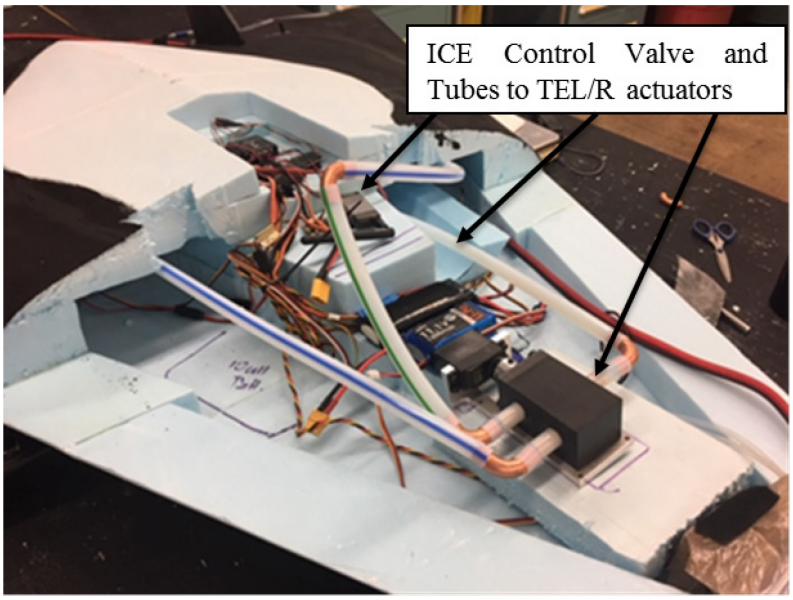

Figure 11-27: 1/7th Scale ICE Foam with Innovative Control Effectors.

11.5 CONCLUSIONS

Flight tests with 1:7 scale models of the ICE/SACCON hybrid aircraft are underway to assess the viability of air jet actuator control as an alternate form of flight control, enhancing the survivability of advanced aircraft. Various experimental methods were executed to detail a complete analysis the ICE effectiveness, while not compromising flight safety. Nearly 50 flights of two different scale and varying weight ICE aircraft have been flown successfully; however, critical aircraft flying quality deficits prevented open air flight testing of the ICE system which would yield clear and definitive results. The primary area of deficient flying qualities was the extreme roll sensitivity.

The ICE system demonstrates both measurable and effective control power, both statically and in captive carry environments, however testing in free flight is the source of the desired data, which must be obtained to be compared with the measurements obtained from wind tunnel measurements and numerical simulations. Flight tests have qualitatively demonstrated through visual observation that the aircraft responds in roll to compressed air ICE actuation. Thus, flight test will be continued to solve the roll stabilization issue through an analysis of vertical tail and elevon control sizing and yaw-to-roll control blending in an attempt improve basic flying qualities shown through repeatable and stable attitude and flight path control.

11.6 ACKNOWLEDGEMENTS

Support by the US Air Force Office of Scientific Research under grant FA9550-16-1-0098 with program manager Douglas Smith and interim program manager Ivett Leyva is gratefully acknowledged.

This material is based in part on research sponsored by the US Air Force Academy under agreement number FA7000-13-2-0009 and FA7000-15-2-0003. The U.S. Government is authorized to reproduce and distribute reprints for Governmental purposes notwithstanding any copyright notation thereon.

The views and conclusions contained herein are those of the authors and should not be interpreted as necessarily representing the official policies or endorsements, either expressed or implied, of the US Air Force Academy, the US Department of Defense, or the US Government.

11.7 REFERENCES

[1] Gillard, W.J., Innovative Control Effectors (Configuration 101), Tech. Rep. AFRL-VA-WP-TR-1998-3043, Air Force Research Laboratory Wright Patterson, 1998.

[2] Huber, K.C., Vicroy, D., Schutte, A., and Hubner, A., UCAV Model Design and Static Experimental Investigations to Estimate Control Device Effectiveness and Stability and Control Capabilities, AIAA Paper 2014-2002.

[3] Williams, D., Seidel, J., Osteroos, R., and McLaughlin, T., Flight Control Derivatives using Active Flow Control Effectors on the ICE/SACCON UCAS Model, AIAA Paper 2019 #TBD.

[4] ATI Industrial Automation Eternet Axia F/T Sensor Manual. Article online at https://www.ati-ia.com/app_content/documents/9610-05-Ethernet%20Axia.pdf. 06 March 2017.

[5] Crawford, B., Berson, T., Brandt, S., and Osteroos, R., Full Scale, Open Air Innovative Control Effectors (ICE) Evaluation, Department of Aeronautics, USAF Academy, CO, May 2017 (unpublished).

Chapter 12 – CONCLUSIONS AND NEXT STEPS

Clyde Warsop
BAE Systems AIR
UNITED KINGDOM

Douglas R. Smith
USAF/European Office of Aerospace Research and Development
UNITED KINGDOM

Daniel N. Miller
Lockheed Martin Corp.
UNITED STATES

12.1 OVERVIEW

A North Atlantic Treaty Organization technical task group (AVT-239) was commissioned to investigate the feasibility of applying Active Flow Control (AFC) to low-observable combat aircraft configurations. A wide range of active flow control technologies were explored and performance and integration assessments were undertaken on two aircraft configurations (ICE and SACCON/MULDICON). The results of these investigations were used to undertake a design of experiments trade study to assess the feasibility of using a suite of AFC technologies for flight control during a typical ingress/egress mission phase relative to a conventional mechanical flap-based control suite. The study suggests that AFC technology is both feasible and reasonable for application to the ICE and SACCON/MULDICON platforms. Areas highlighted for future R&D investment include: AFC valve reliability/maintainability and the maturation of technology, integration, and manufacturing readiness to level 5 or greater. Further assessments are proposed to explore the application of AFC to the take-off/landing and manoeuvring mission phases. A comprehensive framework for integrating flow control into the aerodynamic design of a next generation UAV and assessing its system impact on that aircraft has been established.

12.2 BACKGROUND

Future manned and unmanned military vehicles will rely on surface geometries with smooth, continuous outer mould lines to enhance survivability. This requirement to be seamless invokes a very critical challenge for vehicle control and suggests that new flight control effector strategies may be needed. Strategies that do not involve seams, gaps or moving surfaces have been studied previously and continue to evolve towards ever-improved efficiency and ease of integration.

New seamless flight control effector strategies using Active Flow Control (AFC) offer the potential for enhanced survivability of future military air vehicles. Flow control technologies have a wide range of uses from separation control for improving high alpha performance, to lift augmentation and full 3-axis flight control. To date, the exploitation of flow control technologies on production platforms has been limited, often due to the complexity of their integration, power requirements and their impact on cruise performance. Successfully implemented flow control technologies have the potential to revolutionise the performance and manoeuvre characteristics of modern, low-observable air and maritime platforms.

A NATO STO workshop (May 2013, AVT-215, Stockholm) explored many of these innovative control effector technologies including geometric, seamless and virtual shaping technologies (morphing structures, pneumatics, plasmas, etc.). A key objective of the workshop was to explore, assess and baseline the current state of the art in innovative control effector technologies with a view to steering future research activity. The conclusion of the workshop was that the application of these novel technologies, both in isolation and in combination, offers a promising route for the manoeuvring of a vehicle constrained by low observability considerations.

The AVT-239 task group was set up in response to this conclusion and to raise the Technology Readiness Level (TRL) sufficiently to allow exploitation on future NATO aircraft. The group has focussed on the identification of appropriate flow control technologies and the high level assessment of these technologies with respect to a number of key metrics applied to two representative low-signature air vehicle concepts (ICE and SACCON).

The task group identified two candidate conceptual aircraft platforms to conduct this study: the innovative control effector (a.k.a. ICE) [1], [2] and the stability and control (a.k.a. SACCON) [3] configurations, both shown in Figure 12-1.

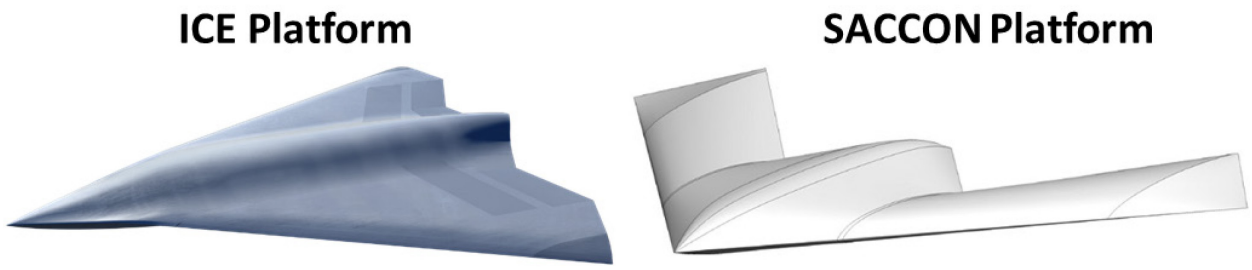

Figure 12-1: ICE and SACCON Tailless Platforms Selected for Investigation.

12.3 OVERVIEW OF TECHNOLOGIES

A wide range of AFC technologies (Figure 12-2) were initially reviewed with a view to down select the most promising for further investigation reviewed. These covered technologies included:

- Fluidic thrust vectoring;
- Trailing edge circulation control;
- Apex- and mid-span leading edge blowing;
- Trailing edge slot blowing;
- Sweeping jets;
- Plasmas; and
- Boundary layer separation control.

Following an initial assessment of the technologies a subset was chosen for further investigation and analysis and to provide a focus for the integration and performance assessments.

For the ICE configuration the technologies down-selected were yaw fluidic thrust vectoring, leading edge blowing at the apex, leading edge blowing at the mid-span and trailing edge tangential blowing. For the SACCON configuration the technologies assessed include pitch fluidic thrust vectoring, trailing edge circulation control with dual-slot, supercritical blowing and sweeping jet actuation at the leading edge and ahead of the conventional trailing edge control effector hinge line.

12.4 OVERVIEW OF ASSESSMENT STUDIES

A Quality Function Deployment (QFD) process [5] was applied to make an objective (or at least less subjective) assessment of the technology applied to the chosen aircraft configurations. An overview of the QFD trade study process is illustrated in Figure 12-3. Generally, engineering analysis and design was

conducted across four metric groups: Performance, Integration, 'Ilities' and Maturity. In each group Key Performance Parameters (KPPs) were defined and subsequently used to score a technology in the QFD matrix. Weighting values were assigned across the metric groups and KPPs to reflect their relative importance in the overall assessment. The trade study results were used to generate KPP response plots (or bar graphs) across the four AFC configurations to permit side-by-side relative comparisons. The resultant KPP scores for each configuration also permit assessment of AFC feasibility against the defined criteria.

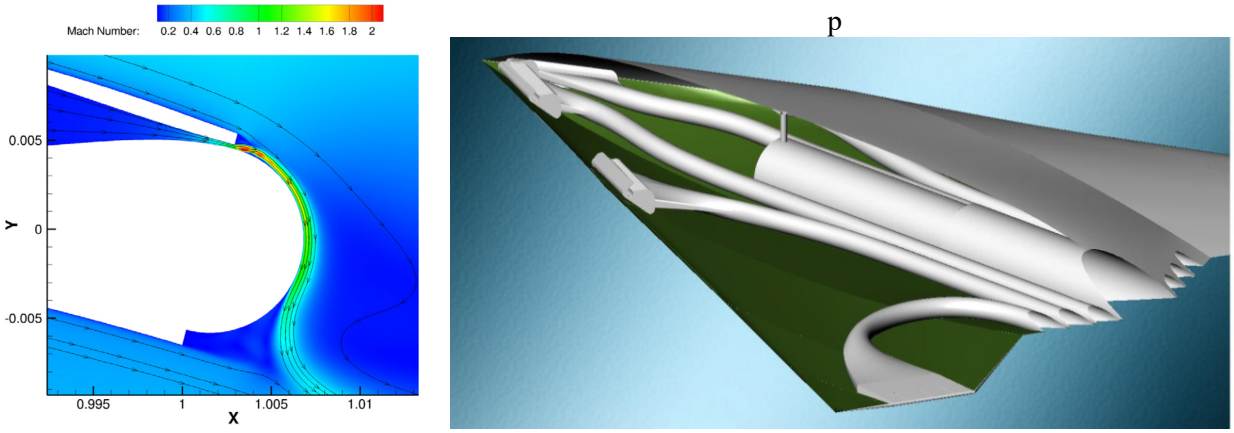

(a) Supercritical Trailing Edge Circulation Control.

(b) Apex, Mid-Span Leading Edge Blowing and Trailing Edge Tangential Blowing.

(c) Fluidic Thrust Vectoring.

(d) Sweeping Jets (Image: Ref. [4]).

Figure 12-2: Examples of Flow Control Technologies Assessed.

In order to score the AFC technologies for each of the KPPs, a representative flight mission needed to be identified. For the scoring described here, the mission was a typical ingress/egress mission phase (30,000 ft, Mach 0.9 for ICE and 30,000 ft, M 0.8 for SACCON).

Aerodynamic data [6], [7], [8] for each of the flow control technologies applied to each configuration was generated by means of a combination of wind tunnel testing and validated Computational Fluid Dynamics. These data were then used to undertake flight control simulations for a defined set of turbulence and gust disturbance conditions [9], [10]. The outcomes from these simulations were then used to determine the AFC performance (ability to provide adequate control, cost in terms of bleed air requirement) and as inputs to size the AFC system on the aircraft for the integration assessment [11]. The output from the integration design and assessment activity provided data for input into the 'ilities' [12] and maturity assessments.

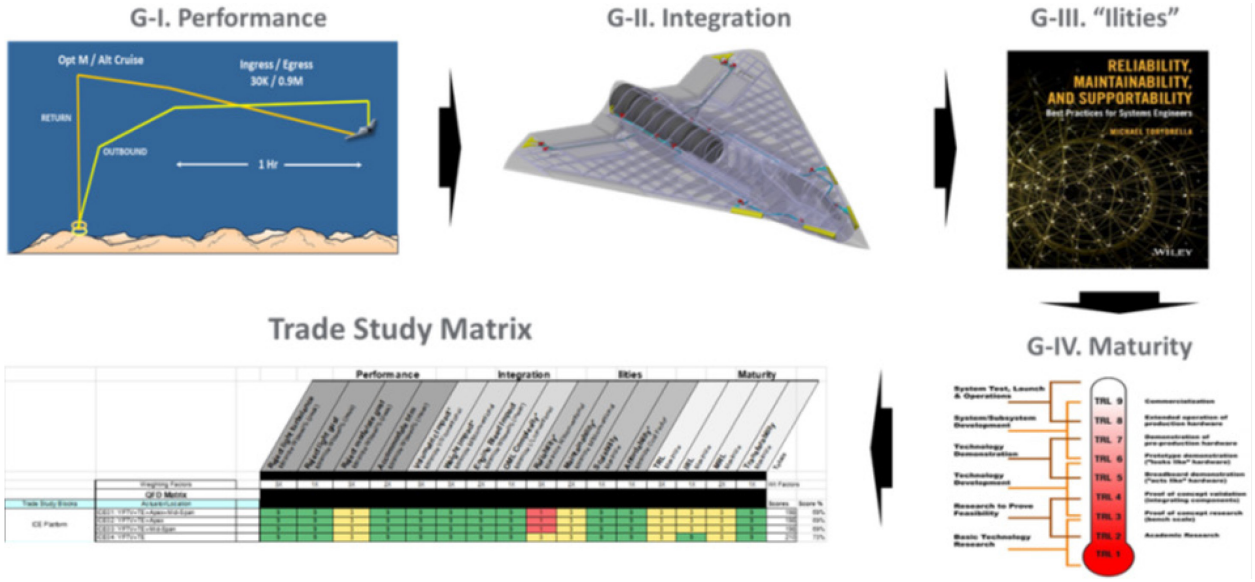

Figure 12-3: Trade Study Process Incorporates Analysis and Design Task Across Four Groups of Metrics.

12.5 KEY ACHIEVEMENTS AND OUTPUTS

The AVT-239 task group has successfully evaluated a range of AFC technologies at a conceptual design/integration level as applied to the ICE and SACCON/MULDICON configurations. The following sections present the key outcomes.

12.5.1 Feasibility of AFC

The trade study suggests that AFC technology is both feasible and reasonable for application to the platforms investigated and can provide the required control power during an ingress/egress mission.

In particular:

- Flight control simulations show that sufficient control power can be generated across all KPPs and at a peak bleed flow rate acceptable for a modern turbofan engine. The performance metric results suggest AFC is feasible from a performance standpoint.
- The nominal AFC engine bleed impact KPP is approximately 0.5%. This level of bleed flow is acceptable to most modern turbofan engines and suggests a 1% impact to aircraft range.
- The peak engine bleed mass flow requirement to overcome the moderate gust case is 1.8% and 3% for the SACCON and ICE configurations respectively.
- The size, weight, and outer mould line impact results suggest very reasonable levels for AFC and the possibility to integrate alongside a conventional system (as a redundant control to permit safe developmental and operational testing).
- The AFC system volume for the ingress/egress mission phase is of the order of 5 – 10% of the conventional control system.
- The AFC system weight impact for the ingress/egress mission phase is of the order of 25% of the conventional control system.

- The Outer Mould Line (OML) complexity factor KPP is a measure of surface discontinuities (e.g., seams, gaps) that generally drive up platform complexity and cost. The nominal AFC system OML metric is 15% of the conventional system.
- The preferred AFC technology for both the ICE and SACCON configurations features trailing edge tangential blowing/circulation control supplemented by yaw thrust vectoring for the ICE configuration.
- DoD readiness level KPPs for technology and manufacturing are 3 – 4 for the configurations considered.
- Readiness level KPPs for integration are the least mature with the integration interaction between different control effectors, AFC and conventional, least understood.
- The transferability KPP suggests that all configurations are excellent. A level 6 suggests the technology can be hypothetically developed on one UAV platform and then "cross-decked" or transferred readily with no major developmental obstacles from an aerodynamic standpoint.

12.5.2 Most Promising AFC Technologies

Of the technologies investigated, trailing edge tangential blowing/circulation control and yaw fluidic thrust vectoring proved to be the most effective and efficient for the transonic ingress/egress mission role. This was probably to be expected since it is a technology that modifies the 'inviscid' circulation around the wing. The following remarks with respect to this technology have resulted from the findings of the study:

- CC functions most efficiently in terms of minimising the engine bleed mass flow for a given control effect when the slot blowing velocity is maximised. This leads to operating the control effector at supercritical conditions to achieve supersonic nozzle exit velocities. To achieve effective operation at the required nozzle pressure ratios of 3 or above it is important to consider the detailed design of blowing slot geometry to achieve proper expansion and attachment of the flow to the curved trailing edge. This can be achieved by adopting convergent-divergent or convergent with aft-facing step nozzle geometry. Typical blowing slot heights for full-scale application are of the order of 1 mm or less so for ease of manufacture the adoption of the simpler convergent nozzle with aft-facing step is preferable.
- CC technology has been shown to be an effective and efficient technology for the subsonic flight regime. However, at supersonic flight speeds it is unlikely to work due to the different aerodynamic mechanisms through which lift is generated.

Fluidic thrust vectoring, particularly in the yaw plane has been shown to be a useful and efficient technology for finless configurations such as ICE. While not explored for the SACCON/MULDICON configuration in this study due to constraints on available data and effort, it is likely that this technology will be equally applicable to the latter configuration class. However, it appears that a well-designed CC system is capable of achieving adequate yaw control authority when used in differential mode to take advantage of its ability to modulate both thrust and drag on opposite wings.

For the configurations and attached flow conditions examined in the present study, Sweeping Jet Actuator (SJA) technology appears to be an inefficient means of providing control authority. This is thought to be primarily due to the SJA impacting the boundary layer flow rather than circulation. SJA technology is expected to be able to provide greater benefit for flight regimes where flow breakdown occurs, for example, at high angles of attack during take-off/landing or during aggressive flight manoeuvres. SJAs may also have a beneficial role to play to allow conventional trailing edge control effectors, particularly on highly swept trailing edges to be effective at higher deflection angles.

12.5.3 Evaluation and Assessment Process

This study has successfully developed and evaluated a systematic approach to the multi-disciplinary assessment of AFC technology to an aircraft configuration at the early conceptual design stage.

The approach provides a way of making a quantifiable and traceable cost-benefit assessment of AFC and is offered as an approach that could, with suitable adaptations to the KPPs, be applied to the assessment of other mission phases of the current configurations/technologies or to other configurations/technologies.

12.6 NEXT STEPS

In light of the achievements and outcomes of the AVT-239 studies, a number of follow-on steps are proposed to extend the scope of the present studies to other, more challenging flight regimes and to mature the technologies towards industrial deployment. These include:

12.6.1 Extend Performance Assessments to Other Mission Phases

With the confidence gained that AFC could play a beneficial role for the signature-critical ingress mission phase, it is proposed that other mission phases be explored including take-off, landing and manoeuvring to determine if conventional controls could eventually be significantly reduced in size or ultimately eliminated.

The present study has only explored the ingress mission phase where flow control is deployed as a means of achieving gentle manoeuvres, trim changes and disturbance rejection in order to negate the requirement to deflect conventional control surface as part of a signature control objective. As such it has been assumed that flow control is used alongside conventional control surfaces rather than as a replacement – which is penalising in terms of the need to install and operate with redundant systems.

With the knowledge and experience now gained, it is possible that other, more challenging sectors of the mission envelope should be explored to ascertain whether flow control could be used to replace conventional control surfaces entirely. These more challenging flight regimes are likely to place higher demands on mass flow required for the flow control systems. The impact this may have on engine performance or consideration of cases where thrust settings are low (e.g., landing approach) may well demand a need for appropriately sized accumulators and alternative sources of “blowing” air. Additional mass flow requirements would also have an impact on the sizing of piping for the distribution of “blowing air”. Assessments need to be made to understand how piping sized for less than peak mass flow demands can perform when operating at peak mass flow conditions.

It is therefore proposed that a new AVT task group is set up to carry out this activity based on the approaches already developed within the current activity.

12.6.2 Extend System and Manufacturing Readiness Levels

The current study has highlighted potential performance issues with respect to reliability, maintainability and manufacturability of active flow control systems. These deficiencies appear to primarily result from two main sources:

12.6.2.1 Improve Reliability of Fluidic Bleed Control Valves

The current level of fail-safe/redundancy built into present day control valves for bleed air systems is insufficient to achieve the probabilities of ‘mission abort’ and ‘loss of control’ currently considered acceptable for conventional control systems. This would limit the application of AFC to configurations where the AFC sits alongside a conventional control surface system.

The current probability of loss of output of a dual lane fault tolerant electro-mechanical valve is of the order 10^5. This may be acceptable for an AFC system that operates in parallel with a 'fall-back' conventional control system. However, valve architecture suitable for an 'AFC only' aircraft needs to have a probability of loss of output several orders of magnitude higher than this. Development is required to realise architectures and concepts for electro-mechanical fluidic control valves that provide sufficient levels of fail-safe and redundancy to allow the AFC system to achieve the often quoted probability of loss of control output of the order 10^{-9} [2]. While this may not be an insurmountable challenge it is likely to require significant development effort and thought about, not only redundancy in the actuator architecture itself, but also consideration of the provision of multiple control valves to supply independent regions of an AFC actuator.

12.6.2.2 Improve Design of AFC Nozzles to Improve Efficiency and Manufacturability

While bleed air system distribution components such as ducts, connectors, bellows, gimbals, etc. have sufficient performance, reliability and are of sufficiently low mass to meet AFC requirements the same cannot be said to be true for the AFC nozzles themselves.

For duct sizing purposes it has been assumed in this study that the bleed air achieves a peak Mach number of 0.3 within the ducts themselves. This is a value based on past experience to avoid issues associated with compressibility induced losses. To obtain good AFC efficiency a high quality of uniformity of the flow through the very high aspect ratio exit slots of the AFC nozzles is required. This requires the transition of the bleed air supply from the relatively small diameter, aspect ratio supply pipe to the plenum chamber supplying the AFC slot. There is significant opportunity for optimising the design of the AFC plenum and flow conditioning components (diffusers, splitting flow paths and internal slot guide vanes) to ensure minimal pressure losses and maximum flow uniformity (velocity amplitude and direction) across the nozzle exit.

In addition to identifying the need for optimising flow conditioning within the AFC actuator nozzles this study has highlighted the complexity and the small dimension / high-tolerances of the nozzles themselves (slot heights for CC devices are typically of the order of 1 mm or less). These tolerances need to be ensured across large actuator spans and throughout the service-life of the aircraft. This introduces concerns with respect to durability and maintenance. Therefore, there is a need to:

- Validate and mature the manufacturing routes to realise high-tolerance, small dimension features in fluidic end effectors (blowing slots). In addition to meeting manufacturability and load carrying requirements these components also need to be resistant to through-life degradation and be compatible with maintainability needs.
- Develop reliable and fail-safe system components and architectures for bleed air distribution and control. These need to be compatible with achieving acceptable mission completion probabilities and the levels of fail-safe/redundancy to meet acceptable aircraft loss probabilities. Redundancy/fail-safe of the control valves would be a key focus of this activity.
- Improve current understanding of the transient behaviour of fluidic flight control effectors:
    - Technologies such as Fluidic Thrust Vectoring (FTV) are understood to have transient response times that are of the order of the convective time of the jet flow. Thus, if control valves are located close to the actuator exit orifices, the time constant of the vectoring response tends to be dominated by that of the control valve. Generally, FTV response times are well within the requirements demanded by considerations of air vehicle control. One aspect of FTV operation that is currently unclear is the closed loop response of the engine with regard to transient operation of the vectoring system (i.e., the impact of rapid/intermittent demand on the bleed on compressor performance). Further studies are required in this area.
    - The response times of flow control technologies that affect circulation around and flow attachment/detachment on a lifting surface (e.g., trailing edge circulation control, leading edge/apex blowing and sweeping jets) are influenced by the response of the bleed air control

valve/blowing slot system and by the response time of the external flow to local changes caused by the actuator. The response times of the flow control valve/blowing slot are arguably equal to or better than a mechanically actuated control surfaces (and have been assumed so in the present studies). However, the response time of the external flow to local changes caused by the actuator are less well known and warrant further investigation. Generally, an instantaneous change in angle of attack of a wing or deflection of a control surface does not result in an instantaneous change in lift or moment. In reality the lift changes asymptotically over a period of time associated with the convective time of the flow over the aircraft. The response times to step changes in angle of attack and vertical gust for an aerofoil are described by the well-known Wagner (angle of attack), and Kussner (gusts) functions. For an aerofoil the typical time to achieve 90% of the steady state lift is of the order of the convective time associated with the aerofoil travelling 5 to 7 chord lengths. On an aircraft travelling at Mach 0.7 at 30,000ft and having a typical wing root chord of 10m this would equate to a lag time of approximately 0.3 s. For flapped aerofoils having step changes in flap deflection the indicial response times are significantly faster – of the order of 1 or 2 chord length convective times [13] (equating to a time constant of 0.05 s). There is currently no reason to suspect that the aerodynamic response to a fluidic actuator affecting changes in circulation is significantly different to that for the deflection of a conventional control surface. However, it would seem prudent to explore and validate this assumption. Such a study should involve both experimental and numerical validation to explore the relationships between control valve operation and the resulting generation of loads on the aircraft. The outputs of such studies could then be incorporated into a full aircraft system response model to explore overall vehicle response to disturbance rejection.

- For an aircraft with both conventional control and AFC-based control, the aerodynamic interaction between the two systems during transition from one to the other needs to be understood, as does the coupling between the individual AFC technologies. The current study assumed that the control effects from different technologies were linearly superimposable.

12.7 CONCLUSIONS

12.7.1 Technical Achievements

The results of the study suggest that AFC technology is both feasible and reasonable for application to the platforms investigated and can provide the required control power during ingress/egress. For these specific mission phases, both tailing edge tangential blowing/circulation control and yaw fluidic thrust vectoring appear to be the most promising technologies.

Areas highlighted for future R&D investment include:

1) AFC valve reliability;
2) AFC maintainability;
3) Reducing bleed flow for moderate gusts; and
4) Maturing technology, integration, and manufacturing readiness to 5+.

Further investigation of AFC should be done on the ICE, SACCON/MULDICON and other platforms for the manoeuvre and take-off/landing flight regimes to determine if conventional controls could eventually be significantly reduced in size or ultimately eliminated. There is also concern regarding the flow transients associated with AFC, particularly where operation of AFC has an impact of flow circulation or separation and the response time of the control effect to operation of the actuator is significant. It is proposed that a follow-on NATO AVT activity is initiated to explore these broader issues associated with AFC.

Finally, the effort of the group has established a comprehensive framework for integrating flow control into the aerodynamic design of a next generation UAV and assessing its system impact on that aircraft. It is the hope of the group that this framework will become the enduring standard by which future novel control technologies are assessed.

12.7.2 Operational Opportunities

AFC could enable future manned and unmanned military vehicle designs with few or no moving surfaces and reduced impact on outer mould lines (reducing seams and gaps). Such devices can either provide fluidic augmentation of conventional control concepts or, potentially, completely replace existing conventional control effector systems. Full replacement of movable parts by non-movable fluidic control systems would contribute to a smoother overall aircraft shape. These measures have the potential to reduce the radar signature of future aerial vehicle configurations.

Replacing existing conventional control and lift augmentation systems with AFC systems could also provide an opportunity to reduce weight and complexity. AFC allows replacement of multiple single-function systems (e.g., Flap, Elevator, Rudder and Aileron) by multi-function effectors that combine lift and control elements about more than one axis in a single unit. Taken together, these measures could significantly reduce the complexity and increase the redundancy of control / lift augmentation systems.

The emerging balance and blending of performance, agility and signature to accomplish and survive typical future combat aircraft missions is a frequently discussed topic within design offices. Expected threats will have a pronounced influence on the concurrent aerodynamic and low-signature shaping. Mission-related trade-offs between the aerodynamic and flight-physical performance-agility package and the RCS and IR-signature reduction efforts may create very different designs (Figure 12-4).

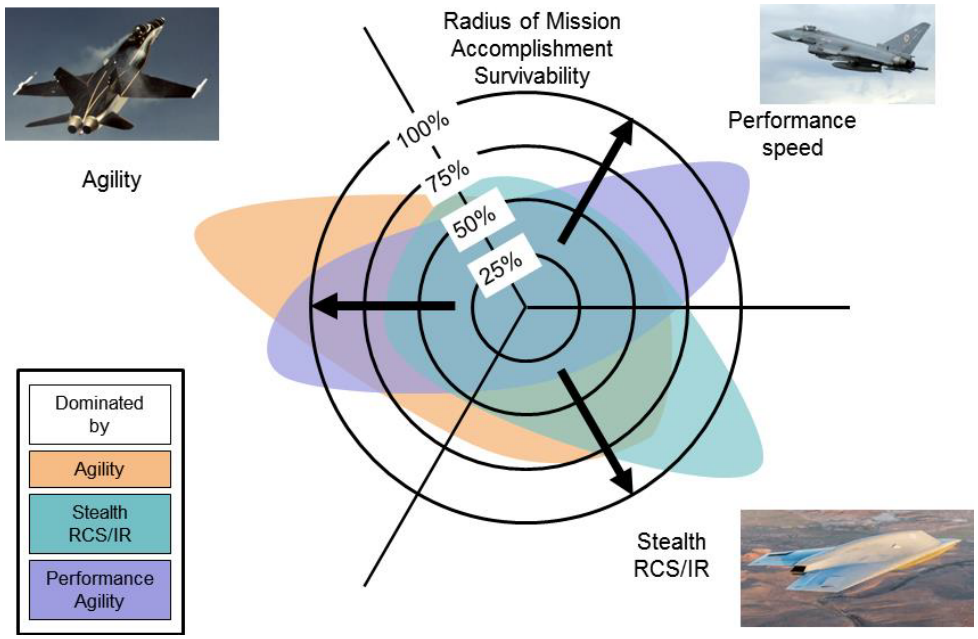

Figure 12-4: Speed, Agility and Stealth to Achieve Mission Accomplishment and Survival.

All mission drivers of the future will tend towards compact topologies combining many aspects of stability, control and engine-integration. Countering high threat surveillance, tracking and missile seeker lock will force RCS-levels well below -30 dB (Figure 12-5). The design-competing objectives can potentially be

harmonized by a fluidic control augmentation in order to enhance agility and stealth capabilities. As shown in Figure 12-4, this could contribute to enhanced survivability and higher mission completion probability for any aircraft configuration operating in a highly contested environment.

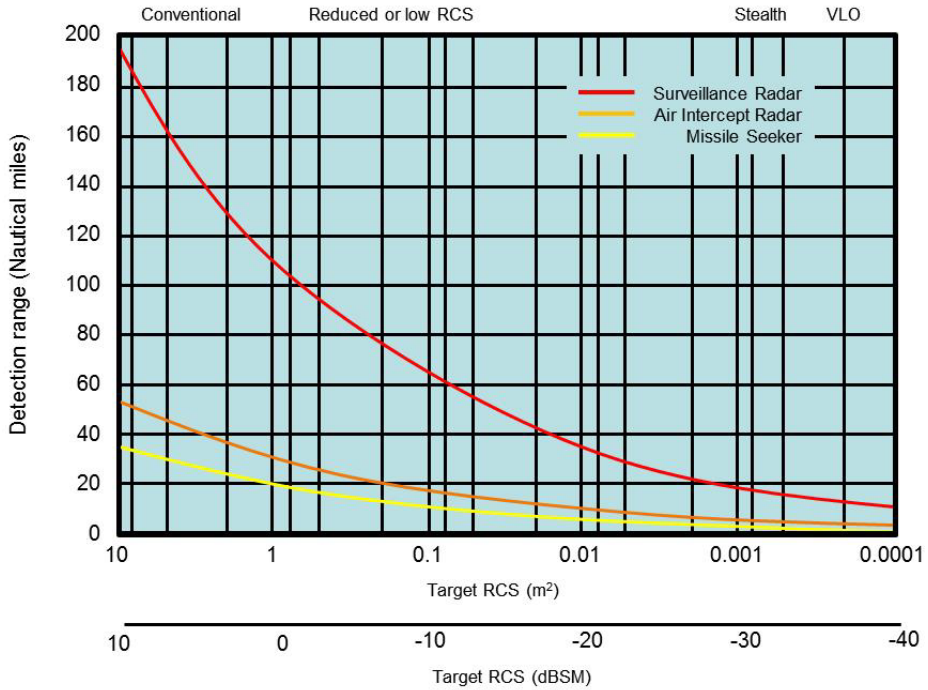

Figure 12-5: Typical Detection Range for Surveillance, Intercept and Missile Seeker Radars vs. Target RCS (adapted from Ref. [14]).

Furthermore, a significant complexity reduction of current mechanical control and lift augmentation systems could lead to reduced maintainability as well as a reduced need for maintenance capabilities. Both will have a direct impact on reducing system's Life Cycle Costs and hence, increasing affordability.

Next generation military aircraft will confront increasingly contested and increasingly sophisticated threat environments. To enhance the survivability of future aircraft in these environments will require new ways of flying aircraft. Legacy approaches, using deflecting surfaces that open gaps and seams in the aircraft surface, are at odds with the demand for enhanced survivability. Novel approaches, involving seamless technologies without deflecting surfaces, offer the promise of full aircraft flight control without compromising low detectability.

12.8 ACKNOWLEDGEMENTS

The authors would like to thank BAE Systems, DSTL, and Lockheed Martin Aero for their generous contributions of time and resources without which this effort would not have been possible. The authors would also like to thank the members of the group for their continuous dedication to the effort and unfailing participation in the bi-annual meetings. Finally, the authors gratefully acknowledge the leadership and guidance of Dr. Jonathan Irving who served as a co-chair during the early years of the task group.

The opinions, findings, conclusions and/or recommendations expressed in this document are those of the authors and do not reflect the views or opinions of, nor do they constitute a recommendation or endorsement by, the United States Air Force.

12.9 REFERENCES

[1] Dorsett, K.M., and Mehl, D.R., Innovative Control Effectors (ICE), Phase 1 Final Report, WL-TR-96-3043, January 1996.

[2] Dorsett, K.M., Fears, S P., and Houlden, H.P., Innovative Control Effectors (ICE) Phase II, Phase II Final Report, WL-TR-97-3059, August 1997.

[3] Cummings, R.M., Introduction: SACCON Uninhabited Combat Aerial Vehicle Experimental and Numerical Simulations, *Journal of Aircraft*, Vol. 49, No. 6, November – December 2012.

[4] Sieber, M., Ostermann, F., Woszidlo, R., Oberleithner and K., Paschereit, C.O., Lagrangian Coherent Structures in the Flow Field of a Fluidic Oscillator, 68th Annual Meeting of the APS division of Fluid Dynamics, Nov 2015, https://gfm.aps.org/meetings/dfd-2015/55e6c09f69702d060d900000, doi: doi.org/10.1103/APS.DFD.2015.GFM.V0015.

[5] Miller, D.N., Williams, D.R., Warsop, C. and Smith, D.R., NATO AVT-239 Task Group: Approach to Assess Prospects of Active Flow Control on a Next-Gen Tailless Aircraft, AIAA SciTech 2019, January 2019.

[6] Warsop, C., Forster, M., and Crowther, W.J., NATO AVT-239 Task Group: Supercritical Coanda Based Circulation Control and Fluidic Thrust Vectoring, AIAA SciTech 2019, January 2019.

[7] Williams, D.R., Seidel, J. and Osteroos, R., NATO AVT-239 Task Group: Flight Control Derivatives Using Active Flow Control Effectors on the ICE/SACCON UAS Model, AIAA SciTech 2019, January 2019.

[8] Phillips, E., Jentzsch, M., Menge, P., Taubert, L., Forster, M. and Wygnanski, I, On the Use of Active Flow Control to Change the Spanwise Flow on Tailless Aircraft Models, Thus Affecting their Trim and Control, AIAA SciTech 2019, January 2019.

[9] Niestroy, M., Williams, D.R. and Seidel, J., NATO AVT-239 Task Group: Flow Control Simulation of the ICE Aircraft, AIAA SciTech 2019, January 2019.

[10] Hutchin, C., NATO AVT-239: Control Effectiveness and System Sizing Requirements for Integration of Fluidic Flight Controls on the SACCON Aircraft Configuration, AIAA SciTech 2019, January 2019.

[11] Maines, B., and Miller, D.N., NATO AVT-239 Task Group: Air Vehicle Integration Considerations for Active Flow Control on a Future UAS, AIAA SciTech 2019, January 2019.

[12] Miller, D.N., Williams, D.R., Warsop, C. and Smith, D.R., NATO AVT-239 Task Group: Approach to Assess Prospects of Active Flow Control on a Next-Gen Tailless Aircraft, AIAA SciTech 2019, January 2019.

[13] Hariharan, N., and Leishman, J.G., Unsteady Aerodynamics of a Flapped Airfoil in Subsonic Flow by Indicial Concepts, Journal of Aircraft, Vol. 33, No. 5, 1996, pp. 855-868, doi:10.2514/3.47028.

[14] Kopp, C., The Russian Philosophy of BVR Air Combat, http://www.ausairpower.net/APA-Rus-BVR-AAM.html, 2008.

REPORT DOCUMENTATION PAGE

1. Recipient's Reference	2. Originator's References	3. Further Reference	4. Security Classification of Document
	STO-TR-AVT-239 AC/323(AVT-239)TP/901	ISBN 978-92-837-2226-7	PUBLIC RELEASE

5. Originator

Science and Technology Organization
North Atlantic Treaty Organization
BP 25, F-92201 Neuilly-sur-Seine Cedex, France

6. Title

Innovative Control Effectors for Manoeuvring of Air Vehicles

7. Presented at/Sponsored by

Summary Report of the NATO STO AVT-239 Task Group.

8. Author(s)/Editor(s)	9. Date
Multiple	November 2020
10. Author's/Editor's Address	**11. Pages**
Multiple	252

12. Distribution Statement

This document is distributed in accordance with NATO Security Regulations and STO policies.

13. Keywords/Descriptors

Active flow control; Circulation control; Conceptual design; Flight control; Fluidic thrust vectoring; UCAV; Sweeping jets

14. Abstract

A North Atlantic Treaty Organization technical task group (AVT-239) was commissioned to investigate the feasibility of applying Active Flow Control (AFC) to low-observable combat aircraft configurations. A wide range of active flow control technologies were explored and performance and integration assessments were undertaken on two aircraft configurations (ICE and SACCON/MULDICON). The results of these investigations were used to undertake a design of experiments trade study to assess the feasibility of using a suite of AFC technologies for flight control during a typical ingress/egress mission phase relative to a conventional mechanical flap-based control suite. The study suggests that AFC technology is both feasible and reasonable for application to aircraft concepts represented by the ICE and SACCON/MULDICON platforms. Areas highlighted for future R&D investment include: AFC valve reliability/maintainability and the maturation of technology, integration, and manufacturing readiness to level 5 or greater. Further assessments are proposed to explore the application of AFC to the take-off/landing and manoeuvring mission phases. A comprehensive framework for integrating flow control into the aerodynamic design of a next generation UAV and assessing its system impact on that aircraft has been established.

NORTH ATLANTIC TREATY ORGANIZATION

BP 25
F-92201 NEUILLY-SUR-SEINE CEDEX • FRANCE
Télécopie 0(1)55.61.22.99 • E-mail mailbox@cso.nato.int

SCIENCE AND TECHNOLOGY ORGANIZATION

DIFFUSION DES PUBLICATIONS
STO NON CLASSIFIEES

Les publications de l'AGARD, de la RTO et de la STO peuvent parfois être obtenues auprès des centres nationaux de distribution indiqués ci-dessous. Si vous souhaitez recevoir toutes les publications de la STO, ou simplement celles qui concernent certains Panels, vous pouvez demander d'être inclus soit à titre personnel, soit au nom de votre organisation, sur la liste d'envoi.

Les publications de la STO, de la RTO et de l'AGARD sont également en vente auprès des agences de vente indiquées ci-dessous.

Les demandes de documents STO, RTO ou AGARD doivent comporter la dénomination « STO », « RTO » ou « AGARD » selon le cas, suivi du numéro de série. Des informations analogues, telles que le titre est la date de publication sont souhaitables.

Si vous souhaitez recevoir une notification électronique de la disponibilité des rapports de la STO au fur et à mesure de leur publication, vous pouvez consulter notre site Web (http://www.sto.nato.int/) et vous abonner à ce service.

CENTRES DE DIFFUSION NATIONAUX

ALLEMAGNE
Streitkräfteamt / Abteilung III
Fachinformationszentrum der Bundeswehr (FIZBw)
Gorch-Fock-Straße 7, D-53229 Bonn

BELGIQUE
Royal High Institute for Defence – KHID/IRSD/RHID
Management of Scientific & Technological Research
for Defence, National STO Coordinator
Royal Military Academy – Campus Renaissance
Renaissancelaan 30, 1000 Bruxelles

BULGARIE
Ministry of Defence
Defence Institute "Prof. Tsvetan Lazarov"
"Tsvetan Lazarov" bul no.2
1592 Sofia

CANADA
DGSIST 2
Recherche et développement pour la défense Canada
60 Moodie Drive (7N-1-F20)
Ottawa, Ontario K1A 0K2

DANEMARK
Danish Acquisition and Logistics Organization
(DALO)
Lautrupbjerg 1-5
2750 Ballerup

ESPAGNE
Área de Cooperación Internacional en I+D
SDGPLATIN (DGAM)
C/ Arturo Soria 289
28033 Madrid

ESTONIE
Estonian National Defence College
Centre for Applied Research
Riia str 12
Tartu 51013

ETATS-UNIS
Defense Technical Information Center
8725 John J. Kingman Road
Fort Belvoir, VA 22060-6218

FRANCE
O.N.E.R.A. (ISP)
29, Avenue de la Division Leclerc
BP 72
92322 Châtillon Cedex

GRECE (Correspondant)
Defence Industry & Research General
Directorate, Research Directorate
Fakinos Base Camp, S.T.G. 1020
Holargos, Athens

HONGRIE
Hungarian Ministry of Defence
Development and Logistics Agency
P.O.B. 25
H-1885 Budapest

ITALIE
Ten Col Renato NARO
Capo servizio Gestione della Conoscenza
F. Baracca Military Airport "Comparto A"
Via di Centocelle, 301
00175, Rome

LUXEMBOURG
Voir Belgique

NORVEGE
Norwegian Defence Research
Establishment
Attn: Biblioteket
P.O. Box 25
NO-2007 Kjeller

PAYS-BAS
Royal Netherlands Military
Academy Library
P.O. Box 90.002
4800 PA Breda

POLOGNE
Centralna Biblioteka Wojskowa
ul. Ostrobramska 109
04-041 Warszawa

PORTUGAL
Estado Maior da Força Aérea
SDFA – Centro de Documentação
Alfragide
P-2720 Amadora

REPUBLIQUE TCHEQUE
Vojenský technický ústav s.p.
CZ Distribution Information Centre
Mladoboleslavská 944
PO Box 18
197 06 Praha 9

ROUMANIE
Romanian National Distribution
Centre
Armaments Department
9-11, Drumul Taberei Street
Sector 6
061353 Bucharest

ROYAUME-UNI
Dstl Records Centre
Rm G02, ISAT F, Building 5
Dstl Porton Down
Salisbury SP4 0JQ

SLOVAQUIE
Akadémia ozbrojených síl gen.
M.R. Štefánika, Distribučné a
informačné stredisko STO
Demänová 393
031 01 Liptovský Mikuláš 1

SLOVENIE
Ministry of Defence
Central Registry for EU & NATO
Vojkova 55
1000 Ljubljana

TURQUIE
Milli Savunma Bakanlığı (MSB)
ARGE ve Teknoloji Dairesi
Başkanlığı
06650 Bakanliklar – Ankara

AGENCES DE VENTE

The British Library Document
Supply Centre
Boston Spa, Wetherby
West Yorkshire LS23 7BQ
ROYAUME-UNI

Canada Institute for Scientific and
Technical Information (CISTI)
National Research Council Acquisitions
Montreal Road, Building M-55
Ottawa, Ontario K1A 0S2
CANADA

Les demandes de documents STO, RTO ou AGARD doivent comporter la dénomination « STO », « RTO » ou « AGARD » selon le cas, suivie du numéro de série (par exemple AGARD-AG-315). Des informations analogues, telles que le titre et la date de publication sont souhaitables. Des références bibliographiques complètes ainsi que des résumés des publications STO, RTO et AGARD figurent dans le « NTIS Publications Database » (http://www.ntis.gov).

NORTH ATLANTIC TREATY ORGANIZATION

BP 25
F-92201 NEUILLY-SUR-SEINE CEDEX • FRANCE
Télécopie 0(1)55.61.22.99 • E-mail mailbox@cso.nato.int

SCIENCE AND TECHNOLOGY ORGANIZATION

DISTRIBUTION OF UNCLASSIFIED STO PUBLICATIONS

AGARD, RTO & STO publications are sometimes available from the National Distribution Centres listed below. If you wish to receive all STO reports, or just those relating to one or more specific STO Panels, they may be willing to include you (or your Organisation) in their distribution.

STO, RTO and AGARD reports may also be purchased from the Sales Agencies listed below.

Requests for STO, RTO or AGARD documents should include the word 'STO', 'RTO' or 'AGARD', as appropriate, followed by the serial number. Collateral information such as title and publication date is desirable.

If you wish to receive electronic notification of STO reports as they are published, please visit our website (http://www.sto.nato.int/) from where you can register for this service.

NATIONAL DISTRIBUTION CENTRES

BELGIUM
Royal High Institute for Defence – KHID/IRSD/RHID
Management of Scientific & Technological Research for Defence, National STO Coordinator
Royal Military Academy – Campus Renaissance
Renaissancelaan 30
1000 Brussels

BULGARIA
Ministry of Defence
Defence Institute "Prof. Tsvetan Lazarov"
"Tsvetan Lazarov" bul no.2
1592 Sofia

CANADA
DSTKIM 2
Defence Research and Development Canada
60 Moodie Drive (7N-1-F20)
Ottawa, Ontario K1A 0K2

CZECH REPUBLIC
Vojenský technický ústav s.p.
CZ Distribution Information Centre
Mladoboleslavská 944
PO Box 18
197 06 Praha 9

DENMARK
Danish Acquisition and Logistics Organization (DALO)
Lautrupbjerg 1-5
2750 Ballerup

ESTONIA
Estonian National Defence College
Centre for Applied Research
Riia str 12
Tartu 51013

FRANCE
O.N.E.R.A. (ISP)
29, Avenue de la Division Leclerc – BP 72
92322 Châtillon Cedex

GERMANY
Streitkräfteamt / Abteilung III
Fachinformationszentrum der Bundeswehr (FIZBw)
Gorch-Fock-Straße 7
D-53229 Bonn

GREECE (Point of Contact)
Defence Industry & Research General Directorate, Research Directorate
Fakinos Base Camp, S.T.G. 1020
Holargos, Athens

HUNGARY
Hungarian Ministry of Defence
Development and Logistics Agency
P.O.B. 25
H-1885 Budapest

ITALY
Ten Col Renato NARO
Capo servizio Gestione della Conoscenza
F. Baracca Military Airport "Comparto A"
Via di Centocelle, 301
00175, Rome

LUXEMBOURG
See Belgium

NETHERLANDS
Royal Netherlands Military Academy Library
P.O. Box 90.002
4800 PA Breda

NORWAY
Norwegian Defence Research Establishment, Attn: Biblioteket
P.O. Box 25
NO-2007 Kjeller

POLAND
Centralna Biblioteka Wojskowa
ul. Ostrobramska 109
04-041 Warszawa

PORTUGAL
Estado Maior da Força Aérea
SDFA – Centro de Documentação
Alfragide
P-2720 Amadora

ROMANIA
Romanian National Distribution Centre
Armaments Department
9-11, Drumul Taberei Street
Sector 6
061353 Bucharest

SLOVAKIA
Akadémia ozbrojených síl gen M.R. Štefánika, Distribučné a informačné stredisko STO
Demänová 393
031 01 Liptovský Mikuláš 1

SLOVENIA
Ministry of Defence
Central Registry for EU & NATO
Vojkova 55
1000 Ljubljana

SPAIN
Área de Cooperación Internacional en I+D
SDGPLATIN (DGAM)
C/ Arturo Soria 289
28033 Madrid

TURKEY
Milli Savunma Bakanlığı (MSB)
ARGE ve Teknoloji Dairesi Başkanlığı
06650 Bakanliklar – Ankara

UNITED KINGDOM
Dstl Records Centre
Rm G02, ISAT F, Building 5
Dstl Porton Down, Salisbury SP4 0JQ

UNITED STATES
Defense Technical Information Center
8725 John J. Kingman Road
Fort Belvoir, VA 22060-6218

SALES AGENCIES

The British Library Document Supply Centre
Boston Spa, Wetherby
West Yorkshire LS23 7BQ
UNITED KINGDOM

Canada Institute for Scientific and Technical Information (CISTI)
National Research Council Acquisitions
Montreal Road, Building M-55
Ottawa, Ontario K1A 0S2
CANADA

Requests for STO, RTO or AGARD documents should include the word 'STO', 'RTO' or 'AGARD', as appropriate, followed by the serial number (for example AGARD-AG-315). Collateral information such as title and publication date is desirable. Full bibliographical references and abstracts of STO, RTO and AGARD publications are given in "NTIS Publications Database" (http://www.ntis.gov).

ISBN 978-92-837-2226-7